NATIONAL AND KAPODISTRIAN UNIVERSITY OF ATHENS

SCHOOL OF SCIENCE
DEPARTMENT OF GEOLOGY & GEOENVIRONMENT

MINERALOGY AND GEOCHEMISTRY OF AGIOS IOANNIS, LARYMNA, GREECE (LARCO GMMSA) Ni-LATERITE

MSc Thesis

KONSTANTINA GOUTZIOUPA

Supervisor: Assoc. Prof. Athanasios Godelitsas

Athens, Greece

January, 2021

Dedicated to the memory of my Beloved Grandfather ***Athanasios***

And to my Grandmother ***Eftychia***

ACKNOWLEDGEMENTS

First and foremost, I am grateful to my supervisor Dr. Athanasios Godelitsas (University of Athens, Greece) for his crucial guidance during my MSc Thesis long journey. My scientific sufficiency has been validated under his great expertise.

'LARCO GMMSA' is gratefully acknowledged for the provision of laterite samples from Agios Ioannis, Larymna area and their collaboration during my MSc Thesis. Additionally, I thank Dr. Athanasios Apostolikas and Mr. Serafim Maras (LARCO GMMSA) for offering me their authorization to visit Agios Ioannis of Larymna avtive mine area providing me with laterite samples directly from its mining front, and, consequently, for support in the whole implementation of the present work.

I would also like to express my gratitude to my former supervisor, Dr. George Alevizos (School of Mineral Resources Engineering, Technical University of Crete, Greece), who inspired me to get interested in the science of laterites.

I am grateful to Dr. Maurizio Petrelli (Department of Physics and Geology, Università degli Studi di Perugia, Italy) for his valuable assistance in the LA-ICP-MS measurements.

Especially, I would like to thank Dr. Yiannis Sanakis (Institute of Nanoscience and Nanotechnology, National Center for Scientific Research Demokritos, Greece) for his cooperation concerning Mössbauer measurements.

Furthermore, Dr. Petros Tsakiridis (School of Mining Engineering and Metallurgy, National Technical University of Athens, Greece), Dr. Dionisios Gasparatos (Department of Natural Resources Management and Agricultural Engineering, Agricultural University of Athens, Greece), Dr. Argyrios Papadopoulos (Hellas Gold, Olympias Mine, Chalkidiki, Greece) and finally, Dr. Michail Samouhos (School of Mining Engineering and Metallurgy, National Technical University of Athens, Greece) are thankfully acknowledged for their collaboration in the laboratory measurements during my MSc Thesis.

SUMMARY

Ni-laterite ores from central Greece deposits are currently used in the LARCO GMMSA smelting plant to produce Fe-Ni. In the frame of research regarding new insights into the mineralogy and geochemistry of the ores, composite samples were collected from a model laterite profile of Agios Ioannis, Larymna (Lokris area). At the same time, the surrounding hanging wall (Upper Cretaceous; in our case ~90 Ma) and footwall limestones (Triassic-Jurassic; in our case ~145 Ma) were also examined. The PXRD investigation of the studied samples of this Ni-laterite deposit confirmed the presence of crystalline Fe-oxides/oxyhydroxides (hematite and goethite) and Ni-bearing Mg-Fe-phyllosilicates (mainly chlorite-group and serpentine-group minerals) as the major mineral components. The subsequent study of the Ni-phyllosilicate by means of ^{57}Fe-Mössbauer indicated that Fe^{3+} is exclusively the Fe component of the mineral. Mössbauer spectroscopy also showed that a possible constituent of the phase can be superparamagnetic α-Fe. The SEM-EDS study of the typical laterite ore, in microscale, confirmed the well-known occurrence of Ni-bearing phyllosilicates in mixture with Fe-oxide phases. However, SEM-EDS performed in material from a thin green-black layer ('garnierite') ocurring in the base of the deposit, revealed, except the aformentioned minerals, peculiar phases containing Al-Si-Mn-Ni-Co-Cr-V-Cu-Ca, implying the presence of potential mineral nanoparticles and nanominerals. In accordance, the nanoscopic study by TEM-EDS proved the existence of such micro-areas, consisting most probably of an amorphous/disordered Ni(-Cr)-Co-bearing Mn-(oxy)hydroxide/oxide (hydrated) phase, the so-called 'asbolane' by previous authors. The bulk chemical analyses by ICP-OES/MS indicated that, except for major elements (Si, Al, Fe and Mn), the studied industrial laterite ore contains a variety of useful and potentially hazardous trace elements (Ni, Co, V, ΣLREE, ΣHREE, Sc, As and Pb, max values: 9212 ppm, 1480 ppm, 379 ppm, 1221 ppm, 253 ppm, 76 ppm, 81 ppm and 67 ppm, respectively; average values: 3941 ppm, 659 ppm, 317 ppm, 678 ppm, 111 ppm, 71 ppm, 51 ppm, and 53 ppm, respectively), with remarkable positive geochemical anomalies with respect to HFSE and REEs (REE+Y+Sc, max: 2150 ppm; average: 1173 ppm), as well as in most of compatible elements, whereas they are depleted in specific LILE. It should be mentioned that, as stands for Ni showing an increase towards deeper horizons of the deposit, Co is also exceptionally increased (3534 ppm and 7940 ppm, respectively) in the green-black layer at the base of the deposit, as well as in the footwall limestone. Complementary point anayses of Ni-bearing phyllosilicates by LA-ICP-MS confirmed that, despite rather low Ni-content in the ore (average 3941 ppm, i.e., ca. 0.4 wt.%), the metal concentration in these phases is 5.81 wt.%. On the other hand, Co and ΣREE+Y+Sc are remarkably lower (164 ppm and 40 ppm, respectively), meaning that the above critical metals are not consistent to Ni and they are preferentially contained in Fe-oxides/oxyhydroxides and other phases examined by SEM-EDS, such as REE-fluorocarbonates and -phosphates. In general, the REEs are concentrated just below the middle horizons of the studied deposit, which was formed in a period of ~55 Ma. The significant enrichment of specific horizons of the Larymna laterite in REEs and, moreover, an observed negative geochemical Ce anomaly (Ce/Ce*), indicate that post-diagenesis/deposition phenomena have taken place in the frame of further supergene/epigenetic processes, during the laterite genesis.

Keywords: Laterite, Nickel, Cobalt, Rare Earth Elements, Mineral Nanoparticles, Nanominerals.

ΠΕΡΙΛΗΨΗ

Τα μεταλλεύματα νικελιούχου λατερίτη από κοιτάσματα της κεντρικής Ελλάδας χρησιμοποιούνται από την εταιρεία ΛΑΡΚΟ Γ.Μ.Μ.Α.Ε. (LARCO G.M.M.S.A.) για την παραγωγή σιδηρονικελίου (Fe-Ni). Στο πλαίσιο της παρούσας έρευνας συλλέχθηκαν δείγματα λατερίτη από ένα τυπικό λατεριτικό προφίλ της περιοχής του Αγίου Ιωάννη Λάρυμνας (ευρύτερη περιοχή Λοκρίδος). Ταυτόχρονα, εξετάστηκαν και οι υπερκείμενοι και υποκείμενοι ασβεστόλιθοι. Η διερεύνηση με PXRD επιβεβαίωσε την παρουσία Ni-φυλλοπυριτικών ορυκτών και κρυσταλλικών οξειδίων/(οξυ)υδροξειδίων του Fe (αιματίτη και γκαιτίτη) στο μετάλλευμα. Η περαιτέρω μελέτη των Ni-φυλλοπυριτικών με φασματοσκοπία ^{57}Fe-Mössbauer έδειξε ότι στις φάσεις αυτές ο σίδηρος εντοπίζεται κυρίως με την τρισθενή του μορφή Fe^{3+}, και ότι είναι πιθανή η παρουσία υπερπαραμαγνητικού α-Fe. Η μελέτη με SEM-EDS σε μικροκλίμακα επιβεβαίωσε τις φάσεις που αναγνωρίστηκαν με PXRD και Mössbauer. Επιπλέον, η έρευνα με SEM-EDS, που εκτελέστηκε σε υλικό από ένα λεπτό πρασινόμαυρο στρώμα («γαρνιερίτης»), το οποίο εμφανίζεται στη βάση του κοιτάσματος, αποκάλυψε, εκτός από τα προαναφερθέντα ορυκτά, ιδιαίτερες φάσεις που περιέχουν Al-Si-Mn-Ni-Co-Cr-V-Cu-Ca, υποδηλώνοντας πιθανώς την παρουσία νανοσωματιδίων ορυκτών και νανο-ορυκτών. Σε συμφωνία με το παραπάνω συμπέρασμα, η νανοσκοπική μελέτη με TEM-EDS απέδειξε την ύπαρξη τέτοιων περιοχών στο υλικό, οι οποίες αποτελούνται πιθανότατα από μια άμορφη/με αταξία στη δομή (ενυδατωμένη) φάση (οξυ)υδροξειδίου/οξειδίου Mn που φιλοξενεί Ni(-Cr)-Co, η αποκαλούμενη «ασβολάνης» από προηγούμενους συγγραφείς. Οι ολικές αναλύσεις με ICP-OES/MS έδειξαν ότι, εκτός από τα κύρια στοιχεία (Si, Al, Fe και Mn), το συγκεκριμένο μετάλλευμα λατερίτη περιέχει μια ποικιλία χρήσιμων και δυνητικά προβληματικών ιχνοστοιχείων (Ni, Co, V, ΣLREE, ΣHREE, Sc, As, και Pb με μέγιστες τιμές: 9212 ppm, 1480 ppm, 379 ppm, 1221 ppm, 253 ppm, 76 ppm, 81 ppm, και 67 ppm αντίστοιχα, και με μέσες τιμές: 3941 ppm, 659 ppm, 317 ppm, 678 ppm, 111 ppm, 71 ppm, 51 ppm, και 53 ppm αντίστοιχα), με αξιοσημείωτες θετικές γεωχημικές ανωμαλίες των ιχνοστοιχείων υψηλού δυναμικού πεδίου (HFSE) (δηλαδή: Th, U, Ta, Nb, W κ.τ.λ.) και των στοιχείων της ομάδας των σπάνιων γαιών (REEs) (REE+Y+Sc με μέγιστη τιμή: 2150 ppm και με μέσο όρο: 1173 ppm), καθώς και των συμβατών στοιχείων, ενώ παρατηρείται απεμπλουτισμός στα λιθόφιλα ιχνοστοιχεία μεγάλης ιοντικής ακτίνας (LILE). Πρέπει να αναφερθεί ότι στη βάση του κοιτάσματος, καθώς και στον υποκείμενο ασβεστόλιθο, το κοβάλτιο (Co) αυξάνεται σε πολύ υψηλό ποσοστό (3534 ppm και 7940 ppm αντίστοιχα). Συμπληρωματικές αναλύσεις των Ni-φυλλοπυριτικών ορυκτών με LA-ICP-MS επιβεβαίωσαν ότι, παρά τη χαμηλή περιεκτικότητα σε Ni στο μετάλλευμα (μέσος όρος 3941 ppm, δηλαδή περίπου 0,4% κ.β.), η συγκέντρωση του μετάλλου σε αυτές τις φάσεις είναι 5,81% κ.β.. Βέβαια, το Co και τα ΣREE+Y+Sc είναι σημαντικά χαμηλότερα (164 ppm και 40 ppm, αντίστοιχα), γεγονός που σημαίνει ότι τα παραπάνω κρίσιμα μέταλλα δε συνυπάρχουν με το Ni και, κατά προτίμηση, εμπεριέχονται σε οξείδια/(οξυ)υδροξείδια Fe και άλλες φάσεις, που εξετάστηκαν από SEM-EDS, όπως REE-φθοριοανθρακικά και -φωσφορικά ορυκτά. Ο σημαντικός εμπλουτισμός του λατερίτη της Λάρυμνας σε REEs σε συνδυασμό με την παρατηρούμενη αρνητική γεωχημική ανωμαλία δημητρίου (Ce/Ce*) υποδηλώνουν ότι έχουν λάβει χώρα φαινόμενα μετα-διαγένεσης/απόθεσης στο πλαίσιο μεταγενέστερων επιγενετικών διεργασιών καθόλη τη διάρκεια της δημιουργίας του λατερίτη.

Λέξεις-κλειδιά: Λατερίτης, Νικέλιο, Κοβάλτιο, Σπάνιες Γαίες, Νανοσωματίδια Ορυκτών, Νανο-ορυκτά.

TABLE OF CONTENTS

1. INTRODUCTION

1.1 Basic and critical raw materials and metals

In June 2011, the European Commission emitted a first report entitled Critical Raw Materials for the EU (European Commission, 2011). This report identified a list of 14 raw materials which were defined critical on the basis of their high economic importance and their potential risk of supply. Among these raw materials, most of them are of a primary importance for modern technology, renewable energy and industry (hybrid and electric car industry, wind turbine technology; aerospace industry, portable electronics and so on…). An updated report was published three years later in which 6 raw materials were added to the previous list (European Commission, 2014), and in 2017, a new version assessed a revised list of 26 critical raw materials and groups of raw materials (European Commission, 2017). The assessment above is based on data from the recent past and shows how criticality has evolved since the first list was published, and it does not forecast future trends.

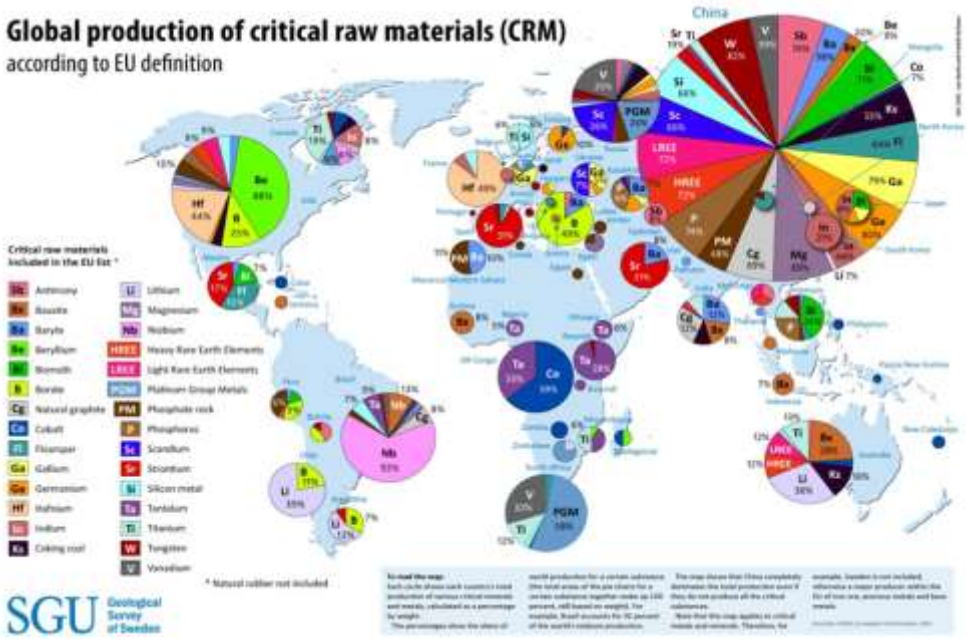

Figure 1. *Global production of Critical Raw Metals (CRM) according to EU definition (Source: Sveriges Geologiska Undersökning; https://www.sgu.se/mineralnaring/kritiska-ravaror).*

The European Union recently updated the list of raw materials considered as critical for its industry on the basis of their high economic importance and their relative supply risk. The 2020 assessment (Fig. 1) follows the same methodology as in 2017. It uses the average for the most recent complete 5-year period for the EU without the United Kingdom (EU-27). It screened 83 materials (5 more than in 2017) and, where possible, looked more closely than previous assessments at where criticality appears in the value chain: extraction and/or processing. This list now defines 26 critical raw materials that include among others, rare earth elements (REE), scandium (Sc), vanadium (V) and cobalt (Co). Raw materials, particularly metals, are very important for sustainable functioning, since they are essential for the high-tech products such as electrical and electronic devices, photovoltaic systems, batteries, catalysts, optical fiber

cables, synthetic fuels, etc.. European industry needs sufficient access to certain mineral raw materials for the sound functioning of the EU's economy (Melfos et al., 2012).

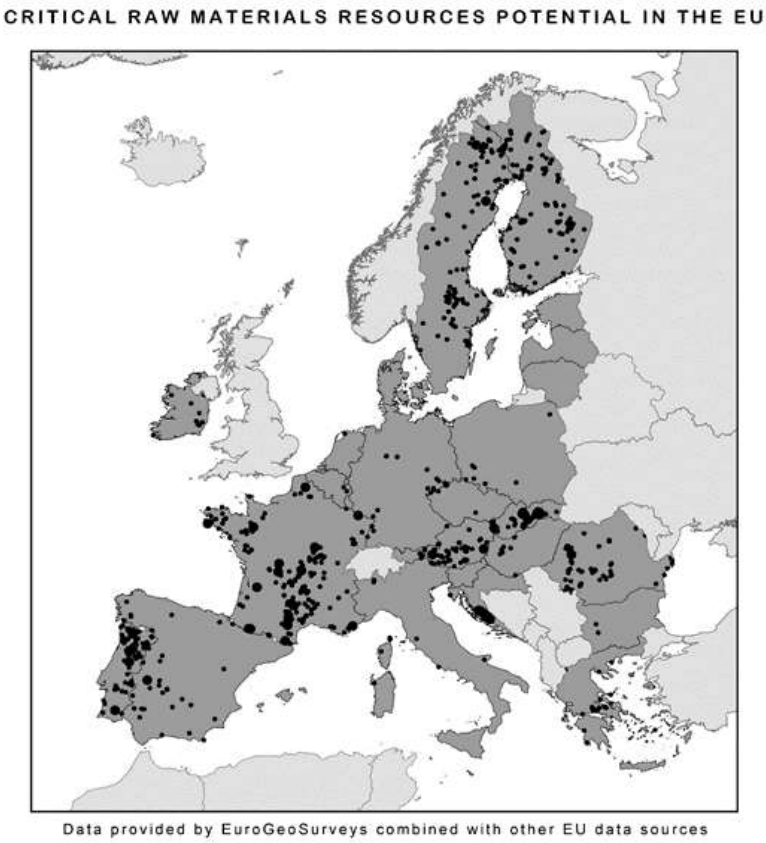

Figure 2. *CRM deposits EU-27 (2020) (Source: European Commission report on the 2020 criticality assessment; https://eur-lex.europa.eu/legal-content/EN/TXT/?uri=CELEX:52020DC0474).*

Due to their low concentrations in earth's crust, the critical metals are produced as by-products of other metals which are mined (Melfos et al., 2012). In fact, recent investigations have shown that the latter elements can be accumulated during weathering in consequence of residual and secondary enrichment. The process of co-beneficiation is from now on, one of the major challenges for society, as most deposits (Fig.2) are extracted for only one metal (sometimes a few), leaving wastes with other metals at a low content, which nevertheless could constitute the potentially future reserves, when better extraction processes are available. Among the different possible primary resources of these critical metals, lateritic deposits are particularly targeted. These environments are also characterized by significant concentrations of transition metals (e.g., Mn, Cr, Ni), which are not defined as critical to date but remain of primary economic importance (Ulrich et al., 2019). Besides, Ni has always been classified in the European Union as a Priority Substance, and, as already mentioned, Ni is also accompanied by other metals, seldom extracted up to now, such as Mn, Cr and Sc. Another valuable metal present in Ni-laterite ores is the Co. Hence, the laterite cover can also host supergene Co mineralization of economic interest (Llorca et al., 1991). On the other hand, weathering horizons are particularly investigated. In such environments, REE (Fig. 3) and other rare metals show limited mobility and thus may be locally enriched through successive processes of leaching and concentration in neoformed silicates, oxides or phosphates.

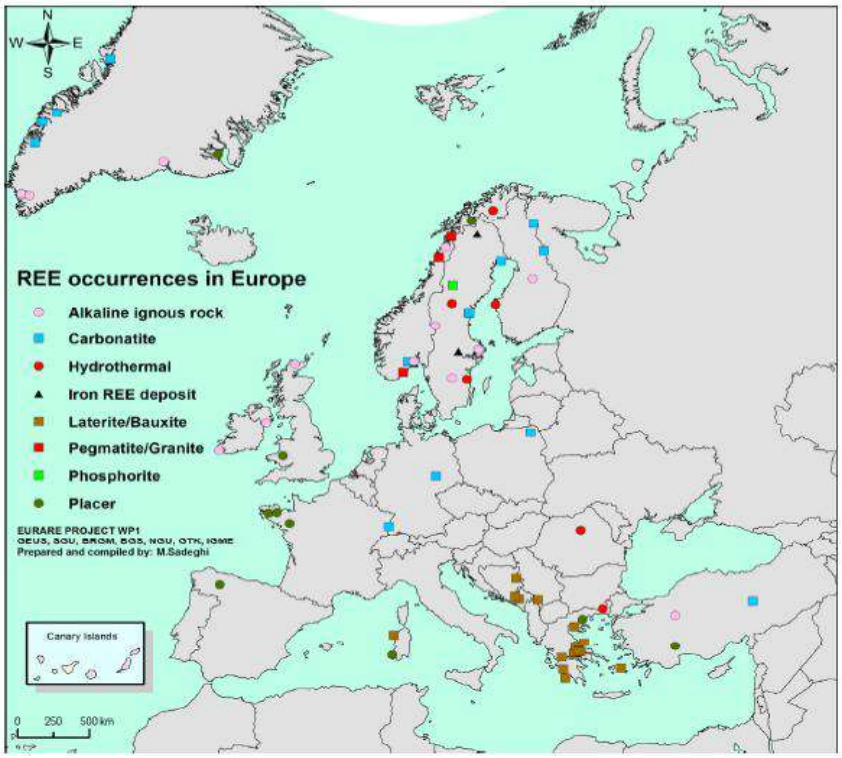

Figure 3. *Main REE occurences in Europe (Sadeghi et al., 2014).*

Consequently, several investigations of the potential occurrence of critical metals (including REE and Sc) have been done recently in Ni-Co laterite deposits (Figs. 4 and 5), which are exploitable reserves of Ni, commonly Co and, rarely Sc, and are developed on ultrabasic basements worldwide, e.g., Cuba, Dominican Republic, Indonesia, Australia, New Caledonia (Ulrich et al., 2019).

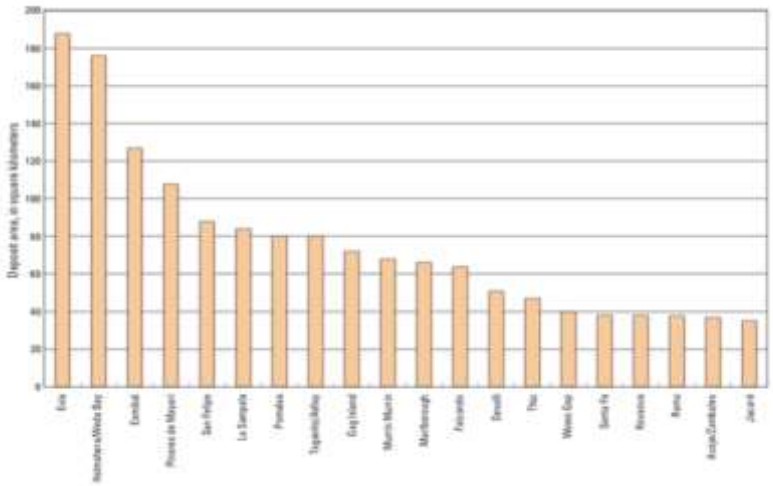

Figure 4. *Deposit areas for the 20 largest exploited Ni-Co laterite deposits (see Fig. 5 below for deposit locations) (Berger et al., 2011).*

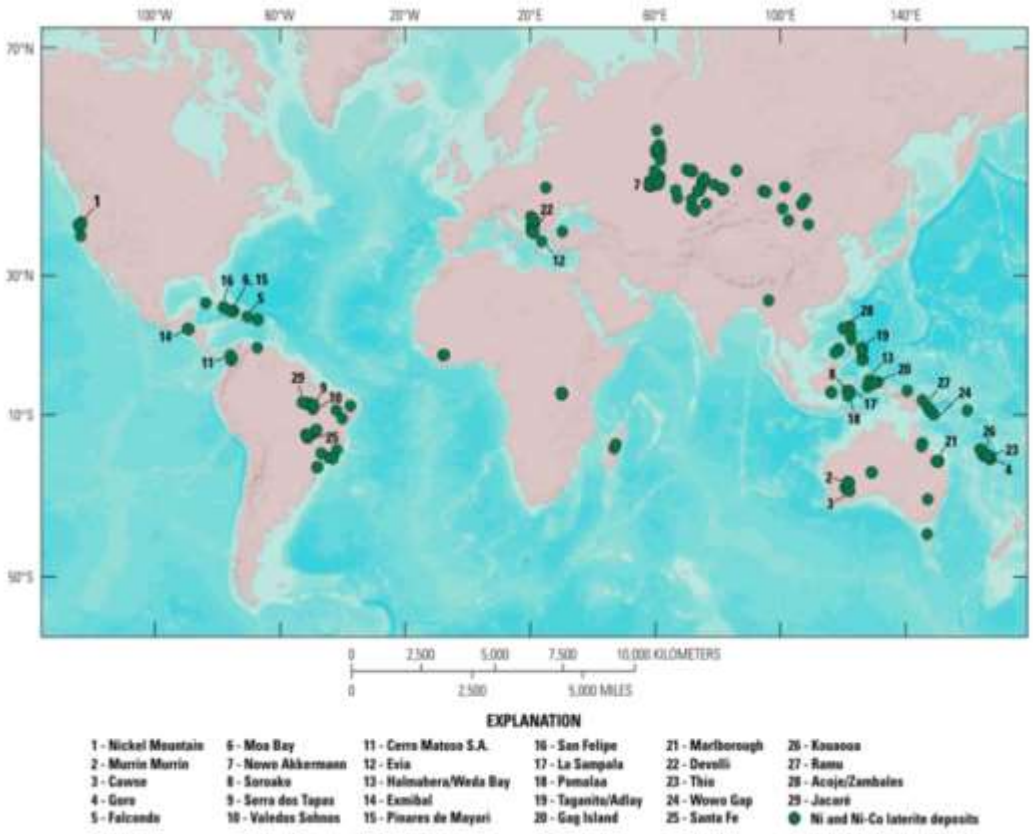

Figure 5. *Global distribution of Ni and Ni-Co laterite deposits (Marsh et al., 2010).*

1.1.1 Nickel

Nickel (Ni) is a transition group metal with 14 known isotopes, five of which are stable. It has the same oxidation state (+2) as, and a similar ionic size to, Fe and other similar transition group metals, so it can substitute for Fe in many minerals. In the earth's crust Ni abundance averages 80 parts per million (ppm), but, as it is greatly concentrated in the core, it is actually the 5th most common element on the planet. Nickel occurs with Fe in meteorites, and in small quantities in plants, animals and seawater. Nickel is classified by the European Commission as a non-critical element with a high economic importance, as it is a transition element of strategic significance. Nickel is an important metal with the total global consumption of about 2 million tons per year. It is sourced from both sulphide and laterite (Fig. 6), but currently laterites are becoming more attractive for Ni production due to the depletion of high grade Ni sulfide ores (Farrokhpay et al., 2017). Ni-bearing lateritic ores, with average Ni content of 1-1.6%, are formed by tropical and sub-tropical surface weathering. In subtropical and tropical climates intense weathering of ultramafic rocks may lead to Ni enrichment. Nickel dispersed in silicates and sulphides within the host rock is remobilised and deposited as hydroxides, limonite and goethite, in weathered layers near the surface and as silicates (garnierite) at deeper levels. Serpentine-rich zones in saprolite (a fine-grained clay produced by weathering of bedrock) at the base of laterites may restrict the circulation of groundwater and thus the amount of Ni enrichment. This also interferes with beneficiation due to individual grains needing to be crushed toliberate ore from gangue intergrowths. There is a wide range of economic grades in laterite

deposits, from 0.4-1.2% Ni, generally lower than in those of magmatic origin (British Geological Survey).

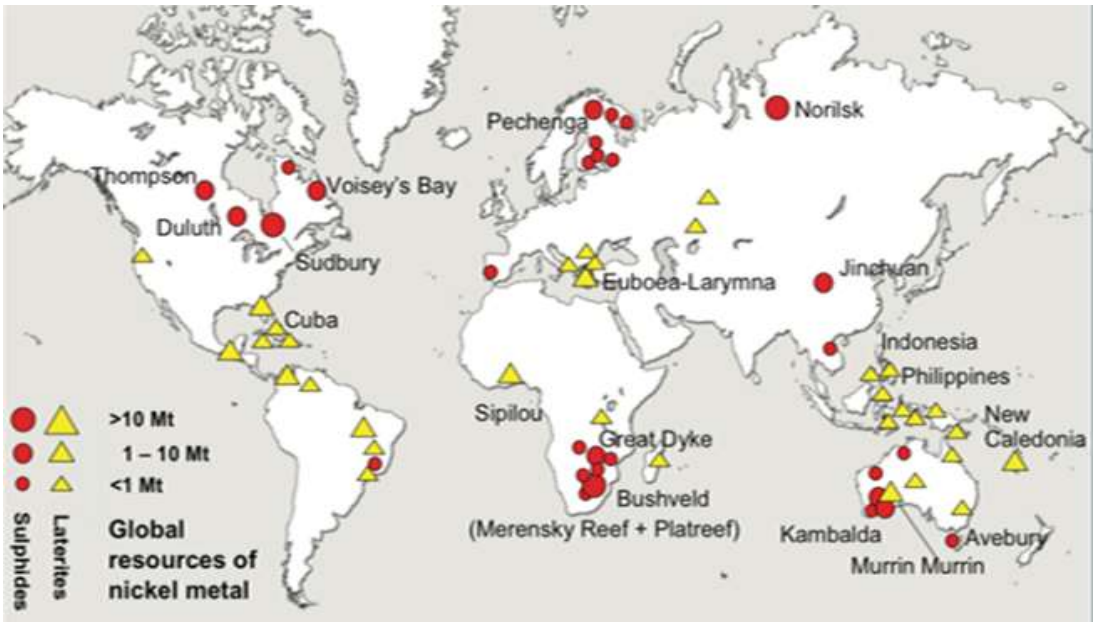

Figure 6. *The global distribution of significant laterite and sulphide Ni deposits. (Hoatson et al., 2006).*

The majority of the world's Ni resources (Fig. 7) occur as laterite ores which are exceptionally complex, low grade and expensive to treat using conventional smelting and high temperature/pressure autoclave methods (Xu et al., 2013). Laterites are generally processed by hydro or pyro-metallurgy and, therefore, preconcentration of Ni before such processes is very important (Farrokhpay et al., 2017). It is highly anticipated that increasing demand for Ni will be met largely by supply from lateritic deposits as processing techniques improve (British Geological Survey).

Figure 7. *Map of countries with the largest Ni mining activities (Commodity.com).*

1.1.2 Cobalt

Cobalt (Co) is one of the first transition series of elements. It lies between Fe and Ni and close to Cu in the Periodic Table and in nature shows a strong spatial association with these metals. Unlike them, however, Co is not widespread in nature: even in ultrabasic rocks, where it is most common, the average concentration is only 110 ppm. With a crustal abundance of only 25 ppm is one of the least familiar metals it is also one of the rarest. Although there are no common rock-forming minerals of Co, concentrations of the element in such minerals as olivine, spinel and chlorite are important primary sources of the element in lateritic and hydrothermal deposits (Smith, 2001). Thirty-four Co minerals have been recognized-principally sulphides, selenides, arsenides, sulpharsenides, carbonates, sulphates and arsenates. The main ore minerals of Co are the sulphides cobaltite, linnaeite and carrollite and the hydrated oxide 'asbolane'. Commonly, Co is associated with 'asbolane' or as a substitute of Fe in the crystalline lattice of goethite or some phyllosilicates, such as chlorites. Cobaltiferous pyrite is a further source. Workable deposits generally contain 0.1-0.4% Co and belong to one of four geologically distinct types: 1. sediment-hosted-largely Precambrian-typified by the copperbelts of Congo Democratic Republic and Zambia, which since the 1970s have contributed between 25 and 50% of the world's mine production; 2. mid-Tertiary to Recent Ni-rich lateritic deposits generated by tropical and subtropical weathering of peridotitic rocks, most notably in New Caledonia, Cuba and Australia; 3. primary magmatic Ni-Cu sulphide concentrations, such as Sudbury, Noril'sk, Voisey's Bay and Bushveld; and 4. a more diverse group attributable to hydrothermal and volcanogenic processes, the most important of which in terms of current and future production are the ophiolite-hosted Co-As deposit at Bou Azzer, Morocco, and the epigenetic Cu-Au-Co concentrations of the Idaho Co Belt, U.S.A. The last group also includes the formerly important Outokumpu-type massive sulphide and five-element (Ni-Co-Ag-As-Bi), vein-type deposits. Globally, Co is mined as a by-product of copper and Ni deposits in the Republic of the Congo-DRC (40%), in Zambia (20%), in Canada, in Australia, in Cuba, etc.. China imports large amounts of Co (almost all the DRC's production) in order to produce refined Co which is exported to the USA and the EU (Melfos et al., 2012).

1.1.3 Rare Earth Elements and Scandium

Rare Earth Elements (REE) or Rare Earths (RE) or Rare Earth Metals (REM) are a group of 17 metals, which is the largest chemically related group in the Periodic Table of Elements. The group of REEs includes the 15 elements of the series of lanthanides [or more correctly of lanthanoids (Ln)]. REE have very similar chemical properties which tend to vary gradually along the group. However, geoscientists traditionally exclude Sc, due to its small ionic radius, grouping either Y and lanthanides or only the latter into the REE family (Chakhmouradian et al., 2012). Also, some classifications exclude Pm which is a radioactive element not found in nature (Hoatson et al., 2011). During weathering processes, the chemical behavior of REE depends on several factors including Eh, pH, the presence in soil of organic and inorganic ligands, exchange sites on clays, mineralogical distribution of REE in the parent material, and especially the nature of the host rock-accessory minerals association. It has been supported that REE are fractionated during weathering processes, the weathered residual products being enriched in light REE (from La to Eu) and depleted in heavy REE (from Gd to Lu) (Braun et al., 1990). Usually, lanthanides of low atomic number (La-Eu) are referred to as LREE, while the heaviest lanthanides (Gd-Lu) are referred to

as HREE (Hoatson et al., 2011). Y is classified with the HREEs because its ionic radius is almost identical to that of Ho (Chakhmouradian et al., 2012). However, this distinction is somewhat arbitrary and the term middle REE (MREE) is sometimes used for the elements between Eu-Dy (British Geological Survey, 2008). In some classifications the most transient elements Sm and Eu can be found in either LREE or HREE, while the elements Y and Sc, despite their small atomic weight are included in the HREEs because their presence, ionic radius and properties of their behavior is closer to the HREEs than to LREEs (Hoatson et al., 2011). In other classifications the Sm-Dy elements constitute the MREEs, while the remaining Ho-Lu elements are referred to as HREE. According to Gambogi (2013), the La-Gd elements belong to the LREEs, while the Tb-Lu elements belong to the HREEs. Y is included in the HREEs, while Sc is not classified as either LREE or HREE.

In a global scale, the large REE deposits (Fig. 8) are associated with carbonatites and alkaline-peralkaline igneous rocks and hydrothermally altered silicate rocks, including pegmatites. On the contrary, REE concentrations by metamorphic or diagenetic processes are low (Hoatson et al., 2011). Economic concentrations of both LREE and HREE are found in laterized granites, rhyolites and carbonatites of different compositions. Supergene concentrations of REE are more likely to contain REE grades and tonnages that may be economically viable when the parent lithologies contained elevated REE concentrations. Within the laterites, REE may occur as: 1) trace components in residual minerals; 2) residual REE minerals; 3) secondary REE phases including REE-rich colloids; 4) trace components of Fe and Mn oxides; and 5) exchangeable cations on clays, and trace components in residual minerals. The lateritic REE deposits have important advantages over those of primary deposits. Some advantages include: 1) ease and cost of mining are low with near surface ore (< 100 m); 2) soft ore that is easy and cheap to open-pit mine; 3) ease and cost of REE extraction and processing are low; and 4) large areal extent of the deposit defines larger exploration targets and increased options for development. Also, lateritic REE enrichment greatly expands the resource potential by including source lithologies that would be normally be considered to be sub economic (Cocker, 2012).

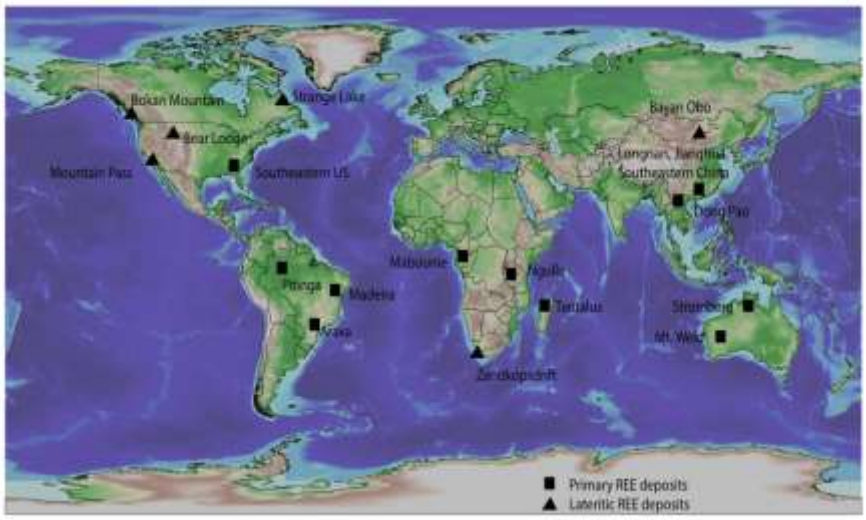

Figure 8. *Primary and lateritic REE deposits (Cocker, 2012).*

Scandium (Sc) is a transition metal in the Group 3 (IIIB)-the 21st element-of the Periodic Table and has several remarkable applications for the modern industry

(Teitler et al., 2018). Sc is considered as a strategic metal, which together with lanthanide elements and yttrium (Y) are classified as REE by the International Union of Pure and Applied Chemistry (IUPAC), because these elements share some similar chemical properties, such as the common occurrences as trivalent ions in nature (Qin et al., 2020). In fact, Sc has historically been regarded as a heavy REE owing to its ionic radius and chemical properties (Teitler et al., 2018). Nonetheless, it is generally excluded from the discussion of REE in economic geology due to its insignificant enrichment in many REE deposits developed over granite. In addition, Sc is relatively immobile and thus it is considered to be a conservative element like titanium (Ti), zirconium (Zr), and niobium (Nb), which is strikingly distinct from other REE with higher mobility in a variety of environments (Qin et al., 2020). Sc has unique properties, highly valued for many applications (Chasse et al., 2017). However, the controls of unique geochemical behaviors of Sc with respect to other REE are poorly understood (Qin et al., 2020). Despite a crustal abundance of ca. 22 ppm, comparable to common elements such as copper or lead, current Sc production is limited to 10 t to 15 t per year. The large ratio of ionic radius to charge of Sc^{3+} hinders the concentration of Sc during most geochemical processes (Chasse et al., 2017), and because of the fact it exclusively occurs in the (+3) oxidation state, it lacks affinity to combine with the common ore-forming anions (Teitler et al., 2018). Solely as a by-product of uranium, tungsten, REE or titanium ore processing, most exclusively in China and to a lesser extent in Kazakhstan, Russia and Ukraine. So far, the quoted high prices and lack of an organized market for Sc have prevented its widespread commercial adoption. However, increasing needs in energy saving technologies together with recent development of Sc extraction techniques have raised interest for this metal.

1.1.4 Uses of basic (Ni) and critical metals (Co, REE, Sc)

Nickel is primarily used in the manufacturing of stainless steel products which now accounts for two thirds of global Ni demand worldwide. Nickel demand for batteries (Fig. 9) is forecast to increase dramatically in the future (Le Gleuher, 2017).

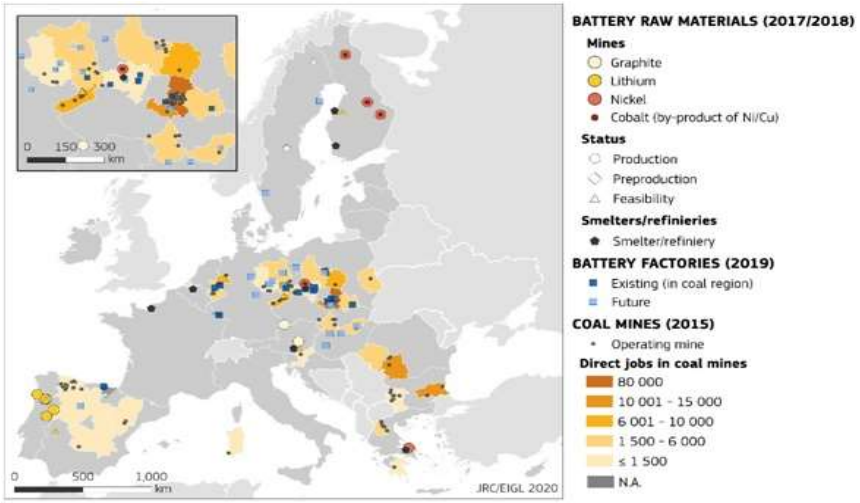

Figure 9. *Battery raw material mines, battery factories and coal mines (Source: European Commission report on the 2020 criticality assessment; https://eur-lex.europa.eu/legal-content/EN/TXT/?uri=CELEX:52020DC0474).*

Cobalt has been used for a long time as a pigment in glass and porcelain industry. Recently it was classified as one of the critical metals due to its unique applications in lithium ion batteries, in resistant superalloys, in green-energy systems and in magnets (Melfos et al., 2012). While there are established markets for Ni (stainless steel, alloys and plating) and Co (chemicals, super alloys, catalysts), a significant growth sector for both metals is in Li-ion batteries, as mentioned above. Growth in the Li-ion battery market is driven by the increased consumption of portable electronic devices (mobile phones, laptops, tablets), the electric vehicle (EV) market and growing applications for utility energy storage. Forecast annual demand growth for Ni sulphate for batteries is 22.5% compound annual growth rate to 2025 and 15.6% for Co. The lithium-ion battery market is primarily being driven by electric vehicles which are increasingly adopting cathode chemistries high in both Ni and Co because of their high energy density, long cycle life, safety and power output. These require high purity Ni and Co sulphates as precursor material for cathode production. Co and Ni are used in the majority of cathode chemistries available, with a growing shift towards Ni-Co-Mn (NCM) and Ni-Co-Al (NCA) chemistries over chemistries that do not use Ni or Co. Li-Co-oxide (LCO) chemistry remains the chemistry of choice for many applications in the portable consumer electronics market, given its high-energy density (Australian Technical Report, 2018).

As for REE, the demand for them has been increased in the last years exactly due to their applications in a wide range of consumer products such as automotive catalytic converters, photovoltaic systems, wind turbines, flat panel displays (cell phones, screen TVs, computers, portable DVDs), permanent magnets, hybrid and electric vehicles. They are also strategic raw materials with important defense uses in jet fighter engines, space-based satellites and communication systems (Melfos et al., 2012). Scandium is embedded in the very fabric of modern society and is critical for technology and industry, making it one of the most valuable elements with increasing industrial applications. End-uses range from biomedical research to electronic devices, lasers and ceramics but the demand is driven by energy issues (hybrid and electric cars, wind turbines). More specifically, Sc finds applications in Al-Sc superalloys, increasing tensile strength and improving weldability while maintaining light weight, an energy-saving factor in aerospace and automotive industries. In solid oxide fuel cells, the addition of Sc to the electrolyte improves conductivity and lowers the operating temperature, extending fuel cell life (Chasse et al., 2017). The addition of small (<1 wt.%) amounts of Sc to Al dramatically increases its weldability and its resistance to stress, corrosion and heat, while maintaining a light weight. Scandium is therefore mainly used as hardening additive to aluminium (Al) to form Al-Sc alloys, with current applications in aerospace industries and manufacturing of high-quality sports equipment. In addition, Sc finds promising application in the development of Solid Oxide Fuel Cells (SOFCs), wherein the replacement of Y by Sc improves conductivity and lowers the operating temperature, extending fuel cell life. Also, Sc is notably used in high temperature lights, lasers and ceramics manufacturing (Teitler et al., 2018).

Therefore, as Ni, Co and Mn are used in many applications including alloys manufacturing, electrode materials for lithium-ion batteries (LIBs), etc., and, hence, their recovery from primary and secondary resources is of great interest (Chagnes et al., 2017). However, although the European Union (EU) is highly dependent on critical (because of their economic value) and rare metals that are very important for a sustainable development, European industry is not able to cover its demands from native sources. Hence, it imports commodities from third countries (Fig. 10).

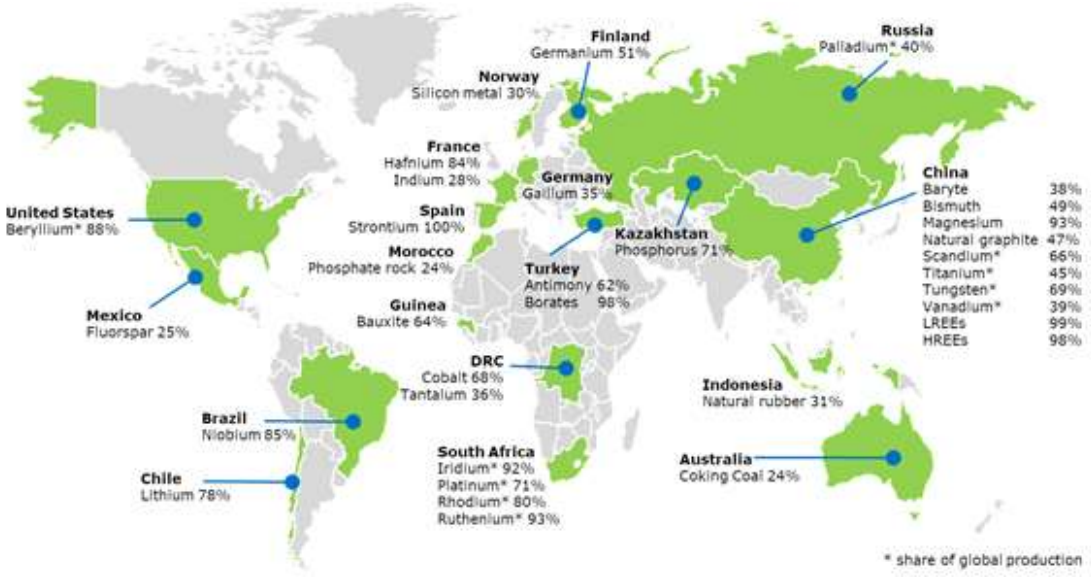

Figure 10. *Biggest supplier countries of CRMs to the EU (Source: European Commission report on the 2020 criticality assessment; https://eur-lex.europa.eu/legal-content/EN/TXT/?uri=CELEX:52020DC0474).*

1.2 Laterite deposits

1.2.1 Terminology

The term laterites is used for the product of in situ chemical disintegration of silicate rocks that takes place in hot and humid climates under the effect mainly of the penetrating water, thus resulting in reserves rich in Fe and aluminum oxides. The term *laterite* is derived from the latin word 'later', meaning 'brick' (Unesco-IUGS, 1979) and was first used by the Englishman F.H. Buchanan in 1807 to describe the hardened clay with a high Fe content used in India for the manufacture of building materials (Marsh et al., 2011). At the International Conference on Lateritization Methods in Trivandrum, India in 1979, W. Schellmann proposed the following definition for laterites: *laterites are those products of intense aerial disintegration of rocks, whose Fe and aluminum contents are higher than the respective contents of kaolinitization products and which consist mainly of kaolinite, goethite, hematite, gypsum and quartz*. Since then, a large number of definitions have been given for laterite ores by various researchers, who have in common the fact that they refer to the geological conditions of formation as well as the mineralogical composition of the ore. One of them is the following (Zevgolis, 2000): *laterite is the product of the in situ chemical disintegration of silicate rocks, which takes place in hot and humid climates by the energy of penetrating water, resulting in reserves rich in Fe and aluminum oxides.*

1.2.2 Origin, genesis and classification of laterites

Based on the above, the term laterites is essentially used for the product of in situ chemical disintegration, which is called laterite chemical disintegration, of silicate rocks, which takes place in hot and humid climates under the effect mainly of penetrating water. The reactions that take place during laterite disintegration depend mainly on the pH of the environment, the redox potential and the ionic potential. The main factors that regulate the intensity of disintegration are the type of rock (the

presence of water-soluble Fe and Al salts is necessary), temperature and vegetation (make water capable of dissolving the elements), rainfall, geomorphology (facilitation of the accumulation of solutions), etc.. These conditions, in combination with the changes of pH and potential, contribute to the removal of water-soluble (at normal pH values) elements such as potassium, sodium, magnesium, etc., and to the presence of insoluble Fe and Al, thereby creating in situ an enrichment of Fe and Al oxides (laterites), rich mainly in Fe (laterite Fe ore) or in Al (bauxites) (Golightly, 1979). Commonly, laterite development involves disintegration and dissolution of the primary minerals of the peridotite, which leads to (i) leaching of soluble elements (Si, Mg) and (ii) in situ neoformation of mineral phases (mainly oxy-hydroxides) that host the insoluble elements (Fe, Al, and Cr) (Quesnel et al., 2017). Hence, Ni-laterite ore can be physically and chemically divided into two main categories: saprolitic and limonitic. Saprolitic ores are mainly composed of silicates and hydrous silicates, whereas limonitic ores are basically composed of oxides and hydroxides. Nickel, in laterite ore, appears mainly in the crystalline lattice of Fe oxides/hydroxides and silicates, replacing Fe and Mn, respectively (Ribeiro et al., 2020). Nickel, with an intermediate behavior, is preferably concentrated at the base of the lateritic profile, in the saprolite horizon, where it reaches economic concentrations (> 1 wt.%) (Quesnel et al., 2017).

Namely, the lateritization of the parent rocks involves the dissolution of unstable minerals, mainly olivine, and their replacement by others. Therefore the primary minerals are decomposed, some of their components are washed away and secondary minerals are formed from the residue. During lateritization, ions are replaced, while the most important replacement is the replacement of Mg by Ni between ground water and serpentine, chlorite, smectite (Nahon 1992). Nickel, which mainly replaces Mn and Fe in the aluminosilicate lattice (Annersten et al.1982; Nord et al. 1982) and Fe in the oxide, sulfide and alloy lattice (Filipidis 1997 a and b) of ultramafic rocks, has a sufficiently high solubility. Thus in the processes of lateritization it is transported to deeper horizons and precipitated in alkaline areas with pH > 7. The preferential movement of Ni^{2+} to deeper horizons of the laterite soils seems to be a common phenomenon, since most laterite deposits show Ni enrichment in their lower part (Filipidis 1997a and b). Strongly intense disintegration removes from the protolith the most soluble components (Mg, Ca, and Si) and causes the concentration of the least soluble (Fe, Ni, Mn, Co, Zn, Y, Cr, Al, Ti, Zr and Cu).

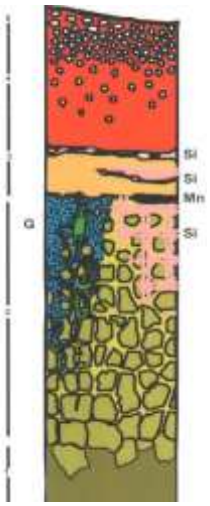

Figure 11. *Schematic profile of laterite weathering in Balkan: 1. Parent rock; 2. Saprolite-clay zone; 3.Goethite zone; 4-5. Pisolithic ferrous cover; G: garnierite; Si: silcrete; Mn: Mn oxides (Skarpelis, 2000).*

A typical laterite profile (Fig. 11) generally consists either of unaltered or serpentinized peridotites at the bottom, overlain by a saprolite horizon. The saprolite horizon contains relicts of the parent rocks with secondary minerals such as serpentine, goethite, and hydrous Mg-Ni-phyllosilicates. In many deposits, the transition between the saprolite and the oxide-dominated zone of the laterite (hereafter 'limonite') is marked by a smectite-rich boundary. In this context, the limonite horizon is developed at the top of the profile and consists of goethite, hematite, maghemite, gibbsite, and Mn-oxy-hydroxides. The topmost section of the horizon is the Fe-cap (i.e., ferricrete) and it is commonly enriched with hematite and goethite. Lateritic regoliths generally consist of many or all of the following horizons (from the base): saprock, saprolite, plasmic zone, mottled zone, ferruginous and/or aluminous duricrust or gravels, and soil (Eggleton 2001); saprolite may comprise over 80% of the total thickness of the profile. They have developed under humid tropical to sub-tropical conditions, under present and/or past climatic regimes. A lateritic regolith developed on ultramafic rocks (Fig. 12) may contain economically significant concentrations of Ni in one or more horizons, and it is these units that define it commercially as a 'Ni-laterite' (Butt et al., 2013).

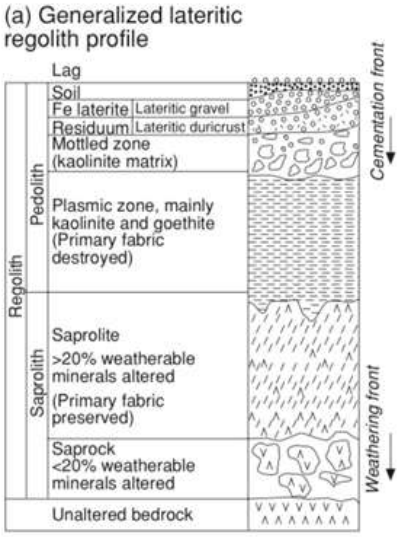

(b) Element mobility in typical lateritic profiles

Host minerals	Leached	Partly retained (in secondary minerals)
Released in the mottled and ferruginous zones		
Aluminosilicates (muscovite, kaolinite) iron oxides; gold	K, Rb, Cs Trace elements; Au	Si, Al (kaolinite)
Released in upper saprolite		
Aluminosilicates (muscovite)	Cs, K, Rb	Si, Al (kaolinite)
Ferromagnesians (chlorite, talc, amphibole)	Mg, Li	Fe, Ni, Co, Cr, Ga, Mn, Ti, V (Fe and Mn oxides)
Smectite clays	Ca, Mg, Na	Si, Al (kaolinite)
Released in the lower saprolite		
Aluminosilicates	Ca, Cs, K, Na, Rb	Si, Al (kaolinite); Ba (barite)
Ferromagnesians (pyroxene, olivine amphiboles, chlorite, biotite)	Ca, Mg	Fe, Ni, Co, Cr, Ga, Mn, Ti, V (Fe and Mn oxides)
Released at weathering front		
Sulfides	As, Au, Cd, Co, Cu, Mo, Ni, Zn, S	As, Cu, Ni, Pb, Sb, Zn, (Fe oxides; sulfates, arsenates, carbonates, alunite-jarosite)
Carbonates	Ca, Mg, Fe, Mn, Sr	

Figure 12. *(a) A generalized lateritic regolith profile showing the different horizons and the terminology used in their description; (b) Generalized pattern of element mobility in lateritic regoliths (Robb, 2005).*

The main minerals generally found in laterites are hematite (Fe_2O_3), goethite (FeOOH), while quartz and aluminosilicate minerals (chlorite, kaolinite, alloisite, nontronite) are often found (Goudie et al., 1983). The intensity of chemical disintegration is mainly affected by the amount of rainfall, the type of rock, the vegetation, the temperature, the topographic relief of the area, by the low aquifer and its fluctuations and in general by the presence of free O_2, CO_2 and humic acids in the water. The order of stability (Fig. 13) of the silicate minerals indicates that the minerals, which crystallize in the early stages of magma crystallization at high temperatures, are less resistant, in contrast to those that crystallize in the later stages at lower temperatures (Elias 2002).

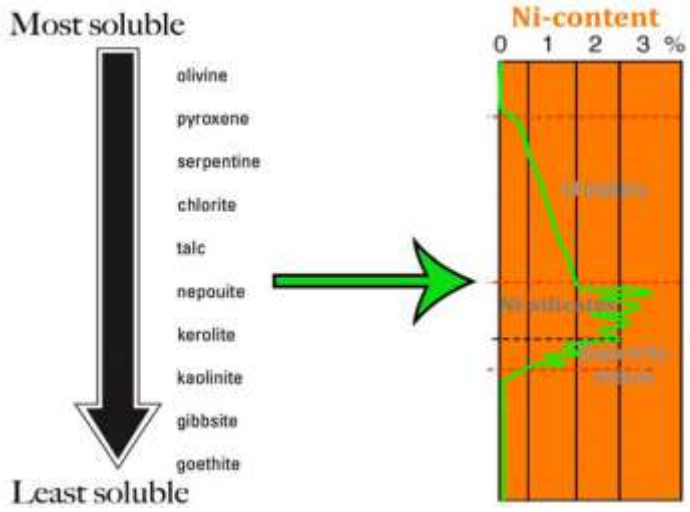

Figure 13. *Mineral stability for idealized mineral assemblage found in the progressive weathering of Ni-laterite deposits and Ni per-descensum concentration model currently proposed by most mining geologists (e.g., Pelletier, 2003) (Myagkiy, 2018).*

1.2.3. Location and environment of laterites

Laterites are formed in tropical or subtropical climates with alternations of dry and humid periods. In humid climates (tropical or subtropical) the destruction of the parent rock is observed, while the alternations of dry and humid periods cause the deposition of materials, which remained as products of the rock dissolution. Dissolved and decomposed materials are transported with the help of water, ending up in oceans. The residue is constantly enriched in insoluble materials. Therefore, continuous enrichment takes place in situ in minerals of high specific weight, resulting in the creation of autochtonous deposits. The intensity of lateritization depends on the nature of the original rock and environmental conditions. In case this type of metallogeny is interrupted by any land subsidence, either the autochtonous deposits will be covered by newer sediments, which will be the roof of the autochtonous laterite deposits, or they will be transported and deposited again, away from the parent rock, and then will be covered by newer sediments, resulting in the creation of heterochthonousdeposits. The differentiation in disintegration that takes place in temperate climates from that of tropical-subtropical climates is large. In temperate climates the alteration of rocks differs in relation to the tropical and subtropical regions since it is not so intense and no total removal of silicon takes place, while in tropical and subtropical climates the degree of rock disintegration is greater and, therefore, the decomposition of silicate ores is more complete. In the tropical regions, the maximum development of disintegration is due to the coexistence of conditions of high temperatures, intense vegetation and heavy rainfall. The concentration of laterite covers on flat surfaces with a relatively mild relief (long periods of tectonic calmness) suggests that low relief is a prerequisite for the formation of residual concentrations. Mild relief results in slow filtration of soil water and significantly reduces the erosion of the disintegration products (Nahon 1992).

1.2.4 Nickel-Cobalt laterites

Nickel-Cobalt laterites are intensely weathered regoliths with one or more horizons and they are defined by economic, rather than geological, criteria, namely that the Ni-Co grades and tonnages are sufficient for them to be mined, processed and

rehabilitated with financial (and social) benefit (Butt et al., 2013). Nickel-Cobalt laterites are sedimentary/surficial (supergene) deposits of Ni±Co (Robb, 2005). In fact, these laterites are a supergene enrichment of Ni and Co derived from the prolonged intense pervasive chemical and mechanical weathering at tropical latitudes of mafic or ultramafic lithologies containing Ni-bearing mafic minerals, i.e., olivine and pyroxenes (Golightly, 1981; Freyssinet et al., 2005; Robb, 2005; Butt et al., 2013), as the formation of secondary concentrations of Ni±Co significant enough for an economic resource requires a protolith lithology that is primarily enriched in Ni (Marsh et al., 2010). This process leaches the mobile constituents of the peridotite (Mg, and Si), whereas the immobile components (Fe, Al, Cr, Ni, Mn, Cu, and Co) are retained and concentrated in the laterite (Eliopoulos et al., 2012). The laterite profile develops from the progressive weathering of ultramafic parent rocks, which occur in accretionary terranes as Alpine-type, as well as large thrust sheets, of obducted ophiolites and in cratonic areas as komatiites. These laterites occur within 20 degrees of the equator, with a few exceptions (Marsh et al., 2010). It is known that the combination of several factors (e.g., soil drainage, chemistry of the system, rate of weathering, parental material etc.) can control significantly the architecture of the laterite profile, as well as the nature and the relative abundance of the different ore types potentially occurring in a single deposit (Putzolu, 2020). Based on the dominant minerals hosting Ni, and generally on the major Ni ore assemblage, Ni-Co laterite deposits are typically classified into the following three main ore types: (i) oxide laterite deposits dominated (also called 'limonitic ores') by Fe-Mn-oxy-hydroxides, (ii) hydrous Mg silicate deposits that contain mostly garnierite-like mineralization and (iii) clay silicate deposits that consist mainly of Ni-rich smectites (Elias, 2002). In fact, the two subtypes (Fig. 14) recognized above, i.e., clay-type (smectite-type) and hydrous Mg silicate-type (garnierite-type), can be recognized among Ni-phyllosilicates endowed laterites (Putzolu et al., 2020).

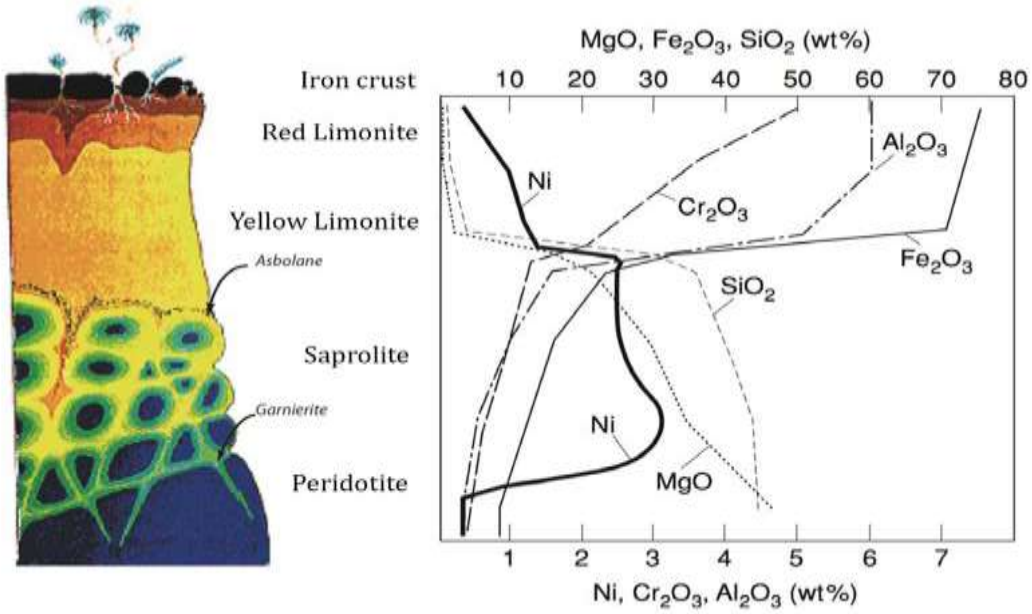

Figure 14. *Subtypes of Ni-laterites developed on serpentinized ultramafic protolith with indicated main Ni ore zones and grades (Aiglsperger, 2016).*

Many world-class laterites (Fig. 15) (e.g., Murrin Murrin, Western Australia; Niquelandia, Brazil) are classic clay ore Ni-Co laterite deposits belonging to the smectite-type, in which the dominant ore minerals are smectites (Putzolu et al., 2020),

whereas, the Ni-Co laterite deposits in New Caledonia, the Dominican Republic, Indonesia, and Guatemala, as well as minor occurrences in California and North Carolina, are also hydrous Mg-silicate subtype deposits (Marsh et al., 2010). This subdivision has important implications for processing and whether a deposit can provide economically viable ore. Most Ni-laterite profiles have two ore types, an oxide component and either a hydrous silicate or a clay silicate component (Brand et al. 1998; Berger et al. 2011). Because of the different processing requirements for the different mineral hosts, most mines tend to exploit only one style of mineralization (Butt et al., 2013).

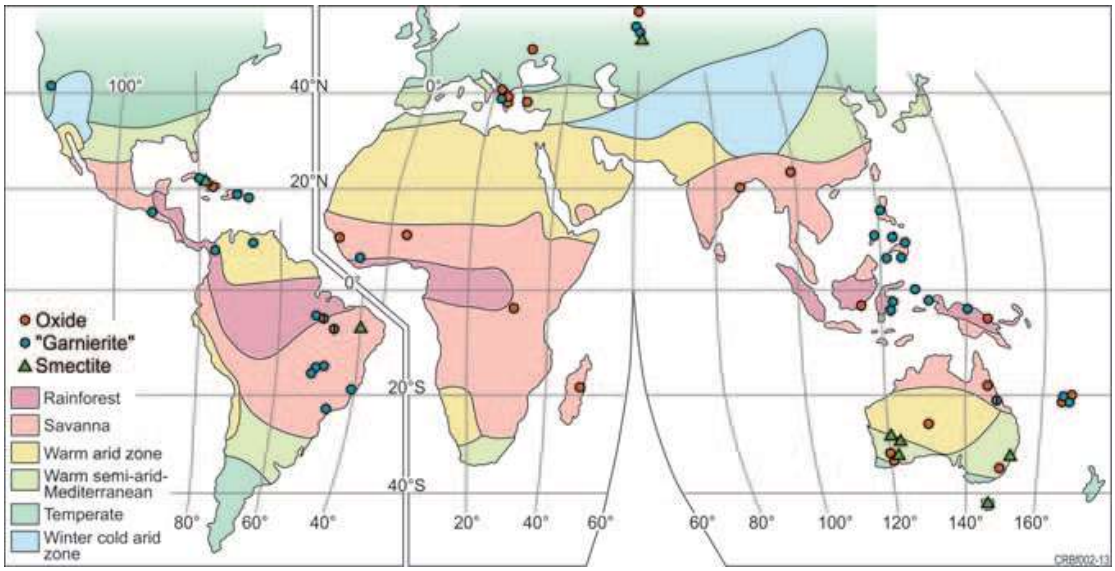

Figure 15. *Worldwide distribution of different types of Ni-laterite (Butt et al., 2013).*

Butt et al. (2013) mention that the richest deposits (> 3 wt.% Ni) formed where oxide-rich regoliths were uplifted and Ni leached downwards to concentrate in neo-formed silicates in the saprolite. Hence, oxide-type ores are characterized by the economic Ni and Co concentrations within the ferruginous saprolite (hereafter oxide zone), which is enriched in Fe- and Mn-(oxyhydr)oxides (Putzolu et al., 2020). In general, these deposits are formed in stable cratons, under condition of high water table and absence of significant tectonics. On the contrary, the genesis of clays during tropical weathering is widely recognized as crucial component during the ore-forming processes related with the formation of Ni-phyllosilicate type sensu lato laterites, where the highest Ni enrichments are observed in the saprolite sections (Putzolu et al., 2020). The Cawse deposit in Western Australia is an oxide ore Ni-Co laterite deposit, as are many of the deposits in Cuba (Marsh et al., 2010). All three mineralogical types of ore may be present in a single Ni-Co laterite deposit. The metalliferous laterite deposits are mineralogically complex, discontinuous, and commonly have Ni enrichment in more than one of the weathering profile (Fig. 16) zones (Lelong et al., 1976). Some deposits are subsequently mechanically weathered, redeposited, reconcentrated, and possibly covered by new sediment (Golightly, 1981).

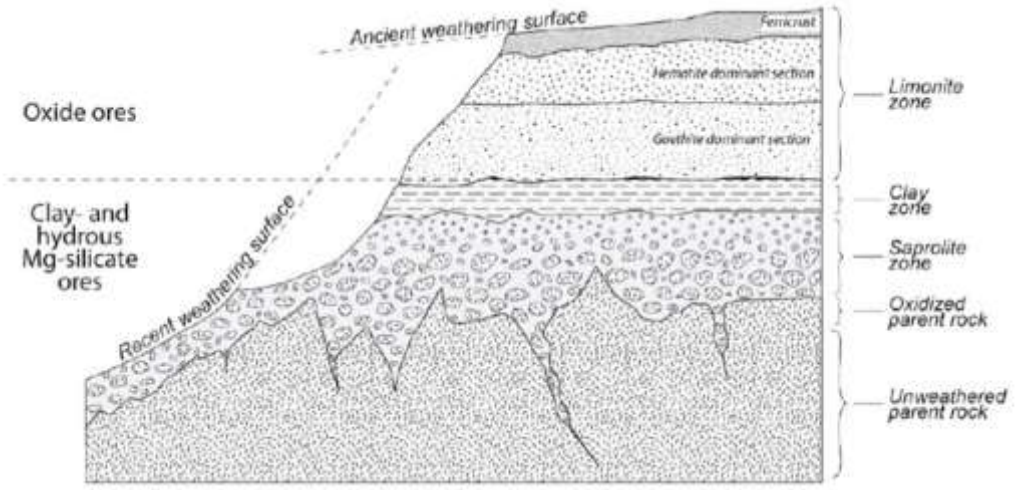

Figure 16. *Idealized cross section through a Ni-laterite weathered profile illustrating all the possible layers. Natural profiles are more complex and contain diverse sequences of any or all of the layers shown. Profiles can be a few to tens of meters thick (Marsh et al., 2011).*

Consequently, generally in Ni-Co laterites, dissolution and leaching of primary Mg-rich silicates leads to the residual enrichment of Fe as ferric oxides/oxyhydroxides in the upper horizons. Downward remobilization and trapping of Ni and Co lead to their local enrichment to economic concentrations, with maximum grades reached in the saprock/saprolite and in the transition horizons, respectively (Teitler et al., 2018). The richest deposits (> 3 wt.% Ni) formed where oxide-rich regoliths were uplifted and Ni leached downwards to concentrate in neo-formed silicates in the saprolite (Butt et al., 2013). In contrast, maximum Sc enrichment occurs in the yellow limonite horizon, where Sc-bearing goethite contains about ten times the Sc content of the parent rock. In the last decade, Sc-rich occurrences with economically attractive grades and tonnages have been identified in some oxide-rich laterites developed after mafic and ultramafic rocks. There, Sc enrichment is interpreted to be largely residual, resulting from the intense leaching of mobile cations during lateritization of the parent rock, while Sc remains trapped and concentrated in neo-formed goethite (Teitler et al., 2018). It is proposed that three main factors control the distribution and intensity of Sc enrichment in laterites derived from mafic and ultramafic rocks: 1) the initial Sc content of the parent rock; 2) the development of goethite-dominated, yellow limonite after long-lived tropical weathering; 3) the local remobilization of Sc from the uppermost horizons through dissolution/recrystallization of goethite and partial replacement of goethite by hematite, thus leading to downward Sc concentration in the yellow limonite. Consequently, harzburgite- and lherzolite-derived yellow limonites yield maximum Sc concentrations up to 100 ppm, together with moderate Ni and Co concentrations (Teitler et al., 2018). There, Sc is potentially a valuable by-product that could be successfully co-extracted along with Ni and Co through hydrometallurgical processing (Teitler et al., 2018). In New Caledonia, recent studies revealed a progressive enrichment through the weathering profile, with Sc concentrations increasing from ~8 ppm in the bedrock (peridotite to serpentinite rocks) to almost 100 ppm in the limonite horizon such enrichment being potentially compatible with mining operation (Munoz et al., 2017).

1.3 Laterites of Europe and Greece

1.3.1. Potential for Ni, Co, REE and Sc

The Ni-Co laterites can occur surficially as in situ deposits (Fig. 17), buried as karst (Albania and Greece), or as linear/fault-hosted deposits (Urals) (Golightly, 1981). Significant Ni-Co-(Sc) laterite resources are found through a geographic area stretching from Serbia in the west through Turkey and beyond into Iran (Herrington, 2017). Ni production is now mainly restricted to Greece, yet the region still accounts for around 1% of world production. However, there is little or no recovery of Co and Sc. Many undeveloped deposits are recorded in the region, but for oxide-dominated mineralization, current metallurgical techniques are largely uneconomic. This disparity stems from the expense and complexity of the metallurgy involved in extracting Ni from the mineralogically diverse and erratic Ni concentrations through a laterite profile (Marsh et al., 2010). Technology changes have the potential to unlock large low-grade redeposited lateritic Ni-Co-Fe deposits like Mokra Gora in Serbia, which alone has an untapped resource of more than 1 Gt of ore with an average grade of 0.7% Ni and 0.05% Co (Herrington, 2017).

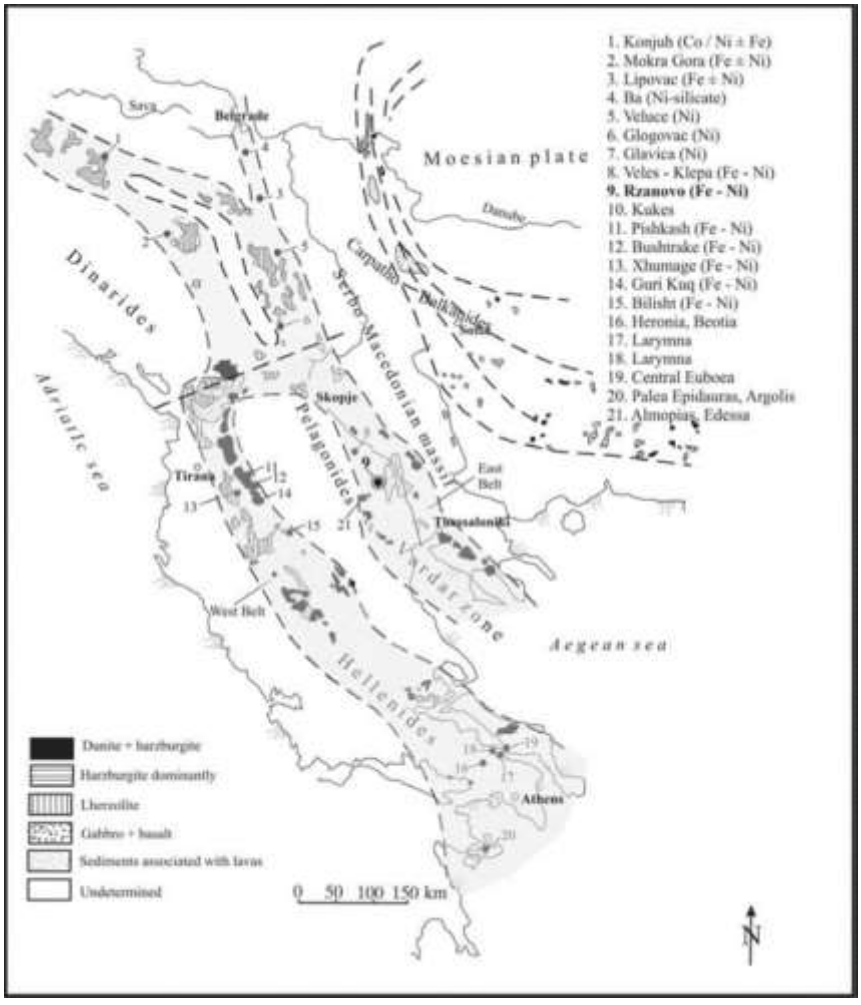

Figure 17. *Location of the principal deposits and occurrences of Ni silicate and nickeliferous Fe ore mineralization in the west and east ophiolite belts of the SE Europe (Modified from Boev et al., 1996).*

Three different processes are used to extract Ni and Co from the respective enriched layers. The processes include either the carbon process or high-pressure acid leaching (HPAL) for the oxide subtype ore, HPAL for clay subtype ore, and a smelting process for hydrous Mg-silicate subtype ore (Elias, 2002). Because of the current metallurgical intricacies encountered while dealing with heterogeneous Ni-Co laterite profiles, a number of recent studies have focused on ore delineation and mineralogical identification, including the application of diffuse reflectance spectroscopy to distinguish ore mineralogy (Wells et al., 2011). A new ore-processing technique, DNi, was developed by Direct Ni to treat the entire laterite profile. This innovation is a hydrometallurgical process capable of extracting 95 percent of the Ni and 85 percent of the Co in laterites (Direct Ni, 2010). With the potential success of the DNi hydrometal-lurgical process or any other low-temperature and low-pressure Ni-Co laterite processing, these supergene deposits will be a much larger contributor to the future production of Ni and Co. Modern techniques of ore delineation and mineralogical identification are being developed to aid in streamlining the Ni-Co laterite mining process (Fig. 18), and low-temperature and low-pressure ore processing techniques are being tested that will treat the entire weathered profile. There is evidence that the production of Ni and Co from laterites is more energy intensive than that of sulfide ores, reflecting the environmental impact of producing a Ni-Co laterite deposit. Tailings may include high levels of magnesium, sulfate, and Mn and have the potential to be physically unstable (Marsh et al., 2011).

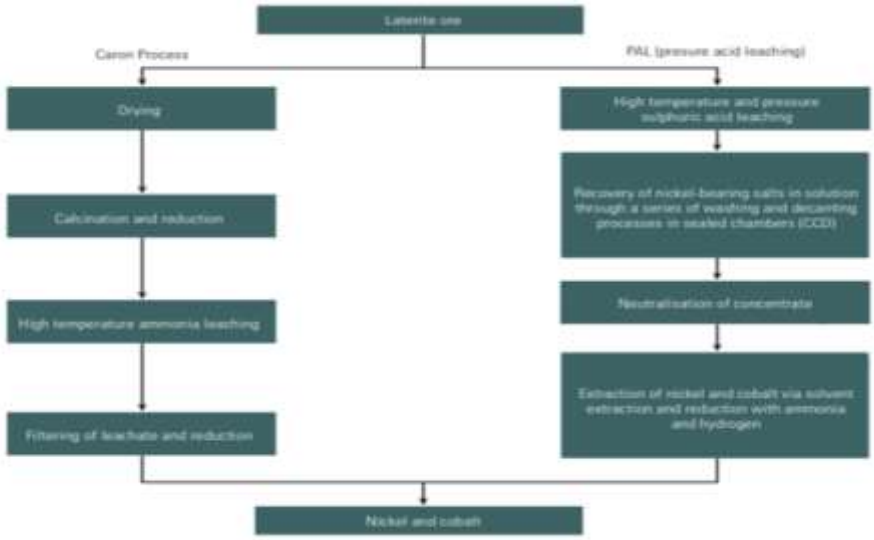

Figure 18. *A flow sheet summarising the processing of lateritic ores (Source: British Geological Survey, 2008).*

Ni-Co laterite ores (Fig. 19) account for over 60% of global Ni supply and Ni is concentrated to over 1.0 wt.% (Butt et al., 2013). Major Ni-laterite deposits developed over peridotite are widely distributed in humid tropical regions, including New Caledonia, which constitutes about 60-70% of the world's Ni resource (Fan et al., 2011, Butt et al., 2013), Indonesia, the Philippines, Brazil, Colombia, Cuba, central Africa, and the Dominican Republic. Despite this, Ni-laterites are also found at higher latitudes (e.g., Australia, Greece, Urals, etc.), where the current climatic regime does not match

with the optimal environmental conditions enhancing lateritization, and thus, they represent fossil paleo-weathering profiles (Tupaz et al., 2020).

More specifically, the New Caledonia ophiolite is of major economic importance since it hosts 10% of the world Ni reserves (McRae, 2018). The country is the third main producer of Ni and is also one of the main producers of Co (~3% of the world production and reserves). Moreover, China has become the largest Ni consumer in the world due to soaring production of stainless steel. More Ni-laterite ores are imported into China because of the depletion of domestic Ni sulfide resources. Consequently, it is of great importance to the Chinese economy to effectively utilize low grade Ni-laterite ore (De-qing et al., 2012). Thus, the expansion of the Ni production strongly depends on the exploitation of these ore deposits. However, the mineralogical complexity of laterite ores is still a challenge for such at ask. Each type of ore may require a different processing route to obtain acceptable recoveries for Ni and Co (Ribeiro et al., 2020). As for Co, the second most important class of deposits consists of mid-Tertiary to Recent laterites, which typically contain 0.1-0.15% Co. Laterites are produced by deep tropical weathering of bedrock, during which certain elements are removed and others enriched by supergene processes. Where the rocks are ultramafic in character, the laterites can show significant enrichments in Co and Ni relative to bedrock. Such laterites may be up to 20 m thick and consist largely of the hydrated Fe oxide, limonite. Typically, they overlie a zone of altered bedrock (saprolite zone), which is the main repository of Ni. The Co is obtained as a byproduct of Ni mining (Smith, 2001).

REE are particularly targeted since China, which produces about 98% of the REE worldwide and is the main EU supplier, has announced a restriction of their exportation to secure their own domestic use. In addition, transition metals like Sc and V, which were not on the 2014 list, are now considered as critical due to an increasing demand in the market (Ulrich et al., 2019). Over 250 lateritic deposits of REE are currently known and many have been important sources of REE. In southeastern China, lateritic REE deposits, known as ion-adsorption type deposits, have been the world's largest source of HREE. The lateritized upper parts of carbonatite intrusions are being investigated for REE in south America, Africa, Asia and Australia, with the Mt. Weld deposit in Australia being brought into production in late 2012 (Cocker, 2012).

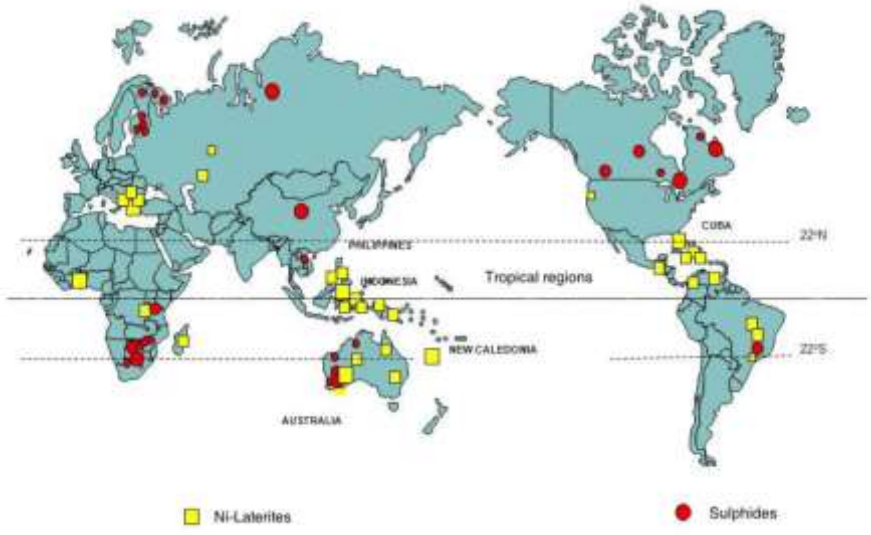

Figure 19. *Global distribution of Ni-Co resources. Laterite-Ni ore deposits are presented in Cuba, New Caledonia, Indonesia, Philippines, Burma, Vietnam, Brazil and Ni sulphide ore deposits in Canada, Russia, Australia, China, South Africa, etc. (Butt et al., 2013).*

Scandium production is limited (~15 t/yr, US Geological Survey, 2018) and it is mainly produced as a by-product of other ore deposits, owing to the rare discovery of terrestrial Sc minerals. As a consequence, growing demands for Sc, essential for several modern industrial applications, have created a strong need to develop alternative Sc resources. It has been recently reported that Sc can be greatly enriched in laterite deposits/lateritic Ni ores developed over ultramafic and mafic rocks, where Sc concentrations up to 100 ppm, showing that the Sc-rich laterite is a potential Sc (by-product) resource (Qin et al., 2020). In such context, significant Sc concentrations (~100 ppm) were recently reported in several Ni-Co lateritic oxide ores developed after mafic-ultramafic rocks. This contribution examines the distribution of Sc in Ni-Co laterites from New Caledonia, the sixth largest Ni producer worldwide (Teitler et al., 2018). Future supply is expected to rely on unusually high-grade (up to 1000 ppm) lateritic Sc ores discovered in eastern Australia. Recently, lateritic deposits with Sc concentrations high enough to mine as a primary product have been reported in eastern Australia. Among these, the Syerston-Flemington deposit contains about 1350 t of Sc at an average concentration of 434 ppm Sc, providing a century-long resource at the present levels of world consumption (Chasse et al., 2017).

Greece is one of the EU countries with the most potential for supplying these strategic metallic raw materials in the future, since it hosts a large number of ore deposits, as the country is the leading producer of Ni and Al in the EU from laterites of central and northern Greece. These deposits also contain significant amounts of Co or REE, which should be considered in the future plans of the processing industries. In fact, Greece is the major Ni supplier in EU and produces 2%-3% of the world total Ni (Melfos et al., 2012). The Fe-Ni-laterite deposits in Greece are a major source of Ni. Greece's Fe-Ni ore resources are currently estimated to be in the range of 200 Mt at 0.9-1.4% Ni (Albandakis, 1980; Eliopoulos and Economou-Eliopoulos, 2000; Valeton et al., 1987). The main mining operations of Ni are based at Agios Ioannis-Nissi (Lokris area), Psachna (Evia), and Kastoria (northern Greece) laterite deposits and the metallurgical facility is located at Larymna. Finally, Ni is recovered by pyrometallurgical methods. These Fe-Ni-laterites, which also contain Co, are mainly allochthonous and are associated with Mesozoic ophiolites. They are intercalated in Mesozoic limestones and show multistage transportation and re-deposition, responsible for a post-sedimentary redistribution of metals, resulting in Mn, Co, Ni-rich zones. Chemical composition of different laterite occurrences in Greece shows that Co is mainly concentrated in the Fe-Ni-rich zones, demonstrating elevated contents which reach 0.10% in Palaiochori, Grevena, 0.14% in Vermio, 0.16% in Kastoria and 0.22% in Lokris. Cobalt in these deposits is concentrated mainly in the mineral ‘asbolane’. The metallurgical process of the Greek laterites in Larymna by LARCO GMMSA, which produces Fe-Ni alloy, does not allow any Co recovering, which can be separated by hydrometallurgical treatment. Consequently, Greece remains a potential region to supply the EU with significant amounts of Co in the future. It should be also mentioned here that the non-economic sulfide ores hosted in the ophiolite complexes in Greece, including Cyprus-type and Fe-Cu-Ni-Co type, at Pindos and Othrys contain up to 2300 ppm Co. Furthermore, the Serbomacedonian and Rhodope metallogenic districts in Greece are among the richest ore provinces in Europe, and can be an exploration target in the near future, especially for critical and rare metals. The epithermal- and porphyry-type mineralizations, and the reduced intrusion-related systems of Northeastern Greece could produce Sb, Te, Mo, Re, Ga, In and PGE as by-products, along with base metals, Au and Ag, if the mining and extractive activities will start. Additionally, as already

mentioned, laterites and bauxites of central and northern Greece which are mined for Ni and Al, respectively, contain significant amounts of Co or REE (Melfos et al., 2012). These secondary types, in which the REE have been further concentrated from a primary enrichment through sedimentary processes or weathering, are economically the most important types in Greece (Eliopoulos et al., 2014). Therefore, the processing industries should focus on the probability for a future exploitation. Finally, the chromitites of northwestern Greece contain significant concentrations of PGE, whereas the coastal sediments between Chalkidiki and Kavala are characterized by REE geochemical anomalies which may be related with the Kavala and Pangeon Mt reduced intrusion-related system, although this has to be clarified. Therefore, the mineral wealth of Greece can contribute significantly to a sustainable and a competitive economy of Europe (Melfos et al., 2012).

1.3.2 Geology and classification

The Fe-Ni-laterite deposits in the Balkan Peninsula are mainly found in the Mirdita-Sub-Pelagonian and Pelagonian geotectonic zones (Fig. 20) and are related to ophiolites of Upper Jurassic to Lower Cretaceous age. They extend from the Bitinca ophiolites in Albania, Kastoria, Palaiochori of Grevena to the west of the Pelagonian massif, and Lokris, central Greece (Laskou et al., 2005). These deposits have been affected by intense tectonism, which has created overthrusting, foliation, folding, and faulting. This has resulted in the transportation of the laterite bodies, disrupting their continuity and in some cases mixing them with underlying rocks. The multistage deposition of the Fe-Ni ores, the redistribution of ore metals, the intense tectonism and the metamorphism, which have affected all the Ni-laterite deposits of Greece, have almost totally changed the initial mineralogical and chemical composition of the ores (Albandakis, 1980; Valeton et al., 1987; Eliopoulos and Economou-Eliopoulos, 2000). The ophiolite masses, which appear in Greece in the form of tectonic covers, are divided into two zones, the inner ophiolite strip of Axios and the outer strip of Pindos-Othrios-Argolida (Mountrakis et al. 1983). Nickel metal-bearing in Greece is associated with the zones of Almopia, Pelagonian, Sub-Pelagonian and the Mesohellenic Trough, which is geologically located between the Sub-Pelagonian-Pindos. The Mesohellenic Trough crosses Greece from the Greek-Albanian border to the Thessalian plain and is covered by sediments of the Upper Eocene-Middle Miocene, which in some places have ophiolites as background. The deposits of the Sub-Pelagonian zone, which exist in the area of Lokris, cover a wide range of different forms of metal-bearing and are representative for almost all the different types of deposits.

Laterite in situ primary deposits are found in Tsouka, Loutsi and Akraifnio. These deposits consist of two horizons, the saprolitic and the limonitic, with the exception of the deposit of Akraifnio, from which the typical saprolitic zone is absent. Nickel is associated with both horizons, but in the deposits that have the saprolitic zone, the contents are particularly high. The metal-bearing bodies are covered by limestones of the Upper Cretaceous. In Tsouka, a layer of conglomerates is found between the metal-bearing and the limestones with chert cobblestones that alternate with small thickness horizons of compact ore. The Fe-Ni-laterite deposits in Greece were formed during the Upper Jurassic, Lower Cretaceous emersion from the disintegration of ultramafic rocks mainly in two geological periods. In the first, which took place in the Cretaceous, the deposits of Lokris and central Evia were formed, as well as the metamorphosed laterites of Skyros and of Pella and Imathia prefectures, while in the second, which took place

in the Tertiary, the deposits of Kastoria and other smaller occurrences in western Macedonia.

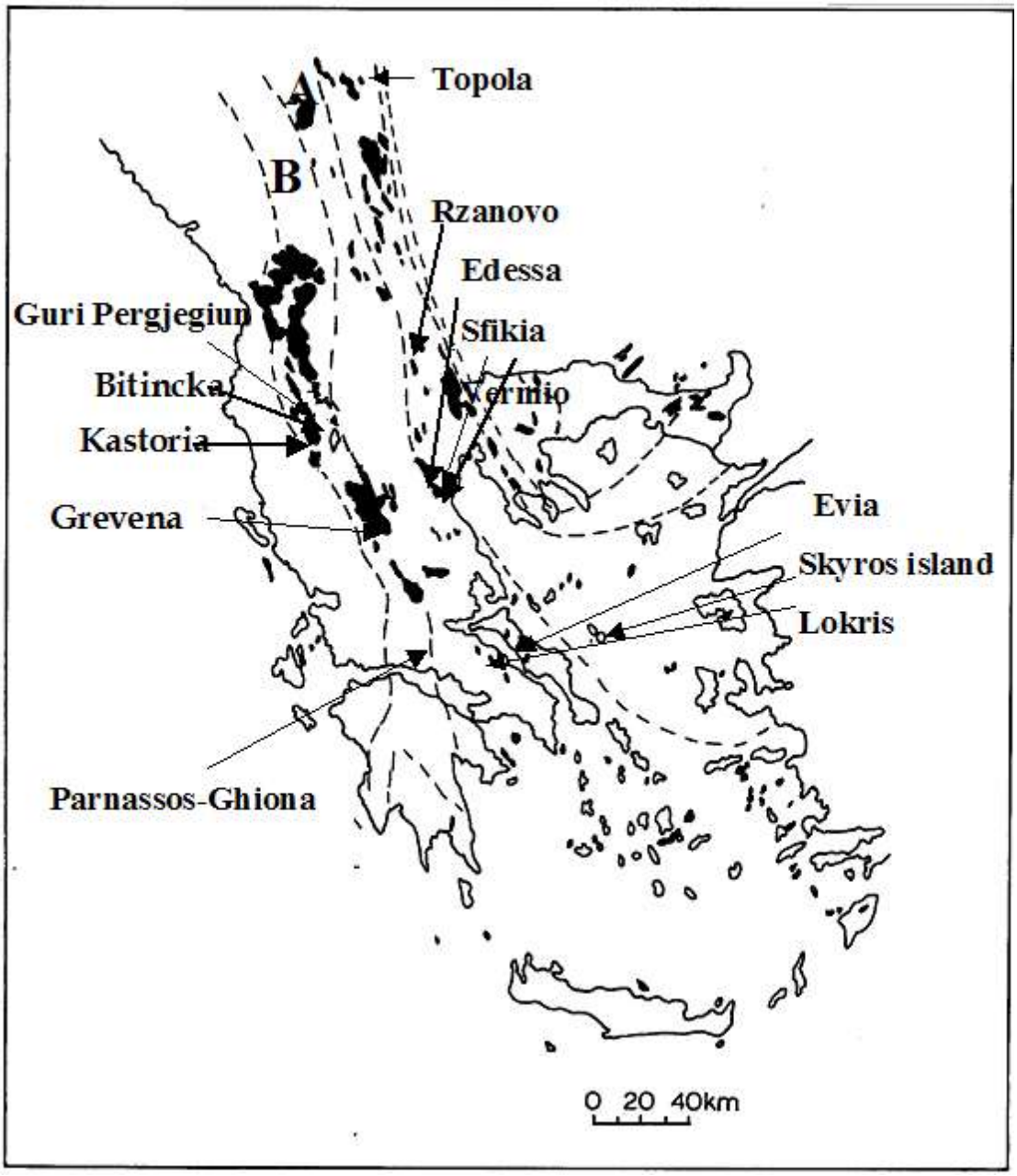

Figure 20. *Sketch map showing Pelagonian (A) and Sub-Pelagonian (B) geotectonic zones of Greece, the distribution of ophiolites and the location of the studied Fe-Ni-laterite deposits in the Balkan Peninsula (Eliopoulos et al., 2010).*

Karstic-type deposits of sedimentary origin are the most widespread, such as those of Agios Ioannis, Kopaida and part of Nissi. The metal-bearing develops unconformably in the form of a layer or lenses on the Paleokarstic surface of oolithic Jurassic carbonate rocks and is subject to Upper Cretaceous limestone layer conformity. The Kopais deposit is an exception, which extends below the lake sediments of the basin and is covered partly by Cretaceous limestones and partly by Quaternary marls

and clays. The development of metal-bearing in these deposits is characterized by the alternation of layers of Fe-Ni ore with a wide range of petrographic constituents. The predominant types of ore are pisolitic, compact, sandstone, mudstone and conglomerate horizons. A peculiarity in Viothia is the karstic mixed-type deposits, such as of the oros Ptoo and a part of the Nissi. There are two ore horizons in Ptoo, the lower one, which corresponds to the typical Fe-Ni ore and has high concentrations in Ni, and the upper one, which consists of Fe-rich clay material. The Nissi deposit is lenticular in shape consisting of mixed lenses and pure Fe-Ni ores. The eastern lens of the deposit is characterized by the presence of Fe-Ni ore in its lower part and bauxite in the upper. This peculiarity is found exclusively in the specific deposit, in which bauxite and Fe-Ni ore coexist. The coexistence of the two different ores is attributed to the supply by two different types of parent rocks. This opinion is based on the high content of titanium in the bauxite horizon, which does not support the origin of the bauxite material from ultramafic, but from mafic rocks. In contrast, the high content of Ni and Co in the Fe-Ni horizon is associated with the disintegration of ultramafic rocks. The parent rocks of mafic composition are estimated to belong to the melange (Fig. 21) of the wider region of Viothia-Evia (Apostolikas, 2010).

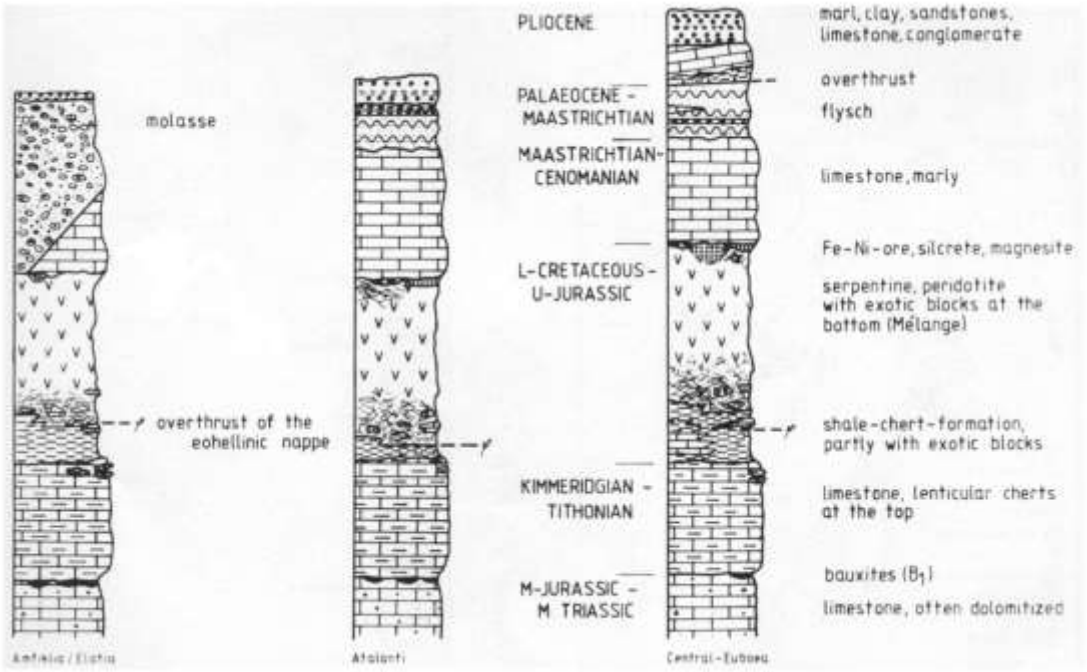

Figure 21. *Stratigraphic position of the serpentinite, peridotite, 'melange' at the bottom of the overthrusted nappe, and of the Ni-Fe ore (Valeton et al., 1983).*

1.3.3 Genesis and formation of the deposits

In Greece, more than 110 small and large occurrences of Fe-Ni ores have been described, which are characterized by the coexistence of Ni, Fe, Cr and Co. The concentration of these elements is directly related to the way ores are created and is due to the laterite disintegration of ophiolite rocks (Alevizos, 1997). The climatic conditions for the formation of laterite deposits existed in two periods, the first is pre-Cenomanian with which the majority of the deposits are associated and the second during the Eocene

with which the laterite disintegration crusts of the Mesohellenic Trough are associated (Apostolikas, 2010). The Fe-Ni-laterites in Greece area were formed mainly by the laterite disintegration of peridotite-type rocks (ophiolites in the zone of eastern Greece), the products of which were transported to the sea where they were deposited, thus giving allochthonous laterite deposits, during the period between Upper and Lower Cretaceous. In situ surface occurrences are found only in the area of Kastoria over serpentinized harzburgites (Boskos et al., 2000). Greek laterites are mainly found in the zone of eastern Greece (Evia and Lokris), as well as in Kastoria (Northern Greece). The Fe-Ni ores of central and northern Greece have been the subject of scientific study by many researchers in the past (Alevizos, 1997). Greek Ni deposits are the poorest in the world, compared to the deposits of New Caledonia and Russia with a Ni content of 2-3%, as well as the deposits of Dominican Republic and Oregon in USA with a Ni content of 1.6-1.7% (Kalles, 1993). The deposits, which are currently under exploitation, are of Agios Ioannis in Larymna, of Evia and Kastoria. Fe ore deposits have been identified in other parts of the country, such as Edessa, Skyros, Grevena, Attica (Parnitha and Dafni), Kozani, Mytilene and elsewhere. The country's total reserves of Ni ores are estimated at 200 million tons, of which 30 million tons are currently considered directly exploitable. Until Finland's recent accession to the European Union, these deposits were the only Ni deposits in the European Community (Alevizos 1997).

The Fe content of the ores is between 20 and 79% and their other components are mainly oxides of aluminum, silicon as well as 2-3% of Mn and Cr oxides (Kalles, 1993). Their average Ni content is approximately 1% (Albandakis, 1984). The main ‘carrier’ of Ni is Ni-chlorite, while minor Ni-ores have been identified, such as nepouite, talc, montmorillonite, takovite, etc. (Albandakis et al., 1980). Nickel is mainly in colloidal form within the Fe-ores. The ore consists mainly of Fe, Si, Al, Cr, Mn and Ni, and in addition to these elements small quantities of Mn, Ca, S, Co, As, etc. are also present. The most important of the other minerals found in these deposits are oxides of Fe (mainly hematite), quartz and chromite. Other occurrences of Fe-Ni deposits in Greece are found in Skyros, Vourino, Edessa, Parnitha, Dafni, etc. (Albandakis, 1974). The Fe-Ni ores of both the eastern Greece zone and the Almopia zone are characterized by most researchers as products of laterite disintegration of igneous rocks (ophiolites). These ores, but also the Fe-Ni deposits in general, are distinguished according to the way of their formation and their stratigraphic placement in two genetic categories: the autochtonous or primary or from disintegration and the heterochthonous or secondary or sedimentary. Augustithis (1962) has introduced a third category, the pseudo-autochtonous. Autochtonous are those ores, which did not undergo any movement from the parent rocks on which they were formed (ophiolites). Heterochthonous are those ores, which were transported from the parent rocks and deposited on sedimentary rocks (limestones). Pseudo-autochtonous are those ores, which were transported from the parent rocks at relatively short distances and have been deposited again on ophiolites, as a result of which they appear as autochtonous ores (Alevizos, 1997).

Most Fe-Ni-bearing ore deposits in Greece are considered to be secondary-sedimentary allochthonous, which have been transported at short or long distances and have been repositioned either on serpentinites or mafic ophiolites or on sedimentary formations (Economou, 1979). In other words, these are entirely mechanical sediments and there was no deposition of a fraction of the ore in the form of chemical sediment, as claimed until now (Skarpelis, 2000). In particular, Katsikatsos (1977) and others

accept the secondary origin for the Greek laterite deposits on ophiolites, Albandakis (1974) and Augustithis (1962) for the deposits of Evia, Albandakis (1974) for the deposits of Lokris, Michailidis et al. (1984) for the deposits of Edessa. A typical allochthonous deposit is the deposit of Agios Ioannis of Larymna, which is found among limestones (Albandakis, 1974; 1984). Residues of old disintegration crusts on ultramafic ophiolite rocks (Ni-laterite deposits with in situ characteristics) have been found in the area of Lokris [in the appearances of the areas of Kastraki, Loutsi, Pavlos (Viothia) and Tsouka (Fthiotida)], in Kastoria and in the area of Vermio (Prophitis Elias deposit) (Valeton et al., 1987; Eliopoulos et. al., 2000; Skarpelis 2006). The category of ores from disintegration includes the deposits of the areas of Karditsa-Kastraki, Pavlos, Loutsi and Tsouka. For this type of ores, the base of the deposit is disintegrated serpentinite of ashy or reddish shade. The ore is limonitic and compact at the bottom and pisolitic at the top. The non-parallel arrangement of the boundaries between the compact and pisolitic part of the deposit is associated with the formation of pisolites. In addition, the irregular arrangement of the above layers suggests that the pisolites come from diagenesis through the circulation of solutions and not from oolitic sedimentation. The category of sedimentary ores includes the deposits of Kokkino and Marmeiko areas. Sedimentary ore is the product of the ore due to disintegration, which was transported from the site of its formation and deposited again (redeposition) (Alevizos, 1997).

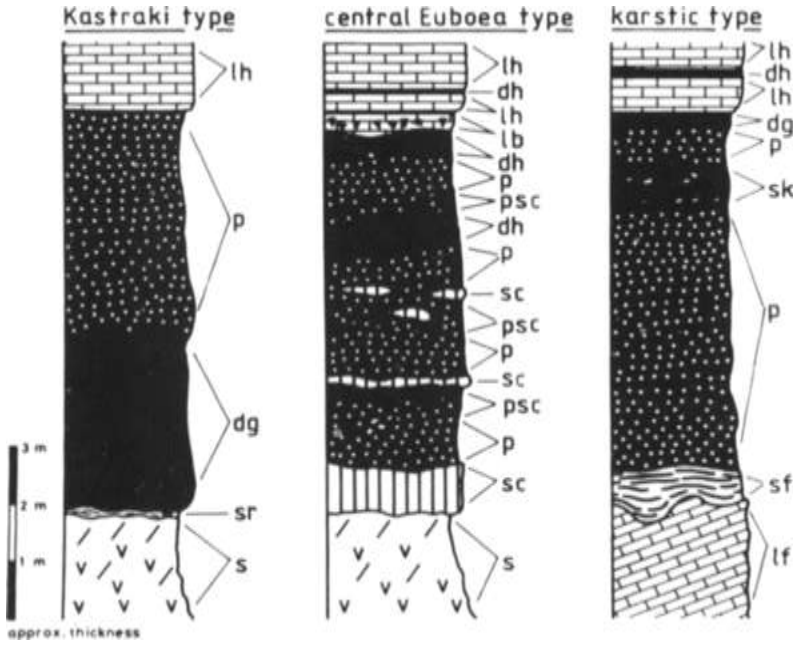

Figure 22. *Major types of Ni-laterites in Evia and central Greece (Rosenberg, 1984).*

Nickel karstic type deposits are common in the area of Lokris (e.g., the deposit of Agios Ioannis, deposit in the area of Nissi, etc.), while deposits on serpentinites are found in Evia, Lokris, Edessa, Vermio. Secondary deposits on sedimentary formations have also been found in the area of Edessa (Valeton et al. 1987, Arnisalo et al. 1999; Alevizos, 1997; Eliopoulos et al., 2000). The Ni-bearing Fe ores of central Evia (Fig. 22), both those found on ophiolites and those on limestones, are heterochthonous.

The deposits of Ni-bearing Fe ores of the Attica basin are considered to be of primary origin, located on the initial site of their formation and that they came from laterite disintegration of the ophiolites. The laterite deposits of the wider area of Edessa are characterized as secondary-sedimentary-allochthonous. Specifically, the deposits of Koupi, Vryta, Flamouria and Mesimeri have been transported at a short or long distance and have been repositioned on serpentinites, giving the impression of primary deposits. These deposits are considered pseudo-autochtonous. The deposits of the Chorafia of Vryta, Flamouria and Platani areas have been repositioned after their transport on sedimentary formations and are characterized as typical secondary deposits. The ophiolite rocks of the Almopia zone are considered to be the parent rocks of these deposits, which during the Lower Cretaceous emersion under suitable conditions were lateritized and formed laterite covers rich in Fe, Ni and Cr. Upon the destruction of these covers due to erosion, before (or concurrently with) the Upper-Cretaceous transgression, their materials were transported by water and deposited in the form of mechanical or mechanical-chemical sediment on serpentinites or sediments. These formations were then covered by the sediments of the middle-upper Cretaceous transgression. Nickel-bearing laterite Fe ores of the wider area of Kastoria are considered stratigraphically equivalent to the Fe ores of mainland Greece, Evia and Albania. These Fe ores are directly associated with serpentinized ultramafic rocks and, in contrast to those of mainland Greece and Evia, have been coated by molasse conglomerates. According to their appearance, mineralogical and geochemical composition, the Ni-bearing Fe ores of Kastoria are characterized as Ni-bearing laterites. The spherical bodies (oval and peloids) of the sedimentary Fe-Ni ores of Greece and Albania were formed during the lateritization of the parent rocks (ultramafic and mafic). These were transported as clastic ‘grains’ together with Fe hydroxides and oxides and clay minerals, formed in the various zones of the laterite disintegration crusts (Alevizos, 1997).

According to Petrascheck (1954), the Ni-bearing Fe ores of Lokris come from the laterite degradation of the ophiolites during the Middle Cretaceous emersion of the zone of eastern Greece, and separates them into sedimentary ores and ores due to degradation. According to this perspective, Maratos (1960) separates the Ni-bearing deposits of Lokris into autochtonous, which are those located on ophiolites, i.e., on their parent rock, and heterochthonous, which are those located on limestones and therefore have been transported away from the area where they were formed due to the laterite degradation of ophiolites (product of laterite degradation of igneous rocks), whereas, the same deposits are classified into two groups of ores, namely ores due to degradation and sedimentary ores, as stated by Alevizos (1997). In this area also exist the deposits of the Sub-Pelagonian zone, which cover a wide range of different forms of metal-bearing and are representative for almost all the different types of Ni deposits (Albandakis 1984). Regarding the deposit of Agios Ioannis of Larymna, Augustithis (1962) concluded from his studies that during the diagenetic and post-diagenetic stage, significant transformations of the mineralogy and the ore took place. He also considers that Ni was originally evenly distributed within the deposit and that it was later concentrated in certain parts of it. According to Moussoulos (1967), the Ni enrichment of the lower part of the deposit took place mainly during the sedimentation stage of the deposit, in colloidal form. Kurzwell (1966), for the Ni-bearing Fe ore of Agios Ioannis of Larymna, discovered that Ni is found in the Fe ore mainly in colloidal form. At the base of the deposits the existence of Ni silicate minerals is emphatically mentioned. These minerals are considered to have been formed during the diagenesis stage of the

deposit, while the Ni in colloidal form was directed towards the base of the deposit. Nickel is considered to have had a uniform distribution within the deposit, which in the post-diagenetic stage was concentrated in certain parts of the deposit (Alevizos, 1997). The Ni-bearing Fe ores of Lokris and, consequently, of the zone of eastern Greece are considered sedimentary, which were deposited in the Upper Cretaceous sea during the Upper Cretaceous transgression (Fig. 23). The deposition of Fe ores was done in the form of chemical sediment (gel).

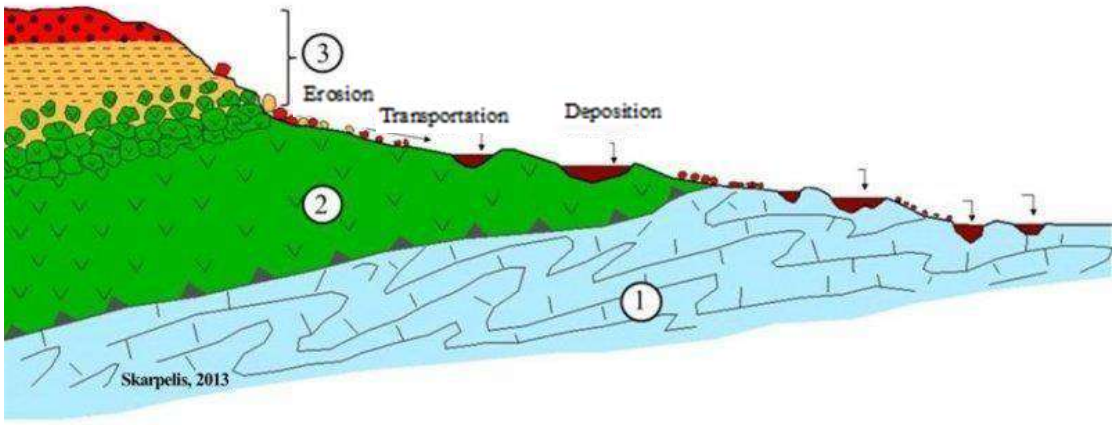

Figure 23. *A simplified sketch depicting the process of producing sedimentary Fe ore. 1. Triassic-Jurassic limestones; 2. Ultra-alkiline rocks; 3. Ni-laterite. The erosion of the laterite begins in terrestrial environments, the erosion material is transported partially mechanically by means of aquatic flows, while deposition takes place in shallow marine environments (Skarpelis, unpublished).*

The ultramafic and mafic rocks of ophiolite complexes of the zone of eastern Greece are considered to be the parent rocks of the Fe-Ni ores of the wider area of Lokris. This perspective coincides with the assessments of various researchers who studied the above ores from time to time. Numerous studies of ultramafic rocks have shown that Ni is found mainly in olivines. The serpentinization of olivines in the presence of water and sulfur makes the number of phases constant (serpentine + brucite + oxides + sulfides). The hydration of Mg-Fe-Ni-olivines in the presence of sulfur converts a portion of Fe and Ni into magnetite and sulfides, according to the reaction: (Mg,Fe,Ni)-olivine + H_2O + S_2 = serpentine + $Mg(OH)_2$ + $FeO.Fe_2O_3$ + sulphide. The ophiolites are inserted into the schist-chert formation, which is the main formation of the Sub-Pelagonian zone. The majority of ophiolite bodies are in the upper level of the schist-chert formation and at their base the formation of ophiolite mixtures (melange) is observed. The multi-mixed formations (melange) were formed in the Upper Jurassic-Lower Cretaceous with the destruction of the ophiolite cover and the resedimentation of its various components in the anterior part of the ophiolite body. The rocks of the ophiolite complexes under suitable conditions underwent laterite degradation, the products of which formed laterite covers rich in Fe, Cr and Ni (Alevizos, 1997).

1.4 LARCO GMMSA deposits

1.4.1 Geotectonic classification

The classification of the studied area concerned into one or more geotectonic zones has been the subject of study by various researchers, whose opinions differ in several cases. The area of Lokris is considered to belong partly to the zone of eastern Greece (Sub-Pelagonian) and partly to the Parnassos-Giona zone (Fig. 24). Sediments of the Parnassos-Giona zone are found in the specific area and the sediments of eastern Greece have been thrusted on them (Alevizos, 1997).

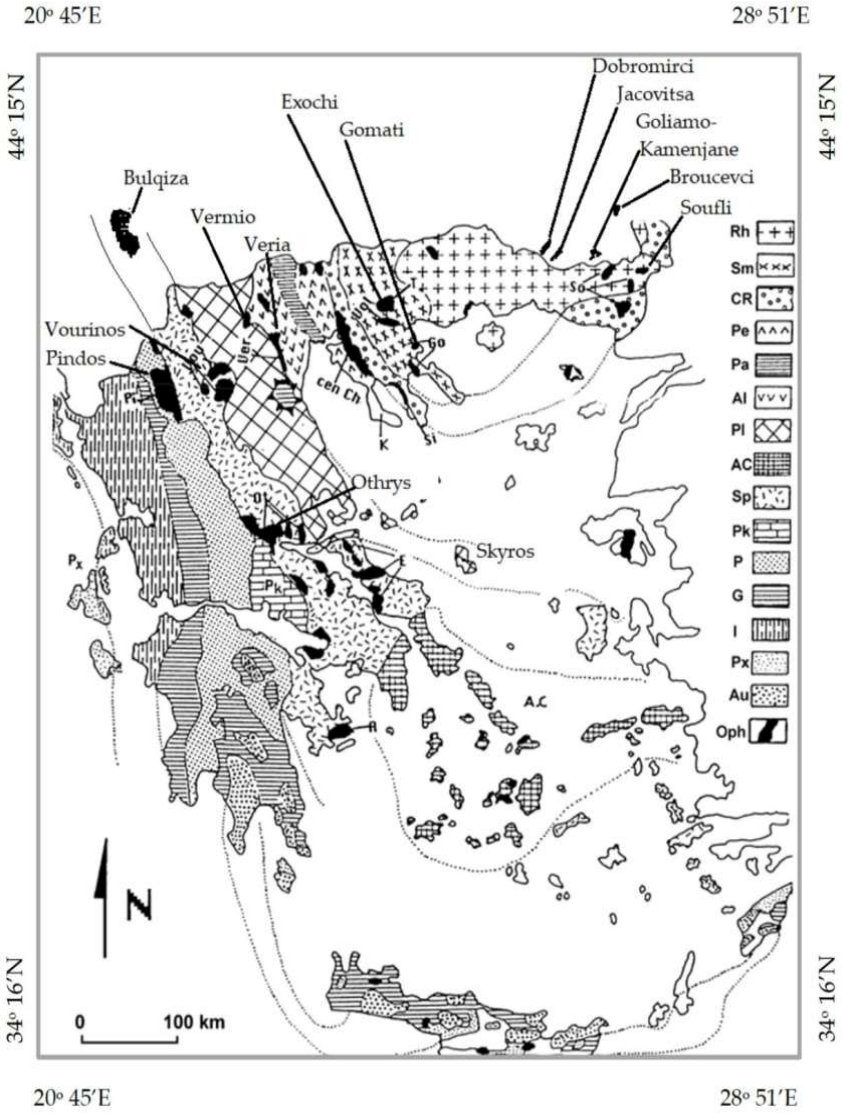

Figure 24. *Simplified map of the structural zones of the Hellenides (after Mountrakis et al., 1983) with main geotectonic features. Symbols: Rh = Rhodope; Sm = Serbo-Macedonian Massif; CR = Circun-Rhodope; (Pe = Peonias, Pa = Paikon, Al = Almopias) = Axios (Vardar); Pl = Pelagonian; AC = Attico-Cycladic; Sp = Subpelagonian; Pk = Parnassos-Giona; P = Pindos zone; G = Gavrovo Tripolis; I = Ionian; Px = Paxos; Au = Plattenkalk – Talea Ori.*

According to Renz (1940, 1955), the zone of eastern Greece is characterized by the schist-chert formation of the Upper Jurassic-Lower Cretaceous period and by the

transgressive Upper Cretaceous rudist-bearing limestones, on which the flysch of Danian-Eocene period develops. The Parnassos-Giona zone consists of a) dolomites and dolomitic limestones with large Megatodon and Gyroporella of the Upper Triassic, b) limestones with small Megalodon at their base and Cladocoropsis mirabilis Felix at their upper parts, c) rudist-bearing limestones of the Upper Cretaceous and d) flysch of Eocene. The main characteristic of the zone of eastern Greece is the presence of schist-chert formation with ophiolites of Upper Jurassic-Lower Cretaceous period. The transgressive rudist-bearing limestones of the Upper Cretaceous, on which the flysch of Eocene has been deposited, develop on the schist-chert formation. The Fe-Ni ores of Lokris are classified in the geotectonic zones according to the place of their formation. The areas of Lokris, where the Fe-Ni ores have as a floor the schist-chert formation with ophiolites, belong to the zone of eastern Greece. The areas where the Fe-Ni ores are located on limestones, on the contrary, belong to the Parnassos-Giona zone, with the exception of the deposit in the area of the village of Pyrgos, which, despite being on Jurassic limestones, is reservedly classified in the zone of Eastern Greece (Alevizos, 1997). Marinos (1958) found that in eastern Greece (Lokris, Othris) there are lateral and vertical transitions of the carbonaceous sediment structure in the Upper Triassic up to the Upper Jurassic. Celet (1962) classifies the northern part of Lokris (Sfigio Mountain) in the Sub-Pelagonian zone and distinguishes the following stratigraphic structure: a) upper Triassic dolomites with large sized Megalodon and Gyroporella, b) gray-dark limestones with small sized Megalodon Orbitopsella praecursor (Lias), c)oolitic limestones, d) thick-bedded dark colored limestones with Cladocoropsis mirabilis FELIX (Kimmeridio), Clippeina jurassica FAVRE as well as algae and crinoidea, e) thin-bedded gray-dark limestones with flints and alternations between yellowish schists and greenish quartz, f) serpentinised ophiolites and with g) transgressive rudist-bearing limestones of the Upper Cretaceous. Finally, it is generally accepted that in the area there is a tectonic fold with approximately A-D axes direction with the presence of vertical cracks parallel to the axes of the folds.

1.4.2 Stratigraphy, structural characteristics and paleogeography

The stratigraphy in the area of Viothia lakes includes a) dolomitic limestones of the Upper Triassic with large Megalodon, Gyroporella, b) limestones of the Lower Jurassic with small Megalodon and Paleodasycladus mediterraneus (PIA) and Orbitopsella at the lower parts and at the upper parts Cladocoropsis mirabilis FELIX, Conicospirillina basiliensis MOHLER, Pseudocyclammina, c) schist-cherts with ophiolites of the Upper Jurassic-Lower Cretaceous, d) transgressive limestones of the Cenomanian up to Paleocene and e) flysch of the Paleocene-Eocene. The schist-chert formation with ophiolites is placed between Lower and Upper Jurassic, with lateral transitions to the limestone or dolomitic sediments. The area of Lokris belongs entirely to the zone of eastern Greece, the stratigraphic structure of which is briefly described by the researcher as follows: sandstones and clay schists compose the oldest formation of this zone, in which basic igneous rocks, as well as limestones of the Upper Paleozoic, are often inserted. Dolomites and dolomitic limestones of the Upper Triassic with Diplopora, Gyroporella and large Megalodon follow in a layer unconformity. The Jurassic limestone structure then develops in layer conformity with dark-coloured limestones with Pinnidae and small Megalodon (Lias), oolitic light-coloured limestones (Dogger) and dark-coloured bituminous compact limestones with Cladocoropsis mirabilis FELIX and other algae (Upper Malm). A bauxite horizon is inserted between the dark-coloured limestones of Lias and the light-coloured oolitic rocks of Dogger.

These formations are overlaid in layer conformity by marls, sandstones, schist-cherts with ophiolites of the Upper Jurassic-Lower Cretaceous, and subsequently rudist-bearing limestones of the Upper Cretaceous with Ni-bearing Fe ores follow in layer conformityalong the transgressive contact. The Cretaceous limestones are overlaid in layer conformity by flysch of the Paleocene-Palaeogene, which consists of sandstones and marls. A characteristic feature of the zone of eastern Greece is the coexistence of the schist-chert formation with ophiolites and the Upper Cretaceous transgression. The schist-chert formation with ophiolites consists of radiolarites, cherts, clay-mixed sandstones, marls and marl limestones. Ophiolites are found in the upper part of the formation, most of which are serpentinised. The Upper Cretaceous transgression is also a reference element of the zone of eastern Greece. The transgressive Upper Cretaceous limestones overlie in layer conformity, either the schist-chert formation with ophiolites, or the Jurassic limestones or the Triassic dolomitic limestones. Between the Upper Cretaceous limestones and the ophiolites or Jurassic limestones Ni-bearing Fe ores are found, as in the areas of Agios Ioannis of Larymna, Marmeiko, Tsouka, Loutsi, Pavlos etc. (Alevizos, 1997). The area of Lokris according to Albandakis (1974) was found to belong entirely to the zone of eastern Greece (Fig. 25), whose main feature is the coexistence of schist-sandstone-chert formation and the Upper Cretaceous transgression. Regarding the stratigraphy from bottom to top the following are found:

- Paleozoic formations, i.e., clay schists, sandstones, gray-dark colored clastic limestones in the form of layers within the clay schists and sandstones as well as diabase and keratophyre tuffs.
- Triassic formations, i.e., it consists mainly of light-colored limestones and dolomitic limestones.
- Jurassic formations and is characterized mainly by gray-dark colored thick-bedded limestones mainly with small sized Megalodon, oolitic limestones with bauxite horizon and bituminous limestones.
- The schist-sandstone-chert formation that consists of radiolarites, cherts, sandstones, marls, marl limestones with ophiolites as the upper formation, mostly serpentinised.
- Cretaceous formations, i.e., Upper Cretaceous limestones mainly with rudists that sometimes overlie in layer unconformity the schist-sandstone-chert formation and sometimes Jurassic limestones or Triassic dolomitic limestones. Ni-bearing Fe ores are found between Upper Cretaceous limestones and ophiolites or Jurassic limestones.
- Flysch in tectonic contact mostly with the Upper Cretaceous limestones with the exception of the normal transition to the flysch in the area of Ftelia two kilometers west of Akraifnio.
- Neogene deposits mainly in the areas of Larymna, Martinos, Theologos and Malesina with marl limestones alternating with marls.
- Quaternary deposits consisting of alluvium deposits of lateral debris, debris cones and detritus.

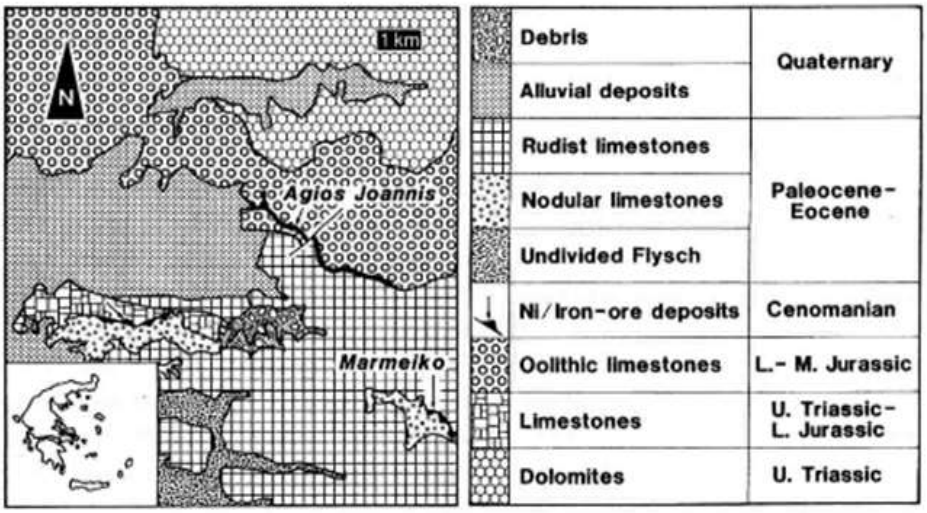

Figure 25. *Geological map of the zone of eastern Greece (Alevizos et al., 2001)*

Regarding tectonics, the following are found:

- pre-Alpine orogenic movements in Paleozoic formations, which are multiple folded and mostly metamorphosed, as a result of upper Paleozoic-lower Triassic orogenic movements. This is made clear by the fact that the Mesozoic formations overlying Paleozoic formations do not show any metamorphism phenomena. The limestones of the lower, middle and upper Jurassic, which underlie the Ni-bearing Fe ore and the transgressive Upper Cretaceous limestonesof the area of N. Kokkino, Thiva, have a folding system with axes direction NE-SW.
- During the Alpine orogeny in the area, apart from the imbricates, local thrust phenomena also took place, due to tangential pressures with the thrust of the upper Jurassic limestones onto the schist-sandstone-chert formation or the thrust mainly of flysch on the heterochthonous limestones of the Jurassic or on the Cretaceous limestones.
- During the post-Alpine tectonics, isostatic movements took place between the Miocene and the Quaternary, which resulted in the creation of vertical cracks of NW-SE and NE-SW direction. The Miocene ruptures contributed to the formation of basins, where mainly conglomerates, sandstones, marls and clays with local lignite deposits were deposited.

The palaeogeography of the wider area of Lokris, according to Albandakis (1974), which belongs to the zone of eastern Greece (Sub-Pelagonian), is characterized by two stratigraphic gaps, which correspond to two different emersions of the zone, one between upper Permian and middle Triassic and the other between Lower Cretaceous and Cenomanian. The Triassic land lasted until the lower Carnio, where we have the beginning of the Triassic transgression. From the Carnio to the upper Jurassic we have a continuous deposition of carbonate sediments (dolomites-limestones) of the neritic phase. At the end of the Jurassic and the beginning of the Paleo-Cretaceous, the deposition of clay-sandstone materials after radiolarites took place in a shallow sea and then magmatization of basic and ultramafic magma followed. Immediately after magmatization, the emersion of the area followed (neokimmeric orogeny) during which

there was intense erosion of the Mesozoic sediment series up to part of the Paleozoic formations with the creation of an endrumpf. The ophiolites at the same time underwent laterite degradation. The lateritization material was carried by the rainwater as clastic sediment on the eroded surface during the Cenomanian transgression in the form of layers or lenses, forming Fe-Ni ores. The depth of the Upper Cretaceous Sea began to increase at the beginning of the Cenomanian-Turonian transgression and so, initially, there was the deposition of rudist-bearing limestones of reefal phase and then fine-grained middle-bedded limestones, developed upwards into microcrystalline limestones. During the Paleocene, from the beginning of flysch deposition due to Alpine orogenic movements, sediments began to emerge. In the Miocene, due to continental movements, closed basins or lagoons were formed, in which mainly clastic sediments were deposited. Finally, due to the quaternary vertical ruptures, the area took its current form.

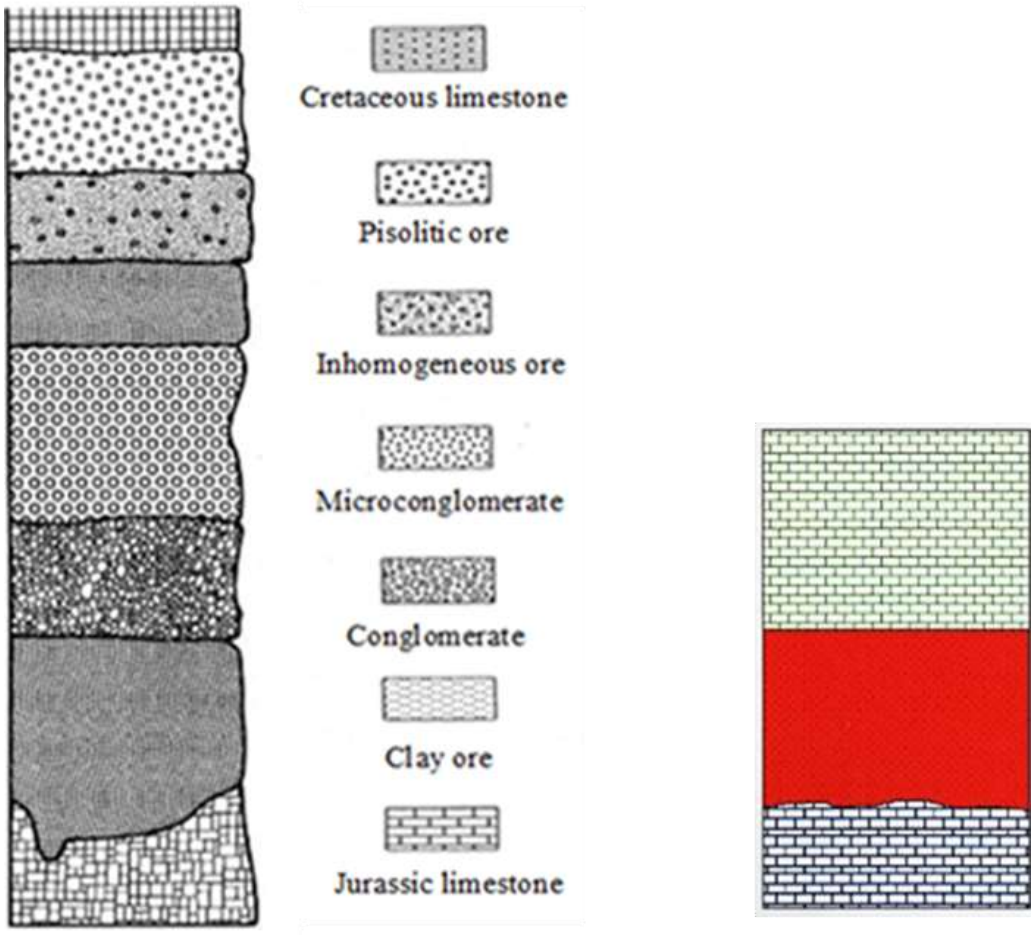

Figure 26. *Schematic lithostratigraphic column of the Agios Ioannis Fe-Ni ore deposit (Alevizos and Mücke, 2001, left; Apostolikas, 2010, right).*

1.5 LARCO GMMSA laterite mining and industry

1.5.1 General

Mineral resources support a large part of Greece's heavy industry and as a growth sector has played an important role in its development. The exploitation of nickeliferous laterite deposits in Greece is performed by the company LARCO General Mining and Metallurgical Company SA (G.M.M.S.A.), which is among the main metallurgical industries for Fe-Ni production in Europe. LARCO GMMSA has a long tradition in innovation, as it is the first company in the world to have introduced granulated ferronickel (Fe-Ni) to the international market in 1976. Its competitors followed two years after and nowadays 70-80% of the Fe-Ni produced in the world is in granulated form. All stainless steel producers, such as Thyssen-Krupp, Outokumpu OY and AB, Acerinox, Glencor, Avesrapolarit, use LARCO GMMSA granulated Fe-Ni in their plants. LARCO GMMSA, which is one of the most important production units of our country with activities mainly in the region, is the one that exploits the Greek laterites. It is a fact that LARCO GMMSA has an important activity for 53 years with special economic importance for the Greek Economy, as it is one of the main metallurgical industries producing Fe-Ni in Europe. More specifically, it is the largest producer of Fe-Ni in Europe, one of the twenty largest in the world ranking and the only one using only indigenous ores. In addition to the exploitation of deposits located in Evia, Viothia and Kastoria, the company has metallurgical plants for the production of Fe-Ni located in the area of Larymna in Lokris, Fthiotis since 1966. This unit is one of the 57 Ni metallurgical plants worldwide and one of the 22 plants processing laterites (http://www.larco.gr). LARCO GMMSA conducts extensive and detailed research that includes geological identification, mapping and exploratory sampling drilling using modern technology. The study and evaluation of the results of the geological research is done via modern and certified computer programs and thus the volume and the quality of the reserves of Ni ores are calculated.

1.5.2 Mining sites

The company disposes of privately-owned mining sites in Evia, Agios Ioannis-Lokris and Kastoria. Additionally, it also has a privately-owned coal mine in Servia of the Kozani prefecture. The company also has a metallurgical plant in Larymna (Fig. 27), Lokris, which employs the majority of the company's employees. LARCO GMMSA was founded in 1963 by Prodromos Athanasiadis Bodosakis. In 1966 the Larymna plant construction was completed. The Evia mining sites entered into full exploitation in 1969 and in 1972 two new electric furnaces were added. In 1977 the longest conveyer belt in Europe with 7.5 km length was installed in order to decrease the transportation cost of the rocks with trucks (http://www.larco.gr).

Figure 27. *The LARCO GMMSA metallurgical plant in Larymna.*

The company's activities are divided as follows:

- Agios Ioannis mines in Viothia, where the rock is extracted from subterranean and superficial exploitations, using privately-owned equipment.
- The Evia mines where the extraction of laterite is performed with a superficial exploitation, using privately-owned equipment.
- The Kastoria mines where superficial extraction is performed with the use of leased equipment.
- The Albania mine located in the Bitincka area, 15 km approximately from the Ieropigi mine in Kastoria. It is a deposit great in size, the overall reserves of which exceed 100,000,000 tons with an average Ni content of 1.2% (Apostolikas et al., 2000).
- The coal mine in Servia, Prefecture of Kozani. There, the coal extraction is performed with superficial exploitation and leased equipment.
- The Metallurgic Complex of Larymna, where the nickeliferous rocks are submitted to process with the pyro-metallurgical method in view of producing Fe-Ni (Ni content: about 25%).

All plants and equipment are owned by LARCO GMMSA; the company performs extended and detailed research, including geological recognition, mapping as well as research and drilling for sampling purposes using state-of-the-art technology. The study and assessment of the geological research results are performed with state-of-the-art and certified computer programs; thus, the volume and quality of Ni-rock reserves can be calculated. The deposits exploited by the company are extracted superficially (open-pit method), while only 2% is extracted underground.

1.5.3 Mines of Larymna area (Lokris)/Agios Ioannis

The mines of Agios Ioannis are located in Neo Kokkino of the Prefecture of Viothia, 7 km away from the metallurgical plant of Larymna. They are the oldest mines and operate with one underground and other surface exploitations. A fourth surface exploitation was created as an extension to the existing surface exploitations. The first underground mine in the area started its operation at the beginning of the last century. And these mines are equipped with modern surface and underground equipment and

additional units of drilling machines. In addition, there are two crushing-sieving facilities as well as an enrichment unit and an ore homogenization unit. The annual production after the magnetic separation amounts to 700 thousand tons of ore with a Ni content of 1.05% - 1.1% (http://www.larco.gr).

1.5.4 LARCO GMMSA metallurgy and Larymna metallurgical plant

The Metallurgical Plants are located in Larymna in the Prefecture of Fthiotida. The plant performs pyrometallurgical treatment of the laterite Fe-Ni ores in order to produce granulated Fe-Ni, of high purity and low carbon content, with a Ni content of 18%-24%, which is the raw material for the stainless steel industries in Europe. The main production line consists of 4 rotary kilns, three of which are about 90 meters long and two of which have a diameter of 4.2 m, while the third has a diameter of 5.2 m. The fourth is 126 meters long and has a diameter of 6.1 m and is one of the largest in Europe. In rotary kilns (Fig. 28) the removal of moisture and the pre-heating of the ore are achieved. Then it consists of 5 electric furnaces 6 meters high. The four of them have a diameter of 12 meters and the fifth has a diameter of 18 meters, while their power ranges from 28 MW-44 MW. There the melting of the roasted material and the reduction of Ni is achieved. Then 2 converters of OBM type follow, with a capacity of 50 tons of metal each. In addition to the above, there are also the necessary auxiliary facilities, such as the 2 units for the production of oxygen and nitrogen, a powder pelletizing unit, a Fe-Ni granulation unit and magnetic enrichment units (http://www.larco.gr).

Figure 28. *Rotary Kiln (R/K) (left) and Electric Furnace (E/F) (right) at the metallurgical plant.*

The exploitation of Greek Fe-Ni ores began at the beginning of our century. The ore was then mainly exported to Germany for the production of Ni-steels. Today the exploitation is carried out by the LARCO GMMSA Company, which is one of the main metallurgical industries producing Fe-Ni in Europe. The company was established in 1965 and during the 70's was one of the main producers of Ni in Europe. LARCO GMMSA remains today the only producer of Ni in the European Union from domestic ores. Finland has a small amount of Ni sulphide ores, but this is not enough to supply Ni metallurgy in that country, so Ni production is heavily dependent on imported ores. The LARCO GMMSA Company currently operates mines in three areas (Agios Ioannis of Larymna, Evia, Kastoria). Also, there are two lignite mines for private use of lignite (Serbia of Kozani, Koroni of Messinia) and the Metallurgical Plant of Larymna. The

ore that comes from the Mines of Kastoria, Agios Ioannis and Evia has different characteristics depending on its origin, as the ore of Evia has a high content of Fe and silicon oxide, while the ore of Agios Ioannis has a high content of Fe but a low content of silicon oxide, and the ore of Kastoria has a high content of silicon oxide but a low content of Fe oxide. The typical composition of the metallurgical mixture is as follows: (i) 55% ore of Evia, (ii) 30% ore of Agios Ioannis, (iii) 15% ore of Kastoria, (iv) solid fuels, coal-lignites, approximately 200-230 kg/tn of natural ore. The above ratio of ores is mainly dictated by the volume of exploitable reserves, the Ni content of the deposits, the potential and capacity of the ores and the general chemical and mineralogical composition (http://www.larco.gr).

Nickel in laterite ores is often finely disseminated in various minerals and the complex mineralogy of laterite ores makes it difficult to achieve any significant Ni upgrading by physical techniques (Farrokhpay, 2017). Laterite ore processing can be performed by pyro or hydrometallurgical routes and the choice depends on the chemical and mineralogical composition of the ore. There are two general methods of processing laterite ores for the extraction of Ni products (Diaz et. al., 1988): 1) pyrometallurgical: (i) smelting to produce matte and (ii) smelting to produce Fe-Ni and 2) hydrometallurgical: (i) reduction roasting and extraction with ammonia to produce Ni oxide (the carbon Process) and (ii) extraction with sulfuric acid in pressurized autoclaves to produce Ni briquettes and powder (Pressure Acid Leaching method, PAL). In general, the hydrometallurgical processing is used for low-content Ni ores, while pyrometallurgy is used for ores with a Ni content above 1.5 wt.% allied to SiO_2/MgO, Fe/Ni, and Ni/Co ratios, respectively, lower than 1.5 and 12, and greater than 30. Among the hydrometallurgical routes, high pressure acid leaching (HPAL), atmospheric leaching (AL), and heap leaching (HL) deserve to be mentioned (Ribeiro et al., 2020). Heap leaching is a process employed in the minerals industry to extract valuable metals from low-grade ores at relatively low capital and operational cost. Practically all heap leaching operations use agglomeration as an intermediate stage between mineral crushing and its stacking. Agglomeration helps to increase permeability by eliminating the migration of fine-grained particles downwards in the heap, thereby lessening the channeling and ponding effects. Good agglomerates in a heap should survive the aggressive acid leaching conditions without disintegration over long period of time and have good permeability, which leads to better interfaces between the leach solution, air, and ores, resulting in improved metal recovery (Xu et al., 2013). The HPAL process is the most efficient for the Ni and Co extraction, however, its high capital investment and operational costs represent a considerable drawback (Ribeiro et al., 2020). More specifically, significant technical challenges such as low agglomerate strength under wet conditions, low Ni recovery remain for Ni-laterite heap leaching process, preventing its adoption in industry (Xu et al., 2013).

The other routes present low selectivity and recovery of the valuable metals allied to high reagent consumption, as in the case of AL and HL. As sulfuric acid is the most expensive input of this hydrometallurgical process, the development of the sulfation-roasting-leaching route arises as an important alternative to reduce acid consumption. The sulfation-roasting-leaching process has successfully been used to extract Ni and Co from laterites due to its flexibility for application to ores with different chemical and mineralogical characteristics. One of the main characteristics of this process is to leave elements such as Fe, aluminum, and Cr in the residues as insoluble oxides. This route presents also a lower capital investment and operational costs, when compared to the HPAL process, and provides high Ni and Co recoveries besides low Fe and

aluminum concentration in the leachate liquor. Fe and aluminum are considered the main contaminants that hamper the downstream stage of the hydrometallurgical process of Ni-laterite ore. For this reason, many studies and reviews of the literature have reported the Fe removal from leachate liquor. Hence, the application of the sulfation-roasting-leaching process for Ni and Co extraction from a laterite ore is promising (Ribeiro et al., 2020).

The production process known as the LM process (named after the late NTUA professor L. Moussoulos, who invented this process) followed at the metallurgical plant, is clearly pyro-metallurgi and belongs to the methods combining pre-smelting roasting in a rotary kiln and metal finishing in a converter with oxygen blowing.This method was developed in Greece on behalf of LARCO GMMSA. It is applied in the facilities of this company in the area of Lokris, in order to exploit the Greek laterite deposits. Greek laterites differ from the rest in the relatively lower water content and in the relatively higher Al_2O_3. The LM method, apart from the exploitation of the peculiar Greek deposits, may cover all types of laterite ores. In particular, LM process (Fig. 29), as applied today in LARCO GMMSA, involves the following steps:

1) crashing and homogenization of the laterite Ni rocks and controlled mixing with solid fuels for the creation of a predetermined composition alloy. The ore is crushed and mixed with a certain amount of solid fuel (lignite, coal).
2) Heating up to 870°C approximately in a rotary kiln, where it is subjected to a controlled carbon-thermal reduction, a pre-reduction of the Ni oxides, as well as part of the Fe oxides.
3) Reducing heating and liquation of the extracted product from the rotary kilns up until 1,450 °C in an open bath immersed arc electric kiln for the production of a Fe-Ni (12-16%) molten alloy and disposal at sea of the produced rust in the Evia Gulf upon its granulation with sea water.
4) Refining of the molten Fe-Ni alloy from the electric furnaces in OBM converters with oxygen blowing and lime addition in temperatures going up until 1,700°C for the production of granulated Fe-Ni alloy (18-24%) using sea water (Moussoulos, 1973).

Thus, the reductive smelting of the fed material allows the formation of two separate phases, one metallic containing all of the Ni and part of the Fe and one slag residue. The residue of the metallurgical process (slag) contains a glassy phase with inclusions of spherical Fe-Ni alloy of varying size from less than 10 to a few hundred microns, and the gang material. The gangue material is mainly composed of small phyllosilicate mineral with an average contents of 39 wt.% SiO_2, 6 wt.% Al_2O_3, 25 wt.% FeO, 7 wt.% MgO, 3 wt.% CaO and 1.5 wt.% Cr_2O_3. The Cr content in the slag glass is relatively high (Economou-Eliopoulos et al., 2016). In summary, the method of exploitation of laterite ores includes the following stages: 1) controlled reduction of the ore; 2) melting in Fe-Ni (22-25% Ni); 3) purification and enrichment of the alloy (25-30% Ni). If pure Ni is demanded: 4) manufacture of anodes (90% Ni) and 5) electrolysis.

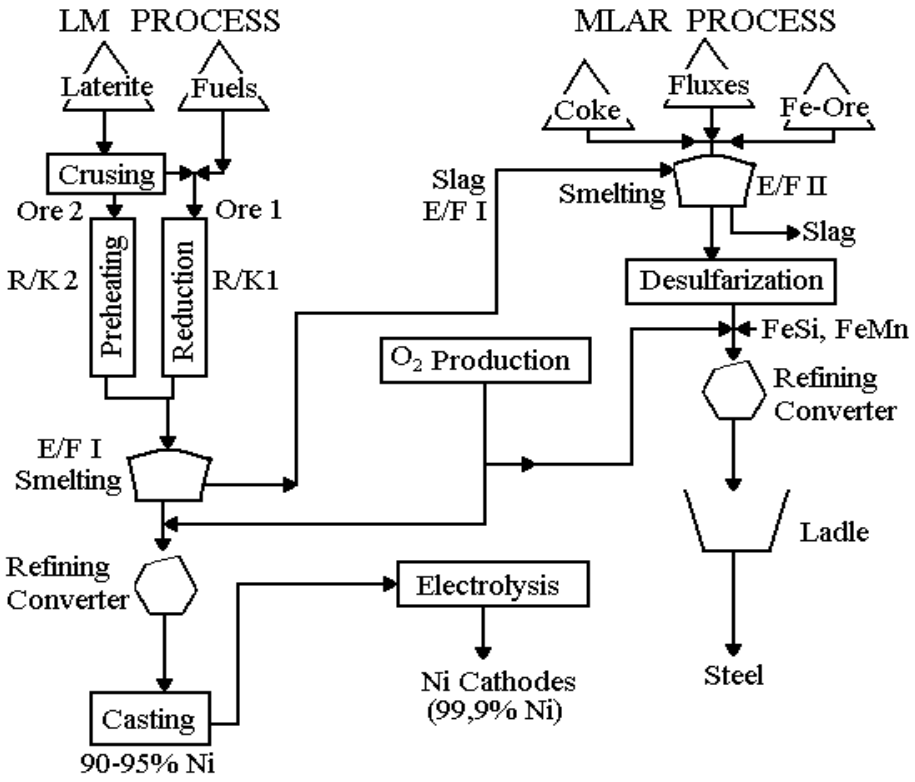

Figure 29. Flow-Sheet of LM Processe (Zevgolis, 2004).

The products by LARCO GMMSA after the metallurgical treatment are the following: 1) powdered Fe-Ni with 18-20% Ni, produced by oxygen converters. Also, free carbon, which has low Ni content. Ferronickel is the final product of LARCO GMMSA. Due to its low content of C, S, P and its high content of Fe (~ 80%), it is considered suitable for stainless steel. It is therefore exported to European stainless steel industries. 2) Slag from reduction electric furnaces: it is produced in a quantity of 1,700,000 t/y. It is used in the cement industry and is an excellent product for sandblasting and paving roads. 60% of this quantity is exported, while the remaining 40% is consumed domestically. 3) Slag from converters: it is produced in a quantity of 70,000 t/y. It is an excellent product for heavy concrete, used in the embedding of oil pump islets, as underwater pipeline housing, etc.. The final result is a high-purity granulated Fe-Ni, with low content in coal, exclusively used for stainless steel production, dispatched from the port of Larymna. More specifically, the basic product from this process is the granulated Fe-Ni 22%, whereas the produced rust's by-products from the electric furnaces and the OBM converters. The purity of the Fe-Ni 22% alloy (P=0.015%, S=0.04% and C=0.02%), its increased content in Fe (75-80%), its content in Co (about 1.1%), which is not priced (with a value equal to 30-50% of the value of the Ni), and is recovered as hydroxide (Moussoulos, 1975), and the granulated form in which it is proposed (facilitating the mechanization of its transportation as a material for stainless steel production), make the Greek Fe-Ni ores some of the most attractive raw materials in stainless steel production metallurgy (Zevgolis, 2004). According to the energy balance of the processes of reduction roasting and reduction melting of Greek Ni-laterites, the system requirements in thermal energy (including the energy of all fuel components in Rotary Kilns (R/K) and Electric Furnaces (E/F) minus the energy

of unburned carbon in the products of R/K, the carbon of the slag and the energy of unburned CO in the gases of the E/F) is 1.8 times the required electricity for the implementation of the reducing roasting. This fact highlights to a large extent the increasing importance of the energy optimization of the reducing roasting in the overall energy efficiency of the pyrometallurgical treatment of laterites. In addition, the energy required to conduct the endothermic reduction reactions during the reducing roasting stage is almost 6% of the total energy required. Therefore, any completion of the reduction of laterite oxides during the reducing roasting stage with the supply of several reducible ores, can significantly contribute to the electricity savings in the E/F, which is a determining cost factor for the metallurgical process.

LARCO GMMSA final product is Fe-Ni, which is exported in its entirety to European stainless steel industries. LARCO GMMSA Fe-Ni, due to its very low content of C%, S% and P% as well as the respectively high content of Fe% (up to 80%) is evaluated as a product of excellent quality suitable for the production of austenitic stainless steel (Zevgolis et al., 2004). The annual production of the company's mines during the last decade ranges from 2 to 2.5 million tons of crushed and homogenized ore. The total annual amount of ore processed by the plant is about 2.2 million tons, whereas the total annual production of LARCO GMMSA, amounts to 16,000-17,000 tons of Ni, which comes from 1,800,000 tons of laterite, covers about 6% of the European market demand for Ni and 1.1% of the world market. This production corresponds to 2-3% of the production of the western world (http://www.larco.gr).

1.6 Scope of the present study

The main purpose of the present MSc Thesis was to re-evaluate previous data on LARCO GMMSA and, in general, of central Greece laterite (Boskos et al., 1996; Economou-Eliopoulos et al., 1997; Boskos et al., 2000; Eliopoulos and Economou-Eliopoulos, 2000; Skarpelis, 2000; Economou-Eliopoulos et al., 2001; Economou-Eliopoulos, 2003; Skarpelis, 2006; Christidis and Skarpelis, 2010; Eliopoulos and Economou-Eliopoulos, 2010; Eliopoulos and Economou-Eliopoulos, 2012; Economou-Eliopoulos et al., 2014; Eliopoulos and Economou-Eliopoulos, 2014; Kalatha and Economou-Eliopoulos, 2015; Economou-Eliopoulos et al., 2016; Gamaletsos et al., 2017; Kalatha et al., 2017; Gamaletsos et al., 2018; Samouhos et al., 2019), and to proceed to new mineralogical and geochemical data, specifically concerning Fe-speciation in Ni-phyllosilicate and nanomineralogy of critical metals such as Co. Hence, for first time in the literature, regarding a laterite ore deposit of Greece (typical LARCO GMMSA laterite ore deposit of Agios Ioannis, Larymna, Lokris, central Greece, particularly at the Agios Ioannis area), powder X-ray diffraction (PXRD), analyses in bulk and microscale (ICP-OES/MS, LA-ICP-MS), microscopic (SEM-EDS) and nanoscopic (TEM-EDS) techniques, together with Mössbauer spectroscopy, were combined for the detailed mineralogical and geochemical characterization and the study of mineral nanoparticles and nanominerals. The above novel mineralogical and geochemical data were used to illustrate new insights into the identification of the specific ore's geochemical fingerprints. The present work gives strong evidence for the importance of nanomineralogy in the characterization of Ni-ores and in general of metal oxide/hydroxide ore deposits. Mineral nanoparticles and nanominerals (Hochella, 2008; Hochella et al., 2008a; Hochella et al., 2008b; Reich et al., 2011; Caraballo et al., 2015; Figs. 30 and 31) related to nanogeoscience issues seem

to be the final frontier of ore mineralogy and geochemistry being playing a vital role in the exploration and exploitation of basic, noble and strategic metal resources.

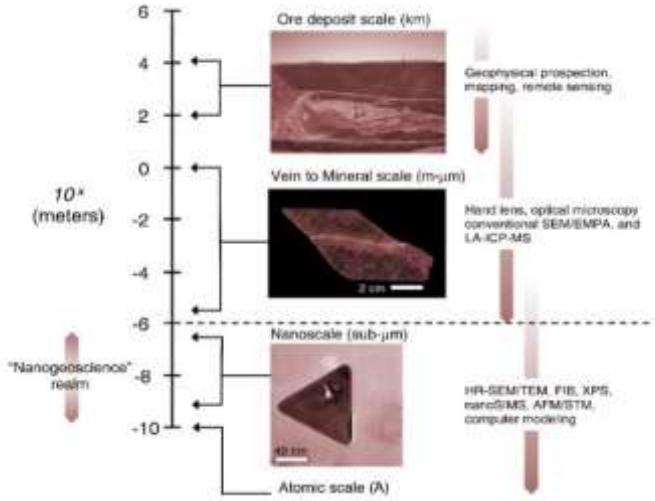

Figure 30. *The dimensional scale of ore deposits research. Vertical scale is depicted in 10xm (−10<x<6), and shows a 10 order-of-magnitude difference between, e.g., a nanoparticle of native gold (~100 nm) and a typical orebody of 1 km^2 size. On the right the analytical/observational techniques are shown for each dimensional range. The segmented line divides the microscopic and nanoscopic realms, which is usually considered the boundary between bulk mineralogy and 'nanogeoscience' (Reich et al., 2011).*

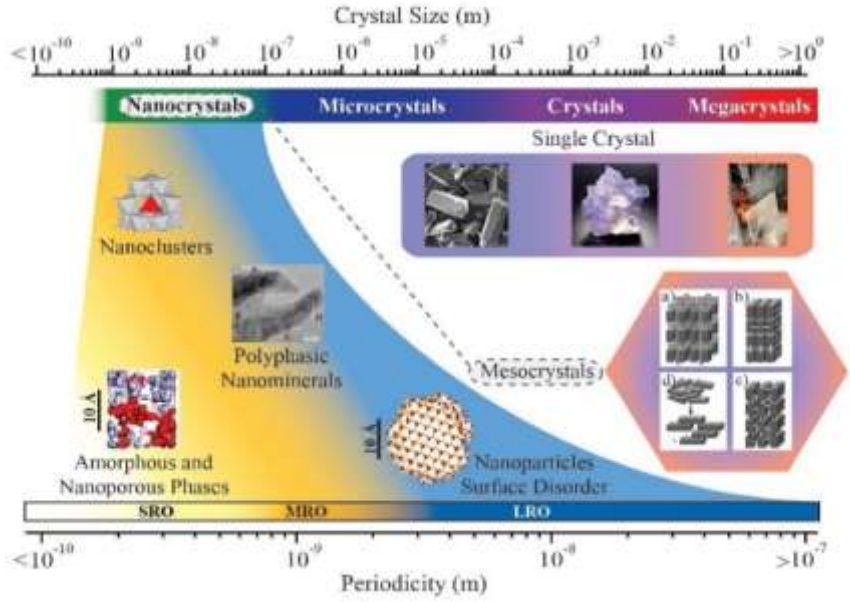

Figure 31. *Schematic categorization of the natural progressive transition between amorphous and crystalline materials. The most relevant emerging areas within mineral crystallinity inenvironmental systems discussed in the main text have been exemplified with some specific cases. The four categories shown within the mesocrystals inset correspond to the alignment of nanoparticles by: (a) organic matrices, (b) physical fields and interparticles forces, (c) mineral bridges, and (d) space constrains (Color online) (Caraballo et al., 2015).*

2. MATERIALS AND METHODS

2.1 Samples and preparation

The investigated typical laterite ore samples were collected from mining sites of the Greek Company LARCO GMMSA. The present investigation is focused on the study of typical LARCO GMMSA laterite samples from Larymna (area of Lokris), which were collected from laterite profile at Agios Ioannis (Figs. 32 and 33). The specimens concerned laterite material (samples L_1-L) and the surrounding hanging wall and footwall limestone (samples LMS_1 and LMS_2, respectively). The material collected from the laterites and the limestones (Fig. 34) was initially grinded appropriately by hand with the use of an agate mortar, in order to obtain a homogenized grain size of ≤ 1mm.

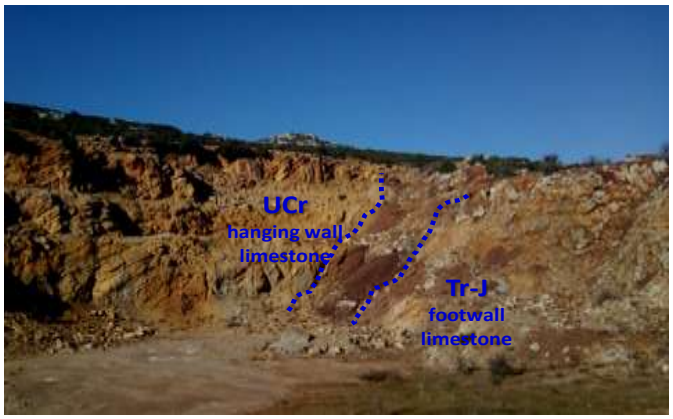

Figure 32. *Representative profile of the studied deposit in sampling site. UCr: Upper Cretaceous hanging wall limestone; Ni-Fe: Fe-Ni ore; Tr-J: Triassic- Jurassic footwall limestone.*

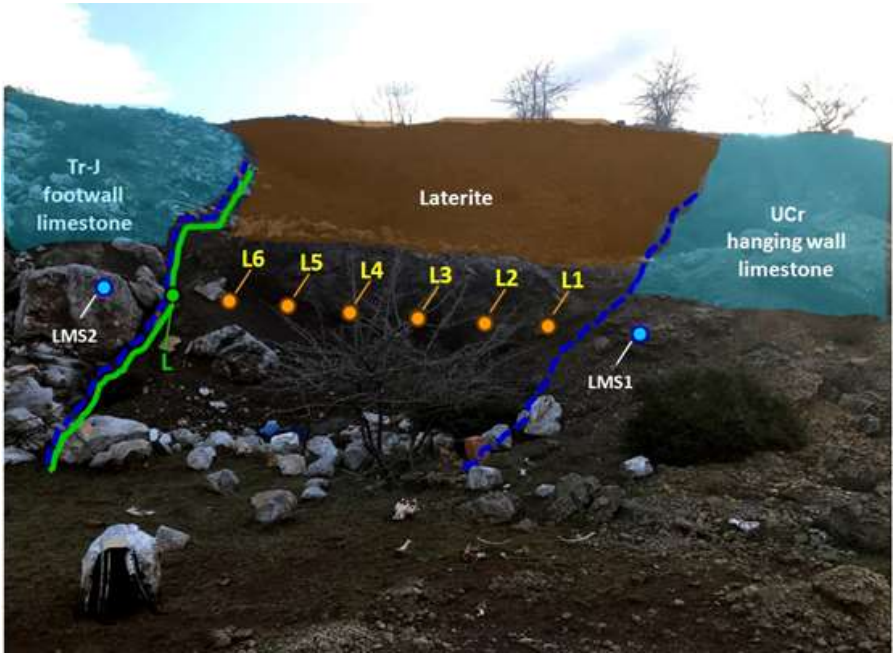

Figure 33. *Occurrence of laterite in sample site, from which samples were collected to be studied.*

Figure 34. *Photographs showing the studed samples from LARCO GMMSA mine: a: hanging wall limestone sample LMS_1; b: laterite sample L_1; c: laterite sample L_2; d: laterite sample L_3; e: laterite sample L_4; f: laterite sample L_5; g: laterite sample L_6; h: laterite sample L (green-black thin layer in the base of the deposit) and i: footwall llimestone sample LMS_2.*

2.2 Powder X-Ray diffraction (PXRD)

Powder-XRD patterns were obtained using a Siemens (currently Bruker AXS) D-5005 X-ray diffractometer, and the EVA 10.0 program of the BrukerDIFFRACplus software package, with regard to raw and acid-treated samples (Cu*Ka* radiation at 40 kV and 40 mA, with graphite monochromator).

2.3 Electron microscopy in microscale (SEM-EDS)

The Scanning Electron Microscopic study and the corresponding Energy Dispersive microanalyses (SEM-EDS) were performed using a Jeol JSM-5600 equipped with an

Oxford EDS, on both free surfaces (raw and acid-treated samples) and whole rock fragments.

2.4 Analyses of Ni-phyllosilicate in microscale (LA-ICP-MS)

According to SEM-EDS, distinct mineral phases, and particularly Ni-phyllosilicate (Fig. 35) hosting Co, were point-analyzed for trace element distribution by means of Laser Ablation Inductively Coupled Plasma Mass Spectrometry/LA-ICP-MS at the Department of Physics and Geology, Perugia University, Italy.

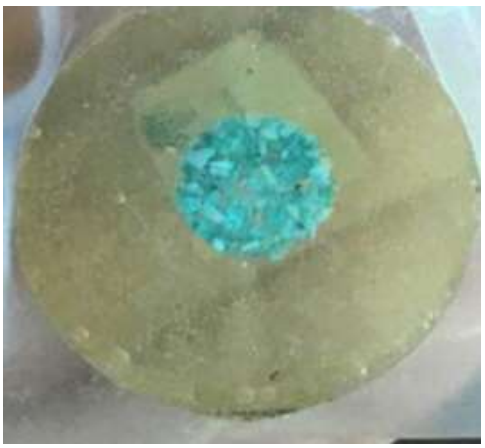

Figure 35. *The selected Ni-phyllosilcate grains, in which LA-ICP-MS analysis was conducted.*

Sample ablation for trace elements analysis has been done using a Teledyne/Photon Machine G2 LA device equipped with a Two-Volume ANU HelEx 2 cell coupled with a Thermo Fisher Scientific iCAP Q, quadrupole-based, ICP-MS. Analyses were performed by using a circular laser beam with a frequency of 8 Hz and a laser density on the sample surface of 3.5 J/cm^2. A beam diameter of 50 µm diameter was used for pyroxene crystals, except in sample 16 were only 20 µm were feasible. Glasses were analyzed with a beam diameter of 110 µm. Data Reduction was carried out following the procedure reported by Longerich et al. (1996), and using the Iolite v.3 software package (Paton et al., 2011). The standard reference glass NIST SRM-610 was used as calibrant with Ca, previously analyzed by EMPA, utilized as internal standard. The USGS BCR2G natural reference material was analyzed as unknown to monitor data quality. Under these operating conditions precision and accuracy are better than 10% for all elements (Günther et al., 1997; Petrelli et al., 2007, Petrelli et al., 2008, Petrelli et al., 2016a, Petrelli et al., 2016b). Glass contamination in mineral analyses was identified by a careful screening of time-resolved signals and the section of the signal that showed a sudden increase in the REEs was removed during data reduction. Contamination by glass, i.e., melt inclusion or glass underlying crystal, is easily recognized by observing spikes in the elemental signal of highly incompatible elements (e.g., La for pyroxene) (Fabbrizio et al., 2021).

Table 1. *Signal intensities for selected elements after the tuning at 85 microns, 8Hz and 3.5 J/cm^2 (Source: Petrelli et al., 2016).*

Isotope	cps
^{139}La	1.11 x10^6
^{208}Pb	0.60x10^6
^{232}Th	1.20x10^6
^{238}U	1.24x10^6

2.5 Mössbauer spectroscopy of Ni-phyllosilicate

Mössbauer spectrometry is based on the quantummechanical 'Mössbauer effect', which provides a nonintuitive link between nuclear and solid-state physics. Mössbauer spectrometry measures the spectrum of energies at which specific nuclei absorb γ rays. Absorption Mössbauer spectra (MS) were collected with a 57Co(Rh) source moving at room temperature (RT), while the absorbers were in a variable temperature cryostat equipped with an electromagnet for magnetic fields up to 7.0 kOe, with the field perpendicular to the gamma-ray beam.

2.6 Analyses in Ni-phyllosilicate in nanoscale (TEM-EDS)

Nanoscale investigation of clay fraction was performed with a JEOL JEM-2100 LaB6 transmission electron microscope (TEM), operating at 200 kV. Grain microstructure was also studied using a bright field detector in scanning (STEM) mode. Elemental analyses were carried out using an Oxford X-Max 100 Silicon Drift Energy Dispersive X-ray spectrometer (EDS), connected to TEM; such obtained characteristic X-ray spectra were further interpreted using the Cliff Lorimer qualitative measurement method (thin-film approximation). Data were acquired in areas ranging from 2 to 5 nm in STEM mode.

2.7 Bulk analyses (ICP-OES/MS)

Further bulk geochemical analyses for major and trace elements were performed, through whole rock analysis by lithium borate fusion, using a Perkin Elmer ICP-OES/MSSPECTRO ARCOS/ELAN® 9000, respectively, following the LiBO2/LiB4O7 fusion and HNO3 digestion. The loss on ignition (LOI) was also measured at 1000°C using standard procedures.

3. RESULTS AND DISCUSSION

3.1 Mineralogy by PXRD

The bulk mineralogical composition of the studied laterite samples were initially investigated by means of conventional powder XRD (PXRD). X-ray diffraction (XRD) investigations were carried out to determine the mineral composition of the bulk laterite material and data recording was started at 3 and ended at 64 °2θ with a step size of 0.020 °2θ and a count time of 1 seconds per step for the bulk sample, and at 3 and ended at 24°2θ with a step size of 0.020 °2θ and a count time of 2 seconds per step for the clay fracture (< 2μm) sample. XRD analyzing of oriented specimens checked the 00l-spacing and the changing of this spacing that is caused after interlayer space saturation. Based on different minerals modification (Starkey et al., 1984; Moore and Reynolds, 1989), the minerals which were presented in oriented mount were identified.

The XRD patterns of the Ni-laterite samples are illustrated in Figures 36-43. On the basis of the PXRD patterns the studied samples contain mainly crystalline Fe-oxide/oxyhydroxide phases (hematite and goethite) and Ni-bearing (Mg-Fe)-phyllosilicates (mainly chlorite-group and serpentine-group minerals) as the major mineral components (Figs. 36-41). PXRD data showed that the Ni-Co-rich sample L, ocurring in the base of the deposit, contains also calcite and bassanite (Fig. 42). Furthermore, simultaneously to mineralogical composition of the raw materials, additional PXRD study was performed on a separated black phase of the sample L, the so called ‘asbolane’ (Fig. 43).

Christidis et al. (2010) thoroughly examined the clay fraction of laterites from central Greece, that they contain smectite, talc, chlorite, serpentine, goethite, hematite, and calcite. More specifically, they claimed that the clay fraction of samples from Agios Ioannis consists mainly of Fe-rich chlorite and Fe-smectite, talc with minor serpentine, hematite, goethite and calcite. In fact, smectite is believed to be a major mineralogical constituent of the Fe-Ni ores of the broader Lokris area (Christidis et al., 2010). Accordingly, Samouhos et al. (2019) presented data about the samples from Agios Ioannis consisting mainly of crystalline Fe^{3+}-oxide (hematite-like) and chlorite-group phyllosilicates, whereas, smectite, goethite, and calcite, were not identified in the LARCO GMMSA ore samples studied therein.

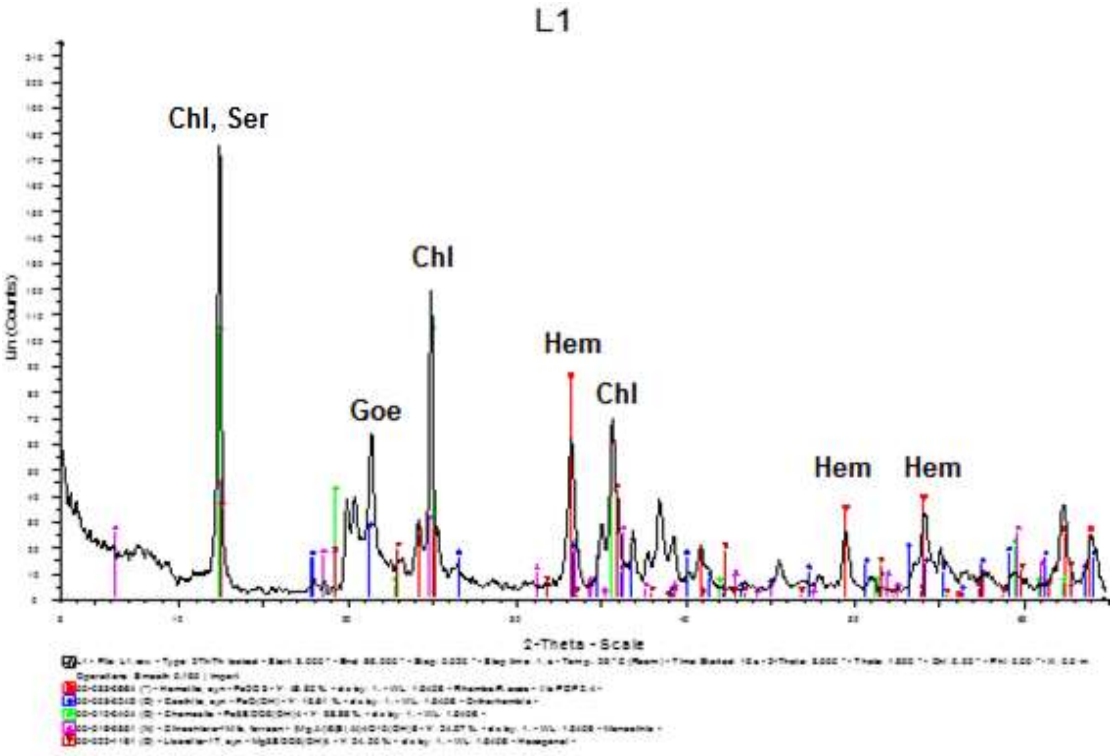

Figure 36. *PXRD pattern of the studied LARCO GMMSA Ni-laterite sample L_1, showing characteristic peaks for hematite (Hem), goethite (Goe), chlorite (Chl) and serpentine (Ser).*

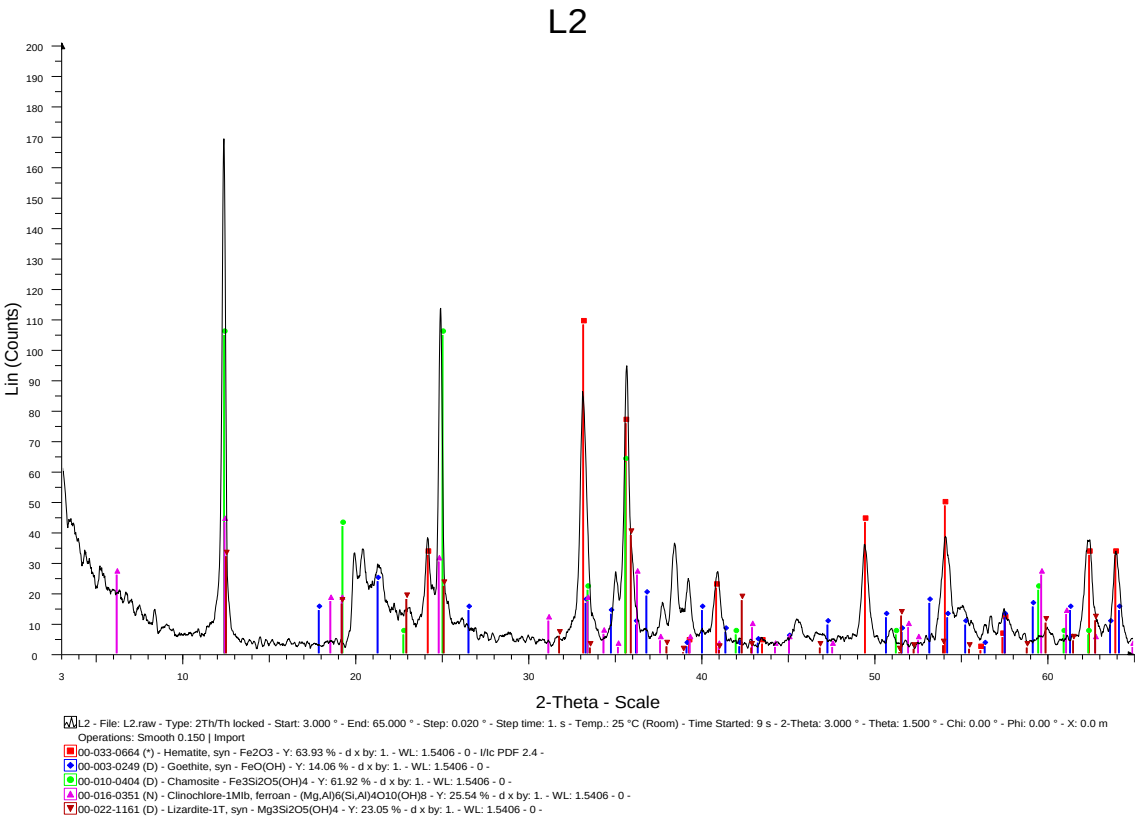

Figure 37. *PXRD pattern of the studied LARCO GMMSA Ni-laterite sample L_2, showing characteristic peaks for hematite (Hem), goethite (Goe), chlorite (Chl) and serpentine (Ser).*

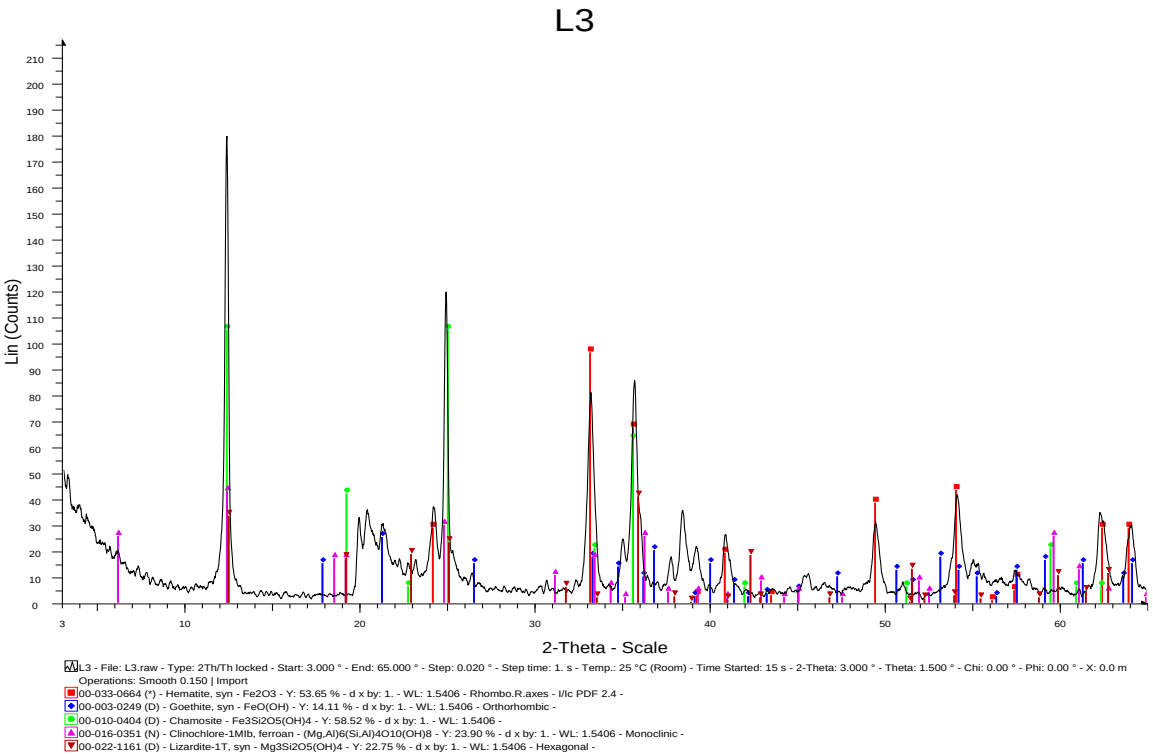

Figure 38. *PXRD pattern of the studied LARCO GMMSA Ni-laterite sample L_3, showing characteristic peaks for hematite (Hem), goethite (Goe), chlorite (Chl) and serpentine (Ser).*

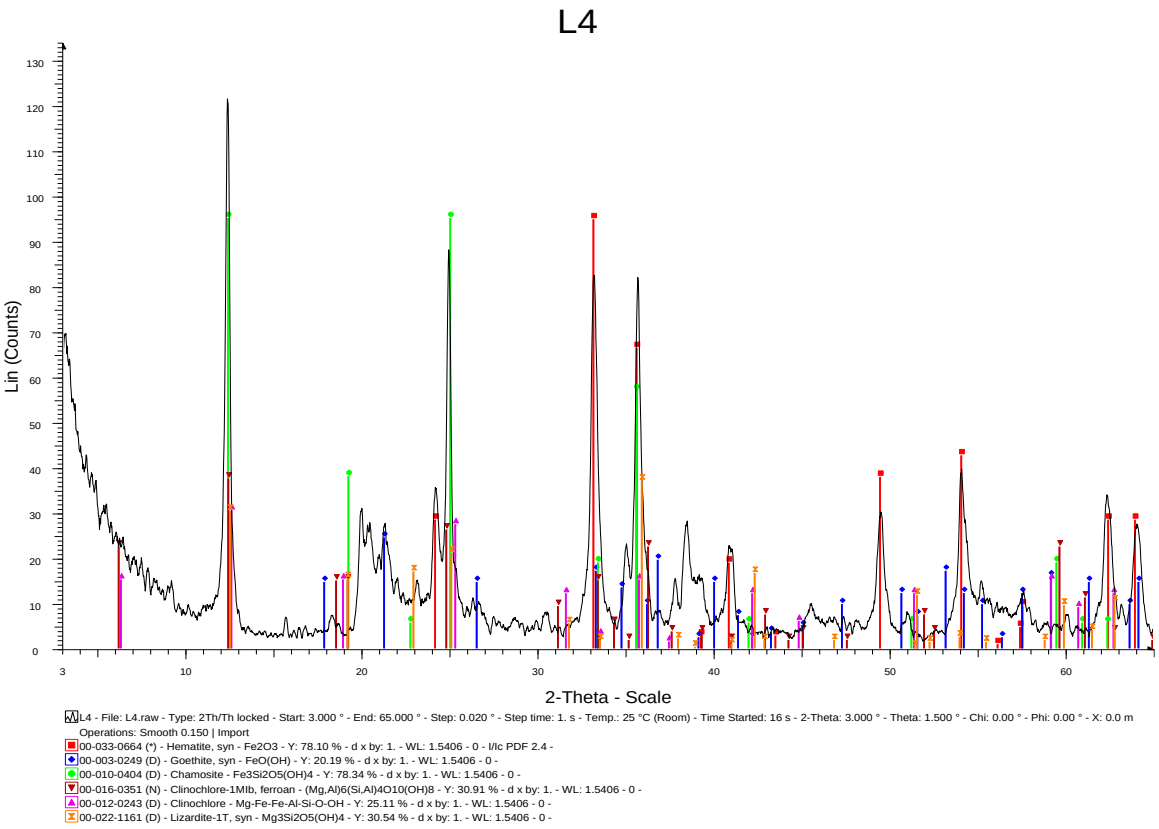

Figure 39. *PXRD pattern of the studied LARCO GMMSA Ni-laterite sample L_4, showing characteristic peaks for hematite (Hem), goethite (Goe), chlorite (Chl) and serpentine (Ser).*

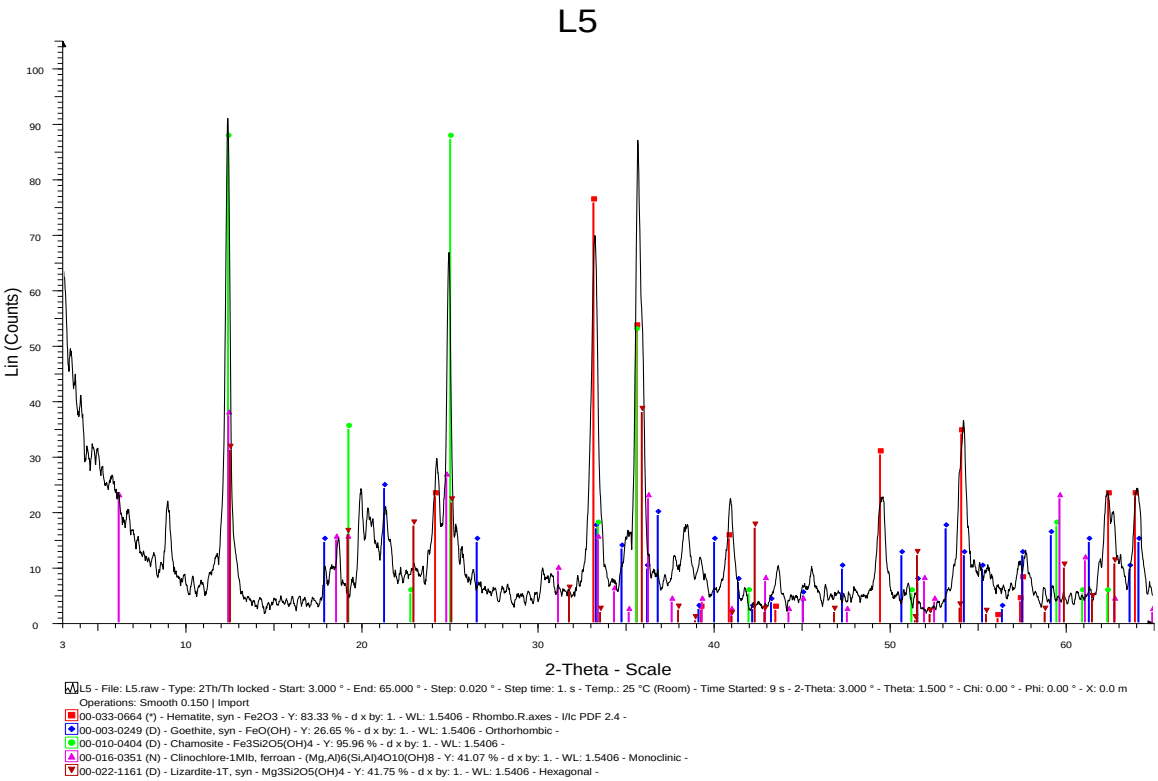

Figure 40. *PXRD pattern of the studied LARCO GMMSA Ni-laterite sample L_5, showing characteristic peaks for hematite (Hem), goethite (Goe), chlorite (Chl) and serpentine (Ser).*

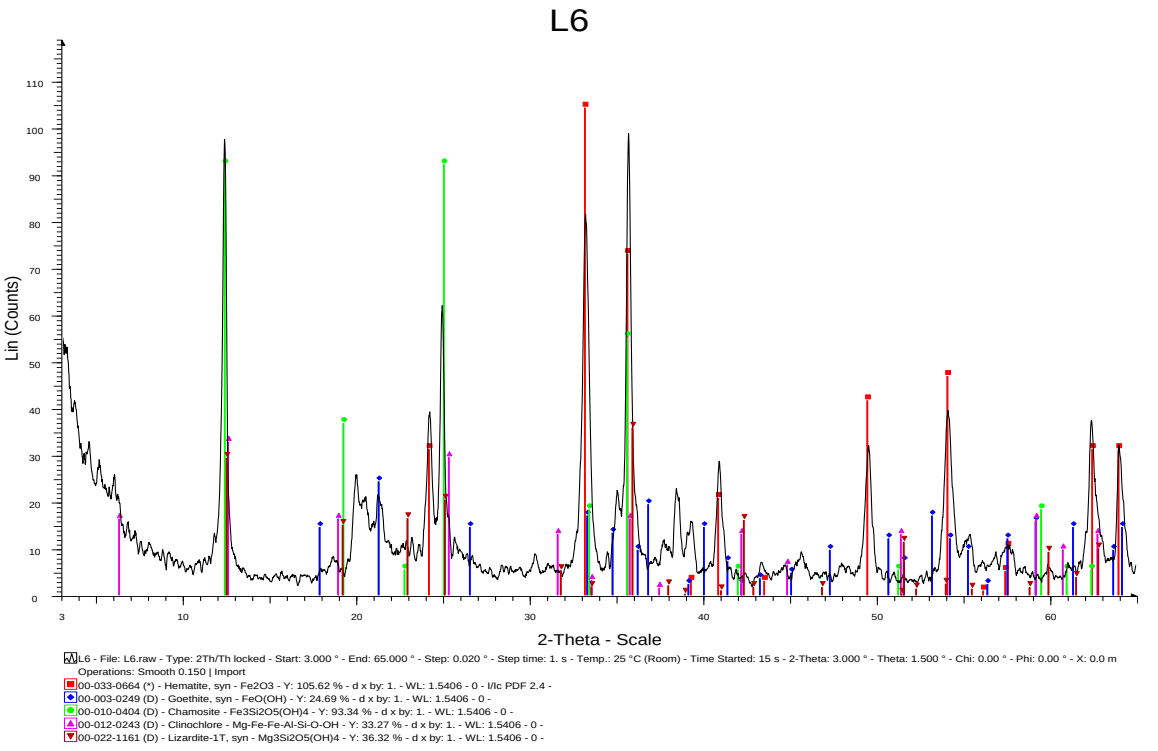

Figure 41. *PXRD pattern of the studied LARCO GMMSA Ni-laterite sample L_6, showing characteristic peaks for hematite (Hem), goethite (Goe), chlorite (Chl), and serpentine (Ser).*

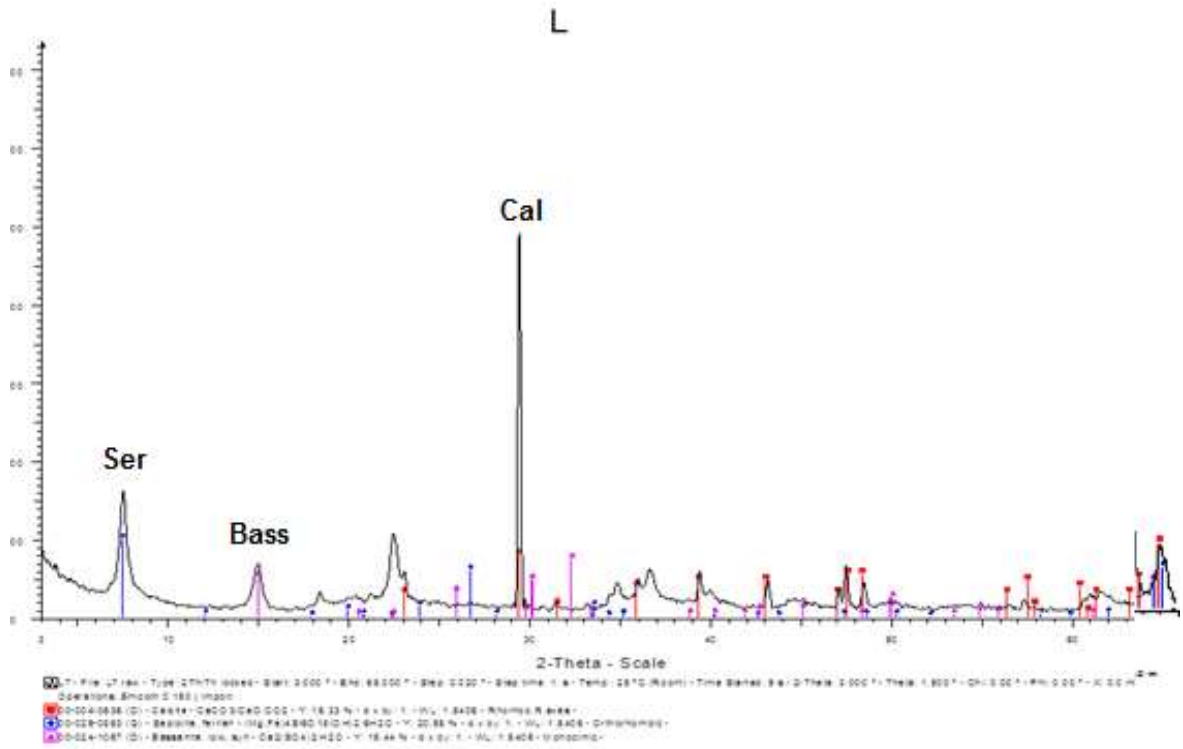

Figure 42. *PXRD pattern of the studied LARCO GMMSA Ni-laterite sample L, showing characteristic peaks for calcite (Cal), serpentine (Ser) and bassanite (Bass).*

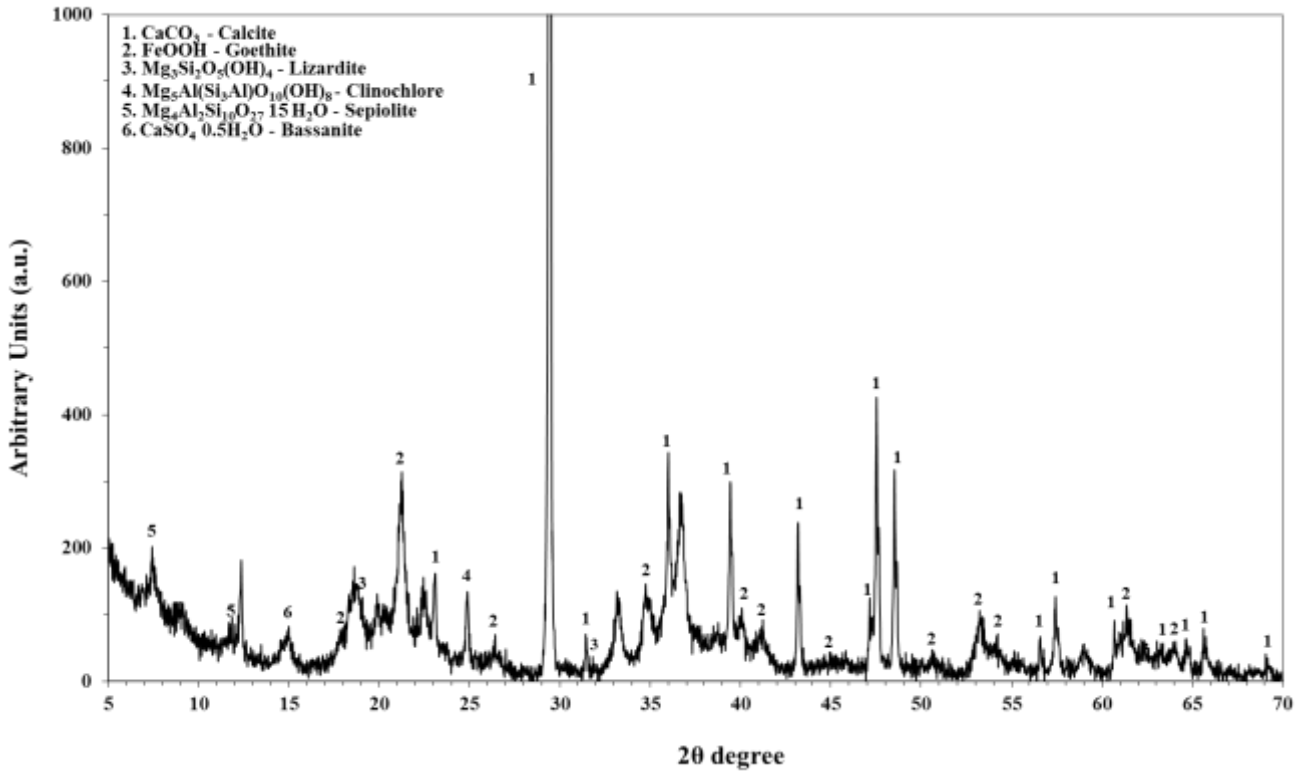

Figure 43. *PXRD pattern of the studied LARCO GMMSA Ni-laterite sample's L separated black phase.*

3.2 Microscopic study and analyses in microscale (SEM-EDS)

The SEM-EDS was used to examine the textural and morphological features as well as the chemical composition (semi-quantitative microanalyses) of the laterite material. The specimens were prepared by drying at room temperature and carbon coating.

The SEM-EDS study was performed to all samples, whereas emphasis was given to most Ni-Co-rich (according to bulk ICP-MS data; see text below) samples L_5 and L. In particular, that was performed to elucidate the nature of the Co-hosting phases inasmuch the PXRD study (see text above) showed Ni-phyllosilicates but no distinct crystalline Co-phases. The SEM images of the samples L_5 and L are shown in Figures 44-48 and 49-52, respectively. The SEM-EDS investigation of the sample L_5 revealed that the major phases are Ni-phyllosilicates and Fe-oxides (mainly hematite), together with traces of detrital (clastic) zircon ($ZrSiO_4$) hosting a part of the bulk Th, and detrital chromite (Cr-spinel). Accordingly, the microscale (SEM-EDS) data presented by Boskos et al. (1996), with regard to Evia Isl. Ni-laterite ore, have indicated that Cr, apart from detrital chromite (46 wt.% of Cr) is considered to be found in hematite by 35 wt.%. Moreover, the characterization using SEM-EDS proved the presence of REE-fluorocarbonates (mostly bastnaesite -type) and -phosphates (monazite and xenotime). The Ni content in hematite-like phase is insignificant, as it does not exceed 0.9 wt.%. Hematite-like phase also contains Cr (0.5-4 wt.%) and Co (1.3 wt.%), as already mentioned, along with Mn (0.3-0.9 wt.%), which does not correspond the typical chemical composition of the mineral.

More specifically, zircon is one of the most prevailing accessory minerals of magmatic, metamorphic and some metasomatic formations of different composition (Lesnov, 2013). As a consequence, the remarkable minor quantities of zircon, which is detectable in the mixed Fe-Si-Mg phase, in the form of detrital (clastic) grains indicates that zircon has been transferred from weathered parent rocks during the lateritization processes at low temperature. The presence of detrital zircons in the Ni-laterites in central Greece has already been reported (Valeton et al, 1987). A strong correlation is observed between Zr and U, Zr and Hf, and, especially the strong correlation between Zr and Th, implies the presence of Th into detrital zircon crystals.

The presence of detrital grains of chromite as well as various REE mineral phases in the Larymna laterite samples has already been reported by Kalatha et al. (2017). The characteristic appearance of detrital chromite micro-grains reveals the presence of a notable Cr enrichment in in the laterite lattice. The overall suggestion is that part of the chromite grains are to some extent altered towards Fe-chromites, whereas there are also rather unaltered grains which fall in the fields of Al chromite and Cr-spinel derived from Alpine-type peridotites (Fig. 45). In general, the presence of chromite grains or fragments is common in the Ni-laterite ores and consistent with contribution of clastic and chemical material from various ultramafic rock types. More specifically, it is a residual component inherited from the ophiolitic parent rocks. These rock types are members of ophiolite complexes, as itis well exemplified by laterites lying on karstified limestones of Triassic-Jurassic age Agios Ioannis area. However, it is rather difficult to conclude regarding the exact parent ophiolites. The high Mn-content of the chromite is a result of serpentinization in the presence of Mn-rich fluids, following lateritic weathering and finally Alpine low-grade metamorphism (Michailidis, 1990). Consequently, if the observed alteration is not exclusively related to primary higher P-T metamorphic processes (i.e., serpentinization), it can be due to transportation from

parent peridotites, or due to in-situ lateritic weathering in tropical climate conditions, or perhaps due to further diagenetic (in fact low-grade metamorphism) and later epigenetic processes. A combination of all above geochemical processes could also be very likely. Similar altered detrital chromites, which however fall into the field of typical Fe-chromite, have been reported in the case of Greek laterites (Michailidis et al., 1984; Valeton et al., 1987; Michailidis, 1990; Eliopoulos and Economou-Eliopoulos, 2000). In fact, different types of chromite fragments (fine or coarse grains of Al-rich or Cr-rich) derived from basic and ultrabasic rocks, have already been described in the Lokris Fe-Ni-laterites (Valeton et al., 1987; Alevizos, 1997; Eliopoulos and Economou-Eliopoulos, 2000). Accordingly, their wide compositional variation reflects contribution from a variety of rocks andmultistage deposition.

REE minerals (of diagenetic and/or epigenetic origin) detected by SEM-EDS, prior to LA-ICP-MS studies (see text below), are mostly REE -fluorocarbonates (mostly bastnaesite -type) and -phosphates (monazite and xenotime) (Fig. 46). Among the main factors controlling the REE content in laterites are the composition of the rock source, the duration of the lateralization process, the size of the ore bodies, the distance of the transportation, the pH and Eh conditions (Economou-Eliopoulos et al., 1997). The most frequent REE minerals in karstic deposits generally are members of the bastnaesite group, including: synchysite-(Nd), bastnaesite-(Ce) and bastnaesite-(Nd), hydroxylbastnaesite-(Nd,La) and hydroxylcarbonate-(Nd,La). The occurrence of REE-phosphates and alkaline earth phosphates, such as neodymian goyasite, monazite-(Nd) and monazite-(La) is relatively rare though (Maksimovic , 2010; Maksimovic et al., 1996). The bastnaesite-group minerals are among the most economically important ones, whereas their origin is related to late stages of magma evolution (Dostal et al., 2016). Xenotime, the major component of which is Y-orthophosphate, is also a phosphate ore and one of the valuable mineral deposits of REE similar to bastnaesite and monazite. Placer xenotime and monazite commonly contain high levels of Th and U in their crystal structures (Chakhmouradian et al., 2012). According to the literature (Samouhos et al., 2019; Kalatha et al., 2015; Kalatha et al., 2017), the REEs in Larymna laterite generally are mainly contained in fine (< 10μm) bastnaesite and hydroxyl-bastnaesite particles. Furthermore, the presence of REEs, at high concentrations, in phyllosilicates and Fe oxide phases cannot be excluded. The REE fluorocarbonate mineral aggregates in the Agios Ioannis laterite deposit might be considered authigenic (e.g., Bárdossy, 1982; Valeton, 1972; Valeton et al., 1987) and are related with the laterite weathering, which is an important process in the REE-enrichment in laterites (Eliopoulos et al., 2000; Alevizos, 1997; Albandakis, 1980; Valeton et al., 1987; Rosenberg et al., 1984; Maksimovic et al., 1993; Economou-Eliopoulos et al., 1997; Panto et al., 2001; Skarpelis, 2006; Kalatha et al., 2015; Goodenough, 2016). The presence of the authigenic hydroxylbastnaesite-(Nd) minerals has already been described at the Agios Ioannis, Lokris, mining area and specifically at the Nissi area deposits, which are located SSW of the Agios Ioannis deposit (Maksimovic et al., 1993; Panto et al., 2001). In fact, the REE minerals as identified by previous authors at the Nissi laterite deposits, have been described within black Mn-oxide assemblages and are dominated by bastnaesite, hydroxylcarbonate-(Nd,La) and hydroxylbastnaesite-(Nd,La) (Rosenberg et al., 1984; Panto et al., 2001). The enrichment of the REE at the Nissi (Patitira) bauxite laterite deposit in Lokris area, concentrated in bastnaesite-group minerals herein is thought to have been caused by long-term leaching and redeposition on karstified limestone, during a subsequent stage under alkaline conditions (Kalatha et al., 2017; Panto et al., 2001; Verplanck et al., 2016; Navrotsky et al., 2008). Marmeiko is another important laterite deposit in Greece, which is located in Lokris.

The deposit is hosted by Upper Jurassic-Lower Cretaceous limestone and contains bastnaesite and monazite as REE-bearing minerals (Economou-Eliopoulos et al., 1997). Furthermore, remarkable minor quantities of Ba (Fig. 48) and V (TEM-EDS study also depicted the occurrence of V; see text below) were detectable by means of SEM-EDS microscopic investigation.

The microscale by SEM-EDS study for the sample L, ocurring as thin layer in the base of the deposit, indicated a dominant 'Al-Si-Ni matrix', and therefore, combined PXRD (see text above) and SEM-EDS data indicated the occurrence of Ni-bearing-phyllosilicates (mainly chlorite-group minerals) (Fig. 51). The presence of chlorite-group minerals in the Larymna laterite samples has already been reported by Kalatha et al. (2017). Eliopoulos et al. (2000), using SEM-EDS, reported that chlorites in nickeliferous laterites from Larymna area contain ca. 0.1-8 wt.% Ni. Additionally, the microscale (SEM-EDS) data presented by Boskos et al. (1996), with regard to Evia Isl. Ni-laterite ore, have indicated that chlorite, comprising 78% of the material, is the main Ni-bearing mineral with ca. 4-5 wt.% NiO. Furthermore, Cr is considered to be found in chlorite by 12 wt.% (Boskos et al., 1996). According to Eliopoulos et al. (2000), who also examined by SEM-EDS bauxitic-laterites from Larymna area (Tsouka, Nissi), chlorites contain ca. 0.1-10 wt.% NiO, whereas Cr and Mn have also been reported to be present in the chemical composition of Ni-bearing phyllosilicates. Herein, the Ni content in the phyllosilicate structures varies (2-23 wt.%), whereas the EDS spectra confirmed additional the elevated presence of Mn (2-25 wt.%) and Co (0.3-19 wt.%). Scanning electron microscopy showed also that the phyllosilicate phases are characterized by minor quantities of Mg indicating a chlorite group-illite free phase.

However, in addition, the study in microscale by SEM-EDS revealed areas with a peculiar composition containing Al, Si, Mn, Ni, Co, Cr, V, and Ca; the latter one perhaps through interference by calcite (Fig. 52). More specifically, SEM-EDS indicated the dominance of a possibly amorphous/disordered Ni-Co-rich Mn-(oxy)hydroxide/oxide (hydrated), the so-called 'asbolane' by previous authors (Figs. 49 and 50). 'Asbolane', occurring as black and often amorphous thin intergrowths with Al-silicates as well as coatings on fractures and containing appreciable quantities of Fe, Ni, and Co, was also observed in samples from the lower transitional zone between laterite and the underlain limestone. Ni-bearing minerals, Mn-Co-Ni 'asbolane' and an unknown Al-Ni-silicate from the studied deposit have already been generally described (Eliopoulos et al., 2012; Baker et al., 2011; Eliopoulos et al., 2000; Alevizos, 1997; Albandakis, 1980; Valeton et al., 1987; Rosenberg et al., 1984; Maksimovic et al., 1993; Economou-Eliopoulos et al., 1997; Panto et al., 2001; Maksimovic, 1997), and more specifically, in the karstic Ni deposit of Larymna in Lokris area with hydrated halloysite (Maksimoviz, 1997; 2003). Finally, remarkable minor quantities of S, Ti and Cu were also detectable in the laterite matrix. Conclusively, concerning the mineralogy of LARCO GMMSA laterite at microscale (see text above), Ni-bearing hydrous silicates, particularly Ni-bearing Mg-Fe-phyllosilicates (mainly chlorite-group minerals), occur in mixture with Fe-oxides, which also contain Mn and Co. Therefore, detailed electron microscopic studies at the nanoscale (TEM-EDS) were additional performed to examine the above preliminary findings.

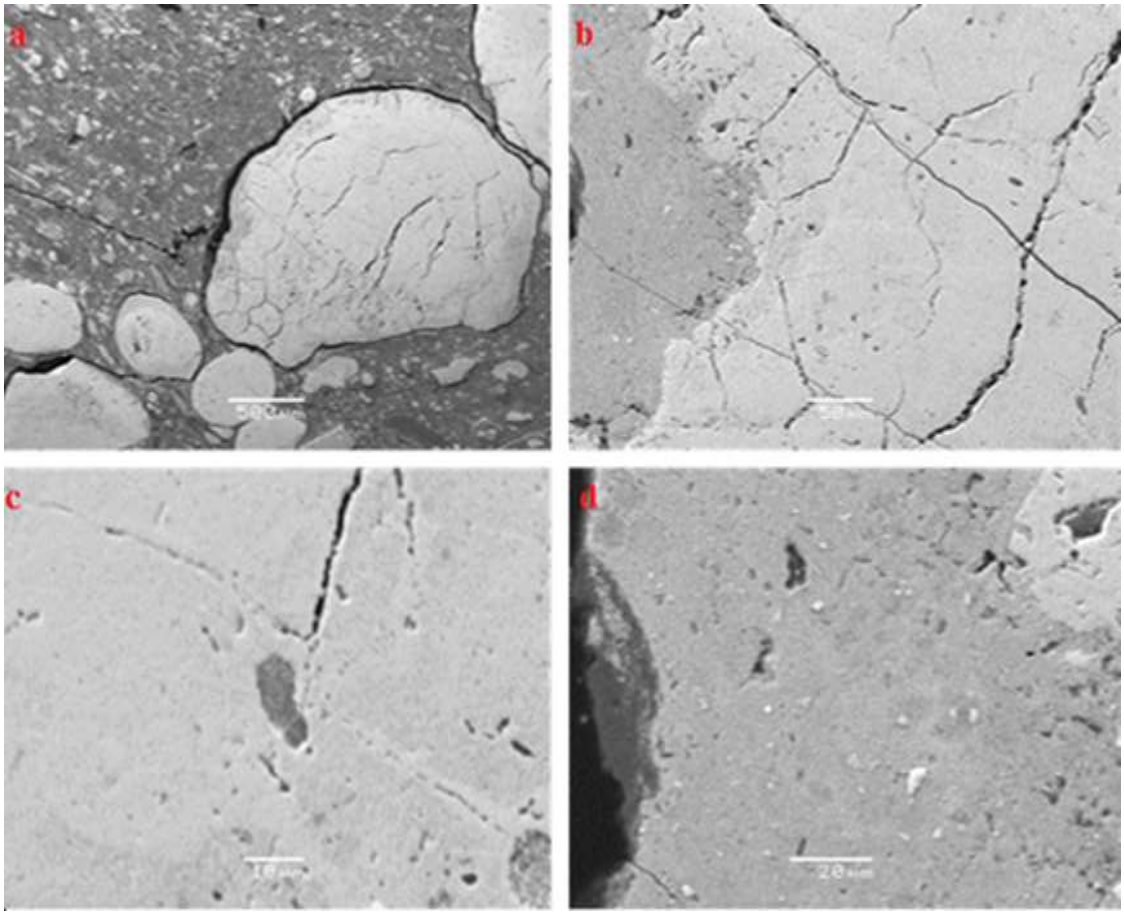

Figure 44. *Representative SEM images of the studied LARCO GMMSA laterite sample* L_5.

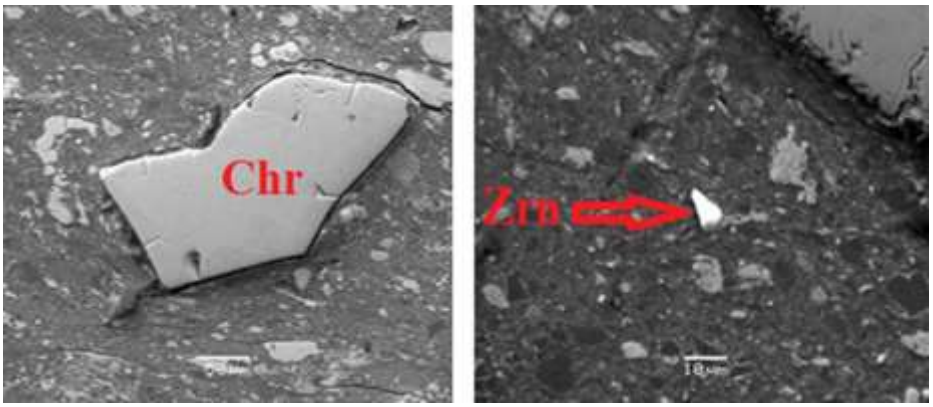

Figure 45. *SEM-EDS data for minor (detrital) mineral phases in polished section of the studied LARCO GMMSA laterite sample* L_5 *(left image: chromite; right image: zircon): 'chr' for chromite; 'zrn' for zircon.*

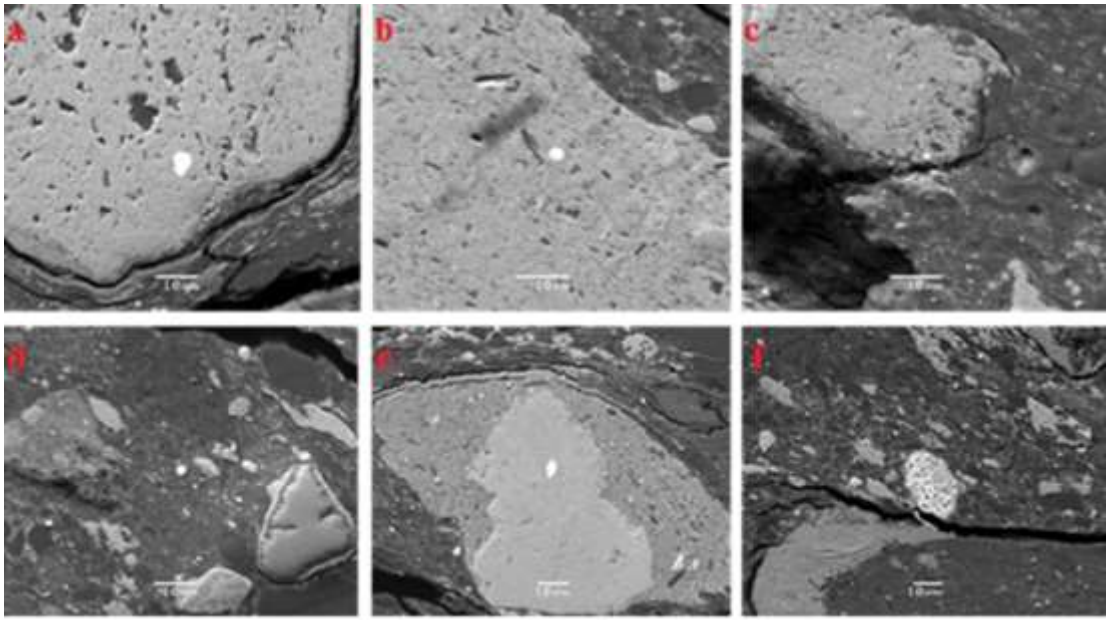

Figure 46. *Representative SEM images of the studied LARCO GMMSA laterite sample L_5, showing the occurrence of REE-minerals (white).*

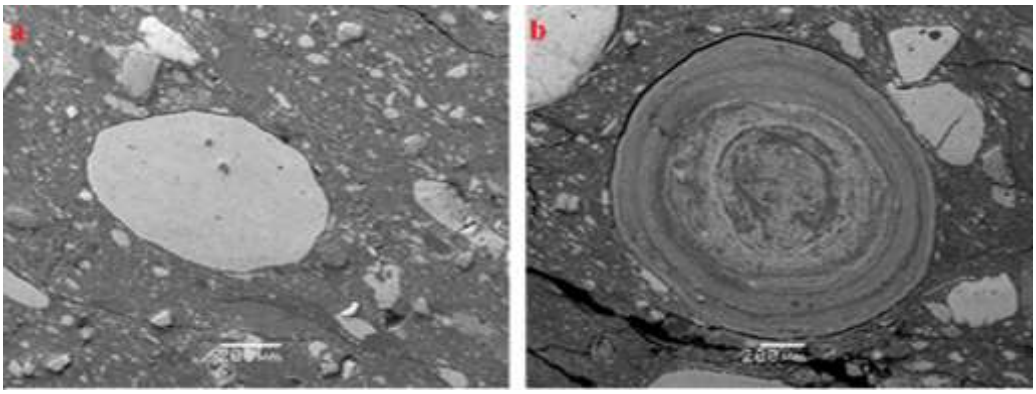

Figure 47. *SEM-EDS data for pisoliths into the studied LARCO GMMSA laterite sample L_5.*

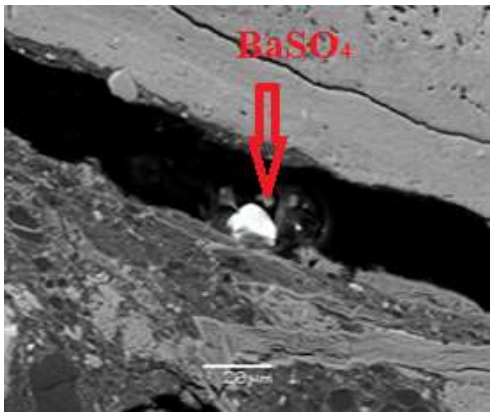

Figure 48. *SEM-EDS data for the presence of baryte ($BaSO_4$) in the studied LARCO GMMSA laterite sample L_5.*

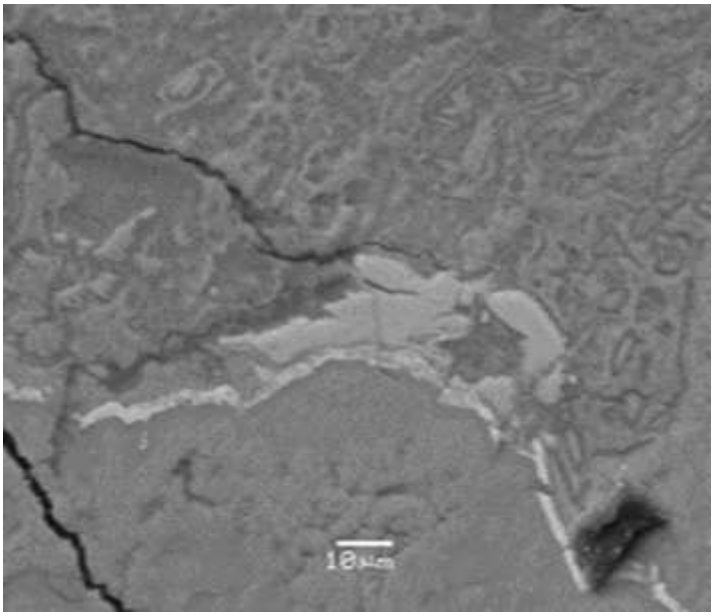

Figure 49. *Detailed SEM-EDS study on the studied LARCO GMMSA laterite sample L revealed the presence of an amorphous/disordered Ni-(Cr)-Co-bearing Mn-(oxy)hydroxide/oxide (hydrated) phase, the so-called 'asbolane' by previous authors.*

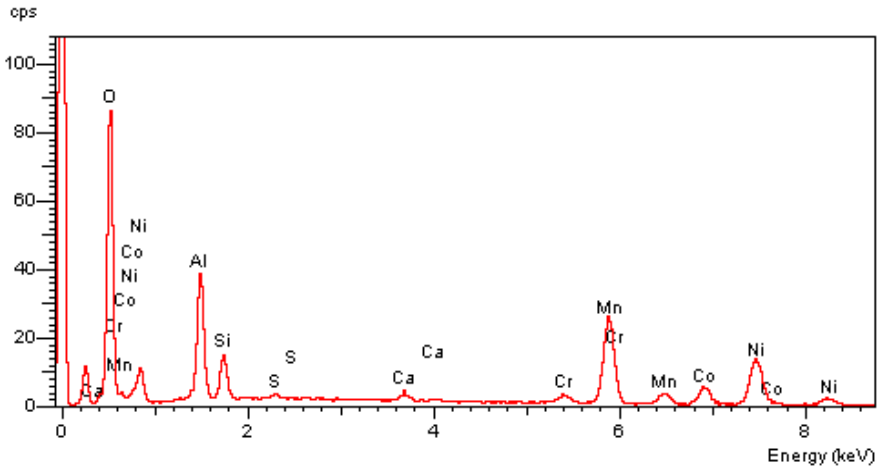

Figure 50. *EDS of the possibly amorphous/disordered Ni-(Cr-)Co-bearing Mn-(oxy)hydroxide/oxide (hydrated) phase, the so-called 'asbolane' by previous authors.*

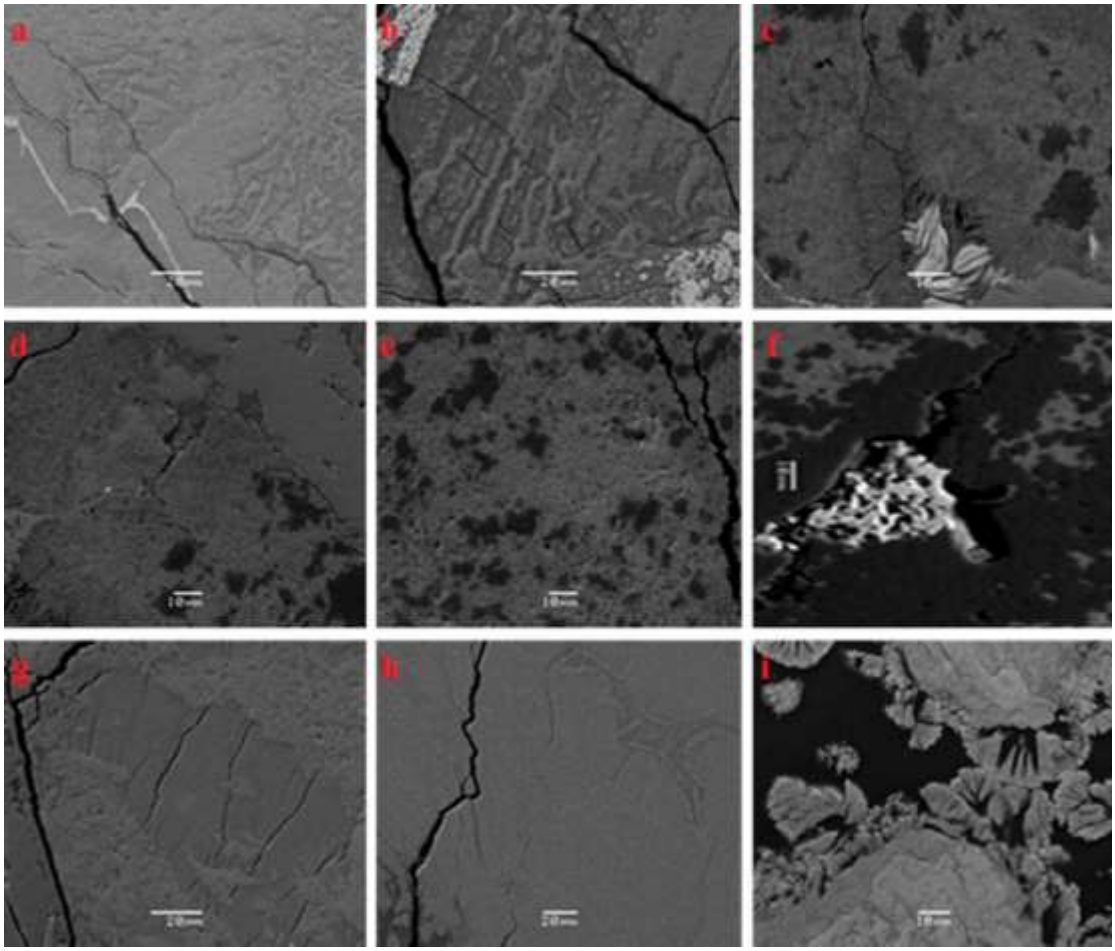

Figure 51. *Representative SEM images of the studied LARCO GMMSA sample L, showing micrograph of the mixed Al-S-Ni phase corresponding to chlorite-group minerals.*

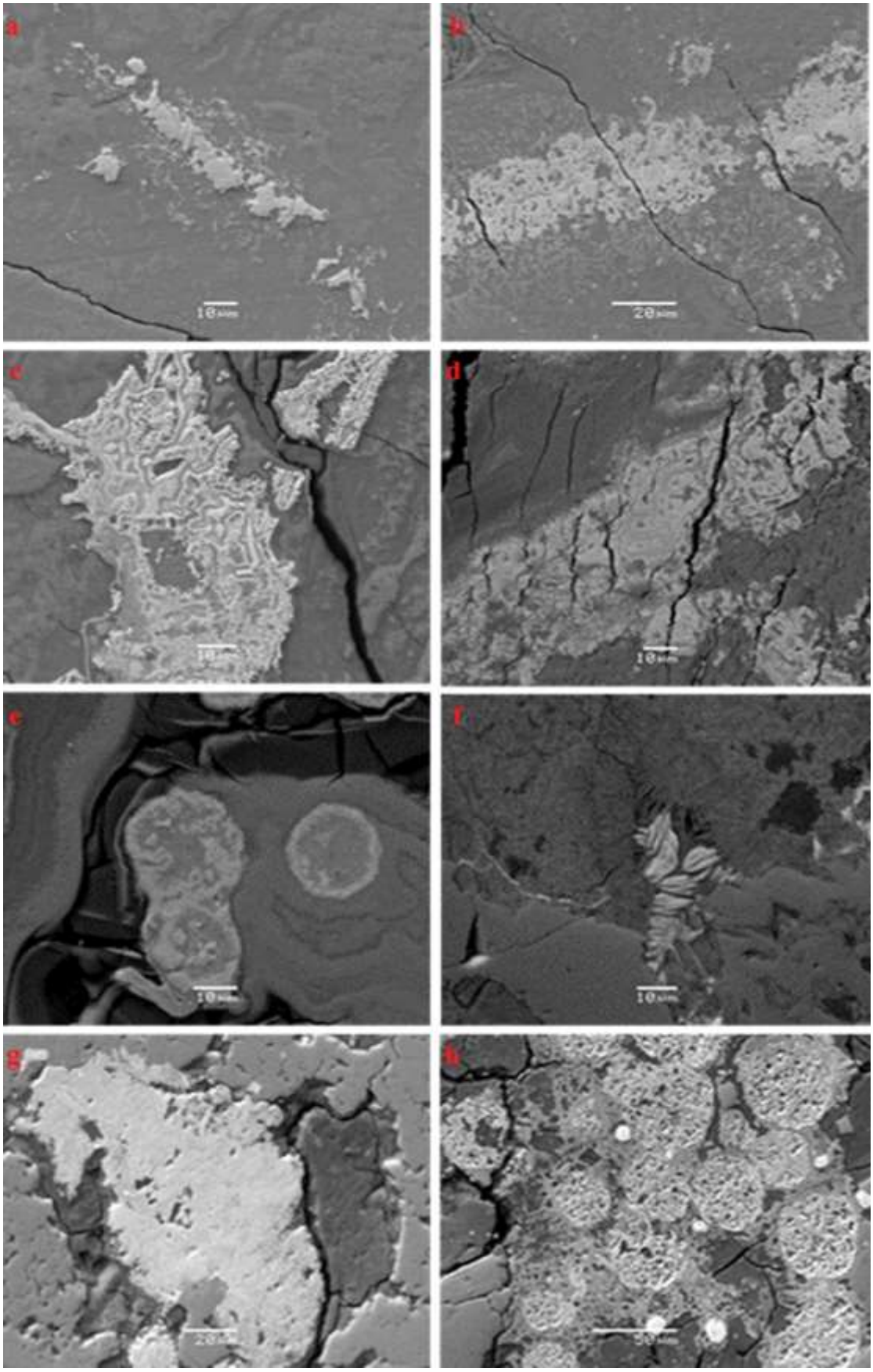

Figure 52. *SEM-EDS data for Al-Si-Mn-Ni-Co-Ca(-Cr) areas into the studied LARCO GMMSA sample L.*

3.3 Trace element analyses of Ni-phyllosilicate in microscale (LA-ICP-MS)

The LA-ICP-MS data about Co and other significant major and trace metals partitioning in Ni-laterite was complementary checked by applying on some selected Ni-phyllosilicate grains, separated from local inclusions into the ore and the thin green-black layer in the base of the deposit (sample L). The results shown in Table 2; Figures 53 and 54 (see below) confirmed the abundance of Ni concentration in the range of 17360-163900 ppm together with elevated Cr (311-444 ppm) and Cu (ca. 62-181 ppm). It is therefore demonstrated that Ni and Cr are associated exclusively with Ni-bearing phyllosilicate (chlorite-group) phases. Additionally, LA-ICP-MS analyses detected measurable quantities of Co (85-340 ppm), U (5-ca. 21 ppm) and Sc (11-ca. 56 ppm), as well as a minor quantity of V. This, in comparison with the SEM-EDS (see text above) and TEM-EDS (see text below) pattern implies, that the Co, U and Sc concentrations are mainly due to Fe- and Mn-(oxy)hydroxide/oxide (hydrated) phases. As for V, which is an element of increased importance in bauxite industry due to its involvement in red mud (Burke et al., 2013), it is most probably due to Fe-oxides, a fact that is in good agreement with the results from the literature, where V is commonly correlated with major elements such as MgO and Al_2O_3 (Huang et al., 2015). Finally, microscale investigation of sample L using LA-ICP-MS proved additional that REE and Yttrium (Y) (REY) occur as secondary/accessory fluorocarbonate mineral aggregates (mainly bastnaesite /monazite/xenotime-group minerals) and mostly due to Fe-(oxyhydr)oxides.

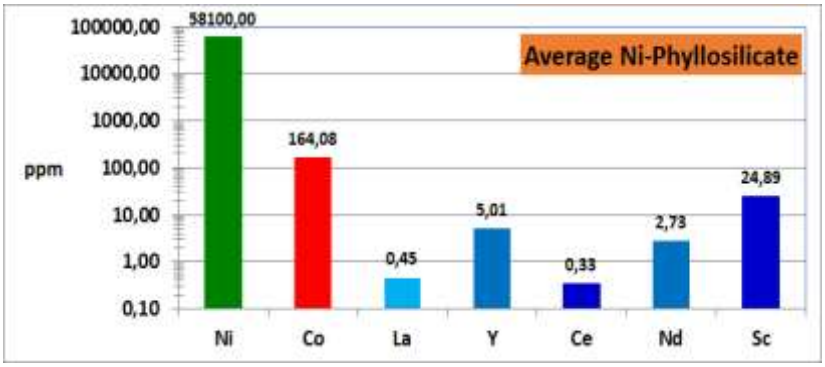

Figure 53. *Concentration of basic and critical metals in Ni-phyllosilicate from LARCO GMMSA laterite.*

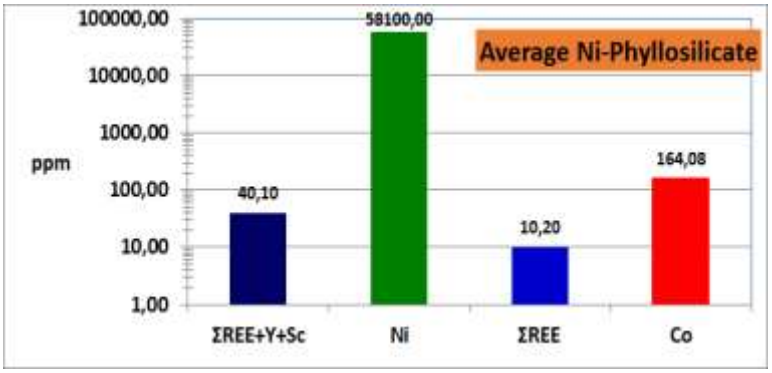

Figure 54. *Summary regarding concentration of basic and critical metals in Ni-phyllosilicate from LARCO GMMSA laterite.*

Table 2. *Trace element concentrations in Ni-phyllosilicate from LARCO GMMSA laterite.*

Description	Ni-phyllosilicate (ppm)															
	ppm	ppm	ppm	ppm	ppm	ppm	ppm	ppm	ppm	ppm	pp	ppm	ppm	ppm	ppm	AVERAGE (ppm)
Ti	4,8	1,96	1,79	1,64	1,33	0,76	0,68	3,36	2,76	2,51	2,4	2,08	1,92	0,5	1,76	2,02
Cr	539	311	290,7	385	416	391	356	317,4	317,4	343,9	311,2	397	444	390	432	376,11
Mn	17,3	8,4	8,31	49	7,26	40	7,1	4,3	3,8	6,8	5,5	5,6	29	5,52	6,11	13,60
Ca	1720	2000	2004	665	1117	533	619	3990	3660	3743	4230	4580	1099	508	1179	2109,80
Ni	163900	98900	88500	32900	53700	39000	28900	21970	22120	17360	21150	62300	93000	37900	89900	58100,00
Co	340	248,4	230,6	191	327	192,3	158	85,1	95,8	75,6	110,9	112,2	150,5	58,8	85	164,08
Y	9,5	7,3	7,11	2,46	4,01	2,162	2,33	4,04	3,962	4,091	4,28	6,97	6,76	2,98	7,16	5,01
La	2,01	0,424	0,435	0,272	0,337	0,212	0,233	0,35	0,311	0,353	0,363	0,584	0,377	0,197	0,359	0,45
V	0,575	0,13	0,143	0,179	0,183	0,053	0,098	0,154	0,115	0,118	0,123	0,208	0,202	0,065	0,128	0,16
Nd	7,49	3,79	3,7	1,719	2,13	1,363	1,5	1,508	1,504	1,66	1,751	3,16	4	1,893	3,79	2,73
Ce	1,57	0,642	0,691	0,313	0,26	0,209	0,245	0,072	0,0488	0,07	0,072	0,322	0,197	0,133	0,1213	0,33
Zr	0,81	0,2	0,16	1,53	0,55	0,67	0,21	0,163	0,074	0,25	0,088	0,19	0,26	0,0523	0,157	0,36
Cu	212	112,5	103,2	140,7	181,2	123,4	89,7	75,2	81,1	74,4	84,1	134,4	136,8	61,6	79,7	112,67
Sc	55,6	30,88	27,98	12,18	21,16	13,15	11,1	25,9	27,82	25,27	26,92	25,26	31,37	13,19	25,6	24,89
Pr	1,291	0,491	0,47	0,267	0,298	0,201	0,233	0,22	0,214	0,243	0,26	0,473	0,458	0,239	0,447	0,39
Pb	0,357	0,118	0,186	0,21	0,21	0,109	0,103	0,292	0,293	0,39	0,368	0,539	0,165	0,108	0,185	0,24
Gd	2,66	1,89	1,762	0,685	1,023	0,611	0,613	0,999	0,959	1,053	1,081	1,8	2,3	0,972	2,27	1,38
Dy	2,39	1,711	1,646	0,598	0,833	0,47	0,531	0,882	0,911	0,862	1,004	1,55	1,634	0,69	1,717	1,16
Sr	3,08	8,26	8,26	1,34	2,69	1,097	1,72	21	19,98	19,42	20,24	9,48	7,36	3,04	10,59	9,17
Sm	3,24	2,08	1,93	0,845	1,119	0,634	0,715	0,921	0,887	0,897	1,006	1,79	2,44	1,005	2,32	1,46
Er	1,47	0,859	0,835	0,314	0,465	0,269	0,254	0,466	0,474	0,486	0,522	0,841	0,771	0,334	0,812	0,61
Yb	1,73	0,834	0,872	0,333	0,489	0,309	0,311	0,587	0,547	0,598	0,596	0,932	0,712	0,327	0,764	0,66
Ba	5,55	41,7	42,8	4,97	12,83	3,26	8,17	154,5	149,9	136,2	136,4	28,4	42	16,35	58,5	56,10
Nb	0,055	0,009	0,012	0,025	0	0	0,02	0,0072	0	0,0115	0	0,0041	0,0059	0	0	0,02
Th	0,182	0,0204	0,0219	0,045	0,0398	0,0187	0,0214	0,072	0,0618	0,0453	0,0462	0,0664	0,0373	0,0296	0,084	0,05
Ho	0,454	0,32	0,291	0,115	0,167	0,0905	0,1013	0,18	0,176	0,1612	0,182	0,286	0,29	0,124	0,309	0,22
Eu	0,783	0,566	0,549	0,24	0,294	0,182	0,188	0,294	0,262	0,282	0,298	0,487	0,66	0,283	0,673	0,40
Tb	0,419	0,291	0,273	0,1056	0,167	0,0808	0,097	0,156	0,154	0,1522	0,158	0,267	0,306	0,131	0,318	0,21
Be	12,63	2,85	2,78	1,6	2,73	1,61	1,36	4,11	3,89	4,13	3,85	3,38	2,4	1,36	2,48	3,41
U	57	15,37	15,79	5,93	11,25	5,31	5,01	11,5	12,22	10,37	11,57	8,74	16,07	7,75	20,84	14,31
Hf	0,021	0,0063	0,0031	0,067	0,017	0,0028	0,015	0,041	0,0048	0,0097	0,0053	0,0085	0,032	0,0062	0,0113	0,02
Tm	0,236	0,139	0,132	0,0528	0,079	0,0444	0,0435	0,0873	0,0773	0,0773	0,0817	0,138	0,1098	0,047	0,1111	0,10
Rb	0,24	0,1	0,09	0,065	0,094	0,039	0,073	0,284	0,256	0,303	0,274	0,177	0,089	0,042	0,121	0,15
Lu	0,267	0,137	0,12	0,0614	0,0833	0,0468	0,0435	0,086	0,0912	0,0814	0,0894	0,156	0,107	0,0478	0,1186	0,10
Ta	0,0038	0,0041	0,0045	0,018	0,0061	0,0022	0,0043	0,0092	0,00082	0,0023	0,00131	0,0014	0,0022	0,0013	0,0011	0,00
Cs	0,0193	0	0,0085	0,02	0	0	0	0,03	0,0193	0,0279	0,0254	0,0098	0	0	0	0,02
Li	46,4	23,69	21,21	26	57	29,91	23,5	37,14	37,57	32,15	34,44	43,5	49,5	26,2	106,9	39,67

Table 3. *The error as 2SE concerning LA-ICP-MS in Ni-phyllosilicate from LARCO GMMSA laterite.*

Description	SE														
Ti	0,7	0,4	0,39	0,63	0,33	0,35	0,41	0,5	0,36	0,34	0,35	0,57	0,39	0,23	0,34
Cr	25	11	9,6	17	20	11	10	8	5,9	8	7,7	16	13	14	13
Mn	1,2	1,6	0,77	13	0,7	12	2	1,7	1,2	1,5	1,3	1,1	2,8	0,37	0,95
Ca	86	48	60	84	41	29	57	110	72	91	130	140	36	25	64
Ni	7500	2800	3000	1300	1400	1500	3300	590	680	530	720	2000	2500	1100	3400
Co	21	6,3	7,5	11	10	7,4	18	3,1	3,1	2,2	3,6	4,6	4,2	2,1	3,5
Y	0,47	0,18	0,2	0,1	0,13	0,061	0,2	0,1	0,096	0,084	0,11	0,27	0,16	0,1	0,32
La	0,11	0,023	0,02	0,022	0,024	0,016	0,021	0,029	0,017	0,018	0,018	0,031	0,021	0,017	0,019
V	0,085	0,031	0,03	0,054	0,037	0,024	0,034	0,099	0,033	0,026	0,027	0,076	0,039	0,025	0,034
Nd	0,44	0,18	0,14	0,092	0,13	0,092	0,1	0,085	0,078	0,1	0,097	0,16	0,17	0,093	0,18
Ce	0,084	0,035	0,033	0,032	0,021	0,02	0,065	0,019	0,0065	0,014	0,025	0,021	0,02	0,016	0,0098
Zr	0,45	0,22	0,13	0,77	0,43	0,7	0,15	0,073	0,011	0,33	0,022	0,032	0,2	0,0091	0,018
Cu	10	3	4,1	3,9	5,9	4,6	7,6	2,2	2,8	2,3	3,1	4,8	4,2	2,6	2,9
Sc	1,9	0,65	0,86	0,41	0,64	0,39	1,1	0,57	0,54	0,48	0,61	0,95	0,76	0,39	0,91
Pr	0,091	0,022	0,021	0,019	0,021	0,012	0,023	0,016	0,015	0,012	0,015	0,022	0,018	0,014	0,025
Pb	0,078	0,023	0,092	0,11	0,15	0,03	0,028	0,048	0,035	0,11	0,092	0,099	0,035	0,031	0,054
Gd	0,3	0,11	0,092	0,066	0,073	0,057	0,068	0,074	0,062	0,055	0,065	0,11	0,14	0,082	0,13
Dy	0,15	0,083	0,091	0,041	0,052	0,043	0,061	0,057	0,047	0,055	0,047	0,11	0,076	0,049	0,093
Sr	0,059	0,028	0,021	0,02	0,018	0,016	0,032	0,031	0,024	0,024	0,026	0,028	0,018	0,015	0,022
Sm	0,21	0,14	0,11	0,067	0,082	0,061	0,067	0,077	0,056	0,063	0,059	0,11	0,11	0,071	0,13
Er	0,11	0,045	0,042	0,026	0,03	0,021	0,034	0,032	0,028	0,028	0,032	0,053	0,05	0,032	0,053
Yb	0,21	0,065	0,071	0,039	0,033	0,029	0,038	0,054	0,041	0,053	0,05	0,077	0,058	0,033	0,065
Ba	0,67	1,2	1,3	0,35	0,66	0,21	0,88	4,3	4,5	3,2	3,5	1,2	1,2	0,77	2
Nb	0,042	0,01	0,012	0,014	0	0	0,022	0,0058	0	0,0095	0	0,0033	0,004	0	0
Th	0,034	0,0043	0,0038	0,019	0,0066	0,0041	0,0061	0,015	0,0078	0,0053	0,0063	0,0072	0,0053	0,005	0,011
Ho	0,038	0,017	0,017	0,012	0,015	0,0078	0,0098	0,014	0,013	0,0091	0,011	0,018	0,015	0,011	0,018
Eu	0,048	0,026	0,032	0,021	0,022	0,017	0,026	0,023	0,017	0,021	0,021	0,032	0,032	0,022	0,041
Tb	0,044	0,016	0,014	0,0083	0,013	0,0084	0,013	0,014	0,01	0,0094	0,012	0,02	0,016	0,011	0,02
Be	0,71	0,26	0,2	0,17	0,27	0,15	0,17	0,33	0,22	0,26	0,26	0,34	0,19	0,16	0,25
U	2,6	0,44	0,53	0,29	0,4	0,2	0,6	0,37	0,37	0,21	0,29	0,28	0,4	0,36	0,72
Hf	0,015	0,0052	0,0023	0,07	0,01	0,0028	0,0088	0,035	0,0027	0,0043	0,003	0,0044	0,02	0,0035	0,0057
Tm	0,041	0,01	0,01	0,0066	0,011	0,0067	0,008	0,0097	0,007	0,0065	0,0063	0,012	0,0099	0,0054	0,0096
Rb	0,059	0,028	0,021	0,02	0,018	0,016	0,032	0,031	0,024	0,024	0,026	0,028	0,018	0,015	0,022
Lu	0,043	0,013	0,01	0,0092	0,0091	0,0062	0,0071	0,011	0,009	0,0071	0,0069	0,014	0,01	0,0053	0,0093
Ta	0,004	0,004	0,0031	0,012	0,0049	0,0026	0,0039	0,0065	0,00086	0,0015	0,00097	0,0015	0,0016	0,0013	0,001
Cs	0,0097	0	0,005	0,013	0	0	0	0,018	0,0052	0,0066	0,0058	0,0062	0	0	0
Li	2,3	0,83	0,83	1,1	2	0,99	3,2	0,91	0,84	0,68	0,67	1,7	1,3	1,3	5,4

Table 4. *The limit of detection concerning LA-ICP-MS in Ni-phyllosilicate from LARCO GMMSA laterite.*

Description	LOD														
Si	430	310	270	290	260	320	310	300	250	250	250	360	290	220	240
Ti	0,66	0,5	0,46	0,35	0,41	0,44	0,48	0,46	0,35	0,36	0,35	0,49	0,49	0,5	0,48
Cr	0,64	0,47	0,37	0,34	0,41	0,34	0,41	0,38	0,42	0,39	0,43	0,51	0,4	0,42	0,41
Mn	0,36	0,25	0,24	0,18	0,22	0,21	0,19	0,19	0,19	0,23	0,19	0,22	0,22	0,21	0,23
Ca	41	24	18	22	21	20	21	24	24	22	18	26	20	21	25
Ni	0,23	0,2	0,49	0,13	0,12	0,14	0,14	0,15	0,14	0,13	0,13	0,18	0,18	0,17	0,15
Co	0,069	0,049	0,04	0,038	0,039	0,041	0,042	0,047	0,05	0,041	0,043	0,051	0,042	0,041	0,036
Y	0,0052	0,0042	0,0034	0,0032	0,0032	0,004	0,0043	0,0049	0,0025	0,0041	0,0037	0,0039	0,0038	0,0041	0,0037
La	0,00076	0,0013	0,0011	0,0012	0,00049	0,00049	0,00045	0,0005	0,0011	0,00076	0,001	0,0016	0,0022	0,0013	0,0012
V	0,088	0,061	0,05	0,044	0,042	0,042	0,048	0,045	0,036	0,047	0,04	0,055	0,046	0,044	0,053
Nd	0,0063	0,0062	0,0037	0,002	0,0023	0,0023	0,0036	0,0041	0,0069	0,002	0,0059	0,0045	0,0085	0,0072	0,0041
Ce	0,0014	0,0014	0,0014	0,0014	0,0014	0,0014	0,0014	0,0014	0,0014	0,0014	0,0014	0,0014	0,0014	0,0014	0,0014
Zr	0,0045	0,0023	0,0037	0,0044	0,0039	0,0035	0,0032	0,0021	0,0018	0,0041	0,0041	0,0045	0,0046	0,0032	0,003
Cu	0,3	0,26	0,18	0,2	0,16	0,21	0,21	0,18	0,17	0,18	0,18	0,2	0,24	0,18	0,19
Sc	0,12	0,07	0,073	0,062	0,066	0,06	0,062	0,062	0,059	0,062	0,055	0,076	0,077	0,078	0,048
Pr	0,0015	0,001	0,0013	0,0011	0,0011	0,0013	0,0017	0,0015	0,0016	0,0012	0,0017	0,0011	0,0011	0,0018	0,0016
Pb	0,015	0,0091	0,0073	0,0067	0,0086	0,0077	0,0073	0,0079	0,0071	0,0072	0,0065	0,0088	0,0082	0,0098	0,0083
Gd	0,0067	0,0028	0,0039	0,0036	0,0059	0,0024	0,0022	0,01	0,0038	0,0038	0,0037	0,0082	0,0072	0,0065	0,0025
Ga	0,04	0,033	0,024	0,024	0,026	0,023	0,023	0,025	0,028	0,03	0,029	0,031	0,035	0,031	0,027
Dy	0,0042	0,0065	0,0034	0,0022	0,0015	0,0037	0,0067	0,0016	0,0014	0,0024	0,0032	0,0018	0,0016	0,0014	0,0028
Sr	0,0052	0,0025	0,0024	0,0029	0,0022	0,0019	0,001	0,0016	0,0018	0,002	0,0014	0,0022	0,0029	0,0027	0,0034
Sm	0,027	0,017	0,018	0,014	0,015	0,017	0,014	0,013	0,014	0,015	0,015	0,013	0,022	0,014	0,017
Er	0,0017	0,0013	0,0025	0,0016	0,0011	0,0011	0,0018	0,0011	0,001	0,0017	0,0017	0,0022	0,005	0,0017	0,002
Yb	0,0035	0,0062	0,0082	0,002	0,0055	0,008	0,0021	0,0023	0,0021	0,0021	0,0035	0,0026	0,004	0,0036	0,0042
Ba	0,011	0,011	0,004	0,0036	0,0098	0,0099	0,0091	0,0073	0,0038	0,012	0,0037	0,011	0,016	0,0038	0,0042
Nb	0,0035	0,0036	0,0041	0,0041	0,0044	0,0055	0,0042	0,0031	0,0026	0,0032	0,0034	0,0029	0,0057	0,0028	0,0033
Th	0,00072	0,00054	0,00045	0,00041	0,00046	0,00047	0,00042	0,00048	0,00043	0,00042	0,00042	0,00054	0,00048	0,00044	0,00048
Ho	0,00058	0,001	0,00036	0,00055	0,00064	0,00037	0,00034	0,00038	0,00059	0,00081	0,00034	0,00043	0,0014	0,00059	0,00095
Eu	0,0019	0,0013	0,0016	0,0014	0,00068	0,0017	0,0024	0,0017	0,0011	0,00062	0,001	0,00079	0,0012	0,0011	0,0013
Tb	0,00097	0,00041	0,00097	0,00072	0,00061	0,00062	0,00095	0,00036	0,00056	0,00077	0,00054	0,0014	0,00037	0,00056	0,00037
Be	0,055	0,045	0,053	0,027	0,028	0,04	0,049	0,032	0,025	0,025	0,028	0,032	0,028	0,021	0,049
U	0,00067	0,0005	0,00042	0,00038	0,00043	0,00043	0,0004	0,00044	0,0004	0,00068	0,00039	0,0015	0,00045	0,00041	0,00079
Hf	0,0018	0,0014	0,0011	0,0011	0,002	0,0012	0,0019	0,0012	0,0011	0,0011	0,0011	0,0024	0,0021	0,0019	0,0022
Tm	0,0034	0,0019	0,002	0,001	0,0015	0,0022	0,0015	0,0021	0,0018	0,0018	0,0015	0,0022	0,0024	0,0019	0,0011
Rb	0,036	0,027	0,024	0,024	0,026	0,022	0,024	0,029	0,028	0,023	0,026	0,03	0,028	0,026	0,025
Lu	0,001	0,00043	0,00036	0,0013	0,00064	0,00065	0,00034	0,00093	0,00059	0,00033	0,00079	0,00074	0,00039	0,00035	0,00068
Ta	0,00061	0,00045	0,00089	0,00058	0,00039	0,00039	0,00062	0,0004	0,00037	0,00061	0,00035	0,00045	0,00096	0,0012	0,00072
Cs	0,012	0,0089	0,0062	0,0069	0,0087	0,0069	0,0075	0,007	0,0079	0,0065	0,0067	0,009	0,0087	0,0075	0,0093
Li	0,16	0,14	0,11	0,11	0,12	0,15	0,12	0,15	0,11	0,12	0,11	0,13	0,13	0,13	0,11

3.4 Solid-state Fe speciation of Ni-phyllosilicate

The redox chemistry of Fe plays a major role in the geochemical cycling of many major as well as trace elements. Mössbauer spectroscopy is one of the few techniques, which can quantify the proportions of Fe^{2+} and Fe^{3+} in both crystalline and amorphous materials. In fact, it is ideal for the identification of Fe^{2+} and Fe^{3+} mineral phases (Fig. 55; Dyar et al., 2006), and, generally, for the determination of the Fe solid-state speciation. Because iron has two common oxidation states (ferrous and ferric), and a ferric ion shows two common coordination numbers (fourfold and sixfold), the crystallization of Fe-silicates and Fe-containing phyllosilicates is complex and difficult to control (Mizutani et al., 1991). Mössbauer spectroscopy has been used in mineralogical, petrological, and geochemical studies, and most of these applications concern the 14.4 keV ^{57}Fe Mössbauer effect. Studies on silicate minerals have demonstrated the applicability of this technique to the investigation of the oxidation states and site population of iron and the identification of iron-bearing minerals. Mössbauer spectroscopy can also be applied to characterize more complicated geological materials, such as multiphase assemblages, for mineralogical identification, determination of the Fe^{3+}/Fe^{2+} ratio, and the semiquantitative analysis of iron distribution in each mineral and lattice site (Bancroft 1973). Mizutani et al. (1991) studied the copolymerization reaction of transition metal ions (Mn, Fe, Co, and Ni) and silicic acid under alkaline conditions, and found that iron and Ni ions gave distinctly crystallized phyllosilicates, whereas Mn and Co ions gave poorly crystallized products. The selective synthesis of iron phyllosilicates was accomplished by controlling the metal ion-to-silicon ratio and hydroxide ion-to-metal ion ratio in the starting mixtures. The oxidation state and coordination number of the iron in the reaction products are based on Mössbauer spectroscopic studies (Mizutani et al., 1991).

Though Greek laterite is a quite important industrial material, the number of publications dealing with the characterization by ^{57}Fe Mössbauer spectroscopy is absent in the literature. Therefore, the Mössbauer data presented herein absolutely concern the very first study that attempts to address Mössbauer investigation of LARCO GMMSA industrial laterites. Mössbauer spectroscopy results, concernig selected Ni-phyllosilicate grains, separated from local inclusions into the ore and the thin green-black layer in the base of the deposit (sample L) are represented in Figures 56-58. Based on these results, the investigation of the two samples using ^{57}Fe Mössbauer spectroscopy revealed that Fe occurs completely as Fe^{3+} due to hematite and goethite.

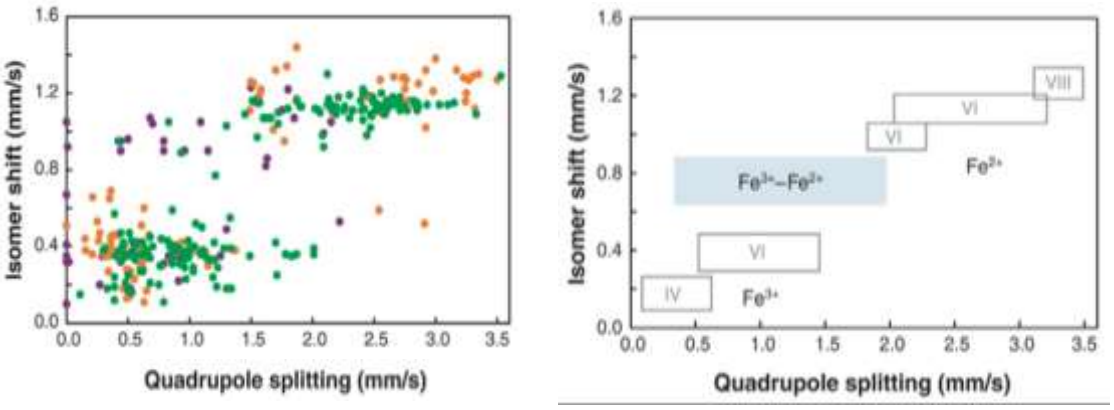

Figure 55. *Room temperature isomer shift versus quadrupole splitting data for common rock-forming minerals (Dyar et al., 2006).*

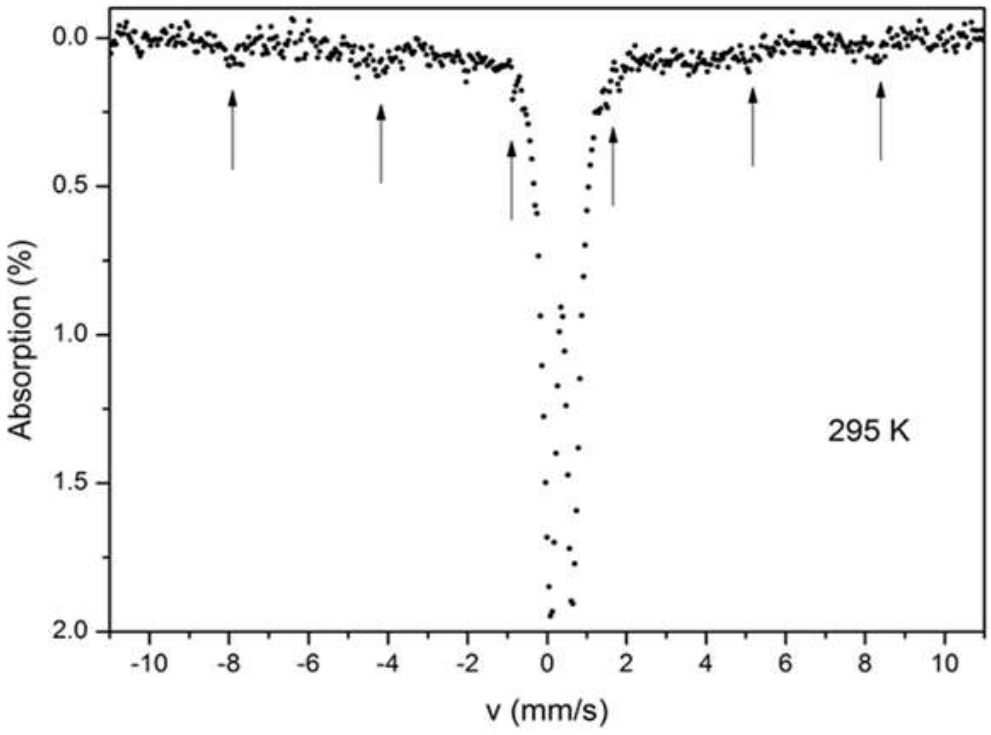

Figure 56. *Characteristic ^{57}Fe Mössbauer spectrum of Ni-phyllosilicate from LARCO GMMSA laterite.*

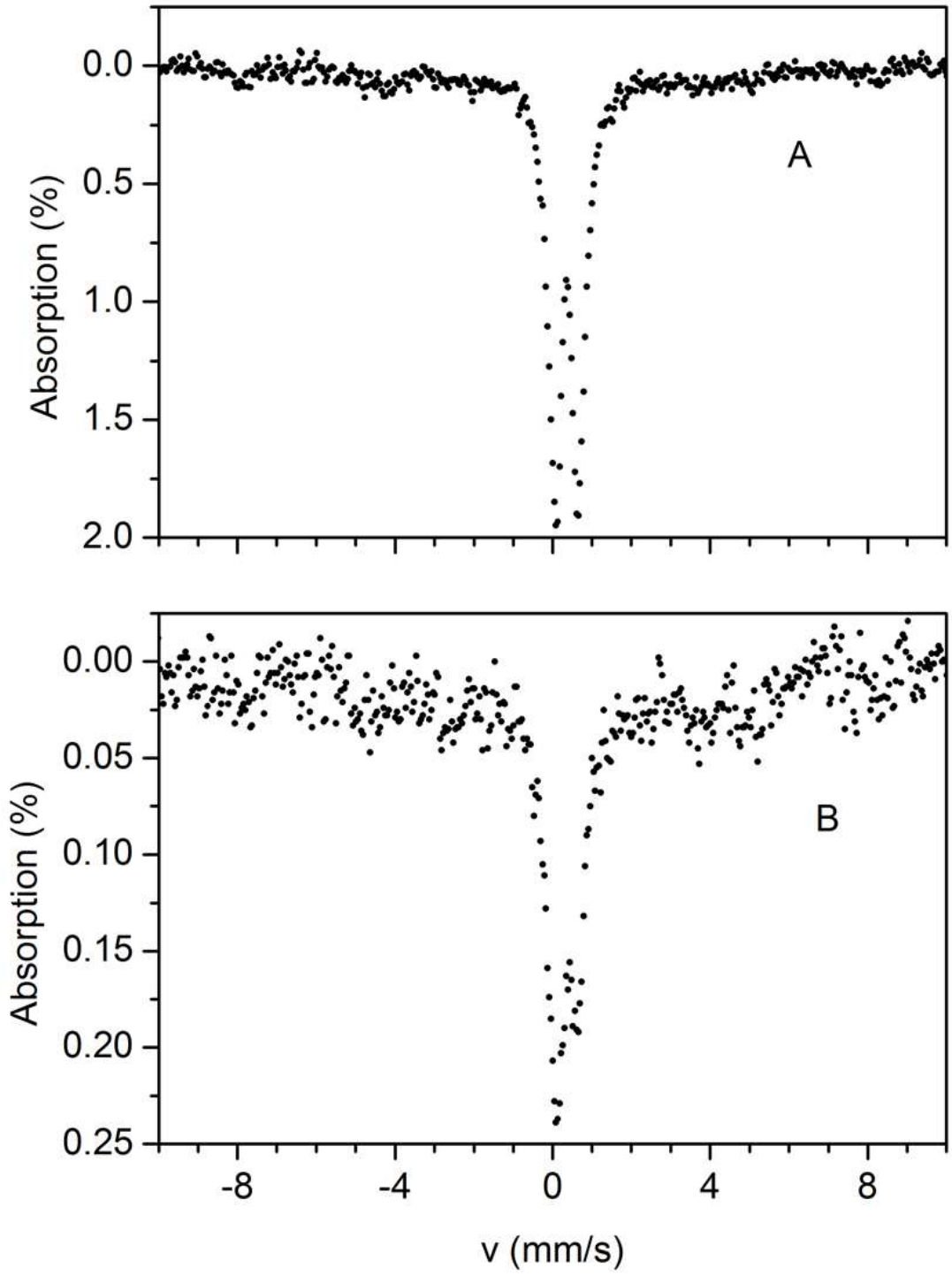

Figure 57. *Characteristic ^{57}Fe Mössbauer spectra measured at room temperature (295 K) of Ni-phyllosilicate from LARCO GMMSA laterite.*

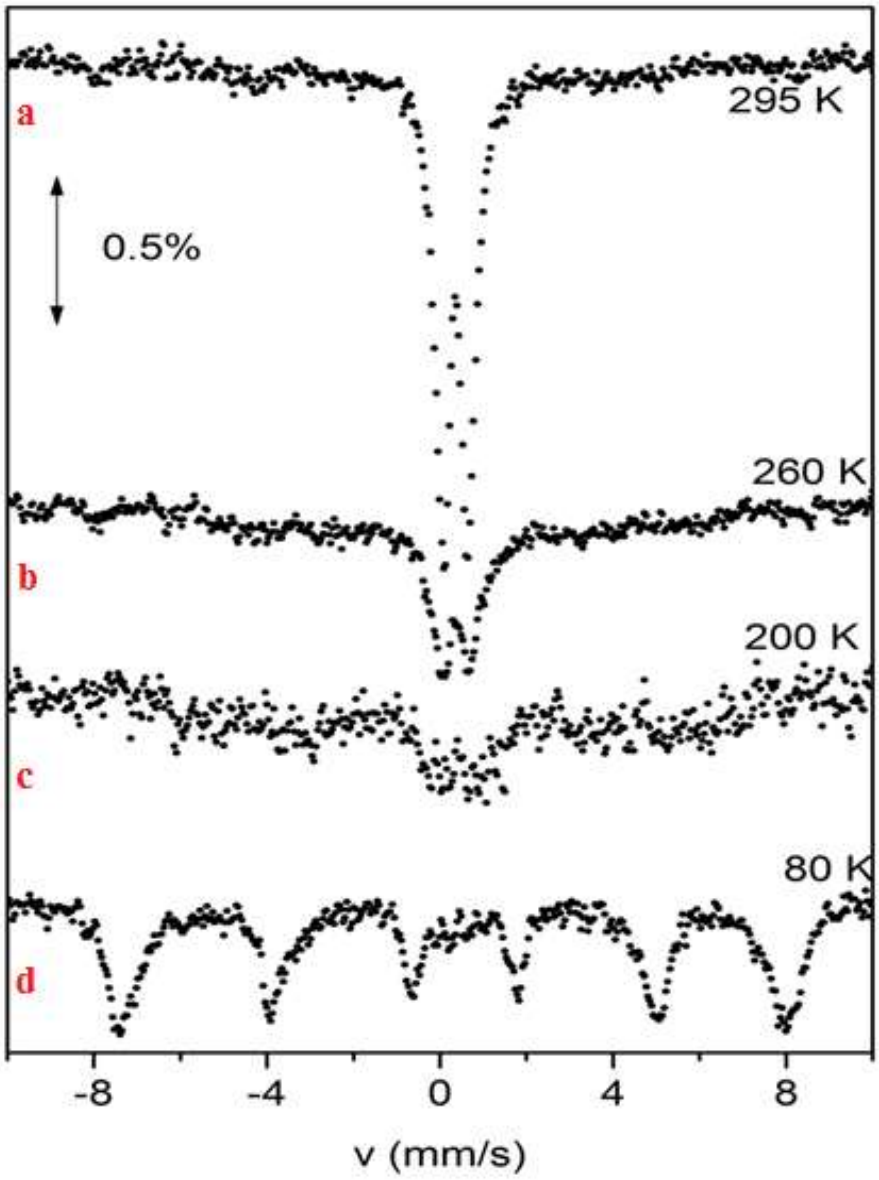

Figure 58. *Characteristic ^{57}Fe Mössbauer spectra measured at room temperature (295 K; spectra a, at 260 K; spectra b, at 200 K; spectra c and at 80 K; spectra d of Ni-phyllosilicate from LARCO GMMSA laterite.*

Mössbauer spectra for the Ni-phyllosilicate sample at 295 K and at 80 K are shown in Figure 58. The spectrum measured at 295 K (Fig. 58; spectrum a) shows a prominent central doublet and, consequently, at 80 K (Fig. 58; spectrum d) a broad six-line pattern. Anila et al. (1981) mention that such a spectrum has been observed for fine particles of α-Fe, β-Fe and γ-Fe. Van der Kraan (1972) had already observed that the Mössbauer spectra particles, which always consist of a similar sixline hyperfine pattern superimposed on a central quadrupole doublet, are those of α-Fe and they are superparamagnetic. In fact, the collapse of the magnetic hyperfine splitting seems to be characteristic of superparamagnetic materials and it can be restored by decreasing the temperature as seen in Figure 58 spectrum d.

Moreover, the isomer shift (IS-given relative to α-Fe at 295 K) values indicate not only that the main contribution originates from paramagnetic Fe^{3+} ions but also that the specific magnetic component corresponds to Fe^{3+} ions most probably located onoctahedral sites (e.g., Hill et al., 1978; Fysh et al., 1983; Cornell et al., 2003; Kuzmann et al., 2003; Dyar et al., 2006). Therefore, it could be probably argued that the recorded Fe^{3+}components correspond to Fe-Cr-diaspore (Fe-Cr-AlOOH where Fe^{3+} substitutes for Al^{3+} ions in octahedral sites, i.e., $^{[6]}Fe^{3+} \leftrightarrow {}^{[6]}Al^{3+}$) and to potential occluded Fe mineral nanoparticles and/or nanominerals (see text below). The latter might be responsible for the magnetic component with the high hyperfine field (Bhf), coming from contribution of a ferrimagnetic mineral with large Fe content, which is probably maghemite-type phase (γ-Fe_2O_3), and also for the collapsing magnetic component attributed to either not well crystallized nano-maghemite or Fe^{3+} dispersed in amorphous minor phases not detected by PXRD. The possible influence by microcrystal fragments of trace chromite cannot be excluded, due to the presence of the phase detectable only by careful SEM-EDS investigation (see text above).

Conclusively, the Mössbauer spectra for both samples show that the major constituent of the laterite ore is superparamagnetic α-Fe [natural Fe^{3+}-oxide (hematite: α-Fe_2O_3) as well as synthetic Fe^{3+}-oxyhydroxide (goethite: α-FeOOH)]. It is known that the particle size influences the shape of the Mössbauer spectrum and the present observations are consistent with the published literature. For sufficiently small sized particles, and, more specifically nanometers, the outer layers decouple completely from the inside and give rise to a paramagnetic fraction superposed on the sextet. In this way the central doublet of the Mössbauer spectrum is due to the interior of the particles while the continuous smooth six-line pattern is due to the surface ions. In our case, these ions are only Fe^{3+}. The fact that the examined particles correspond to Fe containing phases with reduced particle size implies the presence of Fe mineral nanoparticles and/or Fe nanominerals, as also supposed by electron microscopy in nanoscale (see text below).

3.5 Nano-mineralogy and -geochemistry of Co (TEM-EDS)

Additionally, to go in detail in mineral identification in nanoscale, regarding Co, a TEM-EDS study (Figs. 59-95) was performed in the case of the ore sample showing the highest Co content (according to bulk ICP-OES/MS data) which is the green-black thin layer occuring in the base of the deposit exactly over the footwall limestone (sample L). This material is rich in Ni-phyllosilicates, i.e. ‘garnierite’, and also contains small dark Mn inclusions refered as ‘asbolane’ (Chukhrov et al., 1982; Manceau et al., 1987; Apostolikas et al., 2000; Eliopoulos et al., 2000; Maksimovic, 2004; Thorne et al., 2009; Golightly, 2010; Roque-Rosell et al., 2010; Fan et al, 2011; De-qing et al., 2012; Eliopoulos et al., 2012; Melfos et al., 2012; Aiglsperger, 2015; Kalatha et al., 2017).

The TEM-EDS study for the particular sample was performed to elucidate the nature of the Co-hosting phases inasmuch the PXRD study (see text above) showed Ni-phyllosilicates but no distinct crystalline Co-phases. It should be mentioned that the prior study in microscale by SEM-EDS revealed (see also text above) areas with a peculiar composition containing Al, Si, Mn, Ni, Co, Cr, V, Cu and Ca; the latter one perhaps through interference by calcite. Nevertheless, the subsequent study in nanoscale gave evidence for the aforementioned Al-Si-Mn-Ni-Co(-Cr) areas, corresponding most likely to an unknown (oxy)hydroxide/oxide (hydrated) phase.

However, there are also areas consisting only of an amorphous/disordered Ni(-Cr)-Co-bearing Mn-(oxy)hydroxide/oxide (hydrated) phase, the so-called ‘asbolane’ by previous authors. According to the literature (De-qing et al., 2012; Roque-Rosell et al., 2010; Eliopoulos et al., 2012) Ni, Co and Al are detected accumulating in ‘asbolane’. Fan et al. mentioned the importance of the fact that formation of ‘asbolane’ can be connected with the hydrolysed precipitation of heavy metals (such as Ni and Co) in an interlayer space of buserite. The precipitation of phyllomanganate minerals is strongly controlled by redox reactions and forms as veins and surface coatings on minerals and in fractures (Elias, 2001). However, the stability of different domains of phyllomanganate minerals is affected by both the pH and Eh of the weathered laterites. Phyllomanganate, enriched in Ni and/or Co, is probably formed during the late weathering phases (Brand et al., 1998). ‘Asbolane’ could be occasionally found to contain more Ni and Co compared with other Ni-bearing minerals. However, ‘asbolanes’ of various composition (Co, Ni, Co-Ni) differ in some structural features, and are worthy of special consideration (Chukhrov et al., 1982). Aiglsperger (2015) considering high contents of Co in the Ni-laterite deposited in Moa Bay area, Cuba, came to the conclusion that ‘asbolane’ can be the main Co-bearing phase, while De-qing et al. (2012), using electron probe microanalysis (EPMA), reported that ‘asbolane’ contains Co as high as 3.06% in low grade Ni-laterite ore sample from Indonesia. Chemical composition of different laterite occurrences in Greece shows that cobalt is mainly concentrated in the Fe-Ni-rich zones, demonstrating elevated contents which reach 0.10% in Palaiochori, Grevena, 0.14% in Vermio, 0.16% in Kastoria and 0.22% in Lokris (Eliopoulos et al., 2000; Eliopoulos et al., 2012). Cobalt in these deposits is concentrated mainly in the mineral asbolane (Apostolikas et al., 2000). Nickel-bearing minerals, such as Ni-Co ‘asbolane’, from the studied deposit have been described by Maksimovic (2004). The presence of Mn, Co±Ni, as ‘asbolane’, filling fractures in the lower levels of the laterite deposits is a common feature of the Lokris deposits (Kalatha et al., 2017). In fact, several mixtures of similar minerals or pure Ni-Co ‘asbolane’ (black colour) and Al-Ni-silicates (pale green) are common in the lowest part of the deposit, exactly to Fe-Ni ore contact with the basement Triassic-Jurassic limestone. Besides, in modern laterites, ‘asbolane’ is concentrated in the in situ lower part of the profile in the peridotite saprolite or in overlying 'limonite' with intact protolith textures (i.e., ferruginous saprolite) (Golightly, 2010). The association of Co with Mn and Ni in ‘asbolane’ in the Lokris laterite deposits and/or Co-Mn-Ni-(oxy)hydroxide/oxides has been well established by Eliopoulos et al., 2010; Thorne et al., 2009. Eliopoulos et al. (2012) accentuate that the presence of ‘asbolane’, and generally Mn-Co-Ni-rich zones, in the lowest parts of the Agios Ioannis (Lokris) deposit, demonstrates the post-sedimentary redistribution of metals resulting in changes of the mineralogical composition of laterites. As a matter of fact, the preferential occurrence of Ni, Co, and Mn (‘asbolane’ and silicates) within typical Fe-Ni-laterite ores towards the lowermost part of the deposit suggest their deposition was controlled by physicochemical conditions rather than the precursor rocks (Kalatha et al., 2015).

However, we cannot exclude, in nanoscale, a combination of nanophases, like polyphasic nanominerals (Caraballo et al. 2015) or even admixtures of amorphous/disordred nanominerals and mineral nanoparticles (Hochella, 2008; Hochella et al., 2008a; Hochella et al., 2008b):

i) an admixture of two mineral nanoparticles, one crystalline (e.g., a Ni-bearing phyllosilicate) and another amorphous/disordered (i.e., the Ni-Co(-Cr)-bearing Mn-(oxyhydr)oxide (hydrated) the so-called ‘asbolane’).

ii) an admixture of two amorphous/disordered nanominerals, that is the Ni-Co(-Cr)-bearing Mn-(oxyhydr)oxide (hydrated), the so called ‘asbolane’, and another unknown Si-Al-Ni-(oxy)hydroxide/oxide (hydrated) nanophase.

According to the fundamentals of nanogeoscience, mineral nanoparticles are the nanoscale-versions of common minerals (exhibiting although different physicochemical properties compared to the micro and macro-scale analogues), whereas nanominerals are distinct phases existing only in nanoscale without equivalents at larger scales (Hochella, 2002a, b; Hochella, 2006, 2008; Hochella et al., 2008a, b, 2012). In this case, naturally occurring nanoclusters, polyphasic nanominerals, nanoporous phases, amorphous nanomaterials, amorphous-nanocrystalline transitional phases, surface-disordered nanoparticles and mesocrystals, all related to the natural progressive transition between amorphous and crystalline materials, have also to be considered (Caraballo et al., 2015). The present data of Co and Mn highlight the high Co-Mn geochemical affinity in laterite systems. Various factors control the precipitation of Mn-oxy-hydroxides from soil solutions such as oxidation, the catalytic action of other mineral grains, evaporative dehydration, and interaction with microorganisms. The physicochemical conditions of the environment and the soil solutions convey the type of Mn-oxy-hydroxides formed in supergene settings (Tupaz et al., 2020).

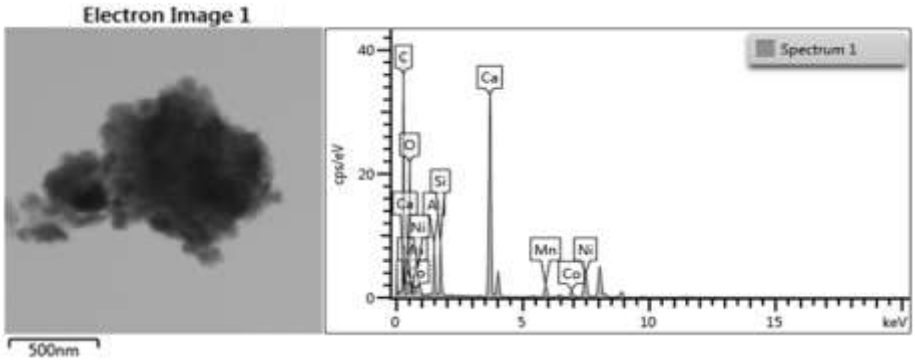

Element	Line Type	k Factor	k Factor type	Absorption Correction	Wt%	Wt% Sigma
C	K series	2.759		1.00	36.64	0.48
O	K series	2.016		1.00	18.29	0.34
Al	K series	1.050		1.00	4.67	0.14
Si	K series	1.000		1.00	4.87	0.14
Ca	K series	0.993		1.00	27.27	0.31
Mn	K series	1.156		1.00	2.22	0.10
Co	K series	1.189		1.00	1.34	0.08
Ni	K series	1.166		1.00	4.71	0.15
Total:					100.00	

Figure 59. *TEM image, spectrum diagram and element distribution table of the studied LARCO GMMSA laterite.*

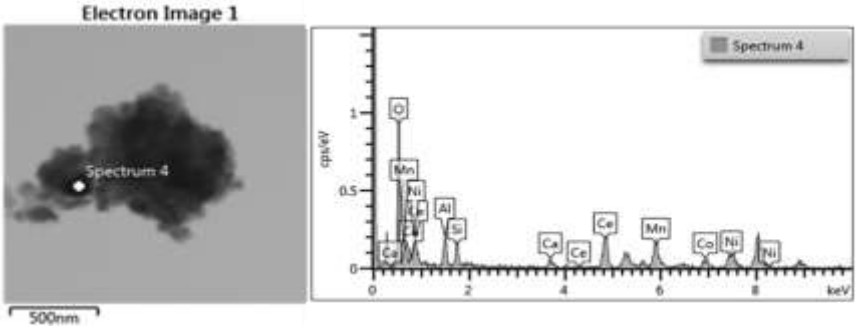

Element	Line Type	k Factor	k Factor type	Absorption Correction	Wt%	Wt% Sigma
O	K series	2.016		1.00	38.36	1.47
Al	K series	1.050		1.00	5.05	0.55
Si	K series	1.000		1.00	4.50	0.49
Ca	K series	0.993		1.00	1.82	0.33
Mn	K series	1.156		1.00	8.45	0.71
Co	K series	1.189		1.00	3.29	0.46
Ni	K series	1.166		1.00	5.86	0.63
Ce	L series	2.059		1.00	32.66	1.52
Total:					100.00	

Figure 60. *TEM image, spectrum diagram and element distribution table of the studied LARCO GMMSA laterite.*

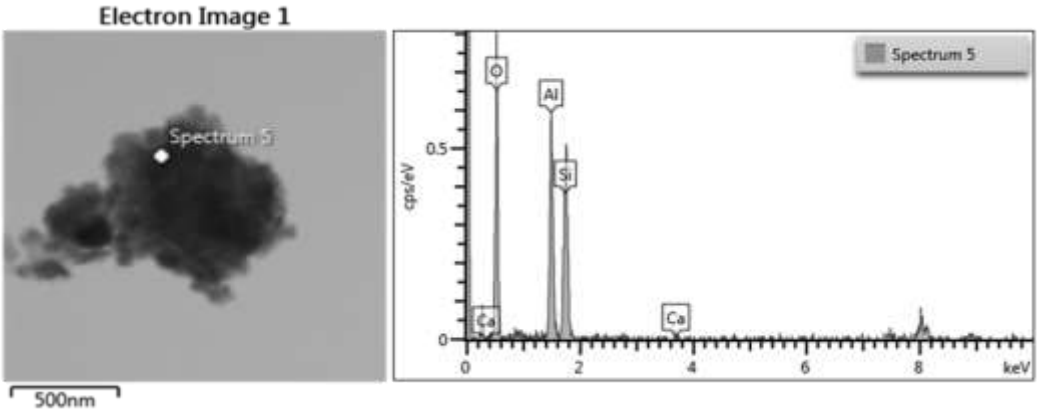

Element	Line Type	k Factor	k Factor type	Absorption Correction	Wt%	Wt% Sigma
O	K series	2.016		1.00	48.78	2.13
Al	K series	1.050		1.00	27.10	1.66
Si	K series	1.000		1.00	23.11	1.63
Ca	K series	0.993		1.00	1.01	0.31
Total:					100.00	

Figure 61. *TEM image, spectrum diagram and element distribution table of the studied LARCO GMMSA laterite.*

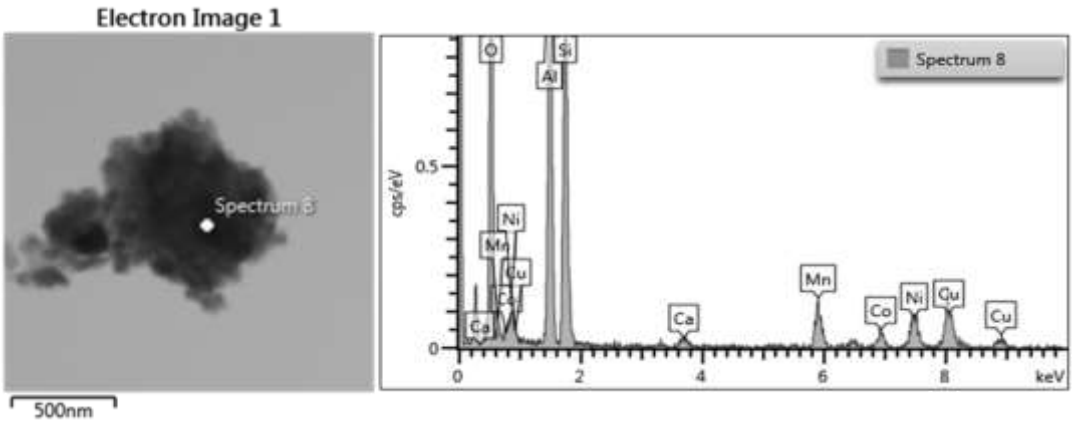

Element	Line Type	k Factor	k Factor type	Absorption Correction	Wt%	Wt% Sigma
O	K series	2.016		1.00	47.44	0.96
Al	K series	1.050		1.00	20.25	0.67
Si	K series	1.000		1.00	17.68	0.64
Ca	K series	0.993		1.00	0.41	0.16
Mn	K series	1.156		1.00	3.78	0.32
Co	K series	1.189		1.00	1.61	0.23
Ni	K series	1.166		1.00	3.41	0.32
Cu	K series	1.248		1.00	5.42	0.40
Total:					100.00	

Figure 62. *TEM image, spectrum diagram and element distribution table of the studied LARCO GMMSA laterite.*

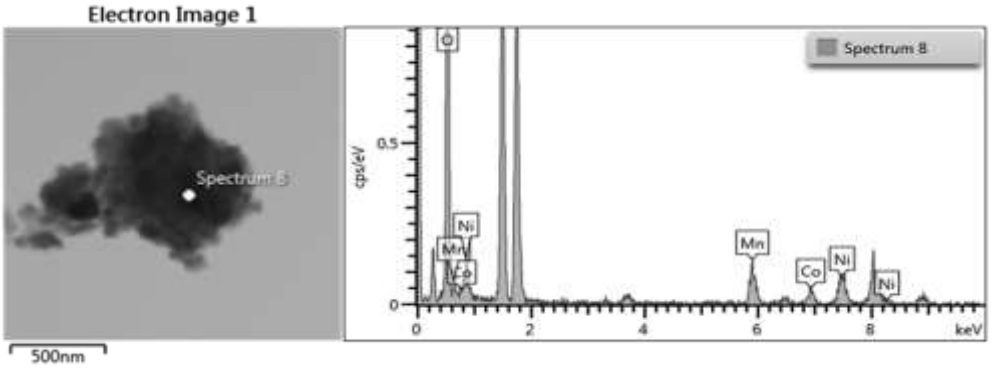

Element	Line Type	k Factor	k Factor type	Absorption Correction	Wt%	Wt% Sigma
O	K series	2.016		1.00	84.62	0.88
Mn	K series	1.156		1.00	6.76	0.57
Co	K series	1.189		1.00	2.93	0.40
Ni	K series	1.166		1.00	5.69	0.58
Total:					100.00	

Figure 63. *TEM image, spectrum diagram and element distribution table of the studied LARCO GMMSA laterite.*

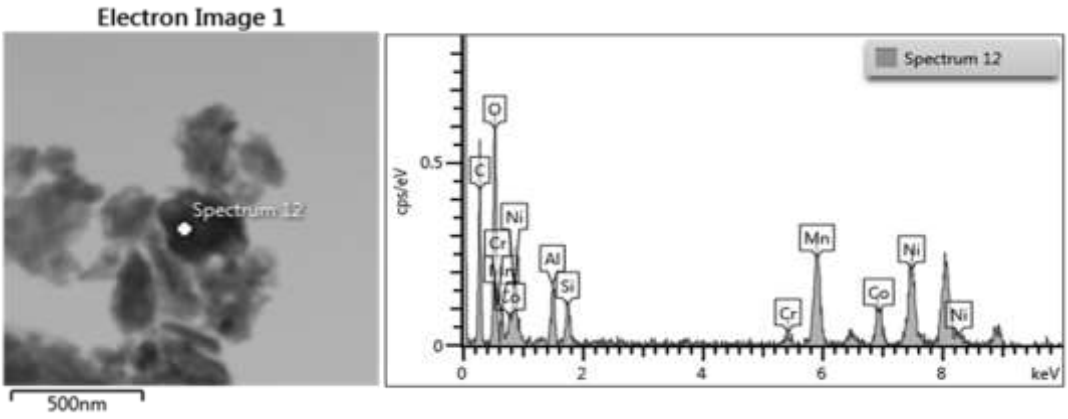

Element	Line Type	k Factor	k Factor type	Absorption Correction	Wt%	Wt% Sigma
C	K series	2.759		1.00	24.04	1.75
O	K series	2.016		1.00	26.67	1.62
Al	K series	1.050		1.00	4.78	0.59
Si	K series	1.000		1.00	3.36	0.53
Cr	K series	1.121		1.00	2.12	0.41
Mn	K series	1.156		1.00	15.70	1.02
Co	K series	1.189		1.00	8.24	0.73
Ni	K series	1.166		1.00	15.10	1.03
Total:					100.00	

Figure 64. *TEM image, spectrum diagram and element distribution table of the studied LARCO GMMSA laterite.*

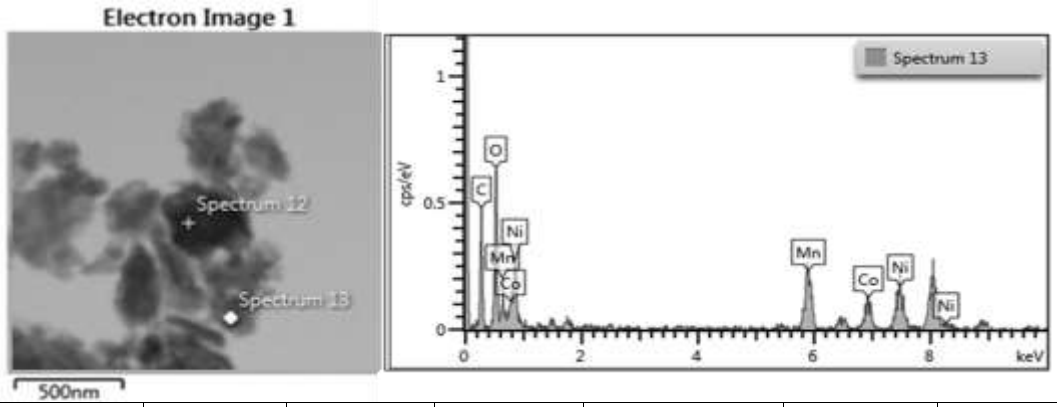

Element	Line Type	k Factor	k Factor type	Absorption Correction	Wt%	Wt% Sigma
C	K series	2.759		1.00	28.69	2.20
O	K series	2.016		1.00	31.56	2.09
Mn	K series	1.156		1.00	17.30	1.32
Co	K series	1.189		1.00	9.05	0.99
Ni	K series	1.166		1.00	13.41	1.25
Total:					100.00	

Figure 65. *TEM image, spectrum diagram and element distribution table of the studied LARCO GMMSA laterite.*

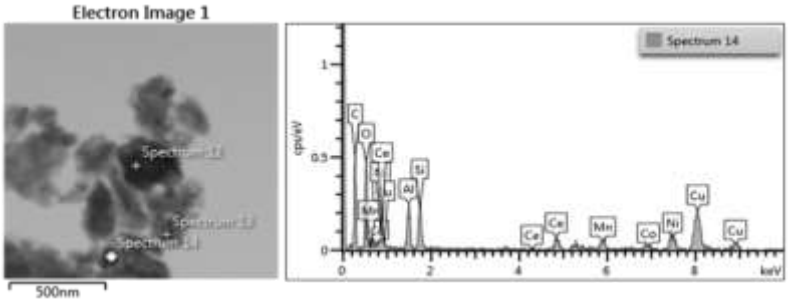

Element	Line Type	k Factor	k Factor type	Absorption Correction	Wt%	Wt% Sigma
C	K series	2.759		1.00	26.55	1.68
O	K series	2.016		1.00	21.54	1.43
Al	K series	1.050		1.00	7.10	0.67
Si	K series	1.000		1.00	7.22	0.68
Mn	K series	1.156		1.00	3.35	0.51
Co	K series	1.189		1.00	1.84	0.42
Ni	K series	1.166		1.00	6.16	0.64
Cu	K series	1.248		1.00	16.00	1.05
Ce	L series	2.059		1.00	10.23	1.26
Total:					100.00	

Figure 66. *TEM image, spectrum diagram and element distribution table of the studied LARCO GMMSA laterite.*

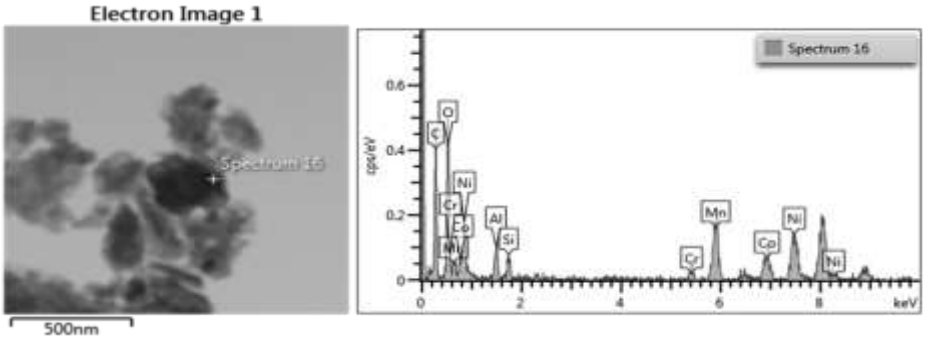

Element	Line Type	k Factor	k Factor type	Absorption Correction	Wt%	Wt% Sigma
C	K series	2.759		1.00	30.22	2.02
O	K series	2.016		1.00	26.02	1.80
Al	K series	1.050		1.00	4.13	0.59
Si	K series	1.000		1.00	2.65	0.49
Cr	K series	1.121		1.00	2.66	0.44
Mn	K series	1.156		1.00	14.91	1.06
Co	K series	1.189		1.00	7.13	0.83
Ni	K series	1.166		1.00	12.28	1.06
Total:					100.00	

Figure 67. *TEM image, spectrum diagram and element distribution table of the studied LARCO GMMSA laterite.*

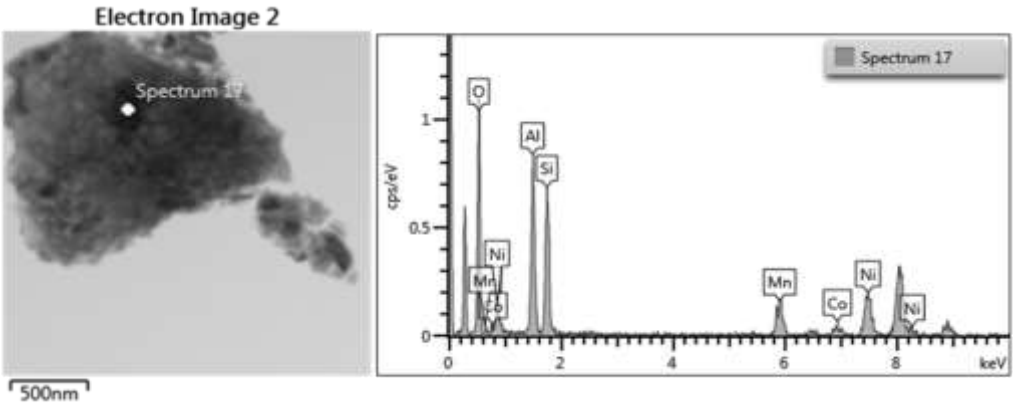

Element	Line Type	k Factor	k Factor type	Absorption Correction	Wt%	Wt% Sigma
O	K series	2.016		1.00	40.34	1.30
Al	K series	1.050		1.00	19.91	0.90
Si	K series	1.000		1.00	18.05	0.86
Mn	K series	1.156		1.00	8.36	0.63
Co	K series	1.189		1.00	2.15	0.41
Ni	K series	1.166		1.00	11.20	0.74
Total:					100.00	

Figure 68. *TEM image, spectrum diagram and element distribution table of the studied LARCO GMMSA laterite.*

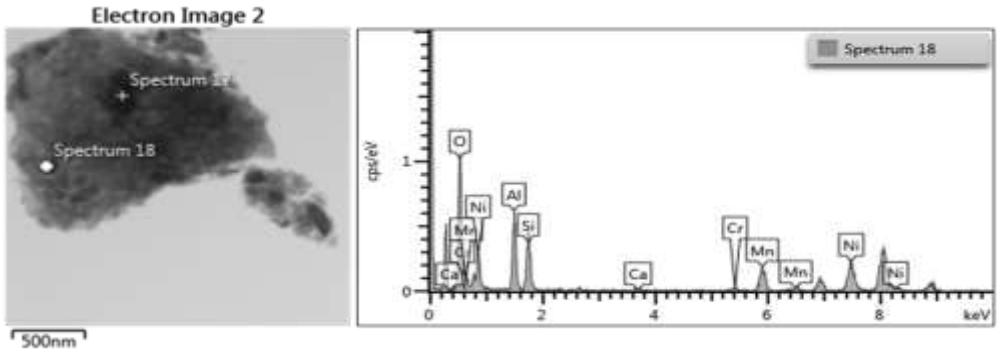

Element	Line Type	k Factor	k Factor type	Absorption Correction	Wt%	Wt% Sigma
O	K series	2.016		1.00	45.57	1.41
Al	K series	1.050		1.00	16.83	0.86
Si	K series	1.000		1.00	12.94	0.79
Ca	K series	0.993		1.00	0.45	0.24
Cr	K series	1.121		1.00	1.02	0.31
Mn	K series	1.156		1.00	10.58	0.70
Ni	K series	1.166		1.00	12.61	0.83
Total:					100.00	

Figure 69. *TEM image, spectrum diagram and element distribution table of the studied LARCO GMMSA laterite.*

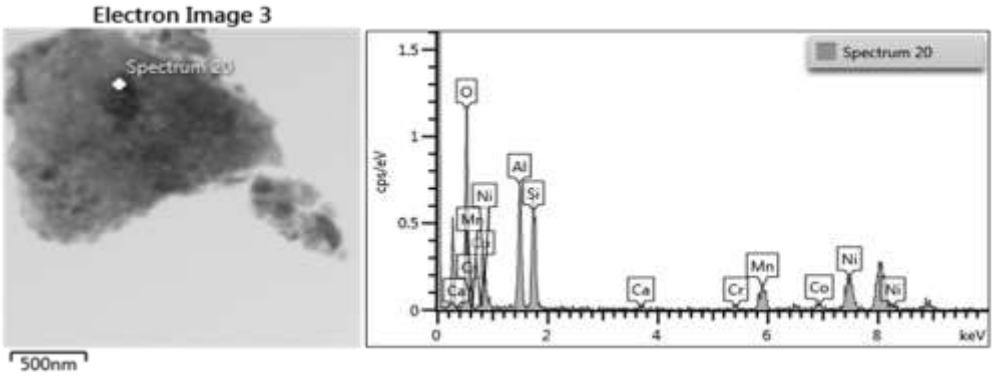

Element	Line Type	k Factor	k Factor type	Absorption Correction	Wt%	Wt% Sigma
O	K series	2.016		1.00	43.97	1.52
Al	K series	1.050		1.00	18.53	1.00
Si	K series	1.000		1.00	16.15	0.97
Ca	K series	0.993		1.00	0.70	0.25
Cr	K series	1.121		1.00	1.25	0.32
Mn	K series	1.156		1.00	6.86	0.69
Co	K series	1.189		1.00	2.06	0.44
Ni	K series	1.166		1.00	10.48	0.87
Total:					100.00	

Figure 70. *TEM image, spectrum diagram and element distribution table of the studied LARCO GMMSA laterite.*

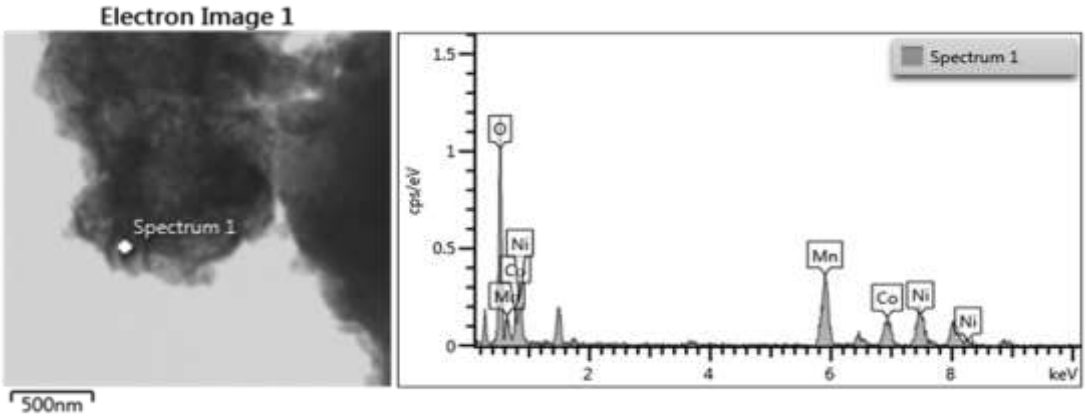

Element	Line Type	k Factor	k Factor type	Absorption Correction	Wt%	Wt% Sigma
O	K series	2.018		1.00	51.81	1.48
Mn	K series	1.154		1.00	24.02	1.11
Co	K series	1.187		1.00	10.14	0.80
Ni	K series	1.164		1.00	14.04	0.91
Total:					100.00	

Figure 71. *TEM image, spectrum diagram and element distribution table of the studied LARCO GMMSA laterite.*

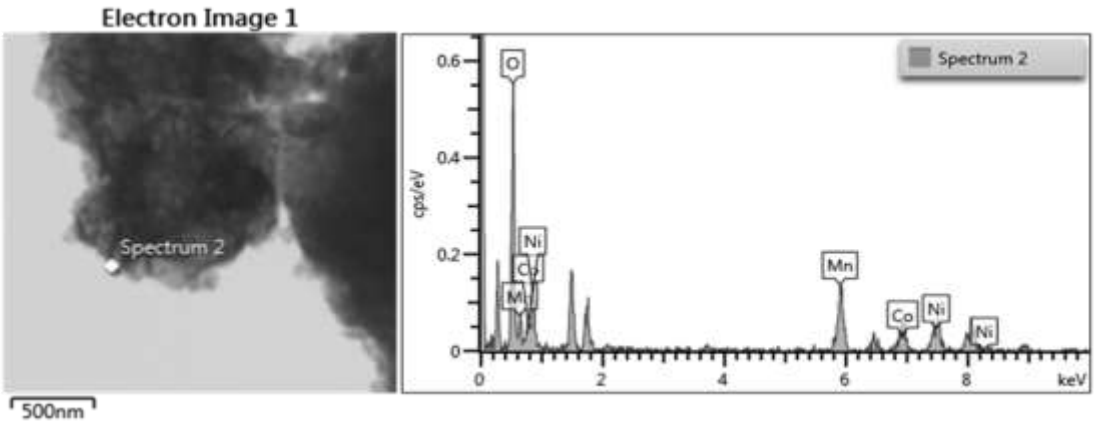

Element	Line Type	k Factor	k Factor type	Absorption Correction	Wt%	Wt% Sigma
O	K series	2.018		1.00	60.15	2.19
Mn	K series	1.154		1.00	21.19	1.60
Co	K series	1.187		1.00	7.84	1.11
Ni	K series	1.164		1.00	10.82	1.27
Total:					100.00	

Figure 72. *TEM image, spectrum diagram and element distribution table of the studied LARCO GMMSA laterite.*

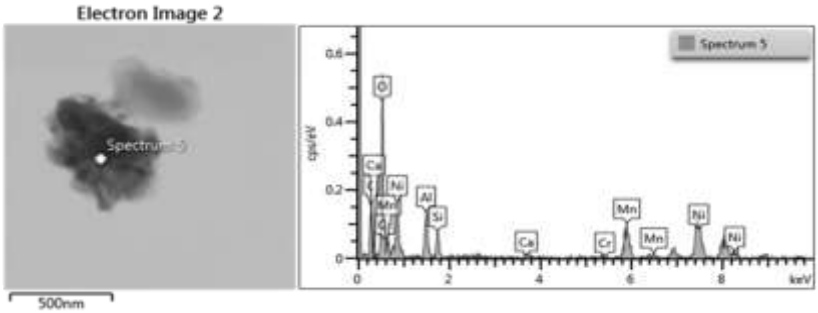

Element	Line Type	k Factor	k Factor type	Absorption Correction	Wt%	Wt% Sigma
C	K series	2.762		1.00	16.38	1.90
O	K series	2.018		1.00	44.72	1.89
Al	K series	1.050		1.00	7.63	0.79
Si	K series	1.000		1.00	4.67	0.59
Ca	K series	0.992		1.00	1.04	0.31
Cr	K series	1.120		1.00	0.58	0.30
Mn	K series	1.154		1.00	10.65	0.91
Ni	K series	1.164		1.00	14.33	1.11
Total:					100.00	

Figure 73. *TEM image, spectrum diagram and element distribution table of the studied LARCO GMMSA laterite.*

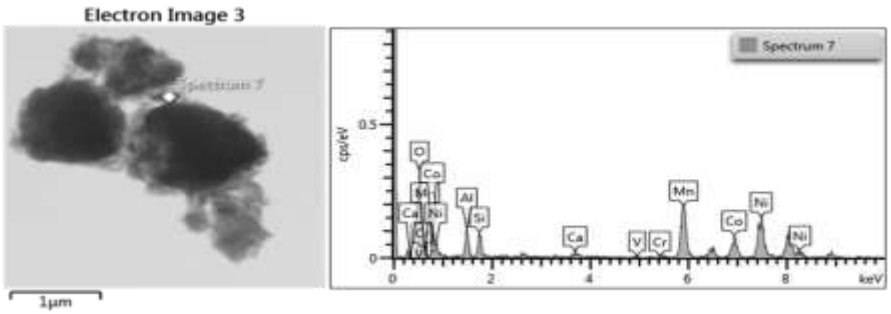

Element	Line Type	k Factor	k Factor type	Absorption Correction	Wt%	Wt% Sigma
O	K series	2.018		1.00	31.00	1.75
Al	K series	1.050		1.00	5.71	0.63
Si	K series	1.000		1.00	5.66	0.61
Ca	K series	0.992		1.00	1.36	0.38
V	K series	1.129		1.00	0.51	0.23
Cr	K series	1.120		1.00	0.38	0.28
Mn	K series	1.154		1.00	25.59	1.17
Co	K series	1.187		1.00	9.79	0.81
Ni	K series	1.164		1.00	20.00	1.10
Total:					100.00	

Figure 74. *TEM image, spectrum diagram and element distribution table of the studied LARCO GMMSA laterite.*

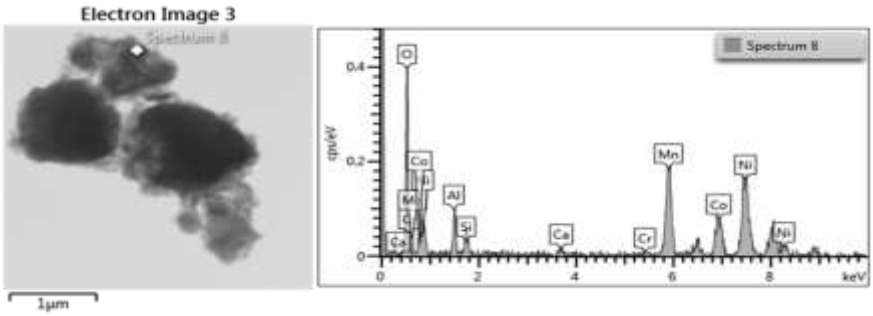

Element	Line Type	k Factor	k Factor type	Absorption Correction	Wt%	Wt% Sigma
O	K series	2.018		1.00	34.29	1.80
Al	K series	1.050		1.00	5.49	0.65
Si	K series	1.000		1.00	2.63	0.56
Ca	K series	0.992		1.00	0.92	0.34
Cr	K series	1.120		1.00	0.70	0.37
Mn	K series	1.154		1.00	22.84	1.32
Co	K series	1.187		1.00	11.15	1.05
Ni	K series	1.164		1.00	21.98	1.38
Total:					100.00	

Figure 75. *TEM image, spectrum diagram and element distribution table of the studied LARCO GMMSA laterite.*

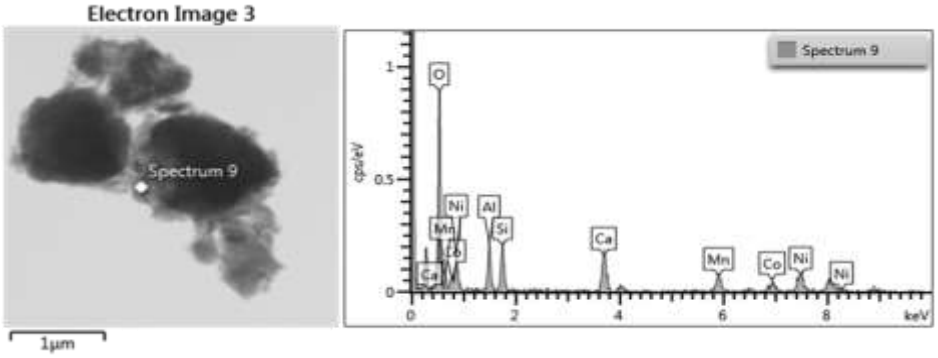

Element	Line Type	k Factor	k Factor type	Absorption Correction	Wt%	Wt% Sigma
O	K series	2.018		1.00	54.32	1.43
Al	K series	1.050		1.00	8.54	0.68
Si	K series	1.000		1.00	8.99	0.69
Ca	K series	0.992		1.00	10.52	0.70
Mn	K series	1.154		1.00	6.37	0.59
Co	K series	1.187		1.00	3.74	0.51
Ni	K series	1.164		1.00	7.52	0.68
Total:					100.00	

Figure 76. *TEM image, spectrum diagram and element distribution table of the studied LARCO GMMSA laterite.*

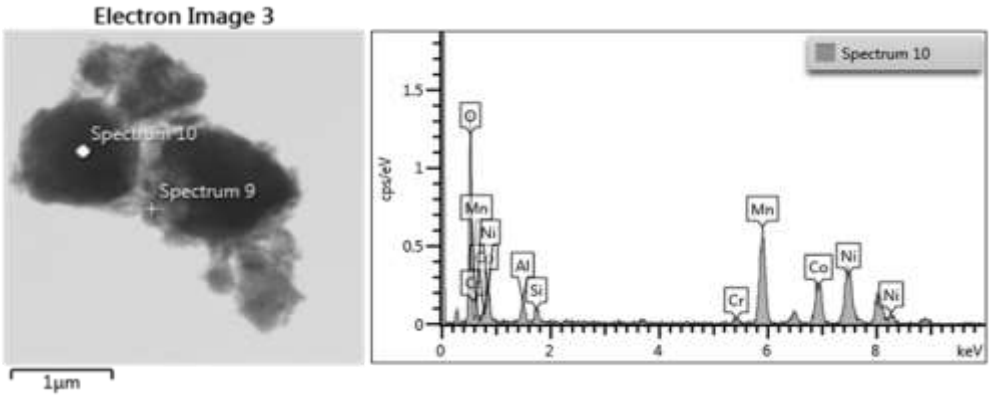

Element	Line Type	k Factor	k Factor type	Absorption Correction	Wt%	Wt% Sigma
O	K series	2.018		1.00	38.59	1.17
Al	K series	1.050		1.00	2.63	0.37
Si	K series	1.000		1.00	1.98	0.33
Cr	K series	1.120		1.00	1.27	0.27
Mn	K series	1.154		1.00	25.26	0.86
Co	K series	1.187		1.00	12.72	0.68
Ni	K series	1.164		1.00	17.54	0.79
Total:					100.00	

Figure 77. *TEM image, spectrum diagram and element distribution table of the studied LARCO GMMSA laterite.*

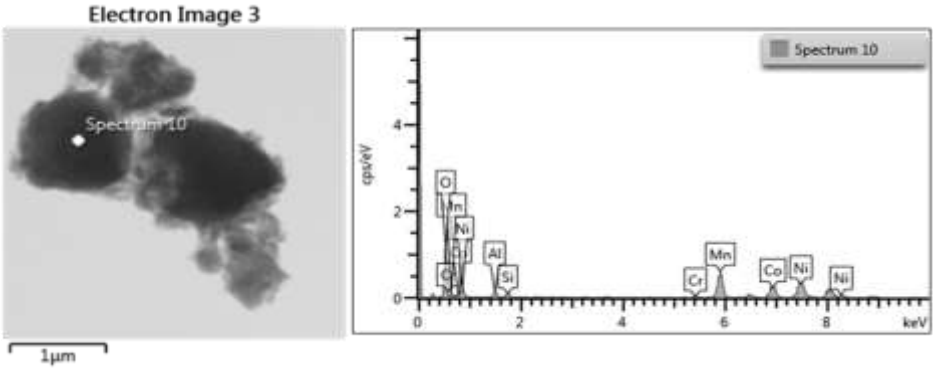

Element	Line Type	k Factor	k Factor type	Absorption Correction	Wt%	Wt% Sigma
O	K series	2.018		1.00	38.59	1.17
Al	K series	1.050		1.00	2.63	0.37
Si	K series	1.000		1.00	1.98	0.33
Cr	K series	1.120		1.00	1.27	0.27
Mn	K series	1.154		1.00	25.26	0.86
Co	K series	1.187		1.00	12.72	0.68
Ni	K series	1.164		1.00	17.54	0.79
Total:					100.00	

Figure 78. *TEM image, spectrum diagram and element distribution table of the studied LARCO GMMSA laterite.*

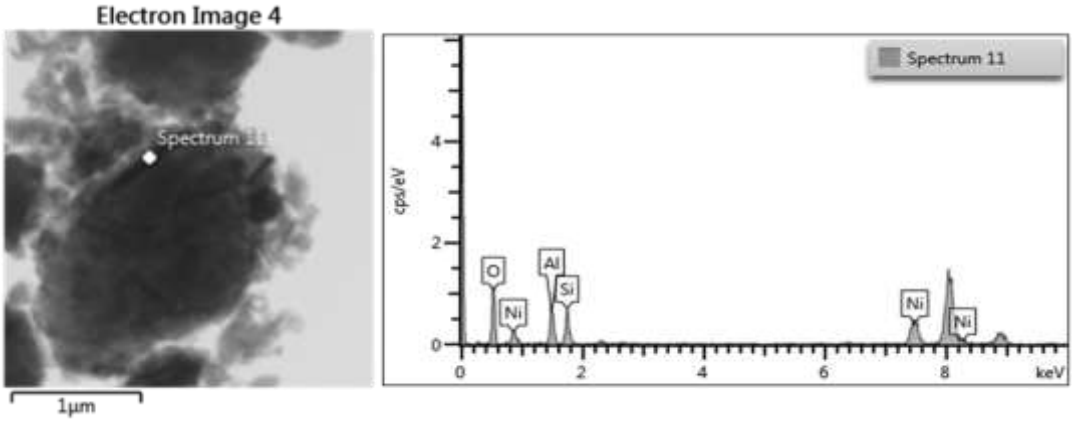

Element	Line Type	k Factor	k Factor type	Absorption Correction	Wt%	Wt% Sigma
O	K series	2.018		1.00	42.58	2.00
Al	K series	1.050		1.00	17.56	1.31
Si	K series	1.000		1.00	15.96	1.24
Ni	K series	1.164		1.00	23.91	1.65
Total:					100.00	

Figure 79. *TEM image, spectrum diagram and element distribution table of the studied LARCO GMMSA laterite.*

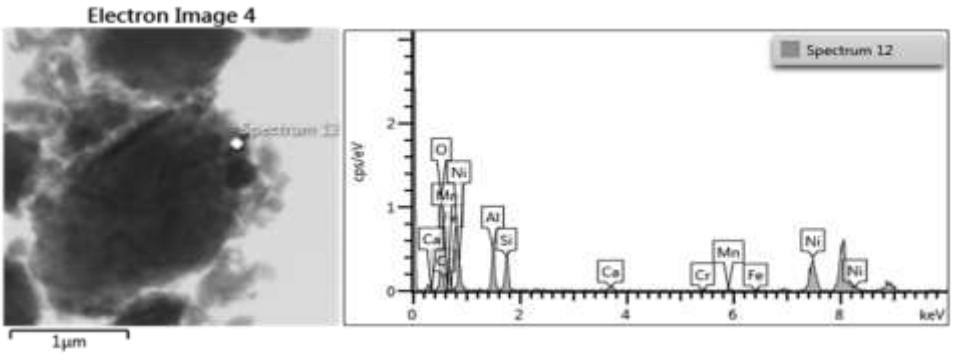

Element	Line Type	k Factor	k Factor type	Absorption Correction	Wt%	Wt% Sigma
O	K series	2.018		1.00	46.40	1.67
Al	K series	1.050		1.00	15.09	0.96
Si	K series	1.000		1.00	12.91	0.91
Ca	K series	0.992		1.00	2.33	0.42
Cr	K series	1.120		1.00	0.26	0.31
Mn	K series	1.154		1.00	0.95	0.35
Fe	K series	1.147		1.00	0.07	0.33
Ni	K series	1.164		1.00	21.99	1.23
Total:					100.00	

Figure 80. *TEM image, spectrum diagram and element distribution table of the studied LARCO GMMSA laterite.*

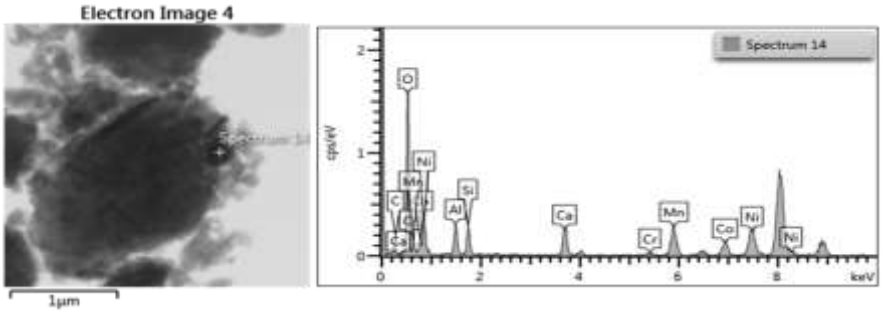

Element	Line Type	k Factor	k Factor type	Absorption Correction	Wt%	Wt% Sigma
C	K series	2.762		1.00	5.76	0.86
O	K series	2.018		1.00	45.84	1.10
Al	K series	1.050		1.00	5.75	0.41
Si	K series	1.000		1.00	5.32	0.38
Ca	K series	0.992		1.00	8.27	0.43
Cr	K series	1.120		1.00	0.72	0.22
Mn	K series	1.154		1.00	11.33	0.55
Co	K series	1.187		1.00	6.29	0.43
Ni	K series	1.164		1.00	10.72	0.61
Total:					100.00	

Figure 81. *TEM image, spectrum diagram and element distribution table ofthe studied LARCO GMMSA laterite.*

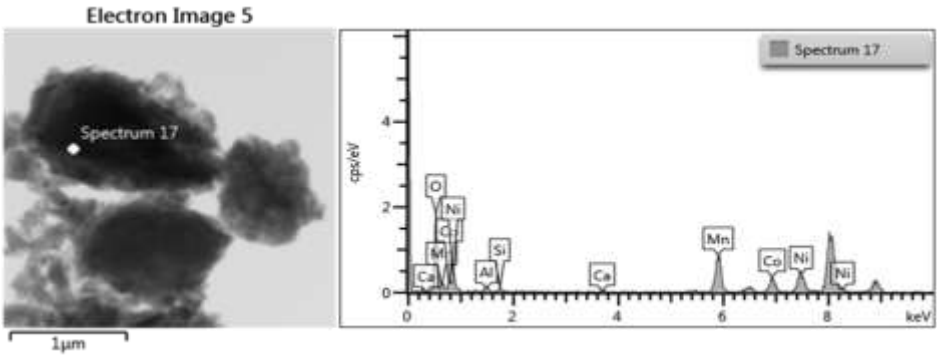

Element	Line Type	k Factor	k Factor type	Absorption Correction	Wt%	Wt% Sigma
O	K series	2.018		1.00	41.74	1.43
Al	K series	1.050		1.00	1.83	0.37
Si	K series	1.000		1.00	1.39	0.33
Ca	K series	0.992		1.00	0.88	0.26
Mn	K series	1.154		1.00	27.89	1.10
Co	K series	1.187		1.00	11.75	0.79
Ni	K series	1.164		1.00	14.51	0.94
Total:					100.00	

Figure 82. *TEM image, spectrum diagram and element distribution table of the studied LARCO GMMSA laterite.*

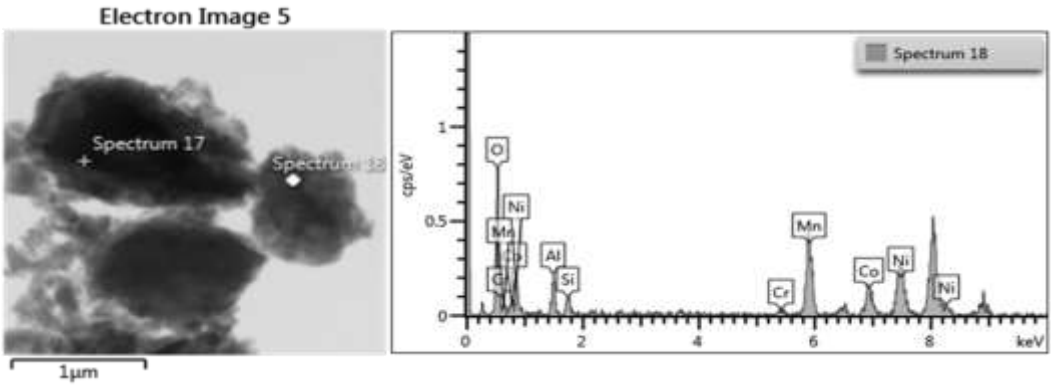

Element	Line Type	k Factor	k Factor type	Absorption Correction	Wt%	Wt% Sigma
O	K series	2.018		1.00	34.84	1.93
Al	K series	1.050		1.00	6.08	0.72
Si	K series	1.000		1.00	3.07	0.59
Cr	K series	1.120		1.00	1.63	0.49
Mn	K series	1.154		1.00	26.42	1.42
Co	K series	1.187		1.00	10.50	1.05
Ni	K series	1.164		1.00	17.45	1.35
Total:					100.00	

Figure 83. *TEM image, spectrum diagram and element distribution table of the studied LARCO GMMSA laterite.*

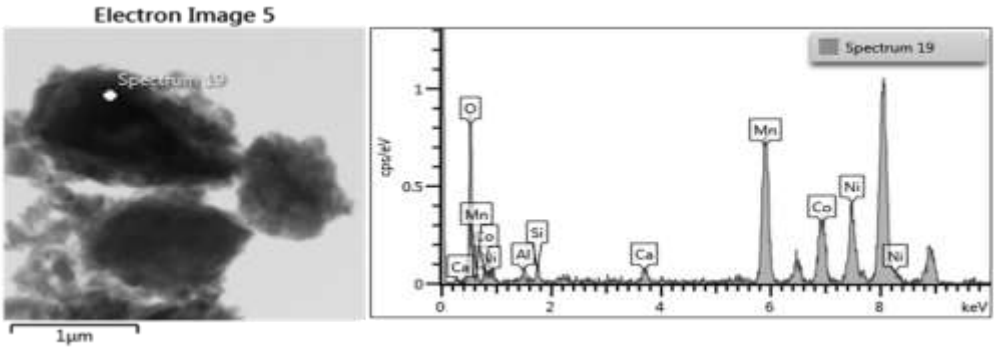

Element	Line Type	k Factor	k Factor type	Absorption Correction	Wt%	Wt% Sigma
O	K series	2.018		1.00	27.61	1.46
Al	K series	1.050		1.00	1.45	0.38
Si	K series	1.000		1.00	1.54	0.37
Ca	K series	0.992		1.00	2.15	0.42
Mn	K series	1.154		1.00	34.48	1.32
Co	K series	1.187		1.00	16.65	1.06
Ni	K series	1.164		1.00	16.11	1.09
Total:					100.00	

Figure 84. *TEM image, spectrum diagram and element distribution table of the studied LARCO GMMSA laterite.*

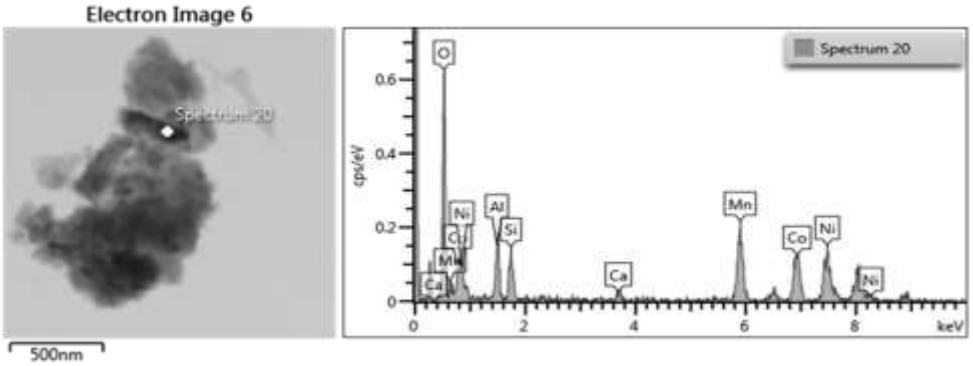

Element	Line Type	k Factor	k Factor type	Absorption Correction	Wt%	Wt% Sigma
O	K series	2.018		1.00	41.31	1.65
Al	K series	1.050		1.00	7.11	0.75
Si	K series	1.000		1.00	5.33	0.70
Ca	K series	0.992		1.00	1.79	0.37
Mn	K series	1.154		1.00	17.84	1.06
Co	K series	1.187		1.00	13.96	0.97
Ni	K series	1.164		1.00	12.65	1.00
Total:					100.00	

Figure 85. *TEM image, spectrum diagram and element distribution table of the studied LARCO GMMSA laterite.*

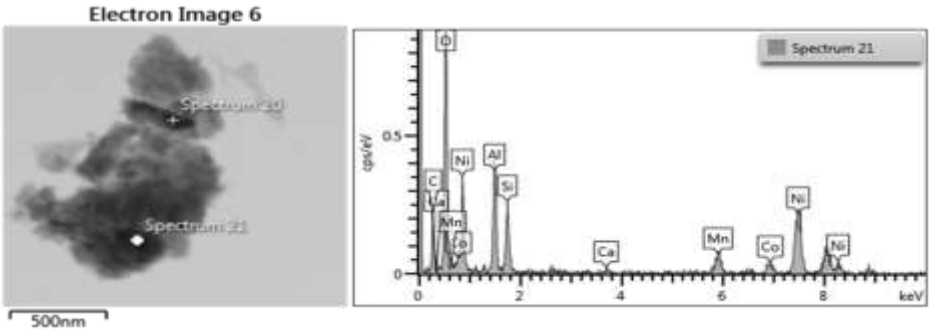

Element	Line Type	k Factor	k Factor type	Absorption Correction	Wt%	Wt% Sigma
C	K series	2.762		1.00	11.58	1.50
O	K series	2.018		1.00	45.47	1.59
Al	K series	1.050		1.00	12.30	0.80
Si	K series	1.000		1.00	6.95	0.65
Ca	K series	0.992		1.00	0.56	0.22
Mn	K series	1.154		1.00	4.27	0.53
Co	K series	1.187		1.00	2.49	0.43
Ni	K series	1.164		1.00	16.38	0.95
Total:					100.00	

Figure 86. *TEM image, spectrum diagram and element distribution table of the studied LARCO GMMSA laterite.*

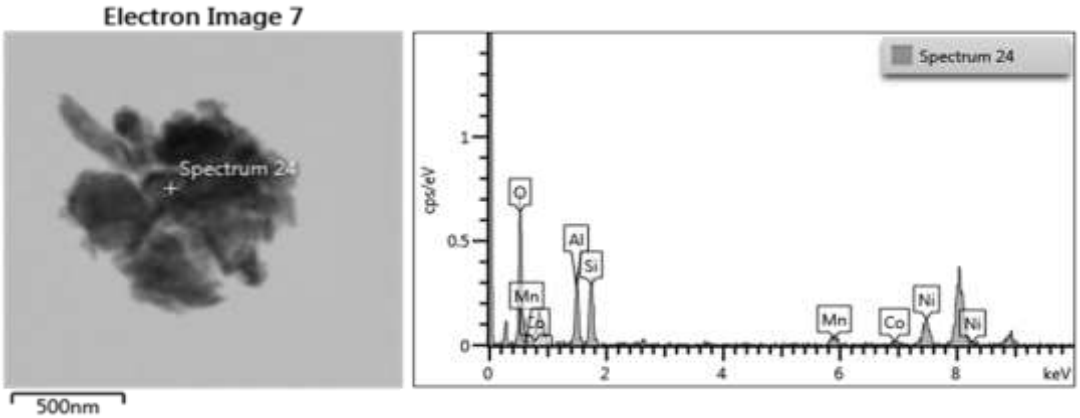

Element	Line Type	k Factor	k Factor type	Absorption Correction	Wt%	Wt% Sigma
O	K series	2.018		1.00	50.08	2.09
Al	K series	1.050		1.00	15.90	1.29
Si	K series	1.000		1.00	16.02	1.31
Mn	K series	1.154		1.00	4.29	0.77
Co	K series	1.187		1.00	1.63	0.57
Ni	K series	1.164		1.00	12.08	1.27
Total:					100.00	

Figure 87. *TEM image, spectrum diagram and element distribution table of the studied LARCO GMMSA laterite.*

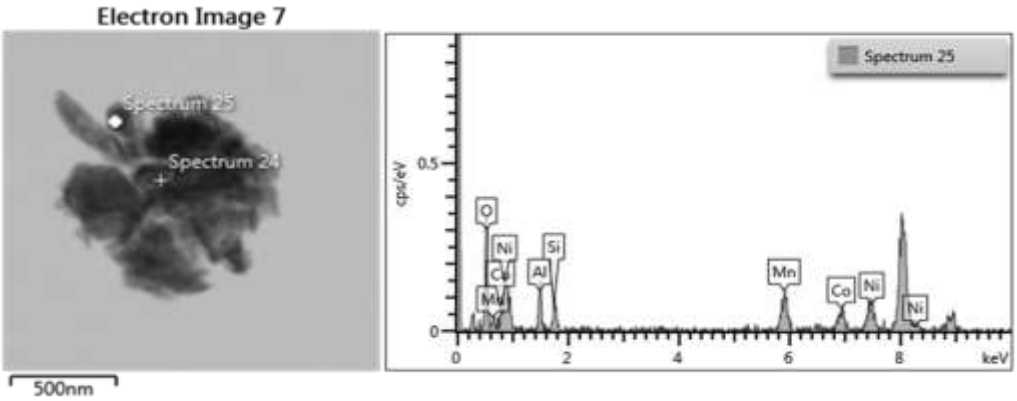

Element	Line Type	k Factor	k Factor type	Absorption Correction	Wt%	Wt% Sigma
O	K series	2.018		1.00	41.03	2.82
Al	K series	1.050		1.00	10.86	1.33
Si	K series	1.000		1.00	6.29	1.17
Mn	K series	1.154		1.00	16.62	1.83
Co	K series	1.187		1.00	11.11	1.60
Ni	K series	1.164		1.00	14.09	1.86
Total:					100.00	

Figure 88. *TEM image, spectrum diagram and element distribution table of the studied LARCO GMMSA laterite.*

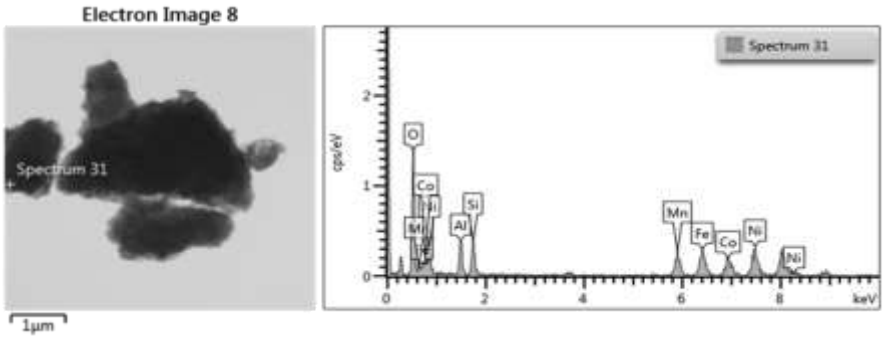

Element	Line Type	k Factor	k Factor type	Absorption Correction	Wt%	Wt% Sigma
O	K series	2.018		1.00	42.05	1.29
Al	K series	1.050		1.00	8.27	0.59
Si	K series	1.000		1.00	7.37	0.58
Mn	K series	1.154		1.00	9.79	0.67
Fe	K series	1.147		1.00	11.52	0.74
Co	K series	1.187		1.00	8.27	0.68
Ni	K series	1.164		1.00	12.73	0.77
Total:					100.00	

Figure 89. *TEM image, spectrum diagram and element distribution table ofthe studied LARCO GMMSA laterite.*

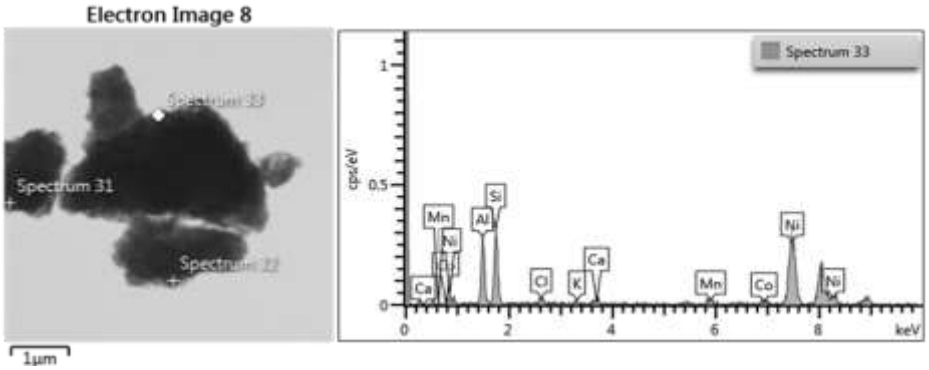

Element	Line Type	k Factor	k Factor type	Absorption Correction	Wt%	Wt% Sigma
Al	K series	1.050		1.00	19.85	1.22
Si	K series	1.000		1.00	21.85	1.28
Cl	K series	1.031		1.00	2.63	0.56
K	K series	1.015		1.00	1.03	0.44
Ca	K series	0.992		1.00	1.80	0.53
Mn	K series	1.154		1.00	2.63	0.64
Co	K series	1.187		1.00	2.61	0.65
Ni	K series	1.164		1.00	47.60	1.60
Total:					100.00	

Figure 90. *TEM image, spectrum diagram and element distribution table of the studied LARCO GMMSA laterite.*

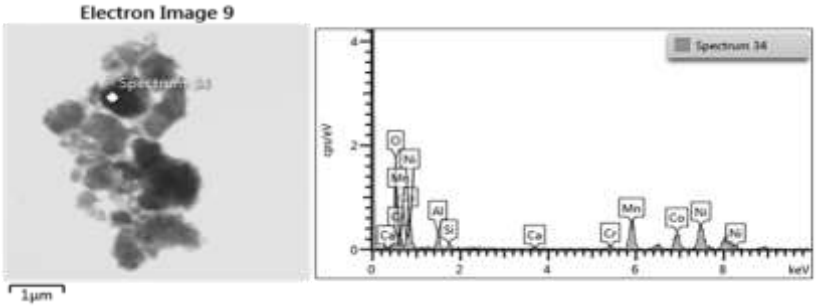

Element	Line Type	k Factor	k Factor type	Absorption Correction	Wt%	Wt% Sigma
O	K series	2.018		1.00	42.08	1.63
Al	K series	1.050		1.00	4.57	0.58
Si	K series	1.000		1.00	1.60	0.41
Ca	K series	0.992		1.00	0.93	0.30
Cr	K series	1.120		1.00	1.94	0.41
Mn	K series	1.154		1.00	19.48	1.08
Co	K series	1.187		1.00	11.78	0.89
Ni	K series	1.164		1.00	17.62	1.08
Total:					100.00	

Figure 91. *TEM image, spectrum diagram and element distribution table of the studied LARCO GMMSA laterite.*

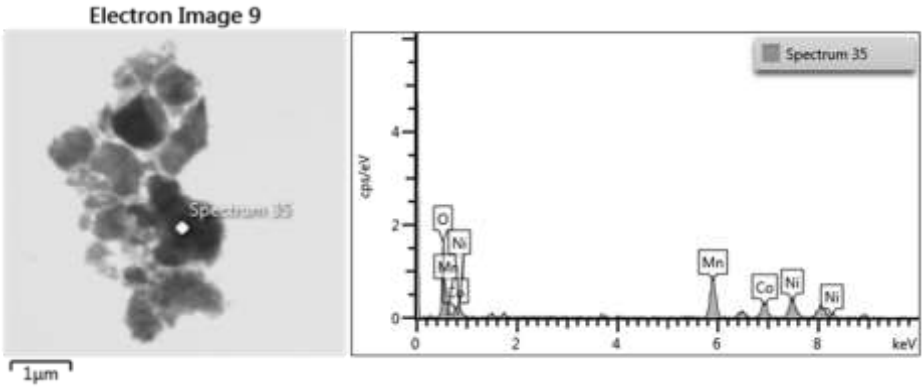

Element	Line Type	k Factor	k Factor type	Absorption Correction	Wt%	Wt% Sigma
O	K series	2.018		1.00	40.09	1.75
Mn	K series	1.154		1.00	31.41	1.42
Co	K series	1.187		1.00	13.37	1.02
Ni	K series	1.164		1.00	15.14	1.14
Total:					100.00	

Figure 92. *TEM image, spectrum diagram and element distribution table of the studied LARCO GMMSA laterite.*

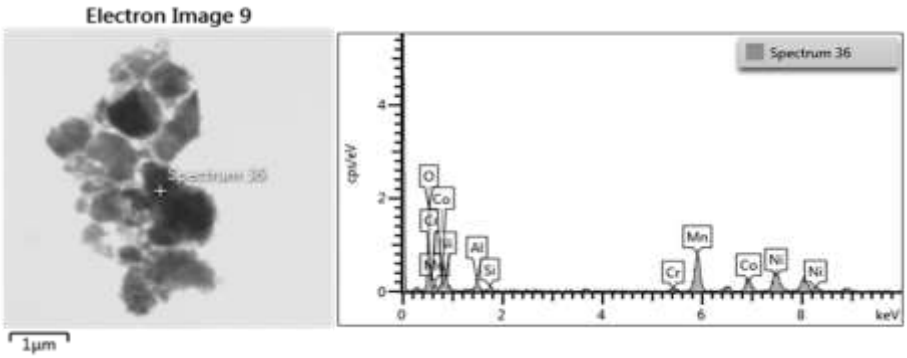

Element	Line Type	k Factor	k Factor type	Absorption Correction	Wt%	Wt% Sigma
O	K series	2.018		1.00	42.46	1.75
Al	K series	1.050		1.00	3.46	0.58
Si	K series	1.000		1.00	1.36	0.40
Cr	K series	1.120		1.00	1.86	0.44
Mn	K series	1.154		1.00	26.26	1.29
Co	K series	1.187		1.00	9.43	0.86
Ni	K series	1.164		1.00	15.18	1.12
Total:					100.00	

Figure 93. *TEM image, spectrum diagram and element distribution table of the studied LARCO GMMSA laterite.*

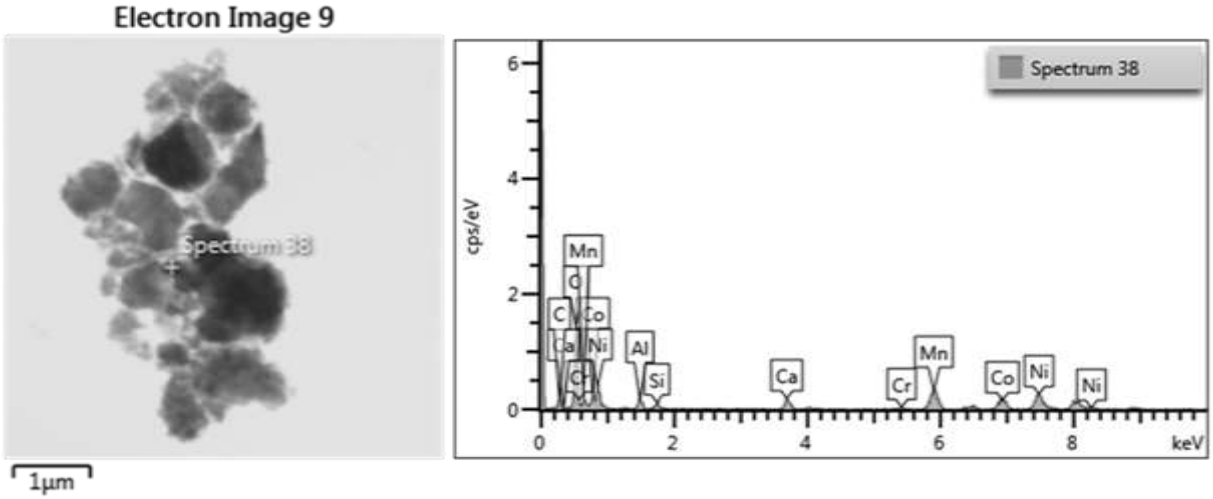

Element	Line Type	k Factor	k Factor type	Absorption Correction	Wt%	Wt% Sigma
O	K series	2.018		1.00	37.27	1.41
Al	K series	1.050		1.00	5.59	0.58
Si	K series	1.000		1.00	3.76	0.48
Cr	K series	1.120		1.00	1.56	0.35
Mn	K series	1.154		1.00	20.22	0.95
Co	K series	1.187		1.00	11.05	0.76
Ni	K series	1.164		1.00	20.54	1.01
Total:					100.00	

Figure 94. *TEM image, spectrum diagram and element distribution table of the studied LARCO GMMSA laterite.*

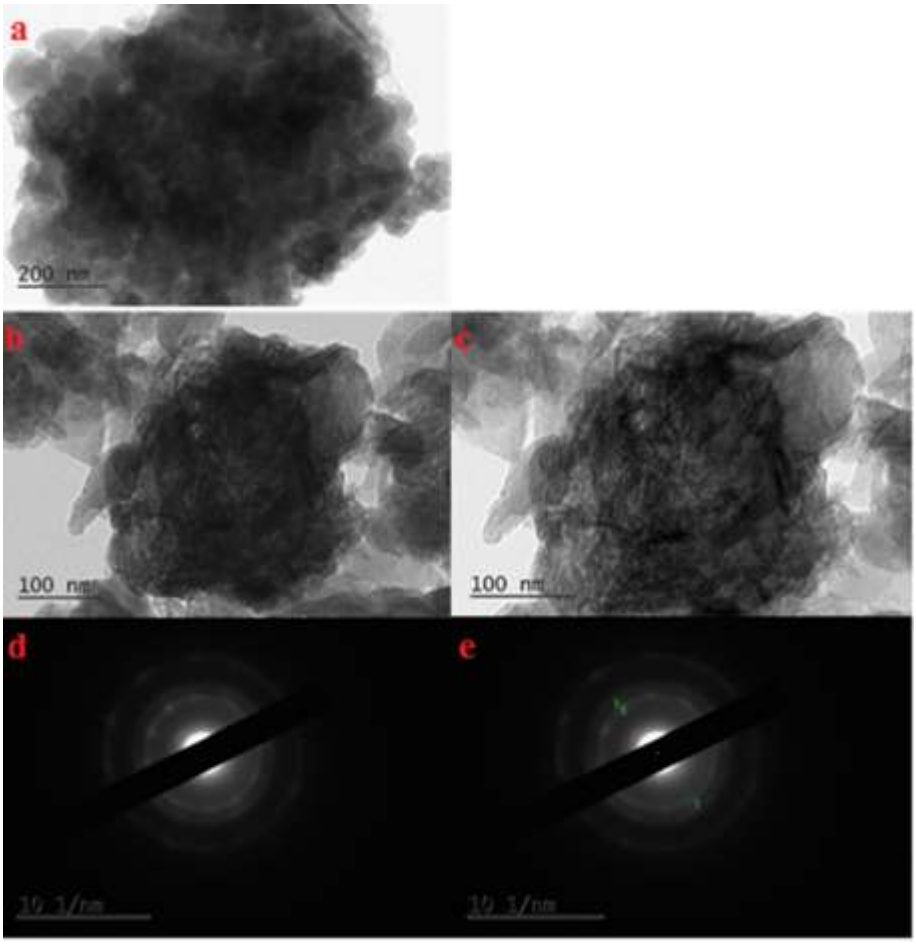
a
200 nm
b
100 nm
c
100 nm
d
e

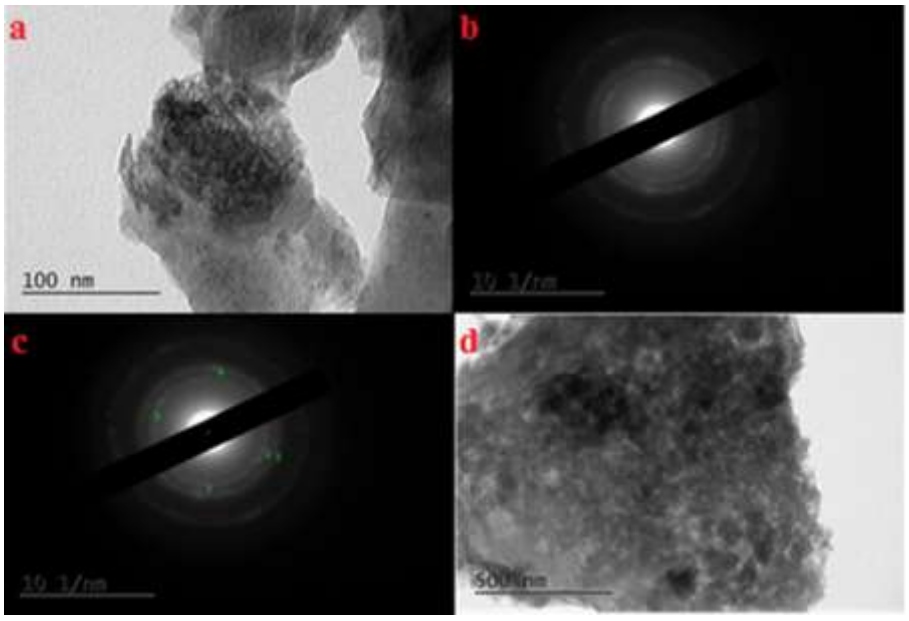
a
100 nm
b
c
d

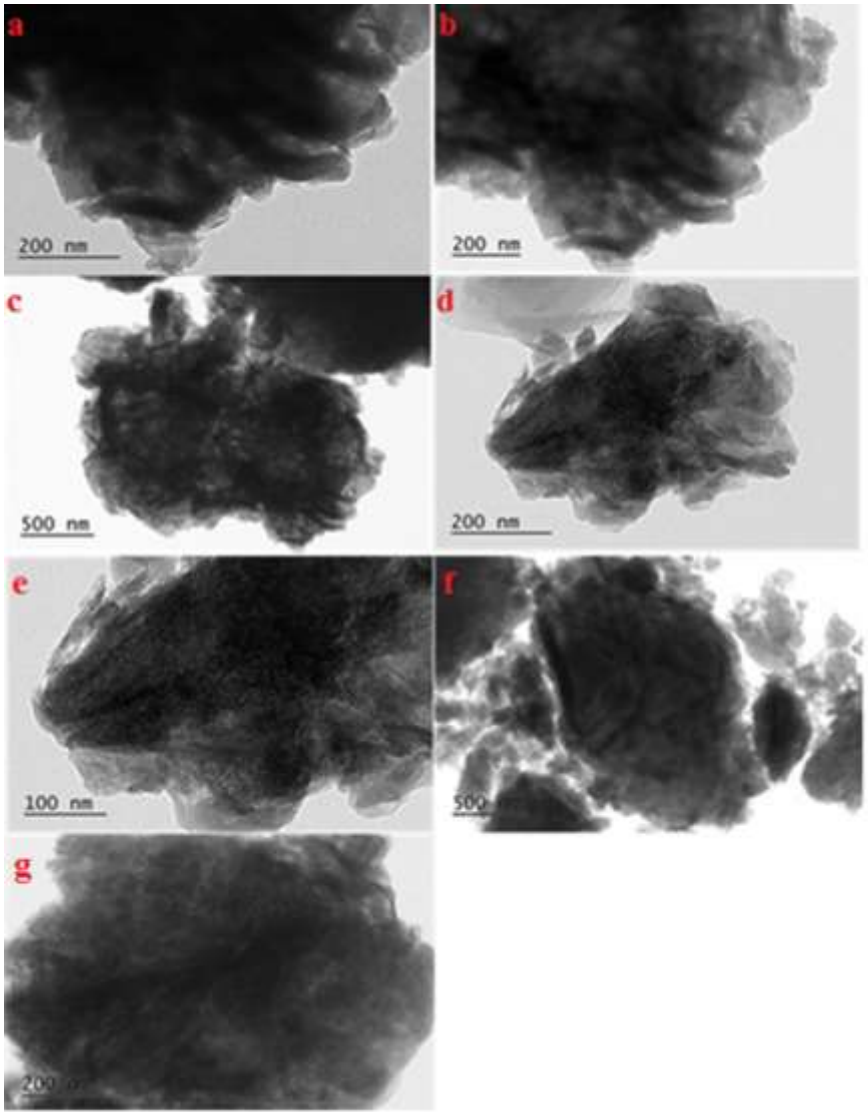
a
200 nm
b
200 nm
c
500 nm
d
200 nm
e
100 nm
f
500
g

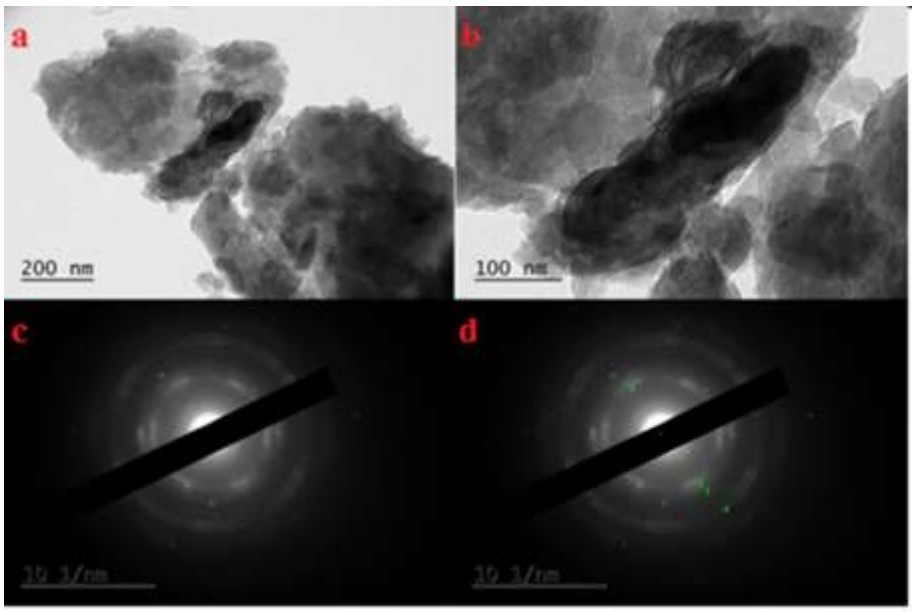
a
200 nm
b
100 nm
c
d

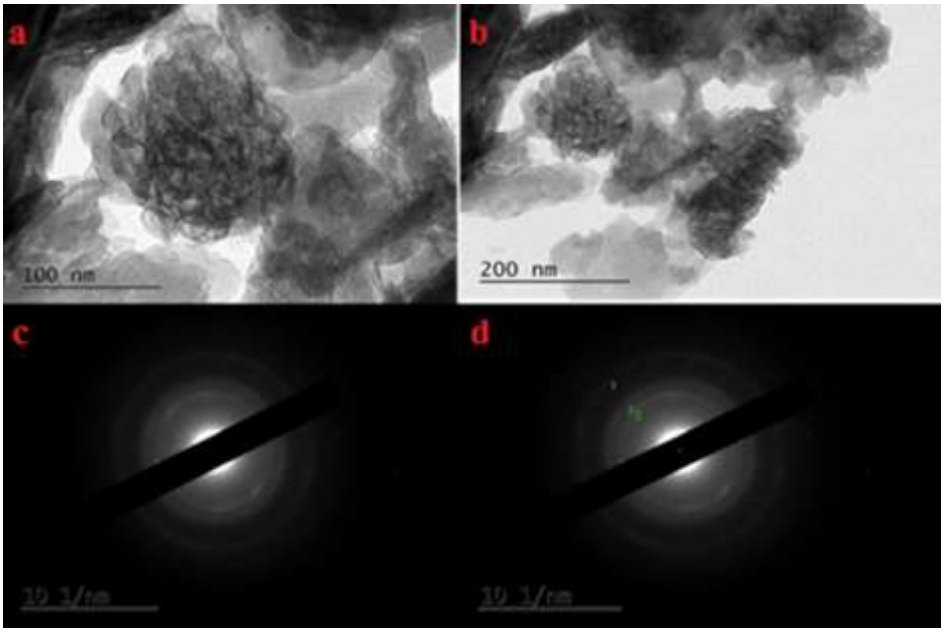
a
100 nm
b
200 nm
c
d

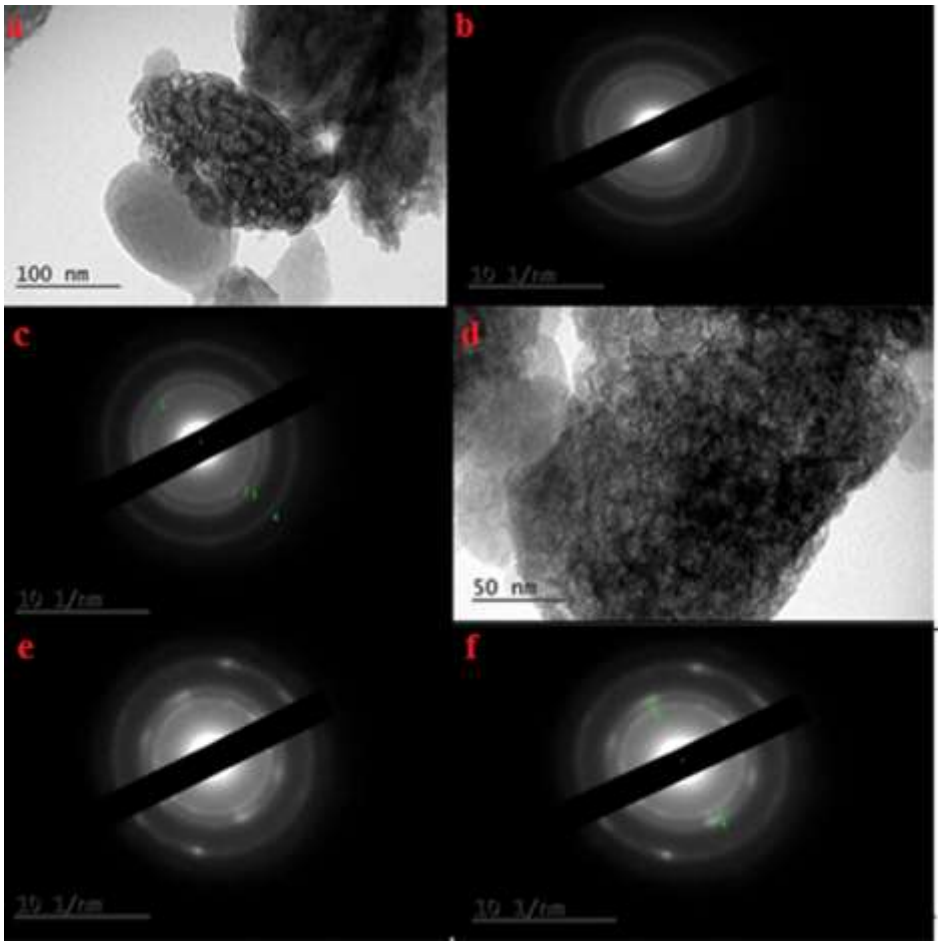
a
100 nm
b
c
d
50 nm
e
f

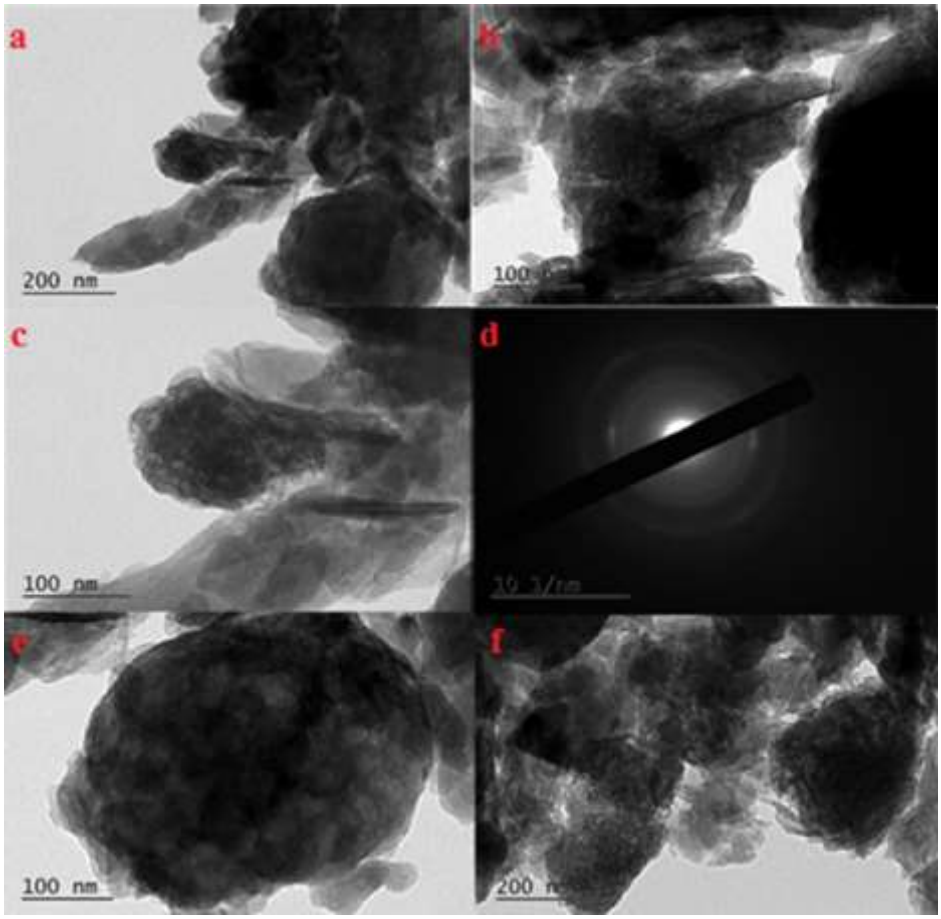

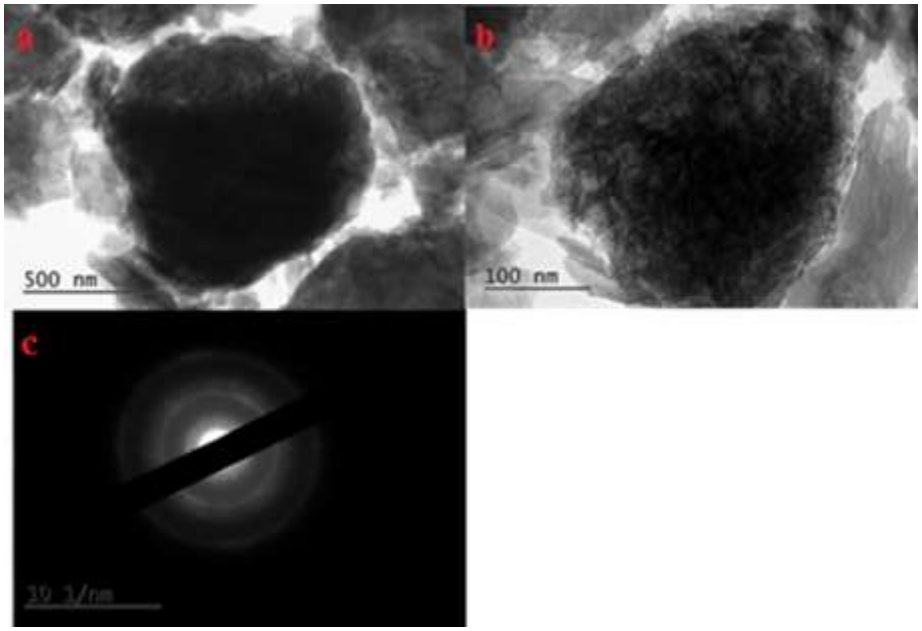

Figure 95. *TEM-EDS data concerning the studied LARCO GMMSA laterite.*

3.6 Bulk geochemistry and implications about the formation of the deposit

The bulk chemical composition of the studied LARCO GMMSA laterite ore has been yielded by means of ICP-OES/MS & Leco measurements. Analytical findings provide convincing evidence that all the illustrated elements can be accurately measured by this analytical technique. The bulk chemical composition of all the studied samples is presented in Table 5. Moreover, the average concentration of elements in the ore is presented in Table 6, while the distribution of key elements and parameters, throughout the horizons of the deposit (and also to the hosting limestones; see also next chapter) is shown in Figures 96-100.

Table 5. *Major and trace element concentrations of the studied LARCO GMMSA laterite ore.*

SampleCode	L1	L2	L3	L4	L5	L6	L
Description	Laterite 1	Laterite 2	Laterite 3	Laterite 4	Laterite 5	Laterite 6	"Garnierite"
	wt%	wt%	wt%	wt%	wt%	wt%	wt%
Fe_2O_3	31,16	32,66	29,30	32,74	37,74	39,10	3,84
SiO_2	28,83	28,59	29,63	27,81	23,33	23,48	17,95
Al_2O_3	24,64	24,84	26,03	24,28	21,10	20,42	20,28
LOI	11,90	10,70	11,30	11,00	10,20	9,90	28,00
TiO_2	1,34	1,34	1,46	1,27	1,41	1,35	0,01
Cr_2O_3	0,86	0,72	0,91	0,57	1,30	1,11	0,21
MgO	0,26	0,23	0,30	0,44	1,27	1,08	0,05
MnO	0,13	0,18	0,21	0,39	0,93	0,32	1,04
CaO	0,26	0,18	0,16	0,27	0,31	0,29	11,81
P_2O_5	0,04	0,04	0,03	0,14	0,14	0,14	0,01
K_2O	0,09	0,06	0,06	0,11	0,10	0,11	0,01
TOT/C	0,07	0,07	0,05	0,11	0,08	0,08	2,62
TOT/S	0,01	0,01	0,01	0,01	0,01	0,01	0,13
Na_2O	0,03	0,02	0,02	0,01	0,01	0,01	0,01
	ppm	ppm	ppm	ppm	ppm	ppm	ppm
Ni	1340,0	1421,2	1750,3	2953,0	6968,6	9212,3	>10000
Co	171,2	140,1	327,5	952,7	1479,9	882,7	3534,0
Y	42,9	52,2	54,4	284,2	763,7	688,0	34,9
La	48,2	66,4	79,6	713,8	497,2	481,0	7,9
Zn	26,0	39,0	59,0	98,0	263,0	387,0	111,0
V	302,0	301,0	379,0	249,0	327,0	344,0	9,0
Nd	24,7	26,6	47,6	182,1	201,8	271,1	30,1
Ce	127,3	103,6	144,1	238,0	263,1	210,0	27,0
Zr	175,4	181,6	180,7	172,2	203,0	203,2	1,1
Cu	41,7	82,4	26,5	22,9	193,9	138,7	211,8
Sc	76,0	60,0	65,0	76,0	75,0	72,0	90,0
As	22,6	27,0	37,8	67,3	80,6	69,2	38,2
Pr	6,5	7,2	11,6	65,4	56,0	66,8	4,9
Pb	39,0	50,8	44,1	50,3	67,2	64,6	2,6
Gd	5,7	6,0	7,5	23,0	57,2	57,7	11,5
Dy	6,4	7,0	7,3	25,6	63,7	53,4	8,3
Sr	27,0	29,9	31,7	124,0	78,6	51,9	11,3
Sm	4,9	5,1	8,2	21,4	40,3	46,3	12,9
Er	4,4	4,9	5,0	19,0	47,1	39,9	4,2
Ga	34,9	24,0	24,3	25,5	32,8	33,2	1,8
Yb	4,2	4,8	4,7	16,5	37,1	29,8	4,3

Table 5. *continued:*

SampleCode	L1	L2	L3	L4	L5	L6	L
Description	Laterite 1	Laterite 2	Laterite 3	Laterite 4	Laterite 5	Laterite 6	"Garnierite"
	wt%	wt%	wt%	wt%	wt%	wt%	wt%
Ba	10,0	14,0	13,0	18,0	18,0	21,0	32,0
Nb	19,3	20,1	20,2	18,7	20,6	20,4	0,1
Th	12,2	12,3	11,6	11,5	15,7	15,6	0,1
Ho	1,5	1,6	1,6	6,2	15,6	13,3	1,5
Eu	1,3	1,3	1,8	4,9	10,8	11,0	3,3
Tb	1,0	1,1	1,2	3,9	9,7	8,6	1,7
Be	0,5	2,0	2,0	4,0	8,0	8,0	14,0
U	3,1	4,9	3,7	4,1	6,0	7,2	58,6
Hf	4,7	4,8	4,7	4,3	5,2	5,5	0,1
Tm	0,7	0,8	0,7	2,7	6,4	5,2	0,7
Rb	2,2	1,2	1,2	3,0	2,4	4,8	0,3
Lu	0,7	0,7	0,7	2,5	5,8	4,6	0,7
Sn	3,0	3,0	3,0	3,0	4,0	4,0	0,5
W	2,6	2,4	2,3	2,5	2,8	3,7	0,3
Sb	1,0	1,3	1,4	1,5	1,8	2,3	0,8
Mo	0,7	1,0	0,9	1,5	1,9	1,4	1,1
Ta	1,2	1,3	1,4	1,2	1,3	1,3	0,1
Bi	0,6	0,6	0,5	0,5	0,7	0,7	0,1
Cs	0,2	0,1	0,1	0,3	0,4	0,4	0,1
Cd	0,1	0,2	0,1	0,3	0,5	0,3	0,7
Se	0,3	0,3	0,3	0,3	0,3	0,3	0,3
Ag	0,1	0,1	0,1	0,1	0,1	0,1	0,1
Tl	0,1	0,1	0,1	0,1	0,1	0,1	2,1
Hg	0,0	0,0	0,0	0,0	0,0	0,0	1,6
Au	0,0	0,0	0,0	0,0	0,0	0,0	0,0
ΣLREE	211,6	208,9	291,1	1220,7	1058,4	1075,2	82,7
ΣHREE	25,8	28,2	30,6	104,2	253,2	223,7	36,2
ΣREE	237,4	237,1	321,7	1324,8	1311,6	1298,9	118,9
ΣREE+Y+Sc	**356,3**	**349,3**	**441,1**	**1685,0**	**2150,3**	**2058,9**	**243,8**
$[Eu/Eu^*]_{NASC}$	1,2	1,2	1,1	1,1	1,1	1,0	1,3
$[Ce/Ce^*]_{NASC}$	1,4	0,9	0,9	0,2	0,3	0,2	0,8
$[La/Sm]_{NASC}$	1,8	2,3	1,7	6,0	2,2	1,9	0,1
$[La/Yb]_{NASC}$	11,4	13,9	17,0	43,4	13,4	16,1	1,9

Table 6. *Average concentrations of major end trace elements n LARCO GMMSA typical laterite ore (excluding the occasional 'garnierite' thin base layer).*

	AVERAGE LATERITE	AVERAGE LATERITE
	wt.%	ppm
Fe_2O_3	33,78	337833
SiO_2	26,95	269450
Al_2O_3	23,55	235517
LOI	10,83	108333
TiO_2	1,36	13617
Cr_2O_3	0,91	9098
MgO	0,60	5967
ΣREE+Y+Sc	**0,12**	**1173**
Ni	**0,39**	**3941**
ΣREE	**0,08**	**789**
ΣLREE	**0,07**	**678**
MnO	0,36	3600
CaO	0,25	2450
P_2O_5	0,09	883
K_2O	0,09	883
TOT/C	0,08	767
Co	**0,07**	**659**
V	0,03	317
La	0,03	314
Y	0,03	314
Zr	0,02	186
Ce	0,02	181
Na_2O	0,02	150
Zn	0,01	145
Nd	0,01	126
TOT/S	0,01	100
Cu	0,01	84
Sc	0,01	71
ΣHREE	0,01	111
As	0,01	51

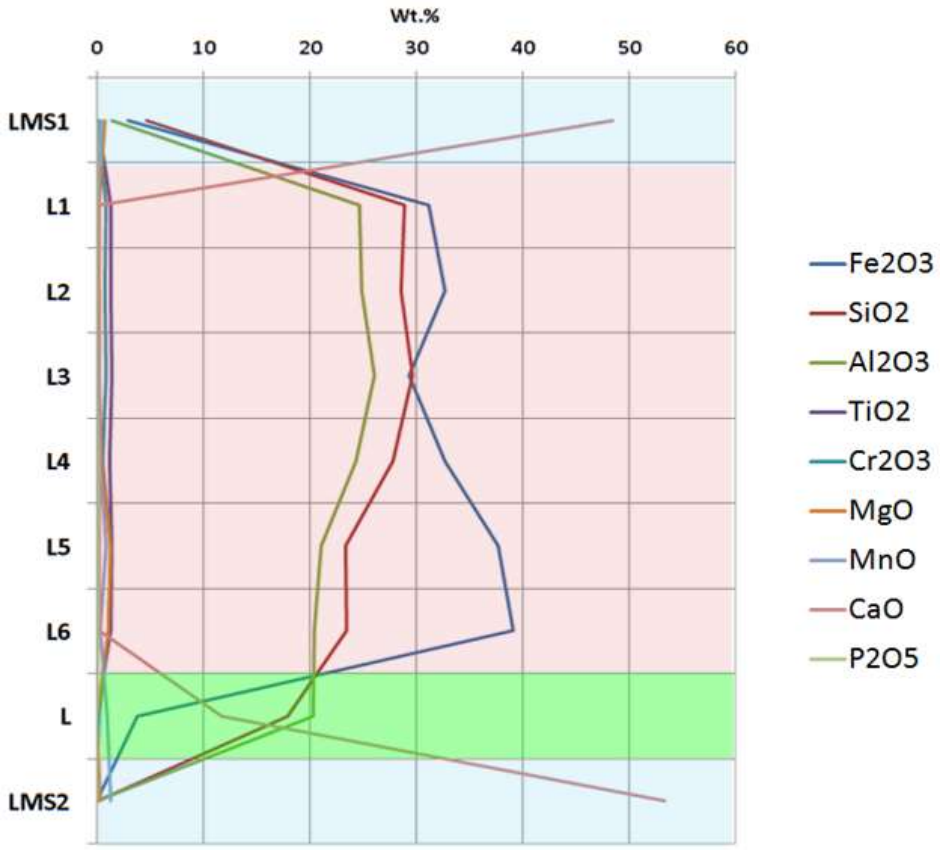

Figure 96. *Distribution of major elements in the studied LARCO GMMSA deposit.*

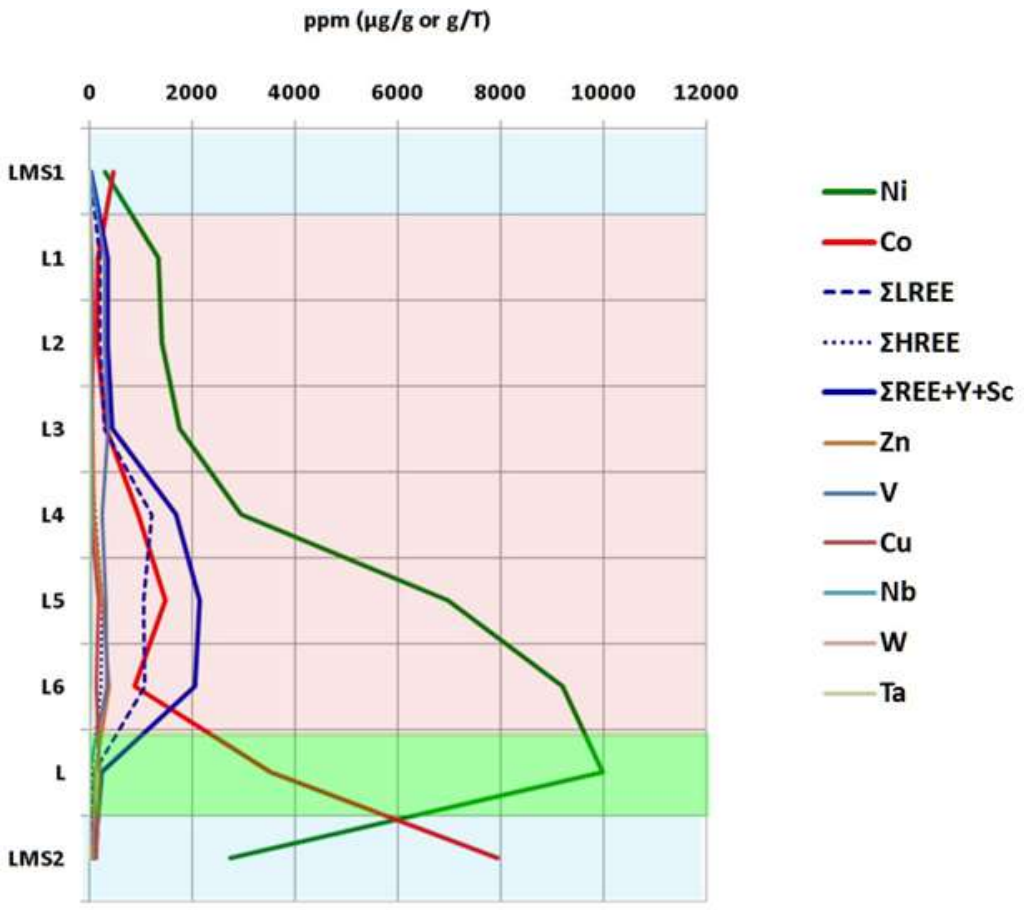

Figure 97. *Distribution of useful trace elements in the studied LARCO GMMSA deposit.*

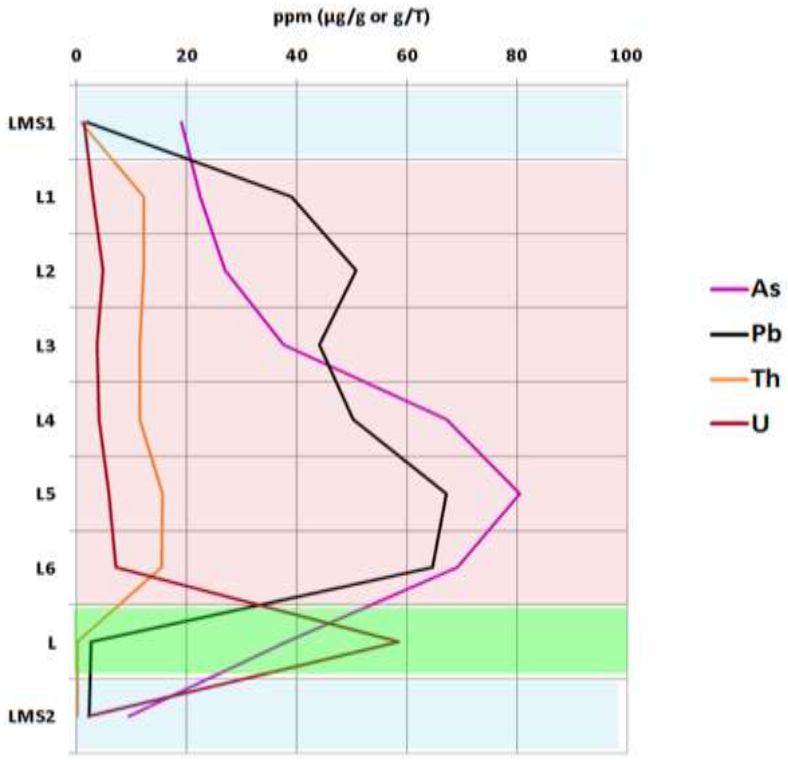

Figure 98. *Distribution of potentially hazardous trace elements in the studied LARCO GMMSA deposit.*

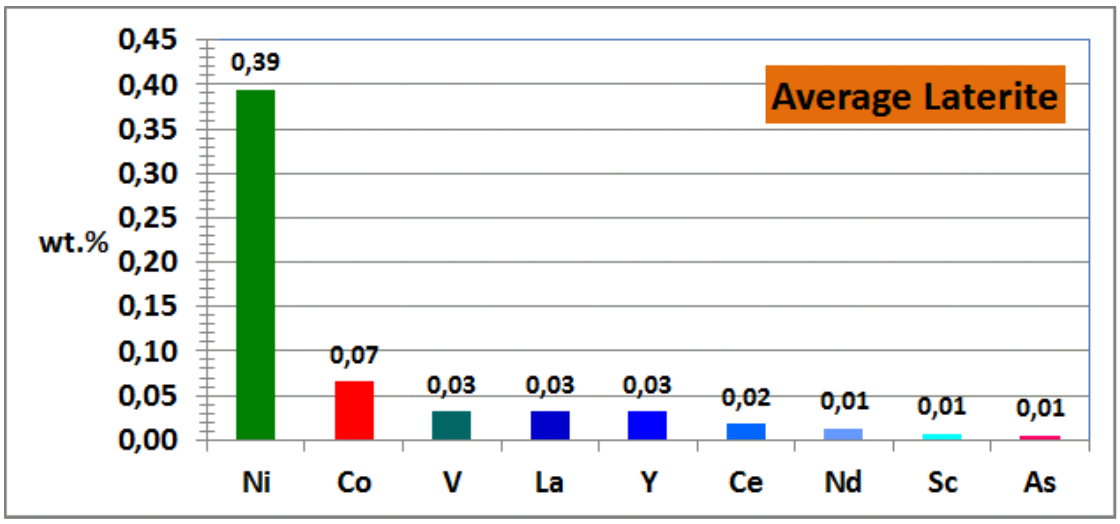

Figure 99. *Concentration of basic and critical metals in the studied LARCO GMMSA laterite ore.*

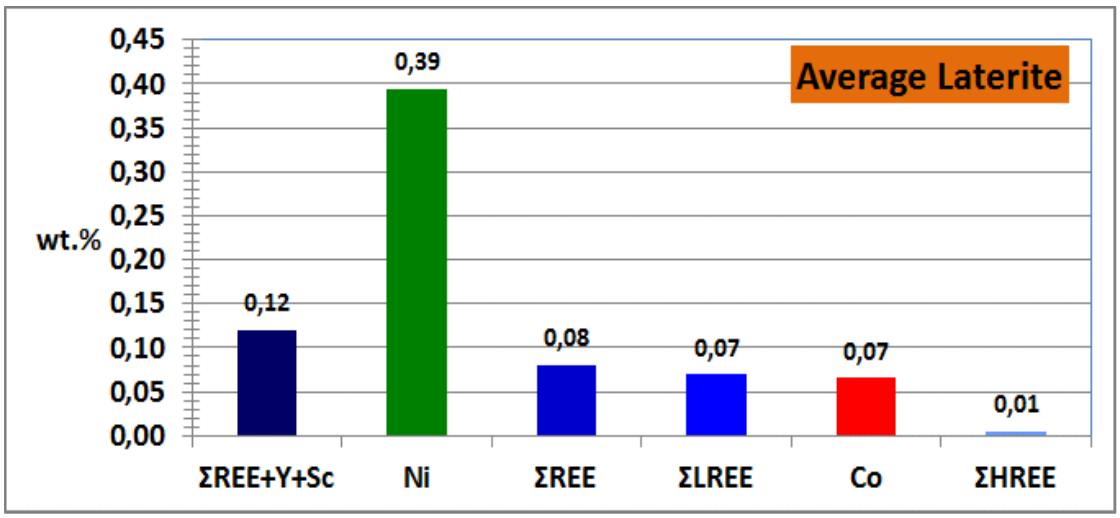

Figure 100. *Summary regarding concentration of basic and critical metals in the studied LARCO GMMSA laterite ore.*

Concerning further geochemical considerations, the UCC-normalized spider diagrams (Rudnick and Gao, 2003) have indicated a clear enrichment in High-Field Strength Elements (HFSE), particularly Sc and actinide element Th [sample L shows a remarkably elevated content of actinide element U (~59 ppm)], REE, and in certain compatible elements (Ni, Co, Cr, Zn, Cu), while there is a depletion in Large Ion Lithophilic Elements (LILE), particularly Rb and K, and Sr [except sample L_4 with high Sr contents (124 ppm)]. V and actinide elements (Th and U) remain relatively constant along the laterite profile (317 ppm, 13 ppm and 4.8 ppm, respectively). It is also notable that the ore exhibits an As geochemical positive anomaly (~81 ppm; Table 5).

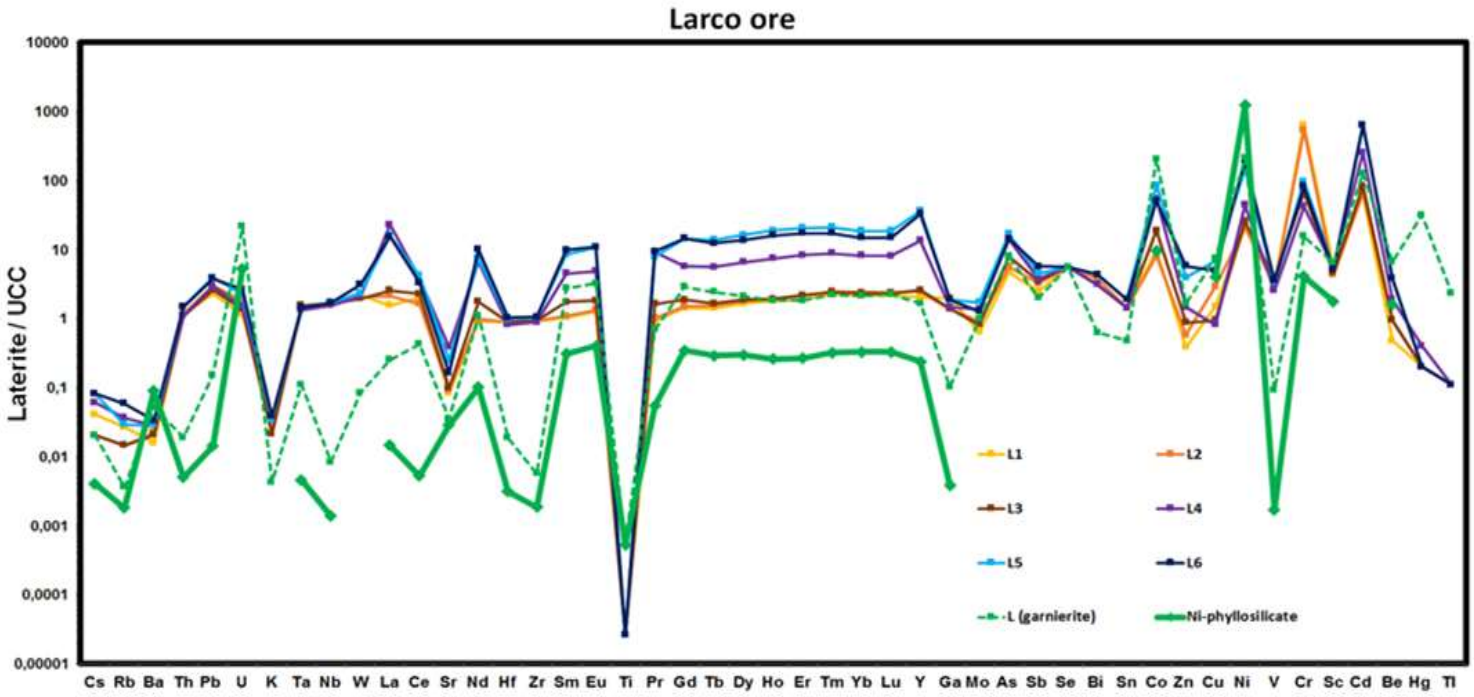

Figure 101. *Upper Continental Crust (UCC)-normalized (Rudnick and Gao, 2003) multi-element spider diagram for the studied LARCO GMMSA laterite ore (ICP-OES/MS) and Ni-phyllosilicate (LA-ICP-MS).*

The studied laterite ore of is characterized by no variations of Si, Al, Fe contents, whereas there are wide vertical variations of major and trace element (Cr, Mn,Co) contents (Fig. 101). SiO_2 and Al_2O_3 behave very similarly all along the profile: lowest concentrations are observed in the bedrock (17.9 wt.% SiO_2 and ~20.3 wt.% Al_2O_3), while their concentrations increase to 28.8 wt.% and to 24.6 wt.%, respectively in the top (sample L_1). At the studied site the Fe content in the ore samples ranges from ~31.2 to 39.1 wt.% Fe_2O_3, and the Cr content from ~0.9 to ~1.1 wt.% Cr_2O_3. Fe_2O_3 and Cr_2O_3 show a typical enrichment, as both elements display higher concentrations (an increased concentration) at the lower laterite layer at the base of the deposit (sample L_6) (39.1 wt.% and ~1.1 wt.%, respectively). Chromium concentrations in the lower portions of the profile indicate a high mobility of Cr during the formation of the deposit. In fact, Cr content is relatively high (~1.1 wt.% Cr_2O_3) compared to other Fe-Ni-laterites from elsewhere in Greece (Valeton et al., 1987; Eliopoulos and Economou-Eliopoulos, 2000; Economou-Eliopoulos, 2003). The mining locations of large Fe-Ni-laterite deposits and occurrences located in the Pelagonian-Sub-Pelagonian zone of Greece extend into Serbia and continue into Turkey (Economou-Eliopoulos et al., 2012) and their metallurgical residues, containing significant amounts of Cr (Valeton et al., 1987; Alevizos, 1997; Eliopoulos and Economou-Eliopoulos, 2000), are potential sources of contamination by Cr. In contrast, other Ni-laterite deposits host chromite with a negligible content of these traces or minor elements (Orphanoudakis et al., 1997). Chromium is usually retained in the Ni-bearing soil, and, therefore, deciphering Cr pathways can therefore help to identify alteration and lateritisation mechanisms and may be a useful tracer for supergene ore deposits (Krüger, 2015). Since lateritic chromites are residually inherited in laterites from weathered ultramafic rocks, the composition of primary chromite cores within Fe-Ni ores may provide evidence for the parent rocks of laterites. The limited compositional variation of primary chromite through vertical laterite profiles maybe related to either in situ weathering or homogeneous composition of the parent rocks on a regionalscale (Economou-Eliopoulos et al., 2003).

It is evident that LARCO GMMSA laterite is preferentially enriched in Ni, Co, REE, Sc, Mn, and As (Table 5). In particular, the samples contain an average of 3941 ppm Ni, 659 ppm Co and 789 ppm ΣREE (Table 6). Nickel concentration in the sample L_1 taken from the top of the deposit, exactly under the hanging wall limestone, is low (1340 ppm Ni), but strongly increases in the L_4 sample reaching 2953 ppm Ni, and finally, reaches the value of ~9212 ppm. Taking into account the above, from top to bedrock the profile is characterized by a progressive enrichment in Ni. Nickel is dominant in the sample L taken from the base of the deposit, exactly over the footwall limestone (> 10000 ppm). Cobalt is commonly associated with Mn-(oxy)hydroxides detected by SEM-EDS (see text above) during the evolutionary process. There is an apparent redistribution of Co along the lateritic profile, which is attributed to the change in pH, oxidation state and tectonic uplift (Yongue-Fouateu, 2006). Co and Mn display very similar behavior along the weathering profile, asthe schematic variations of the composition for the Co and Mn contents along the vertical at the study site (Fig. 101) show in general an increase towards the base of the deposit, and to be precise, at the contact between the ore and the upper Triassic-Jurassic limestone substrate. Both Co and Mn (3534 ppm and 1 wt.%, respectively) are best represented at the base of the profile. The high degree of mobility of Co and Mn, particularly through redox processes, insures that they can change phase during weathering, transport, deposition and diagenesis (Golightly, 1981; Frakes et al., 1992). The highest enrichment in these trace elements was recorded in the Edessa Ni-laterites, which is comparable to that of the western Vermio and Kastoria deposits, with the exception that the Mn content is lower in the latter (Eliopoulos and Economou-Eliopoulos, 2001). Besides, Mn and Co enrichment in chromite of some pseudo-autochthonous Fe-Ni-laterite deposits in the areas east Vermion, Edessa and Olympos (northern Greece) provides evidence for the redeposition of the weathered material (Economou-Eliopoulos, 2003). This enrichment in Ni, Co, and Mn, found in samples from the contact between the lowest part of the laterite and the footwall limestone at the studied LARCO GMMSA deposit, has been attributed to a downward mobilization and concentration towards the footwall limestone of these elements (Table 5). Furthermore, the preferential occurrence of Ni, Co, and Mn towards the lowermost part of the laterite ore suggest its deposition was controlled by physicochemical conditions rather than the precursor rocks.

Significant contents of Sc up to 90 ppm (Table 5) were determined in the studied laterites. In fact, Sc remains relatively constant along the lateritic ore deposit (71 ppm). In contrast to the group of lanthanides (La-Lu) of REE and the Y element, which have a close genetic and spatial relationship with alkaline acidic igneous rocks, Sc has a closer relationship with ultramafic-mafic rocks with high Mg content (Hoatson et. al, 2011 and references therein). In a relevant recent study, Aiglsperger et al. (2016) presented Sc contents up to 120 ppm, which is found with an average content of about 70-80 ppm Sc in the upper zone of limonite in Ni-laterites in Cuba and Dominican Republic. Aiglsperger et al. (2015) and Aiglsperger et al. (2016) also thoroughly revealed that Sc is considered to be found in the minerals of peridotite pyroxenes as a substituent of trivalent Fe, while it is mainly concentrated in the final disintegration products containing Fe and Mn. Latest data yielded by Qin et al. (2020) present concentration of Sc in the laterites ranged from 14.9 to 83.5 ppm showing a certain Sc enrichment in the Ni-laterites from Philippines. In fact, in another recent work (Chasse et al., 2017) first data on Sc speciation in lateritic deposits were provided, proposing a study of the lateritic profile of the Syerston-Flemington deposit (eastern Australia), which developed on an ultramafic-mafic intrusive complex. The presence and association of Sc with Ni and Co in very disintegrated laterite profiles, which are

overlying mafic-ultramafic penetrations in Australia, is considered to be of economic importance (Kalatha et al., 2017). Besides, it has been recently reported that Sc can be greatly enriched in laterite deposits developed over ultramafic and mafic rocks, showing that the Sc-rich laterite is a potential Sc (by-product) resource (Qin et al., 2020). Lateritic profiles over ultramafic-mafic rocks usually show Sc concentrations lower than 100 ppm, corresponding to enrichment by a factor of ten during lateritic weathering, which is similar to the maximum factor of enrichment found in the Syerston-Flemington deposit (Chasse et al., 2017), and both confirmed the fact that Sc concentration in laterite is primarily controlled by the parent rocks (Chasse et al., 2017, 2019; Teitler et al., 2019). Recent investigations of Sc contents in New Caledonia laterites demonstrated by Ulrich et al. (2019) revealed that significant concentrations occur mainly at the top of the lateritic profile (up to 80 ppm Sc). These preliminary data show a clear relation between Sc and Fe enrichments, suggesting that Sc is residually enriched at least during the first steps of weathering. Accordingly, Chasse et al. (2017) and Qin et al. (2020) agree that Sc can be structurally incorporated onto crystalline (in the crystal structure of hematite) and/or into amorphous (goethite) Fe-(oxyhydr)oxides, as indicated by SEM-EDS investigation (see text above). However, little is known about the variation of concentrations in the parent rocks, the concentration factors, and Sc-bearing mineral phases along the weathering (Ulrich et al., 2019). In fact, Chasse et al. (2017) concluded that Sc is adsorbed on goethite and incorporated in the crystal structure of hematite by substituting Fe^{3+}. In parallel, a communication by Muρoz et al. (2017) providing a further study of Sc speciation in New Caledonia laterites by coupling X-ray absorption spectroscopy (XANES/EXAFS) and sequential chemical extraction, demonstrate that Sc is actually mainly integrated in the structure of goethite rather being adsorbed. According to recent studies (Chasse et al., 2017; Samson et al., 2016), anomalies of Sc concentration in the parent rock result from specific conditions of formation and are not shared by all ultramafic-mafic bedrocks. Exceptional concentration of Sc in lateritic deposits thus results from a combination of three circumstances: (1) anomalously high Sc concentration in the parent rock, (2) long time scales of alteration in stable tectonic environment and (3) lateritic conditions during weathering, allowing the trapping of Sc by Fe oxides (Chasse et al., 2017). Based on these implications, the presence of Sc in this deposit may be indicative of the contribution from other rocks.

The As content is significant (up to 80 ppm in sample L_6) (Table 5). The As accumulation in Greek commercial Ni-laterite ores is an issue that has always been mentioned by Eliopoulos et al. (2010), Eliopoulos et al. (2012) and Kalatha et al. (2015). More specifiacally, the elevated As content of the Larymna depositis in accordance with the results that have been previously mentioned by Eliopoulos et al. (2010), who investigated the presence of As in Greek laterites, and presented data that revealed As concentrations for the individual laterite occurrences and deposits from Agios Ioannis, which vary significantly from < 2 ppm to 2600 ppm. However, general geochemical study of Fe-Ni-laterite deposits in the Balkan Peninsula and Turkey, located in the Mirdita-Sub-Pelagonian and Pelagonian geotectonic zones, extending into the Anatolides zone, shows that As contents are generally low, ranging from less than two to a few tens of ppm. In a recent study by Gamaletsos et al. (2018), including As-speciation measurements by micro-XANES, mentioned the elevation of As concentrations, reaching bulk values up to 0.26 wt.% and 1.94 wt.% in Lokris, central Greece, and Gordes (western Turkey) deposits, although the As content seems to be negligible in the majority of the Fe-Ni-laterite ore deposits of the Balkan Peninsula and eastern Turkey. Arsenic is widely distributed in the environment, found in the earth's

crust at levels between 0.5 ppm and 2.5 ppm and concentrated, up to 13 ppm in clayey sediments. The As content in ultramafic rocks is usually very low, unless they have reacted with As-rich crust-derived fluids during subsidence or metamorphism. The analysis of As from Tertiary subsidence peridotites from the Indus Suture Zone of the northwestern Himalayas indicated enrichment in As (6 ppm to 275 ppm of As) while the sulfur content was low (< 50 ppm). Although the content of As in the peridotites of Evia is low, ranging from < 1 ppm of As in the less altered peridotites up to 6 ppm in the very serpentinized ones can be concentrated in allochthonous laterites with post-deposition processes. In the studied laterite As is clearly correlated to Fe, as the lowest part of the deposit, close to its contact with the basement limestone, of the lateritic profile is characterized by an almost progressive enrichment in these two elements. According to Samouhos et al. (2019), As, just like As(III) and As(V), is sorbed onto Al-rich and iron oxide phases (hematite and/or goethite-type phases) and its presence is associated with epigenetic phenomena. It is also suggested that As was enriched in the allochthonous Larymna deposit after the deposition and the diagenesis of the laterite which re-deposited in shallow sea environment. Additionally, Eliopoulos et al. (2010) presented data assuming that the elevated As contents in the Agios Ioannis may be related to the As-sources, including the parent ophiolite complexes, the local conditions of the redeposition environment and the involvement of organic material, which may have played a controlling factor of the physico/chemical conditions during diagenesis and meta-diagenesis stages.

As already mentioned, REEs enrichment is obvious in LARCO GMMSA laterite ore deposit. The studied samples contain significant amounts of REE, and, as can be seen in Table 5, the concentrations of some elements are in all cases higher in comparison to the UCC values. ΣLREE, ΣHREE and ΣREE reach the values of ~1221 ppm, ~253 ppm and ~1325 ppm, respectively (Table 5). Chondrite has been used for normalization of REEs (Fig. 102), because a bulk composition of the earth is assumed to be close to that of chondrite meteorites, which represent the primordial earth (Ohde et al., 1999). The use of this method eliminates the abundance variation between REEs of odd and even atomic number, and allows determination of the extent of fractionation between the REEs, because such fractionation is not considered to have taken place during a meteorite's formation (White 2013). The chondrite-normalized (Fig. 102) and the Av. Shale (Fig. 103) REE patterns of the raw ores show remarkable negative Ce anomalies (a more distinct Ce positive anomaly in sample L_1). There is no considerable Eu anomaly. Europium corresponds to the Eu anomaly trend of Upper Continental Crust/UCC (Fig. 102).

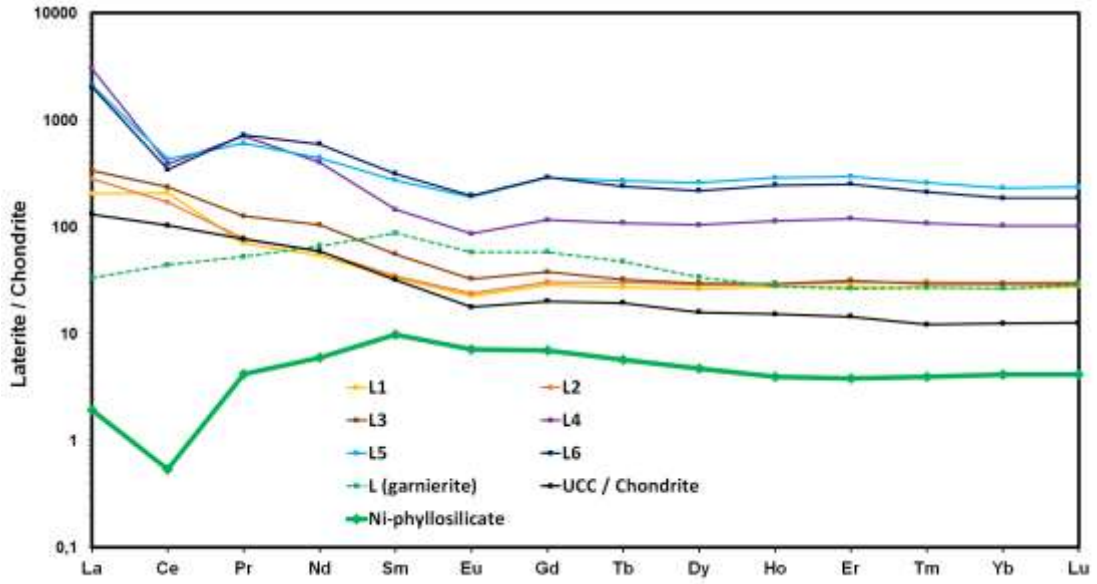

Figure 102. *Chondrite-normalized (McDonough and Sun, 1995) REE patterns for the studied LARCO GMMSA laterite ore and Ni-phyllosilicate (LA-ICP-MS).*

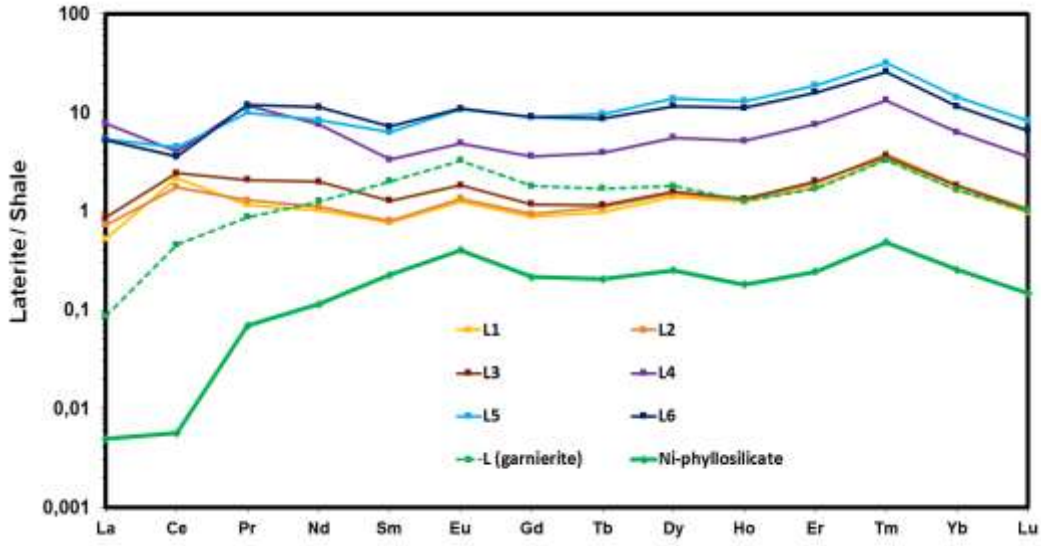

Figure 103. *Av. Shale normalized (Krauskopf and Bird, 1994) REE patterns for the studied LARCO GMMSA laterite ore and Ni-phyllosilicate (LA-ICP-MS).*

A general trend regarding REE behavior within lateritic profiles is that the mobilization of the REE during weathering processes results from different factors related to the parent rock mineralogy, specifically the distribution of the REE in the primary bearing minerals, the stability of these minerals during weathering, and their abundance in the parent material (Braun et al., 1990). The lateritic weathering is an important process in the REE-enrichment in laterites. The mineralogy of the weathered rocks and the physico/chemical conditions (temperature, acidity, redox potential) are among major controlling factors of the composition of the aqueous phase, which in turn can control the degree to which REEs are released to the downward moving fluids in contrast to iron that is quite reactive (Kalatha et al., 2017; Valeton et al., 1987; Maksimovic et al., 1993; Maksimovic et al., 1996; Alevizos, 1997; Economou-

Eliopoulos et al., 1997; Maksimovic, 1997; Eliopoulos et al., 2000; Panto et al., 2001; Maksimovic, 2003; Maksimovic, 2004; Skarpelis, 2006; Maksimovic, 2010; Eliopoulos et al., 2012; Dostal, 2016; Goodenough et al., 2016; Verplanck et al., 2016). It is generally agreed that LREE are less mobile than HREE and there is a consequent enrichment in the LREE relative to the HREE in the soil samples. The lowest parts of the Agios Ioannis (Nissi) are characterized by both Ni and bauxitic laterites with very high values, up to 6440 ppm ΣREE, along with enrichment in Mn, Ni and Co within the lowermost part of laterite and footwall limestone of the Nissi deposit. At the lower contact of bauxite developed over limestone at Parhari, Greece, REE concentrations are greater than thousands of ppm (Eliopoulos and Economou-Eliopoulos, 2000). Such enrichment in REE and the presence of authigenic REE minerals, such as bastnaesite, hydroxylcarbonate-(Nd) and hydroxylcarbonate-(La) (SEM-EDS study depicted the occurrence REE fluorocarbonate minerals; see text above) are consistent with a download mobilization of REE and concentration at the footwall limestone like in the majority of karstic laterite-bauxite deposits with authigenic REE minerals (Maksimovic et al., 1991). REEs typically exist in a trivalent oxidation state, but Ce and Eu are unique in that they can also exist in tetravalent and divalent oxidation states, respectively, giving rise to their anomalous behaviors. Both are very important elements providing some constraints on paleocean chemistry. Cerium is especially interesting to study because it can occur in nature as Ce^{3+}, like the majority of lanthanides, or as Ce^{4+} in oxidizing conditions. The use of the Ce anomaly was first proposed by Elderfield and Greaves as a consequence of the change in the ionic state of Ce as a function of oxidation state. If soluble Ce^{3+} is oxidized to Ce^{4+}, it precipitates from solution as very insoluble CeO_2. Consequently, the solution shows a negative Ce-anomaly. Ce-anomalies are well known in the marine environment. The existence of Ce^{4+} in sea water has been invoked to explain, on the one hand the negative Ce anomaly in sea water, and on the other hand the positive Ce-anomaly in Mn nodules. A major negative Ce-anomaly related to the accumulation of strongly Ce-depleted lanthanite has been observed [$(LREE)_2(CO_3)_38H_2O$] in a fossilised lateritic profile dating from the Pleistocene. Taking into account the existing literature, it seems that the nature of secondary minerals incorporating the REE, and especially Ce, is not known. The main mineral containing Ce^{4+} is cerianite (CeO_2) but its occurrence in nature has rarely been reported. An interesting case is represented in the Afu Hills (Nigeria) where the breakdown of bastnaesite [$Ce_2La_{1.5}(Nd,Pr)_{0.5}(CO_3)$] the weathering of fluocerite [$Ce_2La_{1.5}(Nd,Pr,Th)_{0.5}F_{12}$] oxidizing conditions lead to the formation of La-bastnaesite and cerianite [$(Ce^{4+},Th)O_2$]. Cerianite is also present as a weathering product in the Pocos de Caldas area (Brazil) (Braun et al., 1990). Regularly, the positive anomaly of Ce is also generated as a result of terrigenous input. In addition, factors like paleo-redox, fluviatile colloids enriched by Fe-organics, and scavenging processes could play crucial roles in the occurrence of positive Ce anomalies (Abedini et al., 2015). However, in the continental environment, the geochemistry of Ce is poorly documented and, as a result, it is not clear where and how Ce occurs in lateritic environments and which physicochemical parameters control Ce accumulation. A positive Ce-anomaly has been found in some weathering profiles on various types of source rocks. Lateritic femcretes (Fe crusts), which form on amphibolites, basaltic breccia, and gabbros from the Ivory Coast, display pronounced positive Ce-anomalies. Moreover, a positive Ce-anomaly has been also observed on a lateritic soil developed on the Korhogo granite (Ivory Coast). Positive Ce-anomalies have been also observed on chondrite normalized REE patterns in four lateritic profiles from Cameroon (Braun et al., 1990). According to Gamaletsos (2014), an evident positive Ce geochemical anomaly, i.e., positive Ce^{A},

can also stand for the Parnassos-Ghiona bauxites and, also for all Greek bauxites when their REE values are normalized to the average abundance of REE in the chondrite, PAAS, and Mediterranean bauxite belt, excluding Greek ones. In contrast to the majority of igneous REE deposits, such as carbonatites etc., which do not significantly show evidence of neither positive nor negative Ce^A when normalized to primitive mantle, the Parnassos-Ghiona bauxites exhibit significant Ce^A, when normalized to any reference material [chondrite, North America Shale Composite (NASC), Post-Archaean average Australian Sedimentary rock (PAAS), European Shale (ES), Upper Continental Crust (UCC)] and the average of Mediterranean belt karst-type bauxites). However, it is worthy to note that karst-type bauxites from other areas of Greece do not exhibit similar positive Ce^A and also relative enrichment in HREE. Most of the characteristically REE-enriched geological materials exhibit negative Ce^A, as well as the seawater when they are normalized to NASC and/or to chondrite.

As already mentioned, it has long been suggested that the negative Ce^A (Ce/Ce*) in seawater reflects the oxidation of soluble Ce^{3+} to insoluble Ce^{4+}, which can be then removed as $Ce(OH)_4$. Besides, Ce^{4+} can be incorporated preferentially into Fe-Mn-nodules and Fe-Mn-crusts, exhibiting a characteristic positive Ce^A. Nevertheless, except bauxites, positive Ce^A show specific types of laterites and xenoliths derived from laterites (Gamaletsos et al., 2017). A strong positive Ce^A is also observed in zircon crystals, where Ce^{3+} substitutes in Zr^{4+} sites resulting in a charge deficiency (Grimes et al., 2007). Herein, when the REE values are normalized to the average abundance of REE in the chondrite (Fig. 102), there is a remarkable (rather) positive Ce geochemical anomaly, i.e., sample L_1. There are no REE anomalies in the samples L_2 and L_3. Based on references from the literature (e.g., Braun et al., 1990) the less weathered parent-rocks do not show a positive Ce-anomaly. These anomalies are independent of the parent rocks and the location results from differentiation within the profiles. The slight Ce-positive anomaly in the uppermost part of the profile (sample L_1; Table 5) may reflect the oxidation of Ce^{3+} to Ce^{4+} and its incorporation in other Ce-rich minerals. Additionally, this positive Ce^A in the LARCO GMMSA laterite ore could be probably observed due to paleo-redox conditions. Interpretation of the Ce oxidation state as a paleo-redox proxy requires, however, detailed mineralogical and geochemical investigations, because the Ce oxidation state and REE signature can be inherited and/or modified through successive inorganic and/or organic assisted processes of alteration, aqueous speciation, transport and precipitation/scavenging (Janots et al., 2015). To be precise, there are reservations about whether Ce anomalies can be used as paleo-redox indicators when rocks are rich in organic matter (contain minerals, formed in equilibrium with waters rich in organic matter), and even, when they contain phosphate fossils, such as conodonts, which exhibit Ce^A (+) on their own. In this case, a combination of other geochemical paleo-redox indicators proposed in the literature should be taken into account, such as the ratios Th/U, V/Cr and V/V+Ni, stable isotope measurements ($\delta^{13}C$ and $\delta^{18}O$), but also sedimentological and mineralogical data, such as the possible presence of framboidal pyrite agglomerates or analogous oxide/oxy-hydroxide phases of Fe pseudomorphs with respect to the oxidized ex-iron pyrite (Godelitsas et al., 2010). Generally, it can be concluded that positive Ce anomaly indicates the possibility of a reducing (and possibly anoxic) environment, as shown by the REE geochemical diagrams and in particular by the observed positive Ce anomaly of the sample L_1 (Ce^A or Ce/Ce* = 1.4; Table 5). However, the chondrite-normalized (Fig. 102) REE patterns of the LARCO GMMSA laterite display in general an evident negative Ce geochemical anomaly, i.e., samples L_4, L_5 and L_6 (Ce/Ce* = 0.2, 0.3, 0.2, respectively; Table 5) (Fig. 102), which could be associated with the post-formation of

REEs minerals under, similarly, reductive alkaline conditions [where Ce exists in reduced state (Ce^{3+})]. In general, the aforementioned Ce anomaly has also been observed in Greek lateritic materials, by Skarpelis et al. (1989), Eliopoulos et al. (2000) and Kalatha et al. (2017). In case of LARCO GMMSA ore, the negative Ce anomaly indicates that post-diagenesis/deposition phenomena have taken place. In fact, although the dominant oxidation state of the REE in aqueous solution at 25^{o}C is the 3+ state, Ce behaves differently from the rest of the REE, due to the possibility of being oxidized from Ce^{3+} to Ce^{4+} in a relatively strong oxidizing environment (Kalatha et al., 2017 Maksimovic et al., 1993; Gaines et al., 1997; Braun et al., 1990). Therefore, the positive Ce anomalies occurring in the upper parts of the studied profile, and the negative one at the lowest part of the deposit, in contrast to the rest of the REE transported downward, are probably due to the deference in the breakdown of REE-bearing minerals under similar physico/chemical conditions. Conclusively, further diagenetic and/or supergene/epigenetic processes caused this notable re-distribution of REE, though it is not known if these diagenetic mineralogical transformations were associated with mobilization of REE which has been reported in several Fe-Ni deposits and has been considered as epigenetic (Valeton et al. 1987; Maksimovic et al. 1993). In case of the Ni-Fe deposits in the Lokris area, parent rocks are primarily harzburgites, which represent the erosional outliers of a probable 'complete' ophiolitic nappe that were transformed to serpentinites. Within the serpentine bodies of the basal tectonic melange, xenoliths of basic and sedimentary rocks are included, while a continuous transition from karstic Ni-Fe deposits towards bauxite material in a southern direction has been reported. Although the REE content in ultramafic rocks is usually very low, there is a significant REE content along with other metals such as Al, Fe, Mn, Ni contents in mafic rocks and serpentinites parent rocks (Alevizos, 1997; Valeton, 1987; Rosenberg, 1984). This suggestion implies that the ophiolitic rocks cannot be precluded as a REE source. In fact, according to a recent study, Lesnov (2013) a review of the regularities of REE distribution in minerals contained in mafic and ultramafic rocks as accessory phases was performed. These minerals include garnets, zircons, apatites and perovskites, which can accumulate high concentrations of REE in their structure, as well as chrome spinels, ilmenites, and micas which can accumulate, only limited contents of these trace elements (Kalatha et al., 2017). However, mineralogical characteristics, in particular the occurrence of hematite with inclusions of chromite (Fig. 45) revealed by SEM-EDS (see text above), and which are probably inhered from different sources (Eliopoulos et al., 2012), point to a dynamic cycling of the parent material. The occurrence of the above rare earth minerals described herein and by previous authors, all in the lowermost part of laterite ores at their contact with the carbonate basement may suggest small differences in the conditions during their precipitation and/or variations in the REE source. In addition to the weathering process, the studied profiles as allochthonous laterites lying on a carbonate basement with well-established characteristics of a multistage remobilization and redeposition may have been affected by other processes (Eliopoulos et al., 2000; Aleviozs, 1997; Albandakis, 1980; Valeton et al., 1987; Maksimoviz, 2004; Skarpelis et al., 1989). More specifically, the concentrations level of REEs of Larymna deposit (> UCC values and < carbonatites, pegmatites and alkaline igneous rocks) indicate an origin correlated with metamorphic and diagenetic processes (Samouhos et al., 2019). Based on comments above and suggestions by Eliopoulos et al. (2010), we can support that multistage mineral phase deposition and transformations in the Lokris karst-type laterites is apparent. The significant enrichment of the Larymna laterite in REEs and its negative Ce anomaly illustrate the possibility that the enrichment in REEs originates by the

neighboring metamorphic rocks (Samouhos et al., 2019). Besides, the epigenetic mobilization of REE under reducing (due to the decomposition of organic material) and acidic (due to the decomposition of pyrite) conditions and, subsequently, redeposition under alkaline conditions, during a diagenetic-post diagenetic stage at the Lokris laterite deposits has been well established (Kalatha et al., 2017; Albandakis, 1980; Rosenberg, 1984; Valeton et al., 1987; Maksimovic et al., 1993; Maksimovic et al.,1996; Alevizos, 1997; Economou-Eliopoulos et al., 1997; Maksimovic, 1997; Eliopoulos et al., 2000; Panto et al., 2001; Maksimovic, 2003; Maksimovic, 2004; Skarpelis et al., 1989; Maksimovic, 2010; Eliopoulos et al., 2012). Unfortunately, a comparable study between the Larymna laterite ores and the neighboring parent ophiolitic rocks is not possible due to the lack of available published data. A number of studies concerning the REE content in ophiolites from Greek Peninsula (Samouhos et al., 2019; Bizimis et al., 2000; Katzir et al., 2001, Bortolotti et al., 2008) and Aegean Sea Islands (Karkalis et al., 2016, Stouraiti et al., 2017) have been performed. However these localities are not related to our deposits. Currently, there are no reports on ophiolitic bodies directly related to Larymna laterite deposits in central Greece.

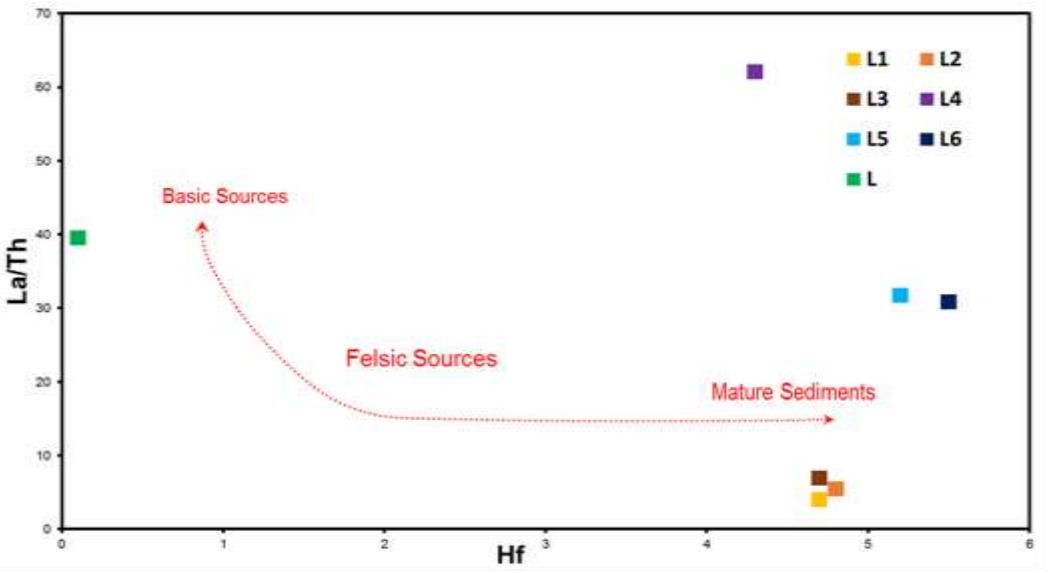

Figure 104. *Binary correlation diagram of La/Th versus Hf (ppm) for the studied LARCO GMMSA laterite ore. The value of UCC (Rudnick and Gao, 2003) is indicated for comparison reason.*

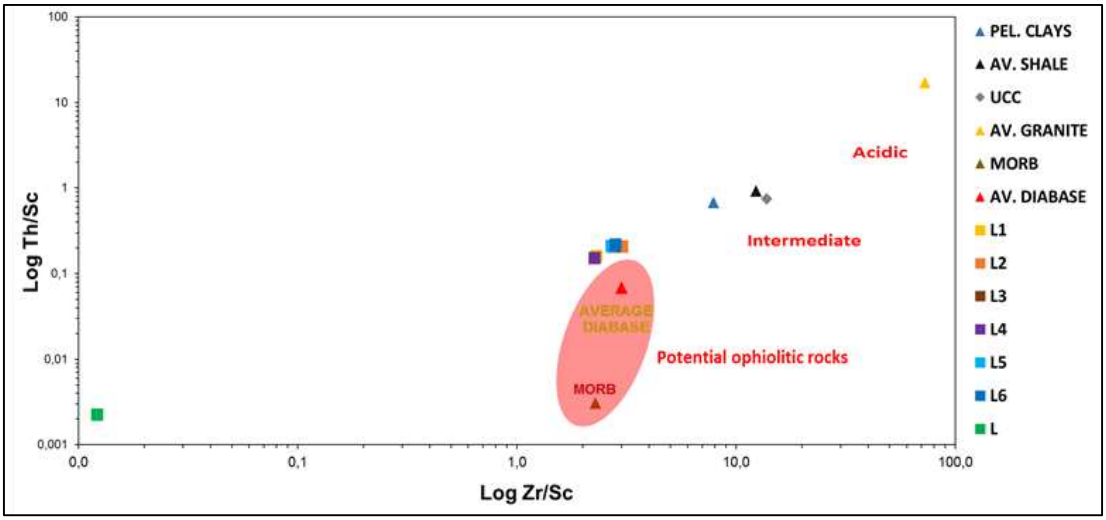

Figure 105. *Binary correlation diagram of Log(Th/Sc) vs Log(Zr/Sc) implying the potential provenance of the studied LARCO GMMSA laterite (after McLennan et al., 1993; Rollinson, 1993; Muftah et al., 2013 and references therein). The values of pelagic clays (Li, 1991 and references therein), avg. shale (Krauskopf and Bird, 1994), UCC (Rudnick and Gao, 2003), avg. granite (Mason and Moore, 1982; Krauskopf and Bird, 1994), depleted morb mantle (Salters and Stracke, 2004) and avg. diabase (Mason and Moore, 1982; Krauskopf and Bird, 1994) are indicated for comparison.*

Furthermore, specific information about the origin of the studied samples can be obtained using discrimination geochemical diagrams based on REE and REE anomalies, i.e., Eu/Eu* and Ce/Ce* (e.g., Rollinson, 1993; Alexander et al., 2000; Mameli et al., 2007; Leybourne and Johannesson, 2008 and references therein; Mondillo et al., 2011; Mongelli, et al., 2014; Mongelli, 2014) (Fig. 106).

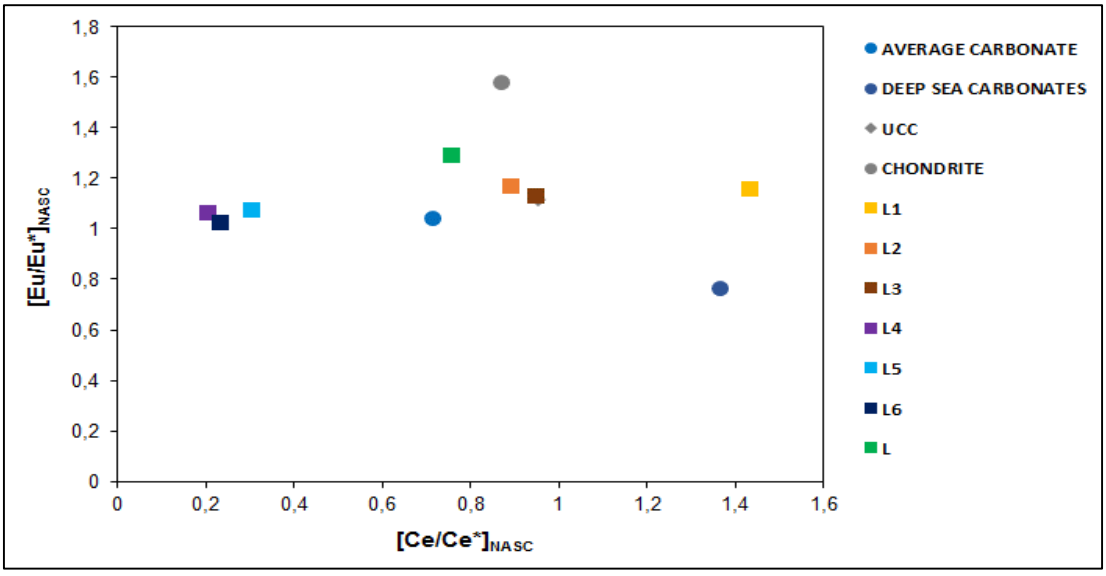

Figure 106. *Binary correlation diagram of Eu vs Ce anomalies (normalized to NASC; Gromet et al., 1984) for the studied LARCO GMMSA laterite (after Leybourne and Johannesson, 2008 and references therein). Eu anomalies calculated as: $Eu/Eu^* = 2(Eu/Eu_{NASC})/(\{Sm/Sm_{NASC})+(Gd/Gd_{NASC})\}$ from Liu et al. (2013). Ce anomalies calculated as: $Ce/Ce^* = 3(Ce/Ce_{NASC})/(\{2\ La/La_{NASC})+(Nd/Nd_{NASC})\}$ after German and Elderfield (1990).*

The REE discrimination diagrams [La/Th vs. Hf; Th/Sc vs. Zr/Sc and Ce/Ce* vs. Eu/Eu*; Figs. 104, 105 and 106, respectively], in accordance to the previous trace element diagrams, clearly support the fact that the studied laterite rocks, and, consequently, the respective layers, have been subjected to serious multiprocessing/repeated weathering, redeposition and intense alteration, due to epigenetic processes. Conclusively, the studied LARCO GMMSA laterite Ni-ore exhibits a rather diverse origin, in contrast to the common consideration that seems to be an ordinary lateritic sedimentary rock subjected to diagenetic processes, exclusively originating in weathering ultrabasic-ophiolitic-rocks. Both whole rock compositions and mineral chemistry of LARCO GMMSA laterite ore deposit indicate that major controlling factors of the composition of the laterites are the conditions during transportation-redeposition of the weathered material and during diagenesis-metadiagenesis stage rather than parent mafic ophiolitic rocks. The Fe-Ni-laterite deposits at the Larymna area are not preserved in situ having been eroded and deposited, as marine sediments and buried by later sedimentary rocks. Evidence of the allochthonous origin of the Larymna Fe-Ni-laterite deposits through repeated marine transgression and regression with associated re-working and deposition in a shallow marine environment, as well as diagenetic and post-diagenetic processes, have been documented in previous publications (Albandakis, 1980; Alevizos, 1997; Eliopoulos et al., 2012; Maksimovic, 2004; Skarpelis, 2006; Valeton et al., 1987). Taking into account all the above, the studied LARCO GMMSA Ni-laterite deposit in Larymna, particularly in Agios Ioannis area, is associated with redeposition and diagenesis in the frame of further supergene/epigenetic processes.

3.7 Hosting carbonate rocks

The studed LARCO GMMSA laterite ore deposit, as already mentioned, have been eroded, transported, and deposited onto karstified Triassic-Jurassic limestones and are conformably overlain by Upper Cretaceous limestones (in our case ~145 Ma and ~90 Ma, respectively), which were also geochemically investigated in detail. The PXRD patterns of the limestone samples are illustrated in Figures 107 and 108. X-ray diffraction patterns of the studied hanging wall (LMS_1) and footwall limestone (LMS_2) proved the presence of calcite as major crystalline phase, as it was expected.

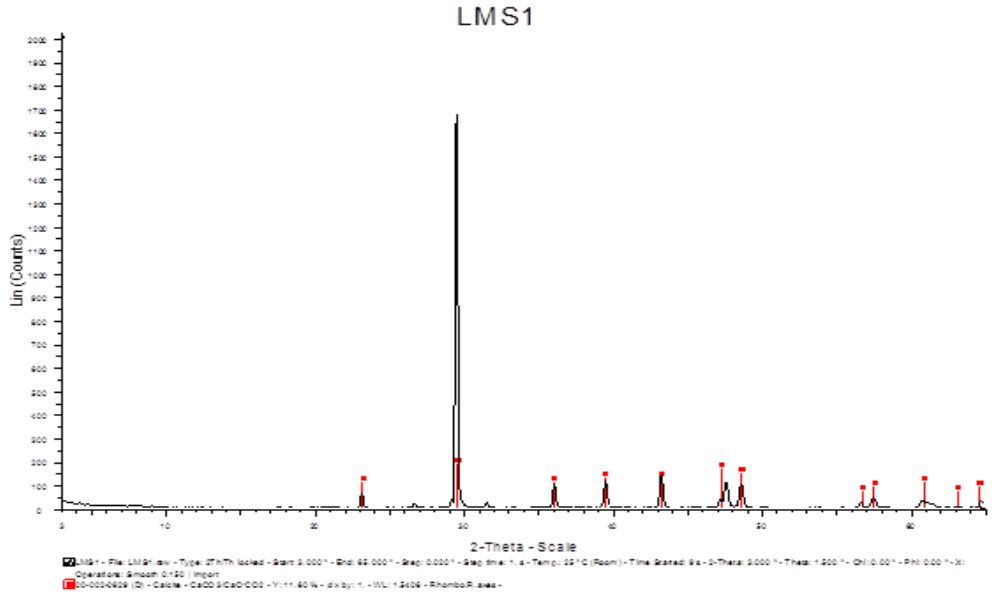

Figure 107. *PXRD pattern of hanging wall limestone LMS_1.*

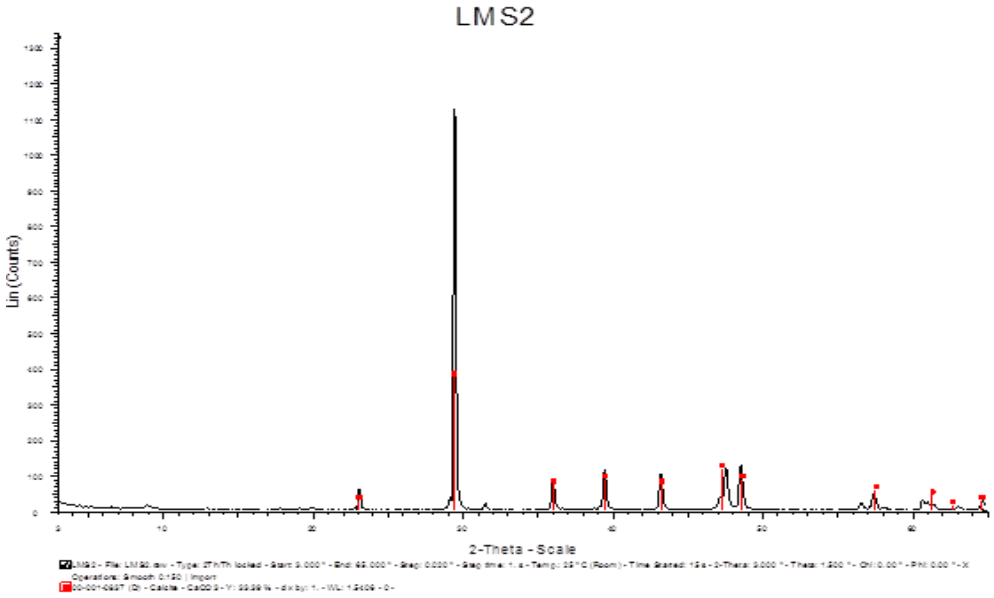

Figure 108. *PXRD pattern of footwall limestone LMS_2.*

The bulk chemical compositions of hanging wall limestone (LMS_1) and footwall limestone (LMS_2), are presented in Table 7.

Table 7. *Major and trace element concentrations of the hanging wall (LMS_1) and the footwall (LMS_2) limestones.*

SampleCode	LMS1	LMS2
Description	Hanging wall limestone	Footwall limestone
	wt%	wt%
Fe_2O_3	2,96	0,07
SiO_2	4,78	0,18
Al_2O_3	1,43	0,07
LOI	40,50	43,20
TiO_2	0,12	0,01
Cr_2O_3	0,07	0,01
MgO	0,73	0,37
MnO	0,47	1,33
CaO	48,47	53,37
P_2O_5	0,01	0,01
K_2O	0,33	0,01
TOT/C	10,84	11,72
TOT/S	0,02	0,01
Na_2O	0,03	0,01
	ppm	ppm
Ni	300,2	2759,7
Co	468,8	7939,5
Y	11,3	45,8
La	5,6	16,5
Zn	5,0	66,0
V	34,0	8,0
Nd	4,3	18,5
Ce	8,3	6,1
Zr	11,4	0,9
Cu	8,1	136,0
Sc	5,0	4,0
As	19,1	9,6
Pr	1,1	3,4
Pb	1,9	2,3
Gd	1,1	5,4
Dy	1,0	3,2
Sr	266,6	169,0
Sm	0,9	4,0
Er	0,6	1,9
Ga	2,3	0,3
Yb	0,5	1,4
Ba	12,0	10,0
Nb	1,5	0,1
Th	0,8	0,1
Ho	0,2	0,7
Eu	0,3	1,0
Tb	0,2	0,6
Be	0,5	0,5
U	1,4	2,1
Hf	0,3	0,1
Tm	0,1	0,2
Rb	10,5	0,2
Lu	0,1	0,2
Sn	0,5	0,5
W	2,4	0,3
Sb	0,1	0,2
Mo	0,9	1,6
Ta	0,1	0,1
Bi	0,1	0,1
Cs	0,7	0,1
Cd	0,2	5,7
Se	0,3	0,3
Ag	0,1	0,1
Tl	0,1	0,2
Hg	0,0	0,1
Au	0,0	0,0
ΣLREE	20,2	48,5
ΣHREE	4,0	14,8
ΣREE	24,2	63,2
ΣREE+Y+Sc	40,5	113,0
$[Eu/Eu^*]_{NASC}$	1,2	1,1
$[Ce/Ce^*]_{NASC}$	0,7	0,2
$[La/Sm]_{NASC}$	1,1	0,7
$[La/Yb]_{NASC}$	11,2	11,5

The bulk chemical compositions (with regard to the trace elements) of the geological materials composing the two studied samples of limetsone, normalized to UCC (Rudnick and Gao, 2003), are presented in Figure 109. It is obvious that both hanging wall and footwall limestones contain relatively low concentrations of trace elements. On the other hand, hanging wall limestone is slightly enriched in Ni (~300 ppm) and As (~19 ppm), whereas footwall limestone differs from the latter, as it is exceedingly enriched incertain compatible elements such as Co [~7940 ppm; much more than Kalatha et al. (2017) reported (680 ppm) in another LARCO GMMSA deposit), Ni (~2760 ppm), and Mn (1.33 wt.%) and Cd (~6 ppm), comparing to UCC (Rudnick and Gao, 2003).

In sedimentary rocks, Co tends to vary with the Fe and Mn content. Commonly, the formation of high valency phases of Fe and Mn is inhibited in the surface environment under acidic and reducing conditions, and, hence, Co is most mobile under

these conditions. It is rapidly removed from solution by co-precipitation and sorption in most oxidizing, near-neutral or alkaline stream water as the dissolved Fe and Mn precipitate out as secondary oxides, hydrous Mn oxides having a particularly strong sorption affinity for Co, due to the fact that Co and Ni are preferentially sorbed to Mn oxide phases, when these phases are present (Kairies et al., 2005). Measurements of Co in seawater suggest that Co is scavenged from the deep sea and hence follows biogeochemical pathways similar to Mn, other measurements of Co in pore waters of marine sediments showed that Co was released into pore waters in the sub-oxic sediment zone during dissolution of sedimentary Mn oxides (Heggie et al., 1984). Accordind to the above authors, solid-phase Co concentrations in surface (oxic) sediments, above the pore water remobilization horizon, are almost double those measured in the deep (anoxic) sediment zone. Besides, Co fluxes to oxic continental margin and hydrothermal sediments are higher than those in the deep sea (Swanner et al., 2014). The sediment and pore-water distributions indicate that a large fraction of sedimentary Co is recycled with Mn between oxic and sub-oxic pore waters and redeposited in surface (oxic) sediments (Heggie et al., 1984). Regardless of the pathway for authigenic Co delivery to sediments, Co released during early diagenesis is immobilized by scavenging with Fe(III) (oxyhydr)oxides and Mn(III/IV) oxides (Swanner et al., 2014).

In sedimentary rocks, Ni is mostly held in detrital ferromagnesian silicate minerals, detrital primary Fe oxides, hydrous Fe and Mn oxides and clay minerals. The levels of concentration in carbonate rocks may reach values as 20 $mg.kg^{-1}$ (Mielke, 1979). Nickel also shows a distinct enrichment in diatomaceous ooze in certain contemporary basins, which suggests that the enrichment mechanism is either linked and involved with anoxic conditions or that Ni is slightly enriched in a heavy-mineral fraction, which accumulates in low-C coarser grained sediments (Francois, 1988).

As for Cd, in sedimentary rocks it is usually found to be enriched in dark shales and soils, depleted in red shales, sandstones and limestones, and about the same in stream sediments. In stream sediments, Cd correlates most significantly with Zn, followed by carbon, weight loss on ignition, Co, readily extractable lead and Mn. This correlation between Cd and Co, readily extractable lead and Mn may be due to relatively high solubility of Cd, Co and Pb in oxidizing waters along with a strong tendency for these metals to adsorb onto Mn oxides that Cd shows the greatest adsorption to clay fractions containing high quantities of organic matter or sesquioxides (Gong et al., 1997). Finally, organic material can sorb trace elements and transfer them to sediments (Broecker et al., 1982; Krauskopf, 1956), and this process is extremely quantitatively significant for metals such as Cd (Algeo et al., 2004; Yee et al., 2003).

Hanging wall and footwall limestones are both enriched in Sr (~267 ppm and 169 ppm, respectively), a fact which is undoubtedly common, as limetsones host significant amounts of Sr. The coprecipitation of Sr with calcite and aragonite has been extensively studied because of the potential applicability of experimental results to geothermometry, diagenetic conditions and processes, and the usefulness of strontium isotopes in understanding subsurface processes. $SrCO_3$ is isostructural with aragonite, although not with calcite, and Sr is generally the most abundant coprecipitate found in marine aragonites of both biogenic and inorganic origin (Katz et al. 1972; Morse et al., 1990). The Sr concentrations, in limestones consisting of $CaCO_3$, indicate diagenetically altered limestones and highlight the complex behavior of carbonate

minerals during diagenesis and the impact on the geochemical information of the primary and secondary phases.

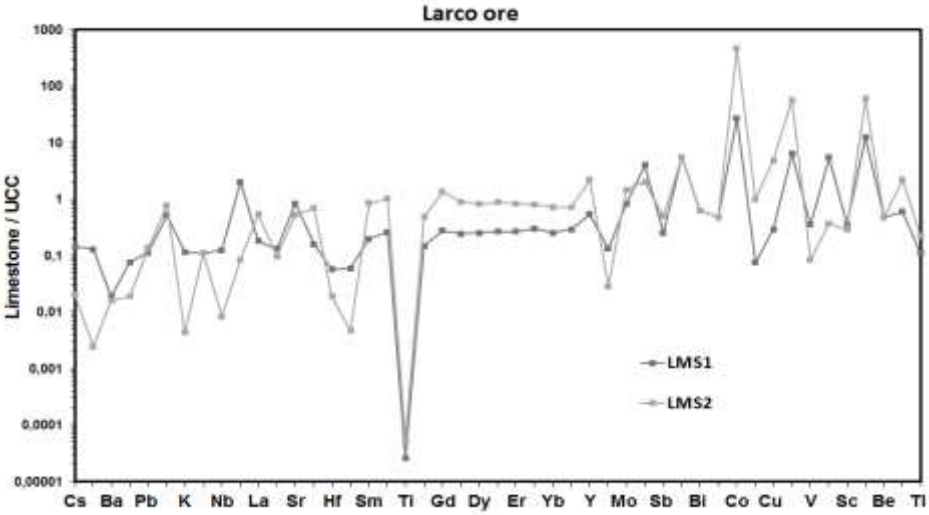

Figure 109. *The UCC-normalized (Rudnick and Gao, 2003) spider diagram for the studied hanging wall (LMS_1) and footwall (LMS_2) limestones.*

Comparing the UCC-normalized spider diagram (Rudnick and Gao, 2003) of LARCO GMMSA laterite embedded between limestones, with the UCC-normalized spider diagram above (Fig. 109), significant enrichment similarities in selected elements can be confirmed. Both laterite and limestone of the studied LARCO GMMSA Ni-laterite ore deposit are enriched in Ni and Co.

The chondrite-normalized (McDonough and Sun, 1995) spider diagram, concerning REE in average, for all geological materials for the studied limestones are presented in Figure 110.

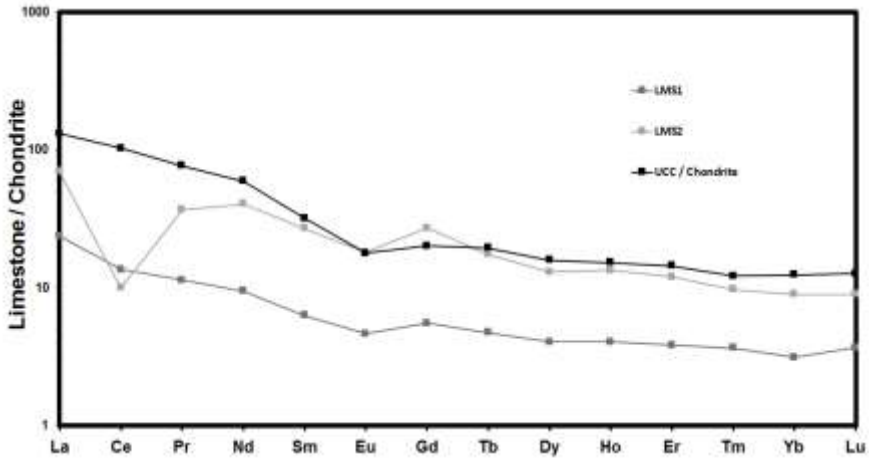

Figure 110. *The REE chondrite-normalized (McDonough and Sun, 1995) diagram for the studied hanging wall (LMS_1) and footwall (LMS_2) limestones.*

During the past few decades, the behavior and mode of distribution of REEs in carbonate rocks were extensively investigated by many researchers. The studies done showed that the important factors influencing enrichment and depletion of REEs in carbonate rocks are 1) the amounts of detrital materials of terrigenous origin; 2) the variation in oxygen level of seawater; 3) the proximity to area of origin; 4) biogenic deposition from seawater; 5) the variation in surface productivity; 6) the lithology and diagenesis and 7) scavenging processes related to depth, salinity, and oxygen level of seawater. The results of recent investigations revealed that geochemical studies on REEs in carbonate rocks furnish a suitable basis for reconstruction of paleogeographic conditions. Commonly, the distribution pattern of REEs in limestones and bauxites can have occurred due to factors such as incorporation of terrigenous (i.e., the character of the carbonate rocks is masked by the terrigenous sediments, of Mn and Fe oxides and of phosphates (Abedini, 2020).

The removal of dissolved Ce(+3) as insoluble form of Ce(+4) preferentially occurs in the upper part of the water column, and, hence, oxic seawater shows a negative Ce anomaly, whereas oxic sediments have a less negative to a positive value. Conversely, in anoxic sediments, Ce is released and the sediments show a negative anomaly (Chen et al., 2012). For example, negative Ce anomalies in marine calcites occur because dissolved oxygen oxidizes soluble Ce^{3+} to insoluble Ce^{4+}. Conversely, $CaCO_3$ precipitating under reducing conditions displays normal or sometimes enriched Ce concentrations. Furthermore, negative Ce anomalies in ancient and modernseep carbonate minerals have been associated with temporary oxic conditions. Therefore, a negative Ce anomaly has long been considered a sensitive indicator of oxidizing conditions (Lin et al., 2017). In other words, the observed Ce anomaly is not limited to marine carbonate, conodonts and ichthyoliths, while the whole-rock Ce anomaly can be used as an indicator of intensity of anoxia and therefore of eustatic sealevel. A positive-trending whole-rock Ce anomaly indicates more oxic conditions. In contrast, negative-trending anomaly indicates more reducing conditions. Concerning the sea level, changes in the positive anomalies would indicate its lowering, as the apparent depth on the redox curve would reflect oxic conditions. Conversely, relative changes negative with time would indicate a rise in sea-level, as the apparent depth reflects anoxic conditions. Cerium anomaly methods have been applied for the Middle Ordovician to Early Silurian quantitative sea-level curve at Dob's Linn, Scotland and in the study of chinese seawater from the Sinian to the early Cambrian in the Yangtze Region. Specifically, in oxic conditions, Ce is less readily dissolved in seawater, which shows negative Ce anomaly (< -0.1) of $\log[3Ce_n/(2La_n+Nd_n)]$. Oxic sediments, on the other hand, are more enhanced with respect to Ce and show less negative to positive Ce anomaly (> -0.1). Conversely, anoxic water would have positive Ce anomalies and anoxic sediments would show negative anomalies. Therefore, changes in the value of the anomaly could be related to redox conditions predicted by the ventilation model of Wilde, with more negative values found during warmer climates and transgressive conditions and more positive values found during cooler to glacial climates and regressive conditions. Thus, whole-rock Ce anomaly is a geochemical parameter that characterizes chemical palaeoceanographic conditions related to relative sea-level changes independent of sedimentological or seismic considerations (Chen et al., 2012). Additionally, this distinct chemical behavior of Ce has enabled it to serve as a marine redox tracer through geologic times. Commonly, the Ce anomalies in marine limestones could indicate paleo-redox conditions in paleo-oceans, and particularly in Tethys (Liu et al., 1988).

A negative Ce anomaly, as also mentioned above, is ubiquitous in well-oxidized open ocean, while study of REE distribution in modern anoxic deep water (e.g., Cariaco Trench) illustrates the paucity of negative Ce anomaly. On the other hand, the extent of negative Ce anomaly in the ocean also varies with water depth. For example, the Ce anomaly profile of North Pacific Ocean shows a sharp decrease in the surface ocean, and stabilizes at intermediate to the deep ocean. In paleo-oceanography studies, Ce anomalies are used to distinguish between oxic and anoxic environments associated with oceanic anoxic events and mass extinction events. In general, most interpretations of marine carbonate Ce/Ce* assume that a negative Ce anomaly represents an oxic or suboxic depositional environment, and a positive Ce anomaly represents anoxic depositional environment (Cao et al., 2020), and is due to the influence of detrital clays (Tobias et al., 2016).

It is more than evident that the footwall limestone (LMS_2) (Fig. 110) shows an evident Ce negative anomaly (Ce/Ce* = 0.2; Table 7), a fact which suggests the deposition under oxic conditions. Moreover, this notable negative Ce anomaly, combined with the elevated Mn content in the certain limestone, may indicate the potential presence of marine ferromanganese (Fe-Mn) (oxyhydr)oxides (hydrated), which are characterized by high sorptive capacity. Manganese oxides are widespread in soils and natural waters, and their capacity to adsorb different trace metals such as Co, Ni, or Zn is well known (Sanchez-Espana et al., 2019). In fact, the Mn oxides have long been recognized as important carriers of minor elementss, some of which (Co, Ni, Cu, Zn) are concentrated up to several percent. Transition metal-bearing Mn oxides have been described as well in deep-sea nodules as in soils or in deposits formed from continental weathering. Whatever their occurrence, these minerals are so poorly crystallized, that their crystal structure are still largely unknown (Manceau et al., 1987). Bau et al. (2014) explain thoroughly that ferruginous and manganiferous metal-rich chemical sediments, such as Fe-Mn crusts and nodules, ironstones, Mn formations (MnFs) and banded iron formations (BIFs) are typical components of the marine sedimentary record of earth's geological history and are widely used as archives of paleoceanographic geochemical proxies and potential metal resources and targets of deep-sea mining (Bau et al., 2014). Deep-ocean polymetallic nodules form on or just below the vast, sediment-covered, abyssal plains of the global ocean. Polymetallic nodules primarily consist of precipitated iron oxyhydroxides and manganese oxides, onto which metals such as Ni, Co, Cu, Ti and REE sorb. The enormous tonnage of nodules on the seabed, and the immense quantities of critical metals that they contain, have made them a target for future mining operations (Hein et al., 2020). Accordingly, Braun et al. (1990) reported a preferedal enrichment of Ce (Ce anomalies from 2 to 10) related to Mn-Fe concretions in a New-Zealand lateritic soil. Additionally, the above approach may also explain the elevated occurrence of Co, as hydrogenetic Fe-Mn crusts are a potential resource for Co, as already mentioned. In fact, Fe-Mn nodules and crusts in the modern global ocean are currently being explored and evaluated as prime targets for future deep-sea mining ventures, predominantly because of their unusual enrichment of critical high-technology metals, such as Ni, Co, Cu, Ti, Mo, Te, Li, Zr, Hf, Nb, Y, REE and Pt, depending on the temperature and composition of the hydrothermal fluid (Bau et al., 2014; Tobias et al., 2017). Another geological material showing positive Ce^A is the desert varnish consisting of Fe-Mn-(oxyhydr)oxides (Thiagarajan et al., 2004).

According to Liu et al. (1988), Tethyan middle-Triassic limestone in China yielded a Ce^A of 0.53 when U/Th was found to be 2.6. In the case of Larymna Tethyan

Cretaceous limestones, the hanging wall sample (LMS_1) show Ce^A (0.72) close to Chinese Triassic, but much lower U/Th ratio (1.75), and therefore, Ce^A values should be carefully considered. Finally, taking into account the carbonates reference domain (Knauth et al., 2009), it can be supported that the footwall limestone is out of the marine and lithification fields related to marine deposition and diagenesis. This rock has been subjected to intense alteration, due to epigenetic processes, in contrast to the hanging wall limestone (LMS_1) that seems to be an ordinary carbonate sedimentary rock subjected to diagenetic processes. In conclusion, the deposition process is similar for both limestones, but the diagenesis to which they have been subjected, is different. Comparing the REE chondrite-normalized (McDonough and Sun, 1995) spider diagram of LARCO GMMSA laterite embedded between limestones, with the REE chondrite-normalized spider diagram above (Fig. 110), it is agreed that there are different enrichment/depletion trends, i.e., it is evident that the limestone of the Larymna LARCO GMMSA ore deposit is clearly depleted in REE, in comparison to REE-enriched laterite. Hence, the distribution of REEs (normalized to chondrite) illustrates different patterns in both rocks (the laterite ore and the limestone) in light of values of conservative indexes such as Ce anomaly. These conspicuous differences like the distribution patterns of REEs and Ce anomaly values between the limestone and the laterite ore demonstrate that the former could not play a significant role in supplying REEs for the latter.

4. OUTLINE AND CONCLUSIONS

Ni-laterite ore from a model laterite profile of Agios Ioannis, Larymna area (Lokris, central Greece), which is currently exploited for Fe-Ni production by LARCO GMMSA, as well as the surrounding footwall Triassic-Jurassic and hanging wall Cretaceous limestones, were characterized by combining diffraction (PXRD), analytical in bulk and microscale (ICP-OES/MS, LA-ICP-MS), spectroscopic (^{57}Fe Mössbauer), microscopic (SEM-EDS) and nanoscopic (TEM-EDS) techniques. On the basis of the present study, the following conclusions can be stated:

- The PXRD investigation of the studied samples confirmed the presence of crystalline Fe-oxides/oxyhydroxides (hematite and goethite), Ni-bearing Mg-Fe-phyllosilicates (mainly chlorite-group and serpentine-group minerals) and calcite as the major mineral components.
- The SEM-EDS study of the typical laterite ore, in microscale, confirmed the well-known occurrence of Ni-bearing phyllosilicates in mixture with Fe-oxide phases, which are associated with traces of detrital zircon and chromite, and REE -fluorocarbonates (mostly bastnaesite -type) and -phosphates (monazite and xenotime) minerals. The Ni content in hematite-like phase is insignificant, as it does not exceed 0.9 wt.%. Hematite-like phase also contains Cr (0.5-4 wt.%) and Co (1.3 wt.%) along with Mn (0.3-0.9 wt.%). However, SEM-EDS performed in material from a thin green-black layer (‘garnierite’) ocurring in the base of the deposit, revealed, except the aformentioned minerals, peculiar phases containing Al-Si-Mn-Ni-Co-Cr-V-Cu-Ca, the latter one perhaps through interference by calcite, implying the presence of potential mineral nanoparticles and nanominerals. The Ni content, according to semi-quantitative microanalyses, in the phyllosilicate structures varies (2-23 wt.%), whereas the EDS spectra confirmed additional the remarkable presence of Mn (2-25 wt.%)

and Co (0.3-19 wt.%). Hence, concerning the mineralogy of LARCO GMMSA laterite at microscale, Ni-bearing hydrous silicates, particularly Ni-bearing phyllosilicates (mainly chlorite-group minerals), occur in mixture with Fe-oxides, which also contain Mn and Co.

- Complementary point analyses of Ni-bearing phyllosilicates by LA-ICP-MS confirmed that, despite rather low Ni-content in the ore (average = 3941 ppm, i.e., ca. 0.4 wt.%), the metal concentration in these phases is 5.81 wt.%. Moreover, LA-ICP-MS analyses confirmed elevated Cr (376 ppm) and Cu (~113 ppm), whereas Co and ΣREE+Y+Sc are remarkably lower (164 ppm and 40 ppm, respectively), meaning that the above critical metals are not consistent with Ni and they are preferentially contained in Fe-oxides/oxyhydroxidesand other phases, examined by SEM-EDS, such as Mn-(oxy)hydroxide/oxide (hydrated) phases and REE-fluorocarbonates and REE-phosphates.
- The study of the Ni-phyllosilicate by means of ^{57}Fe-Mössbauer indicated that Fe^{3+} is exclusively the Fe component of the mineral. Mössbauer spectroscopy also showed that a possible constituent of the phase can be superparamagnetic α-Fe [natural Fe^{3+}-oxide (hematite: α-Fe_2O_3) as well as synthetic Fe^{3+}-oxyhydroxide (goethite: α-FeOOH)]. The examined particles correspond to Fe containing phases with reduced particle size implies the presence of Fe mineral nanoparticles and/or Fe nanominerals.
- TEM-EDS study proved the existence of Al-Si-Mn-Ni-Co(-Cr) areas, corresponding most likely to an unknown (oxy)hydroxide/oxide (hydrated) phase, consisting most probably of an amorphous/disordered Ni-(Cr-)Co-bearing Mn-(oxy)hydroxide/oxide (hydrated) phase, the so-called ‘asbolane’ by previous authors, into the laterite matrix. Consequently, there is a wide possibility of combination of nanophases, like polyphasic nanominerals or even admixtures of amorphous/disordred nanominerals and mineral nanoparticles, a fact that is in accordance with Mössbauer spectroscopy results.
- The bulk chemical analyses by ICP-OES/MS indicated that, except for major elements (Si, Al, Fe and Mn), the studied industrial laterite ore contains a variety of useful and potentially hazardous trace elements (Ni, Co, V, ΣLREE, ΣHREE, Sc, As, and Pb, max values: ~9212 ppm, ~1480 ppm, 379 ppm, ~1221 ppm, ~253 ppm, 76 ppm, ~81 ppm, and ~67 ppm, respectively; average values: 3941 ppm, 659 ppm, 317 ppm, 678 ppm, 111 ppm, 71 ppm, 51 ppm, and 53 ppm, respectively), with remarkable positive geochemical anomalies with respect to HFSE and REEs (REE+Y+Sc, max: ~2150 ppm; average: 1173 ppm), as well as in most of compatible elements, whereas they are depleted in specific LILE. It should be mentioned that in green-black layer from the base of the deposit, as well as in the footwall limestone, Co is exceptionally increased (3534 ppm and 7940 ppm, respectively). Discrimination diagrams (e.g., La/Th vs. Hf; Th/Sc vs. Zr/Sc and Ce/Ce* vs. Eu/Eu*) implied that the studied LARCO GMMSA laterite Ni-ore exhibits a rather diverse origin, and, consequently, it was stated evidently that it does not absolutely originate in ultrabasic and basic-ophiolitic-rocks (due to Th-Zr-Hf presence), as commonly considered. In fact, it is a mature ‘sediment’ subjected to serious multiprocessing/repeated weathering, redeposition and intense alteration processes. The ore’s characteristic epigenetic enrichment in Ni-Co-Mn (‘asbolane’) and Ni bearing phyllosilicates along with REE(-minerals) at the lowest part of the deposit, close to its contact with the basement limestone, and within limestone itself, suggests their deposition was controlled by physicochemical conditions rather than the precursor rocks. This

significant enrichment of the Larymna laterite in REEs combined with its negative geochemincal Ce (Ce/Ce*) anomaly indicate that post-diagenesis/deposition phenomena have taken place inthe frame of further supergene/epigenetic processes.

- Concerning the economic significance of the critical containing metals such as REEs (including Sc) and Co, the presence of Co and Sc in Ni-bearing phyllosilicate (mainly chlorite group minerals) phases as well as in Fe- (mainly hematite) and Mn-(oxy)hydroxide/oxide (hydrated) phases, makes their co-extraction rather difficult on the basis of the current pyrometallurgical method at the smelting plant. In terms of exploitation, Co and Sc, in contrast to REE, could probably be co-extracted with Ni (3941 ppm) in case of typical LARCO GMMSA laterite ore from Larymna area.

LITERATURE

Aiglsperger, T., Proenza, J.A., Lewis, J.F., Labrador, M., Svojtka, M., Rojas-Purón, A., Longo, F., Ďurišová, J., 2016. Critical metals (REE, Sc, PGE) in Ni-laterites from Cuba and the Dominican Republic. Ore Geol. Rev. 73, 127-147.

Abedini, A., Calagari, A.A., 2015. Rare earth element geochemistry of the Upper Permian limestone: the Kanigorgeh mining district, NW Iran. Turkish J. Earth Sci., pp. 365-382.

Albandakis, N., 1974. The nickeliferous Fe-ores of Lokris and Evia. Metal. Miner. Ann. 19, p. 41 (in Greek with English abstract).

Albandakis, N., 1980. The nickel-bearingiron-ores in Greece. Proceedings of the International Symposium of Metallogeny of Mafic and Ultramafic Complexes. 194-213.

Albandakis, N. 1984. Ni-minerals in the deposits of the Sub-Pelagonian zone. Mineral Wealth 31, 9-32 (in Greek).

Albandakis, N.D., Compagnoni, R. and Di Cairano, C., 1980. Mineralogical study of the Ni-Cr-Fe pisolitic deposit of Laryma (Lokris, Greece). UNESCO, IGCP No. 169, Int. Syrup. Metallog. Mafic and Ultramafic Complexes (Abstr.).

Alevizos, G., 1997. Mineralogy, Geochemistry and Genesis of Sedimentary Nickeliferous Fe-ores of Lokris (central Greece), Unpublished Ph.D Thesis. Technical University of Crete, Greece (in Greek).

Alevizos, G., Mücke, A., 2001. Erzpetrographisch-mikroanalytische Untersuchung und Genese der sedimentären Eisennickelvorkommen von Agios Ioannis und Marmeiko (Lokris-Griechenland). N. Jb. Miner. Abh. 176, 67-88.

Algeo, T.J., Maynard, J.B., 2004. Trace-element behavior and redox facies in core shales of Upper Pennsylvanian Kansas-type cyclothems. Chem. Geol. 206 (3-4), 289-318.

Anila, V., Singru R.M., Sharma, V.N., Chander, S., 1981. Mössbauer study of the treatment of nickeliferous laterite ore in argon and hydrogen/water mixtures.Hydrometallurgy 7, 329-337.

Annersten, H., Ericsson, T., Fillipidis, A., 1982. Cation ordering in Ni-Fe olivines. American Mineralogist 67(11/12), 1212-1217.

Apostolikas, A., 2009. Nickel Deposits. Efyra Publications (in Greek).

Apostolikas, A., Frogoudakis, E., Maglaras, K., 2000. Nickel-bearing deposits in Western Macedonia, Greece: Present and perspectives. In Proceedings of the 1st Conference of the Committee of Economic Geology, Mineralogy and Geochemistry of the Geological Society of Greece, Kozani, Greece, 11-14 May 2000.

Arnisalo, J., Mäkelä, K., Bourgeois, B., Spyropoulos, C., Varoufakis, S., Morten, E., Maglaras, C., Soininen, H., Angelopoulos, A., Eliopoulos, D., Lamberg, P., Papupen,

H., Hattula, A., Pietila, R, Elo, S., Ripis, C., Dimou, E., Apostolikas, A., Melakis, M., Economou Eliopoulos, M., Vasillas, N., Pelantonis, S., Amprazis, E., Charou, E., Gustavsson, M., Tiainen, M., Stefouli, D., Deifini, P., Vanturi, G., Stavrakas, Y., Katsoulas, D., 1999. Integrated technologies for minerals exploration; pilot project fornickel ore deposits. Trans. Instn Min, Metall. (Sect. B. Appl. Earth sci.) 108, 151-163.

Augustithis, S.S., 1962. Mineralogical and Geochemical Changes in the Diagenetic and Post-Diagenetic Phases of the Ni-Cr-lron Oolitic Deposit of Larymna/Lokris, Greece. Chem. Erde 22, 5-17.

Baker, J., Cassard, D., Grundfelt, B., Ehinger, S., D'Hugues, P., Gaál, G., Kaija, J., Kurylak, W., Mizera, W., Sarlin, J.; et al., 2011. A New Approach to Mineral Resources in Europe-ProMine. In Proceedings of the Sustainable Production and Consumption of Mineral Resources-Integrating the EU's Social Agenda and Resource Efficiency, Wroclav, Poland, 20-22 October 2011.

Bancroft, G.M., 1973. Mössbauer spectroscopy: An introduction for inorganic chemists and geochemists. Halsted press.

Bau, M., Schmidt, K., Koschinsky, A., Hein, J., Kuhn, T., Usui, A., 2014. Discriminating between different genetic types of marine ferro-manganese crusts and nodules based on rare earth elements and yttrium. Chem. Geol. 381, p. 9.

Berger, V.I., Singer, D.A., Bliss, J.D., Moring, B.C., 2011. Ni-Co Laterite Deposits of the World. Database and Grade and Tonnage Models. USGS Open-File report 2011-1058, p. 26, http://pubs.usgs.gov/of/2011/1058/ and http://mrdata.usgs.gov/laterite (accessed January 2013).

Boev, B., Jankovic, S., 1996. Nickel and nickelferous iron deposits of the Vardar Zone (SE Europe) with particular reference to the R anovoStudena Voda orebearing series, in Faculty of Mining and Geology tip, St. Cyril and MethodiusUniversity, Special issue, Skopje 3, 270-278.

Bizimis, M., Salters, V.J.M., Bonattib, E., 2000. Trace and REE content of clinopyroxenes from supra-subduction zone peridotites. Implications for melting and enrichment processes in island arcs. Chem. Geol. 165, 67-85.

Bortolotti, V., Chiari, M., Marcucci, M., Photiades, A., Principi, G., Saccani, E., 2008. New geochemical and age data on the ophiolites from the Othrys area (Greece): implication for the Triassic evolution of the Vardar Ocean. Ofioliti 33, 135-151.

Boskos, E., Perraki, T., Kolokotroni, K., 1996. The Ni and Cr distribution in the mineralogical phases of the nickeliferous laterites from Evia Island. Miner. Wealth 101, 9-26 (in Greek with English abstract).

Boskos, E., Orphanoudaki, A., Perraki, T., 2000. The Ni distribution in the mineral phases of Greek Fe-Ni-laterite deposits. Proceedings of the 3rd Congress of Mineral Wealth, pp. 107-115.

British Geological Survey, Minerals U.K., 2008. Nickel. Stat. Inf. (www.mineralsuk.com), p. 23.

Brand, N.W., Butt, C.R.M., Elias, M., 1998. Nickel laterites: Classification and features. AGSO J. Austral. Geol. and Geoph. 17 (4), 81-88.

Braun, J.-J., Pagel, M., Muller, J.-P., Bilong, P., Michard, A., Guillet, B., 1990. Cerium anomalies in lateritic profiles. Geochim. Cosmochim. Acta 54, 781-795.

Broecker, W.S., Peng. T.-H., 1982. Tracers in the Sea. Lamont-Doherty Geological Observatory, Columbia University, Palisades, NY, p. 690.

Burke, I.T., Peacock, C.L., Lockwood, C.L., Stewart, D.I., Mortimer, R.J.G., Ward, M.B., Renforth, P., Gruiz, K., Mayes, W.M., 2013. Behavior of aluminum, Asand vanadium during the neutralization of red mud leachate by HCl, gypsum, or seawater. EnvFe. Sci. Technol. 47, 6527-6535.

Butt, C.R.M., Cluzel, D., 2013. Nickel laterite ore deposits: weathered serpentinites. Elements 9, 123-128.

Cao, C., Liua, X.-M., Bataille, C.P., Liu, C., 2020. What do Ce anomalies in marine carbonates really mean? A perspective from leaching experiments. Chem. Geol. 532 (119413), p. 15.

Caraballo, M.A., Michel, F.M., Hochella, M.F.Jr., 2015. The rapid expansion of environmental mineralogy in unconventional ways: beyond the accepted definition of a mineral, the latest technology, and using nature as our guide. Am. Miner. 100, 14-25.

Celet, P., 1962. Contribution a l' etude geologique du Parnasse-Kiona et d'une partie des regions meridionales de la Grece continentale. Ann. Geol. Pays Hell., T. XIII, Athens, p. 45.

Chagnes, A., Omelchuk, K., 2017. Modelling of liquid-liquid extraction of cobalt, nickel and manganese from acidic chloride media. Abstracts of International workshop on Geochemical cycle of Ni, Co and Sc: from mining exploration to ecotoxicity, Nancy, France, 17-19 October, 2017.

Chakhmouradian, A.R., Wall, F., 2012. Rare Earth Elements: Minerals, Mines, Magnets (and More). Elements 8, 333-340.

Chasse, M., Griffin, W.L., O'Reilly, S.Y., Calas, G., 2017. Scandium speciation in a world-class lateritic deposit. Geochem. Perspect. Lett. 3, 105-114.

Chen, L., Lin, A.T.-S., Da, X., Yi, H., Tsai L.L.-Y., Xu, G., 2012. Sea-level changes recorded by cerium anomalies in the Late Jurassic (Tithonian) black rock series of qiangtang basin, North-Central Tibet. Oil Shale, Vol. 29, No. 1, 18-35.

Christidis, G.E., Skarpelis, N., 2010. Clay mineralogy of the sedimentary iron nickel ore of Agios ioannis, NE Viothia: new data and implication for diagenetic

modifications. Proceedings of the 12th International Congress of the Geological Society of Greece. 2553-2561.

Chukhrov, F.V., Gorshkov, A.I., Vitovskaya, I.V., Drits, V.A., Sivtsov, A.V., 1982. On the Nature of Co-Ni Asbolane; a Component of Some Supergene Ores.

Cocker, M.D., 2012. Lateritic, supergene rare earth element (REE) deposits. Proceedings of the 48th Annual Forum on the Geology of Industrial Minerals, Scottsdale, Arizona, USA, April 30-May 4 2012. Arizona Geological Survey Special Paper #9, Chapter 4, p. 18.

Cornell, R.M., Schwertmann, U., 2003. The Iron Oxides: Structure, Properties, Reactions, Occurrences and Uses. 2nd edition, Wiley-VCH Verlag GmbH & Co. KGaA, p. 664, ISBN: 3-527-30274-3.

De-qing, Z., Yu C., Hapugoda, S., Vining, K., Jian, P., 2012. Mineralogy and crystal chemistry of a low grade nickel laterite ore. Trans. Nonferrous Met. Soc. China 22, 907-916.

Diaz, C.M., Landolt, C.A. Vahed, A., Warner, A.E.M, Talor, J.C., 1988. A Review of Nickel Pyrometallurgical Operations, Journal of Metals (September), pp. 28-33.

Dostal, J., 2016. Rare Metal Deposits Associated with Alkaline/Peralkaline Igneous Rocks. In Reviews in Economic Geology; Verplanck, P.L., Hitzman, M.W. (Eds.), SEG: Littleton, CO, USA, Chapter 2, pp. 6-33.

Dyar, M.D., Agresti, D.G., Schaefer, M.W., Grant, C.A., Sklute, E.C., 2006. Mössbauer spectroscopy of earth and planetary materials. Annu. Rev. Earth Planet. Sci. 34, 83-125.

Economou, M., 1979. Origin of magnetite occurrences in ultramafic rocks of Greece. PhD thesis. Athens University, p. 170.

Economou-Eliopoulos, M., Eliopoulos, D., Apostolikas, A., Maglaras, K., 1997. Precious and rare earth element distribution in Ni-laterites from Lokris area, central Greece. Papunen, H. _Ed.., Miner. Deposits: Res. Explor., Where do they Meet?, Balkema, Rotterdam, pp. 411-414.

Economou-Eliopoulos, M., Michaelidis, E., 2001. Apatite in Ni-laterites of the Edessa, northern Greece. In: Piestrrzynsky, A., et al. (Eds.), Mineral Deposits at the Beginning of the 21st Century. Balkema, Rotterdam, pp. 583-589.

Economou-Eliopoulos, M., 2003. Apatite and Mn, Zn, Co-enriched chromite in Ni-laterites of northern Greece and their genetic significance. J. Geochem. Explor. 80, 41-54.

Economou-Eliopoulos, M., Eliopoulos, D.G., Vassilatos, Ch., Soulas M., 2003. Genetic significance of chromite in Fe-Ni-laterite deposits. Implication from western Macedonia, Greece. Miner. Explor. Sust. Devel., Millpress, pp. 69-72.

Economou-Eliopoulos, M., Frei, R., Atsarou, C., 2014. Application of chromium stable isotopes to the evaluation of Cr (VI) contamination in groundwater and rock leachates from central Evia and the Assopos basin (Greece). Catena 122, 216-228.

Economou-Eliopoulos, M., Frei, R., Megremi I., 2016. Potential leaching of Cr(VI) from laterite mines and residues of metallurgical products (red mud and slag): An integrated approach. J. Geochem. Explor. 162, 40-49.

Eggleton, R., 2001. The regolith glossary: surficial geology, soils and landscapes. CRC LEME, Canberra, p. 144.

Elias, M., 2002. Nickel laterite deposits-geological overview, resources and exploitation in Cooke, D., and Pontgratz, J. (Eds.), Giant ore deposits: characteristics, genesis and exploration. Centre for Ore Deposit Research, University of Tasmania, Special Publication 4, 205-220.

Eliopoulos, D., Economou-Eliopoulos, M., 2000. Geochemical and mineralogical characteristics of Fe-Ni and bauxitic-laterite deposits of Greece. Ore Geol. Rev. 16, 41-58.

Eliopoulos, D., Economou-Eliopoulos, M., 2010. As distribution in laterite deposits of the Balkan Peninsula. Proceedings of XIX Congress of the Carpathian Balkan Geological Association, Thessaloniki, Greece 1, 325-332.

Eliopoulos, D.G., Economou-Eliopoulos, M., Apostolikas, A., Golightly, J.P., 2012. Geochemical features of nickel-laterite deposits from the Balkan Peninsula and Gordes, Turkey: the genetic and environmental significance of As. Ore Geol. Rev. 48, 413-427.

Eliopoulos, D., Economou, G., Tzifas, I., Papatrechas, C., 2014. The potential of Rare Earth Elements in Greece. Proceedings of the 1st European Rare Earth Resources Conference, Milos, Greece, 04-07 September 2014, pp. 308-316.

Fabbrizio, A., Schmidt, M.W., Petrelli, M., 2021. Effect of *f*O2 on Eu partitioning between clinopyroxene, orthopyroxene and basaltic melt: Development of a Eu^{3+}/Eu^{2+} oxybarometer.Chem. Geol. 559 (119967), p. 16.

Fan, R., Gerson, A.R., 2011. Nickel geochemistry of a Philippine laterite examined by bulk and microprobe synchrotron analyses. Geochim. Cosmochim. Acta 75, 6400-6415.

Farrokhpay, S., 2017. Processing of fine grained lateritic ores: new challenges. Abstracts of International workshop on Geochemical cycle of Ni, Co and Sc: from mining exploration to ecotoxicity, Nancy, France, 17-19 October, 2017.

Farrokhpay, S., Filippov, L., 2017. A holistic approach to pre-concentrate nickel in laterite ores. Abstracts of International workshop on Geochemical cycle of Ni, Co and Sc: from mining exploration to ecotoxicity, Nancy, France, 17-19 October, 2017.

Filippidis, A., 1997a. Chemical variation of chromite in the Gorgona olivine-orthopyroxenite, Thrace, Greece. Neues Jahrbuch für Mineralogie Monatsheft 8, 113-130.

Filippidis, A., 1997b. Chemical variation of chromite in the central sector of Xerolivado chrome mine of Vourinos, western Macedonia, Greece. Neues Jahrbuch für Mineralogie Monatshefte 8, 354-370.

Frakes, L.A., Bolton, B., 1992. Effects of ocean chemistry, sea level, and climate on the formation of primary sedimentary manganese ore deposits. Econom. Geol. 87(5), 1207-1217.

Francois, R., 1988. A study on the regulation of the concentrations of some trace metals (Rb, Sr, Zn, Pb, Cu, V, Cr, Ni, Mn and Mo) in Saanich Inlet sediments, British Columbia, Canada. Marine Geology 83(1-4), 285-308.

Freyssinet, Ph., Butt, C.R.M., Morris, R.C., Piantone, P., 2005. Ore-forming processes related to lateritic weathering. Economic Geology 100th Anniversary Vol., pp. 681-722.

Fysh, S.A., Clark P.E., 1983. A Mössbauer study of the iron mineralogy of acidleached bauxite. Hydrometallurgy 10, 285-303.

Gaines, R.V., Skinner, H.C.W., Foord, E.E., Mason, B., Rosenzweig, A., 1997. Dana's New Minerals, 8th ed.; JohnWiley and Sons, Inc.: New York, NY, USA.

Gamaletsos, P.N., 2014. Mineralogy and Geochemistry of bauxites from Parnassos-Ghiona mines and the impact of the origin of the deposits, Ph.D Thesis. National and Kapodistrian University of Athens.

Gamaletsos, P.N., Godelitsas, A., Kasama, T., Church, N., Douvalis, A., Goettlicher, J., Steininger, R., Boubnov, A., Pontikes, Y., Tzamos, E., Bakas, T., Filippidis, A., 2017. Nano-mineralogy and -geochemistry of high-grade diasporic karst-type bauxite from Parnassos-Ghiona mines, Greece. Ore Geol. Rev. 84, 228-244.

Gamaletsos, P.N., Kalatha, S., Godelitsas, A., Economou-Eliopoulos, M., Göttlicher, J., Steininger, R., 2018. Arsenic distribution and speciation in the bauxitic Fe-Ni-laterite ore deposit of the Patitira mine, Lokris area (Greece). J. Geochem. Explor. 194, 189-197.

Gambogi, J, Cordier, D.J., 2013. Rare Earths, in Metals and minerals. U.S. Geological Survey. Available from: pubs.usgs.gov/of/2013/1072/OFR2013-1072.

German, C.R., Elderfield, H., 1990. Application of the Ce anomaly as a paleoredox indicator: The ground rules. Paleoceanography 5, 823-833.

Godelitsas, A., Kafantaris, F.-C., Göttlicher, J., 2010. Triassic limestones of Mt. Kithaeron (Greece) as natural analogues of long-term retention of uranium in carbonate rocks: a synchrotron-based study Nuclear Waste Management: Research Challenges for the Future, Mineralogical Society, 28-29 September, Cambridge, UK.

Golightly, J.P., 1979. Nickeliferous laterites: a general description. International Laterite Symposium, by Evans D.J.I., Shoemaker R.S. and Veltman H. (Eds.), AIME, 1979, 3-23.

Golightly, J.P., 1981. Nickeliferous Laterite Deposits. Economic Geology 75th Anniv. Vol., pp. 710-735.

Golighlty, J.P., 2004. Progress in Understanding the Evolution of Nickel Laterites. Special Publications, v. 15, p. 26.

Goodenough, K.M., Schilling, J., Jonsson, E., Kalvig, P., Charles, N.; Tuduri, J., Deady, E.A., Sadeghi, M., Schiellerup, H., Muller, A.; et al., 2016. Europe's rare earth element resource potential: An overview of REE metallogenetic provinces and their geodynamic setting. Ore Geol. Rev. 72, 838-856.

Goudie, A.S., Kenneth, P., 1983. Chemical sediments and Geomorphology. Precipitates and Residue in the Near-Surface Environment, pp. 7-58.

Grimes C. B., John B. E., Kelemen P. B., Mazdab F. K., Wooden J. L., Cheadle M. J., Hanghøj K. and Schwartz J. J. (2007) Trace element chemistry of zircons from oceanic crust: A method for distinguishing detrital zircon provenance. Geology 35 (7), 643-646.

Gromet, L.P., Dymek, R.F., Haskin, L.A., Korotev, R.L., 1984. The 'North American shale composite': Its compilation, major and trace element characteristics. Geochim. Cosmochim. Acta 48, 2469-2482.

Heggie, D., Lewis, T., 1984. Cobalt in pore waters of marine sediments. Nature 311(5985), p. 453.

Hein, J.R., Koschinsky, A., Kuhn, T., 2020. Deep-ocean polymetallic nodules as a resource for critical materials. Nature Rev., Earth & Environment, Vol. 1, pp. 158-169.

Herrington, R., 2017. Palaeo Ni-Co-Sc laterites of Europe: diversity, formationand future potential. Abstracts of International workshop on Geochemical cycle of Ni, Co and Sc: from mining exploration to ecotoxicity, Nancy, France, 17-19 October, 2017.

Hill, V.G., Weir, C., Collins, R.L., Hoch, D., Radcliffe, D., Wynter, C., 1978. Application of Mössbauer spectroscopy to iron-57 bauxite. Hyperfine Interact. 4, 444-447.

Hoatson, D.M., Jaireth, S., Jaques, A.L., 2006. Nickel sulfide deposits in Australia: Characteristics, resources and potential. Ore Geology Reviews 29, 177-241.

Hochella, M.F.Jr., 2002a. There's plenty of room at the bottom: nanoscience in geochemistry. Geochim. Cosmochim. Acta. 66, 735-743.

Hochella, M.F.Jr., 2002b. Nanoscience and technology: the next revolution in the earth sciences, earth plan. Sci. Lett. 203, 593-605.

Hochella, M.F.Jr., 2006. The case of nanogeoscience. Ann. N.Y. Acad. Sci. 1093, 108-122.

Hochella, M. F. Jr., 2008. Nanogeoscience: from origin to cutting-edge applications. Elements 4, 373-379.

Hochella, M.F.Jr., Lower, S.K., Maurice, P.A., Penn, R.L., Sahai, N., Sparks, D.L., Twining, B.S., 2008a. Nanominerals, mineral nanoparticles, and earth systems. Science 319, 1631-1635.

Hochella, M.F.Jr., Lower, S.K., Maurice, P.A., Penn, R.L., Sahai, N., Sparks, D.L., Twining, B.S., 2008b. Nanominerals, mineral nanoparticles, and earth systems. Science 319, 1631-1635.

Hochella, M.F.Jr., Aruguete, D., Kim, B., Madden, A.S., 2012. Naturally occurring inorganic nanoparticles: general assessment and a global budget for one of earth's last unexplored geochemical components. In: Guo, H., Barnard, A. (Eds.), Nature's Nanostructures. Pan Stanford Publishing, Australia, p. 42.

Huang, J.-H., Huang, F., Evans, L., Glasauer, S., 2015. Vanadium: Global (bio)geochemistry. Chem. Geol. 417, 68-89.

Janots, E., Bernier, F., Brunet, F., Munoz, M., Trcera , N., Berge, A., Lanson, M., 2015. Ce(III) and Ce(IV) (re)distribution and fractionation in a laterite profile from Madagascar: Insights from in situ XANES spectroscopy at the Ce LIII-edge. Geochim. Cosmochim. Acta 153, 134-148.

Kairies, C.L., Capo, R.C., Watzlaf, G.R., 2005.Chemical and physical properties of iron hydroxide precipitates associated with passively treated coal mine drainage in the Bituminous Region of Pennsylvania and Maryland.Geochem. 20(8), 1445-1460.

Kalatha, S., Economou-Eliopoulos, M., 2015. Framboidal pyrite and bacterio-morphic goethite at transitional zones between Fe-Ni-laterites and limestones: evidence from Lokris Greece. Ore Geol. Rev. 65, 413-425.

Kalatha, S., Perraki, M., Economou-Eliopoulos, M., Mitsis, I., 2017. The origin of bastnaesite-(La,Nd,Y) in the Nissi (Patitira) bauxite laterite deposit, Lokris, Greece. Minerals 7, p. 19.

Kalles, N., 1993. Prospects of the Greek ferro-nickel industry. Proceedings of the Greek mining industry, Geological Society of Greece, pp. 29-38.

Karkalis, C., Magganas, A., Koutsovitis, P., 2016. Petrological, mineralogical and geochemical data from the Eohellenic ophiolitic nappe in the island of Skyros, Greece. Bull. Geol. Soc. Greece. L 1867-1877.

Katsikatsos, G., 1977. La stucture tectonique dAttique et d'Eubee. VI Coll. on the Geol. of the Aegean Reg., Athens, 1, pp. 211-228.

Katz, A.M.I.T.A.I., Sass, E., Starinsky, A., Holland, H.D., 1972. Strontium behavior in the aragonite-calcite transformation: An experimental study at 40-98 C. Geochim. Cosmochim. Acta 36(4), 481-496.

Katzir, Y., Avigad, D., Matthews, A., Garfunkel, Z., Evans, B.W., 2001. Origin, HP/LTmetamorphism and cooling of ophiolitic melanges in southern Evia (NW Cyclades) Greece. J. Metamorphic Geol. 18, 699-718.

Knauth L.P., Kennedy M.J., 2009. The Late Precambrian greening of the Earth. Nature 460, 728-732.

Krauskopf, K.B., 1956. Factors controlling the concentrations of thirteen rare metals in sea-water. Geochim. Cosmochim. Acta 9(1-2), 1-B32.

Krauskopf, K.B., Bird D.K., 1994. Introduction to geochemistry. McGraw-Hill International Editions, New York, USA, 667 pp. ISBN: 0-07-035820-6.

Krüger, J.C., James, R.H., Herrington, R., Brown, P., Pearce, C.R., Roberts, S., 2015. Behaviour of Cr in laterites and implications for Ni-laterite formation. Abstracts of Goldschmidt.

Kureweil, H., 1966. Zur Mineralogie Ni-führender Verwitterungs- und sedimentärer FeErzen in Lokris, Mittelgriechenland. Berg- und Hüttenm. Mh. 111, 488-497.

Kuzmann, E., Nagy, S., Vértes, A., 2003. Critical review of analytical applications of Mössbauer spectroscopy illustrated by mineralogical and geological examples (IUPAC Technical Report). Pure Appl. Chem. 75, 801-858.

Laskou, M., Economou-Eliopoulos, M., 2005. Micro-organisms as fossils and present-day development in Ni-laterites and bauxites of the Balkan Peninsula. Mineral deposit research: meeting the global challenge: proceedings of the 8th biennial SGA meeting, Beijing, China, 18-21 August 2005: in 2 v. Vol. 2 / ed. by Mao J., Bierlein F.P.-Berlin: Springer, 2005, pp. 873-1613, ISBN 3-540-27945-8.

Le Gleuher, M., 2017. Nickel Market Developments: a review. Abstracts of International workshop on Geochemical cycle of Ni, Co and Sc: from mining exploration to ecotoxicity, Nancy, France, 17-19 October, 2017.

Lelong, F., Tardy, Y., Grandin G., Trescases J.J., and Boulange, B., 1976. Pedogenesis, chemical weathering and processes of formation of some supergene ore deposits, in Wolf K.H., ed., Supergene and surficial ore deposits. Texture and fabrics, v. 3 of Handbook of strata-bound and stratiform ore deposits: Amsterdam, Elsevier, pp. 93-133.

Lesnov, F.P., 2013. Consistent patterns of rare earth element distribution in accessory minerals from rocks of mafic-ultramafic complexes. Cent. Eur. J. Geosci. 5(1), 112-173.

Leybourne, M.I., Johannesson, K.H., 2008. Rare earth elements (REE) and yttrium in stream waters, stream sediments, and Fe-Mn oxyhydroxides: Fractionation, speciation, and control over REE + Y patterns in the surface environment. Geochim. Cosmochim. Acta 71, 5962-5983.

Li Y.-H., 1991. Distribution patterns of the elements in the ocean: a synthesis.Geochim. Cosmochim. Acta 55, 3223-3240.

Lin, Y., Zheng, M., Ye, C., Power, I.M., 2019. Trace and rare earth element geochemistry of Holocene hydromagnesite from Dujiali Lake, central Qinghai-Tibetan Plateau, China. Carbon. Evapor. 34, 1265-1279.

Liu, X., Wang, Q., Feng, Y., Li, Z., Cai, S., 2013. Genesis of the Guangou karstic bauxite deposit in western Henan, China. Ore Geol. Rev. 55, 162-185.

Llorca, S., Monchoux, P., 1991. Supergene cobalt minerals from New Caledonia. Can. Miner. 29, 149-161.

Maksimovic, Z., 1978. Nickel in karstic environment: in bauxites and in karstic Ni deposits. Bull. B.R.G.M., (2), II, 3, 173-183.

Maksimovic, Z., 1997. Hydrous nickel-containing clay-like minerals in the karstic environment. In: H. Kodama, A.R. Mermut, J.K. Torrance (Eds.). Clays of our future. Proc. 11th Intern. Clay Conference. Ottawa, pp. 647-652.

Maksimovic, Z.J., 2003. An unknown Ni-Al hydrosilicate. Acta Geol. Hung., 46 313-320.

Maksimovic, Z., 2004. Karstic nickel deposit in the village Ba, near Ljig, Western Serbia: Ni-bearing minerals and their genesis. Bull. Acad. Serbe Sci. Arts 42 341-361.

Maksimovic, Z., 2010. Genesis of Mediterranean karstic bauxites and karstic nickel deposits. Bull. Acad. Serbe Sci. Arts 46, p. 27.

Maksimovic, Z., Panto, G., 1983. Mineralogy of Yttrium and Lanthanides in the Mediterranean karstic bauxite deposits. Abstracts of the 5th Int. Congr. ICSOBA, Zagreb, p. 32.

Maksimovic, Z., Panto, G., 1991. Contribution to the geochemistry of rare earth elements in the karstbauxite deposits of Yugoslavia and Greece. Geoderma 51, 93-109.

Maksimovic, Z., Skarpelis, N., Panto, G., 1993. Mineralogy and geochemistry of the rare earth elements in the karstic nickel deposits of Lo**k**ris area, Greece. Acta Geol. Hung. 36/3, 331-342.

Maksimovic, Z.J., Panto, G., 1996. Authigenic rare earth minerals in karst-bauxites and karstic Ni deposits. In Rare Earth Minerals, Chemistry, Origin and Ore Deposits; Jones, A.P., Wall, F., Williams, C.T. (Eds.). The Mineralogical Society Series, 7: Washington, DC, USA, Chapter 10, 257-279.

Manceau, A., Llorca, S., Calas, G., 1987. Crystal chemistry of cobalt and nickel in lithiophorite and asbolane from New Caledonia. Geochim. Cosmochim. Acta, Vol. 51, pp. 105-113

Maratos, G., 1960. The Iron-nickel ores of Tsoukas-Loutsiou-Kastrakiou (Lokris). I.G.M.E., p. 65 (in Greek).

Marinos, G., 1958. The geotectonic division of eastern Greece. Geological Society of Greece, Vol. 3, pp. 73-82.

Marsh, E.E., Anderson, E.D, 2011. Ni-Co Laterite Deposits: U.S. Geological Survey, Open-File Report 2011-1259, U.S. Geological Survey: Reston, VA, USA, p. 9.

Marsh, E.E., Anderson, E.D., Gray F., 2010. Ni-Co Laterite Deposits: U.S. Geological Survey, Open-File Report 2011-1259, U.S. Geological Survey: Reston, VA, USA, 9.

Mason B., Moore C.B., 1982. Principles of geochemistry. John Willey & Sons, NewYork, USA, 344 pp. ISBN: 0-471-57522-4.

McDonough, W.F., Sun, S.-S., 1995. Composition of the Earth. Chem. Geol. 120, 223-253.

McLennan, S.M., Hemming, S., McDaniel, D.K., Hanson, G.N., 1993. Geochemical approaches to sedimentation, provenance, and tectonics. Special Papers-Geological Society of America, pp. 21-21.

Melfos, V., Voudouris, P., 2012. Geological, Mineralogical and Geochemical Aspects for Critical and Rare Metals in Greece. Minerals 2, 300-317.

Michailidis, K., 1990. Zoned chromites with high Mn-contents in the Fe-Ni-Cr-laterite ore deposits from the Edessa area in Northern Greece. Mineral. Deposita 25, 190-197.

Michailidis, K., Kassoli-Fournaraki A., Sklavounos S., 1984. Chromites andmagnetite in the laterite ore occurrences of Karydia, Edessa region (NorthernGreece). Sci. Annals, Eac. Sciences, Univ. Thessaloniki, 24, 111-131.

Mielke, J.E., 1979. Composition of the Earth's crust and distribution of the elements. In Review of research on modern problems in geochemistry (Vol. 16, pp. 9-37). UNESCO Report Paris.

Mizutani, T., Fukushima, Y., Okada, A., Kamigaito, O., Kobayashi T., 1991. Synthesis of 1:1 and 2:1 Iron Phyllosilicates and Characterization of their Iron State by Mössbauer Spectroscopy. Clays and Clay Minerals 39(4), 381-386.

Moore, D.M., Reynolds, R.C., 1989. X-ray Diffraction and the Identification and Analysis of Clay Minerals (Vol. 322, p. 321). Oxford: Oxford university press.

Morse, J.W., Mackenzie, F.T., 1990. Geochemistry of sedimentary carbonates, Vol. 48, Elsevier.

Mountrakis, D., Sapountzis, E., Kilias, A., Eleutheriadis, G., Christoforidis, G., 1983. Paleogeographic conditions in western Pelagonian margin in Greece during the initial rifting of the continental area. Canadian Journal of Earth Science 20, 1673-1681.

Moussoulos, L., 1967. Extraction of Nickel, Cobalt, Iron and Chromium from Laterites L.M. and M-LAR Processes. Advances in Extractive Metallurgy, Paper 13, Institution of Mining and Metallurgy, London, April 1967.

Moussoulon, L., 1973. Nickel Metallurgy, First. ed., pp. 50-57, Scientific Editions of the National Technical University of Athens, Athens, 1973.

Moussoulos, L., 1975. A process for the production of electrolytic nickel from ferronickel. Metallurg. Transact. B 6, 641-645.

Muftah, A.M., Pavlakis, P., Godelitsas, A., Gamaletsos, P., Boaz, N., 2013. Paleogeography of the Eosahabi River in Libya: New insights into the mineralogy, geochemistry and paleontology of Member U1 of the Sahabi Formation, northeastern Libya. J. Afr. Earth Sci. 78, 86-96.

Munoz, M., Ulrich, M., Levard, C., Rose, J., Ambrosi, J-P., Cathelineau, M., Teitler, Y., Marcaillou, C., Hesse, B., 2017. Distribution and speciation of Sc in lateritic profiles of New Caledonia using synchrotron-XRF and Sc K-edge XANES spectroscopy.

Abstracts of International workshop on Geochemical cycle of Ni, Co and Sc: from mining exploration to ecotoxicity, Nancy, France, 17-19 October, 2017.

Myagkiy, A., 2018. Mineralization of Nickel in saprolitic ore of New Caledonia: Dynamics of metal transfer and modeling of coupled geochemical and hydrodynamic processes. Ph.D Thesis. Université de Lorraine, p. 116.

Nahon, D.B., Tardy, Y., 1992. The ferruginous laterites. In: Butt CRM, Zeegers H (Eds.). Regolith exploration geochemistry in tropical and subtropical terrains. Handbook Explor. Geochem. 4, Elsevier, Amsterdam, pp. 41-55.

Navrotsky, A., Mazeina, L., Majzlan, J., 2008. Size-driven structural and thermodynamic complexity in iron oxides. Science 319, 1635-1638.

Nord, A.G., Annersten, H., Filippidis, A., 1982. The cation distribution in synthetic Mg-Fe-Ni olivines. American Mineralogist 67(11/12), 1206-1211.

Ohde, S., Mataragio, J., 1999. Instrumental neutron activation analysis of carbonatites from Panda Hill and Oldoinyo-Lengai, Tanzania. J. Radioan. Nuclear Chem. 240(1), 325-328.

Orphanoudakis, A, Mposkos, E, Kastritsis, I, 1997. A study of the mineralogical and geochemical composition of the Fe-Ni-laterite from the area of Paleochori (Grevena). Geological Society of Greece, XXXI: pp. 7-22.

Panto, G., Maksimovic, Z., 2001. Two new rare earth minerals in an unusual mineralization of the Nissi bauxite deposit, Greece. Acta Geol. Hung. 44/1, 81-93.

Petrascheck, W., 1954. Die Eisenerz und Nickelagerstatten von Lokris in Ostgriechenland. Bull.of Inst.Geol and Subsurf. Res, pp. 135-169.

Petrelli, M., Morgavi, D., Vetere, F., Perugini, D., 2016. Elemental imaging and petro-volcanological applications of an improved Laser Ablation Inductively Coupled Quadrupole Plasma Mass Spectrometry.Periodico di Mineralogia 85, 25-39.

Putzolu, F., Abad, I., Balassone, G., Boni, M., Cappelletti, P., Graziano, S.F., Maczurad, M., Mondilloa, N., Najorka, J., Santoro, L., 2020. Ore Geol. Rev. 120 (103431), p. 24.

Qin, H.-B., Yang, S., Tanaka, M., Sanematsu, K., Arcilla, C., Takahashi, Y., 2020. Chemical speciation of scandium and yttrium in laterites: New insights into the control of their partitioning behaviors. Chem. Geol. 552 (119771), p. 15.

Quesnel, B., Le Carlier de Veslud, C, Boulvais, P., Gautier, P., Cathelineau, M., Drouillet, M., 2017. Ni redistribution in laterites: effects of geomorphology on lateral transfer, leading to Ni-enrichment in saprolite. Abstracts of International workshop on Geochemical cycle of Ni, Co and Sc: from mining exploration to ecotoxicity, Nancy, France, 17-19 October, 2017.

Reich, M., Hough, R.M., Deditius, A., Utsunomiya, S., Ciobanu, C.L., Cook, N.J., 2011. Nanogeoscience in ore systems research: principles, methods, and applications. Introduction and preface to the special issue. Ore Geol. Rev. 42, 1-5.

Renz, C., 1940. Die Tektonik der griechischen Gebirge. Pragm. Akad. Athinon, Athens, p. 26.

Renz, C., 1955. Die Vorneogene Stratigraphie der normal sedimentaren Formationen Griechenlands. Inst. Geol. and Subsurf. Res., Athens, p. 9.

Ribeiro, P.P.M., Mendonca de Souza, L.C., Neumann R., Daniel dos Santos I., Dutra A.J.B., 2020. Nickel and cobalt losses from laterite ore after the sulfation-roasting-leaching processing. J. Mater. Res. and Technol. 9, 12404-12415.

Robb, L., 2005. Introduction to ore-forming processes.

Rollinson, H.R., 2014. Using geochemical data: evaluation, presentation, interpretation. Routledge.

Roque-Rosell, J., Mosselmans, J.F.W., Proenza, J.A., Labrador, M., Galí, S., Atkinson, K.D., Quinn, P.D., 2010. Sorption of Ni by 'lithiophorite-asbolane' intermediates in Moa Bay lateritic deposits, eastern Cuba. Chem. Geol. 275, 9-18.

Rosenberg, F., 1984. Geochemie und Mineralogie lateritischer Nickel und Eisenerze in Lokris und auf Euböa, Griechenland, Unpublished Ph.D Thesis. Univ. of Hamburg (in German).

Rudnick, R., Gao, S., 2003. Composition of the continental crust. In Treatise on Geochemistry; Holland, H. D., Turekian, K. K., Eds.; Elsevier-Pergamon: Oxford 3, p. 64.

Sadeghi, M., Jonsson, E., Kalvig, P., Keulen, N., Goodenough, K., Deady, E., Muller, A., Eliopoulos, D., Cassard, D., Bertrand, G., Vuollo, J., Nysten, P., Bergman, T., Söderhielm, J., Arvanitidis, N. and Eurare WP1 team, 2014. Rare Earth Element Resources in Europe with focus on the Nordic countries. 1st International Symposium on Development of Rare Earths, Baotou, China.

Salters, N.J.M., Stracke, A., 2004. Composition of the depleted mantle. Geochem. Geophys. Geosyst. 5 (5), 1-27.

Samouhos, M., Godelitsas, A., Nomikou, C., Taxiarchou, M., Tsakiridis, P., Zavašnikc, J., Gamaletsos, P.N., Apostolikas, A., 2019.New insights into nanomineralogy and geochemistry of Ni-laterite ores from central Greece (Larymna and Evia deposits). Geochemistry 79, 268-279.

Samson, I.M., Chasse, M., 2016. Scandium. In: White, W.M. (Ed.), Encyclopedia of Geochemistry, Encyclopedia of Earth Sciences Series. Springer International Publishing, Cham, Switzerland, p. 5. http://dx.doi.org/10.1007/978-3-319-39193-9_281-1.

Sanchez-Espana, J., Yusta, I., 2019. Coprecipitation of Co^{2+}, Ni^{2+} and Zn^{2+} with Mn(III/IV) Oxides Formed in Metal-Rich Mine Waters.Minerals 9 (226), p. 23.https://www.researchgate.net/publication/332329307.

Skarpelis, N., 2000. Sedimentary nickeliferous iron ores and lateritic weathering crusts in SW Balkan Peninsula: mineralogical textural relationships and genesis. Proceedings of the 1st Conference of the Economic Geology 398-412 (in Greek with English abstract).

Skarpelis, N., 2006. Lateritization processes of ultramafic rocks in Cretaceous times: The fossil weathering crusts of mainland Greece. J. Geochem. Explor. 88, 325-328.

Smith, C.G., 2001. Always the bridesmaid, never the bride: cobalt geology and resources. Transactions of the Institutions of Mining and Metallurgy: Section B, Vol. 110, Issue 2, pp. 75-80, http://dx.doi.org/10.1179/aes.2001.110.2.75 (accessed July 2013).

Starkey, H.C., Blackmon, P.D., Hauff, P.L., 1984. The routine mineralogical analysis of clay-bearing samples. Geological Survey bulletin (USA). No 1563.

Steuber, T., Rauch, M., Masse J.-P., Graaf J., Malkoc, M., 2005. Low-latitude seasonality of Cretaceous temperatures in warm and cold episodes. Nature, Vol. 437, pp. 1341-1344, doi: 10.1038/nature04096.

Stouraiti, C., Pantziris, I., Vasilatos, C., Kanellopoulos, C., Mitropoulos, P., Pomonis, P., Moritz Chiaradia, M., 2017. Ophiolitic remnants from the upper and intermediate structural unit of the Attic-Cycladic crystalline belt (Aegean, Greece): fingerprinting geochemical affinities of magmatic precursors. Geosciences 7.

Swanner, E.D., Planavsky, N.J., Lalonde, S.V., Robbins, L.J., Bekker, A., Rouxel, O.J., Saito, M.A., Kappler, A., Mojzsis, S.J., Konhauser, K.O., 2014. Cobalt and marine redox evolution. Earth and Planetary Science Letters 390, 253-263.

Teitler, Y., Cathelineau, M., Ulrich, M., Ambrosi, J., Munoz, M., Sevin, B., 2019. Petrology and geochemistry of scandium in New Caledonian Ni-Co laterites. J. Geochem. Explor. 196, 131-155.

Technical Report, Sunrise NickelCobalt Project, 2018. New South Wales, Australia, p. 394.

Thiagarajan, N., Aeolus Lee, C.-T., 2004. Trace-element evidence for the origin of desert varnish by direct aqueous atmospheric deposition. Earth Planet. Sci. Lett. 224, 131-141.

Thorne, R, Herrington, R, Roberts, S., 2009. Composition and origin of the Çaldag oxide nickel laterite, W. Turkey. Miner Deposita 44, 581-595.

Tobias, H., Bolton, B., Brugger, J., Etschmann, B., Frierdich, A., 2017. Dynamic Mineral Recrystallization-Implications for sustainable trace metal recovery from deep-sea ferromanganese deposits. Abstracts of 46th Underwater Mining Conference, Berlin, Germany, 24-29 September 2017.

Tupaz, C.A.J., Watanabe Y., Sanematsu K., Echigo T., 2020. Mineralogy and geochemistry of the Berong Ni-Co laterite deposit, Palawan, Philippines. Ore Geol. Rev. 125 (103686), p. 20.

Ulrich, M., Cathelineau, M., Munoz, M., BoFe, M., Teitler, Y., Karpoff, A.M., 2019. The relative distribution of critical (Sc, REE) and transition metals (Ni, Co, Cr, Mn, V) in some Ni-laterite deposits of New Caledonia. J. Geochem. Explor. 197, 93-113.

Valeton, I., Biermann, M., Reche, R., Rosenberg, F., 1987. Genesis of nickel laterites and bauxites in Greece during the Jurassic and the Cretaceous and their relation to ultrabasic rocks. Ore Geol. Rev. 2, 359-404.

Van der Kraan, A.M., 1972. Mössbauer effect studies of superparamagnetic α-FeOOH and α-Fe_2O_3. Ph.D. Thesis, Technical University, Delft.

Verplanck, P.L., Mariano, A.N., Mariano, A.Jr. (Eds.), 2016. Rare Earth Element Ore Geology of Carbonatites. In Reviews in Economic Geology; SEG: Littleton, CO, USA, 2016; Chapter 1, p. 5.

Wells, M.A., Chia, J., 2011. Quantification of Ni-laterite mineralogy and composition: A new approach: Australian Journal of Earth Sciences 58, 711-724.

White, W.M., 2013. Geochemistry. John Wiley and Sons.

Xu, D., Liu, L.X., Quast, K., Addai-Mensah, J., Robinson, D.J., 2013. Effect of nickel laterite agglomerate properties on their leaching performance. Advanc. Powd. Techn. 24, 750-756.

Yee, N., Fein, J. B., 2003. Quantifying metal adsorption onto bacteria mixtures: a test and application of the surface complexation model. Geomicrobiol. J. 20(1), 43-60.

Yongue-Fouateu, R., Ghogomu, R.T., Penaye, J., Ekodeck, G.E., Stendal, H., Colin, F., 2006. Nickel and cobalt distribution in the laterites of the Lomie´ region, south-east Cameroon. J. Afric. Earth Scienc. 45, 33-47.

Zevgolis, E.N., 2004. The evolution of the Greek ferronickel production process, p. 14.

Zevgolis, E.N., Zografidis, C., Perraki, T., Devlin, E., 2000. Phase transformations of nickeliferous laterites during preheating and reduction with carbon monoxide, J. Anal. Therm. Calorim. 100, 133-139.